A TECHNIQUE FOR STUDYING THE ANOMALOUS PENETRATION OF RADIO FREQUENCY RADIATION THROUGH METALLIC SLABS

by

DAVID EARL GABEL

B.Sc., University of Waterloo, 1966

A DISSERTATION SUBMITTED IN PARTIAL FULFILLMENT
OF THE REQUIREMENTS FOR THE DEGREE OF
MASTER OF SCIENCE

in the

Department of Physics

SIMON FRASER UNIVERSITY
OCTOBER 1970

APPROVAL

Name: David Earl Gabel

Degree: Master of Science

Title of Thesis: A Technique for Studying the Anomalous Penetration of Radio Frequency Radiation through Metallic Slabs

Examining Committee:

Date Approved:
October 30, 1970

J. F. Cochran
Senior Supervisor

P. H. Bly
Examining Committee

Leigh Hunt Palmer
Examining Committee

B. Y. Clayman
External Examiner
Assistant Professor
Department of Physics
Simon Fraser University
Burnaby, B. C.

ABSTRACT

A technique for studying the anomalous penetration of radio frequency radiation through metallic crystals has been tested using single crystals of pure gallium. It was found that quantitative observations of the transmission of electromagnetic radiation through gallium single crystals could be made. These crystals had the shape of a hollow box instead of the conventional rectangular slab geometry.

Most notable amongst the profusion of structures seen in a survey of transmission effects in gallium were the Gantmakher resonances and the Gantmakher-Kaner oscillations. The line position, the line width, and the line amplitude of several Gantmakher resonances were found to be consistent with previously reported surface impedance data. Agreement with other size effect data was also obtained for extremal dimensions of sections through the gallium Fermi surface.

Gantmakher-Kaner oscillations due to limiting point resonances were studied in detail in several crystals. A model which was constructed to indicate the possible size and shape of the pieces of surface under investigation showed quantitative agreement with pieces included in a recent theoretical construction of the gallium Fermi surface by Reed.

TABLE OF CONTENTS

LIST OF TABLES

LIST OF FIGURES

ACKNOWLEDGMENTS

I wish to express my sincere gratitude to Professor John Cochran for the many helpful discussions and the continued enthusiastic guidance during the period of this research project. I thank also Miss Pat Goldberg for the careful preparation of gallium single crystals and Mrs. Elsie Waite for typing this thesis.

I also express my sincere regret for the loss of a close friend, Jerry Miller, who was killed in an automobile accident near Boston Bar, British Columbia, March 2, 1968, before he could make his contribution to physics at Simon Fraser University.

Finally, I wish to dedicate this thesis to my dear wife Anita whose invaluable understanding and inspiration has made this endeavor both possible and worthwhile.

Chapter 1

INTRODUCTION

If a metallic conductor is placed in an alternating electromagnetic field of frequency ω, which is less than the plasma frequency ω_p^* of the mobile charge carriers, then an electromagnetic field will be induced in the metal near the surfaces extending to a depth of the order of δ, where δ is the skin depth. If the metal is very pure, then at low temperatures (liquid helium temperatures) the carrier mean free path between collisions, ℓ, may be much longer than the skin depth. At a frequency of 1 Mhz and temperature 1°K, a typical experimental value for the skin depth is approximately 10^{-4} cm. When $\ell >> \delta$ the electric field distribution in the metal is no longer given by the simple exponential behaviour obtained from Maxwell's equations and the usual local form of Ohm's law:

$$E = E(0)\exp\left[-(1-i)z/2\delta_0\right] \qquad \omega\tau << 1 \qquad (1)$$

where δ_0 (classical skin depth) $= \dfrac{\phi}{H(0)} = \dfrac{1}{H(0)}\int_0^\infty H(z)\,dz$

$$= \left(\frac{c^2}{8\pi\omega\sigma}\right)^{1/2}$$

---

*The plasma frequency, $\omega_p = \sqrt{4\pi ne^2/m^*} \approx 10^{16}$ rad/sec for a carrier density $n = 10^{22}$ cm^{-3} and effective mass $m^* = m_o$, where m_o is the free electron mass.

Here ϕ is the flux contained in the metal per unit length of surface, E(0) is the electric field at the surface of the metal, and H(0) is the magnetic field at the surface of the metal.* Instead, the current density at a point $\vec{r}$ in the metal is defined by the electric field in a region having dimensions of the order of ℓ. The conductivity, $\vec{\sigma}$, is now no longer a constant of the metal but rather depends on the spatial distribution of the electric field. Under these anomalous skin-effect conditions it is necessary to replace equation (1) by an equation derived from a microscopic theory developed by Reuter and Sondheimer[1] which predicts a more complicated non-exponential behaviour.[1][2]

Because the current at a given point $\vec{r}$ is determined by the electric field in a region of dimension ℓ about $\vec{r}$, this gives the possibility of measuring effects due to a relatively few carriers on the Fermi surface itself. A useful experimental technique for studying the Fermi surface of a metal has been to look at the transmission through a metal slab or at the reflection from a metal slab of radio and microwave frequency radiation[3][4]. For pure metals with mean free

---

*Throughout this thesis cgs units will be used, in which,

$$\text{curl } \vec{E} = -\frac{1}{c}\frac{\partial \vec{H}}{\partial t}$$

$$\text{curl } \vec{H} = \frac{4\pi \vec{j}}{c} + \frac{1}{c}\frac{\partial \vec{E}}{\partial t}$$

and

$$\vec{F} = e\vec{E} + \frac{e}{c}\vec{v} \times \vec{H}$$

and a time dependence, $e^{-i\omega t}$, is used.

paths greater than the slab thickness, in the presence of a static magnetic field, anomalies in the surface impedance and transmission can be used to gauge the shape of the Fermi surface of the metal. An example of a transmission anomaly is illustrated in the following sketch.

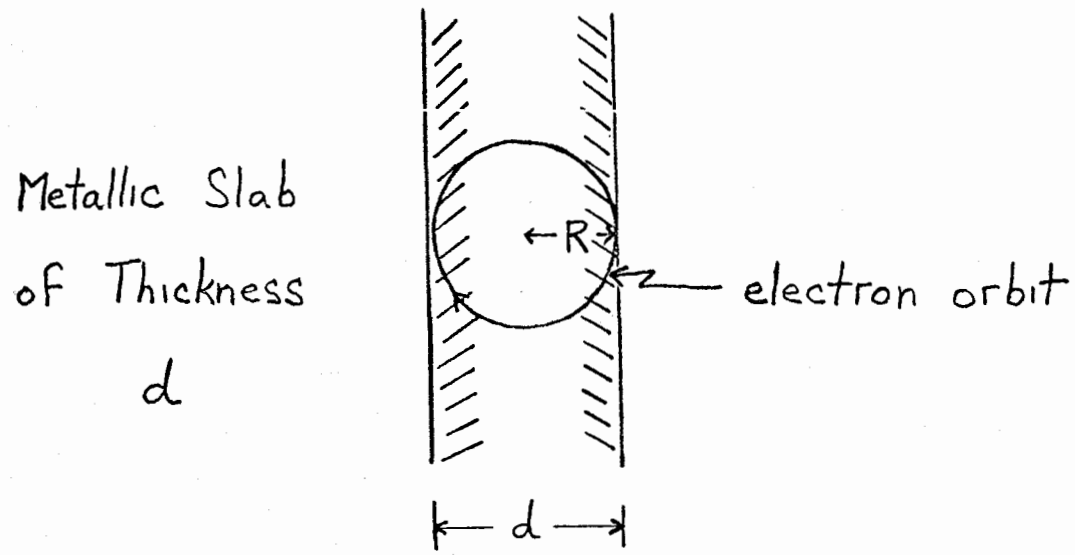

When the diameter of the electron orbit equals the slab thickness, i.e. $2R = d$, there is a transmission anomaly. The strength of the anomaly depends in a complicated way upon the mean free path, ℓ[5][6]. For this reason the mean free path cannot easily be determined from the amplitude of the anomaly.

In general size effects of this nature result from extremal orbits on the Fermi surface. The following sketch helps to illustrate this point.

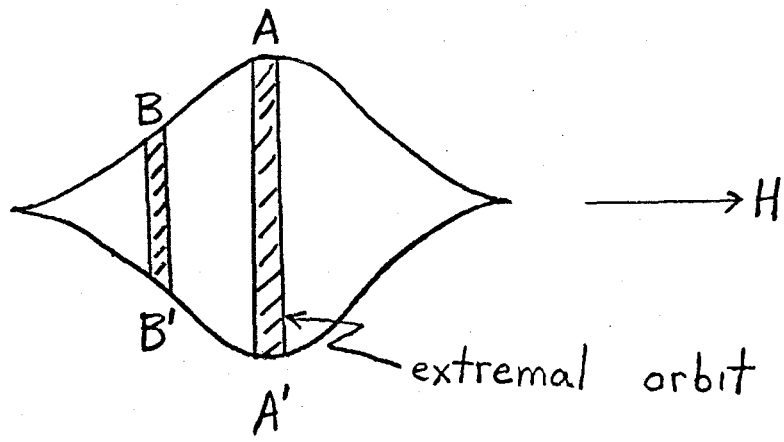

For a Fermi surface of general shape (see above), orbits on the Fermi surface in any plane normal to the magnetic field, $\vec{H}$, (that is, at different values of k_H, where k_H is the characteristic wave vector along $\vec{H}$) may have different cyclotron periods. The dominant response of the system comes from orbits whose periods are stationary with respect to small changes in k_H. These orbits are called extremal orbits, i.e. AA' orbit. Due to a phase cancellation[7], the contribution from orbits such as BB' is minimal. In other words, the contribution to the electric field in the metal from different non-extremal orbits tend to add out of phase and hence do not reinforce one another. However, near the extrema the phase varies only slowly and there is an enhanced signal from these orbits.

In a typical experimental arrangement[3][6][8][10] to measure these anomalies at radio frequencies (called radio frequency size effects) a metal slab is placed inside the

tank coil of an oscillator. If the circuit is operated near its threshold (marginal operation[3][10]) its amplitude of oscillation is sensitive to small changes in the quality factor, Q, and hence is sensitive to small changes in the resistive part of the surface impedance of the specimen. If on the other hand, the circuit is operated in a stable mode, the frequency of oscillation depends on the reactive part of the surface impedance of the specimen[6][8]. Using audio frequency modulation and synchronous detection it is possible to measure the changes that the amplitude and phase of the incident wave suffer upon reflection since these changes are specified by the surface impedance, Z, of the metal. Z is defined as the ratio of the tangential electric and magnetic fields just inside the surface of the metal. The real part of Z, the surface resistance, measures the fraction of incident power that is lost to the sample either through Joule heating or through collisionless mechanisms of direct interaction between the charge carriers and the different Fourier components of the field[9]. The imaginary part of Z, the surface reactance, is related to the phase shift of the reflected wave, or equivalently, to the frequency change of the exciting resonant circuit, i.e. the inductance change of the exciting coil. In this geometry both surfaces of the slab are excited by the radio frequency radiation but in an antisymmetric fashion. This is said to be a bilateral antisymmetric mode of excitation. A fundamental drawback of this method is the

difficulty in calibrating the magnitude of the signal observed. Although calibration is possible (see for example Cochran and Shiffman[6]), most work reported using marginal oscillators gives no information about the absolute strength of the observed surface impedance anomalies.

Another method, although not used as extensively, is a unilateral excitation geometry as developed by Grimes[10]. Rather than monitor the impedance on the driving side of the slab, radiation is detected on the far side due to currents carried across the sample by geometrically resonant orbits. The experimental arrangement, illustrated in Fig. 1-1, page (8), consists of a transmitting coil on one side and a receiving coil on the other side, with shielding cans around the coils to minimize stray coupling. To achieve good shielding it is necessary to have the shielding cans in intimate contact with the metal slab, a condition which is difficult to achieve without damaging the specimen to some extent.

This study on gallium single crystals was undertaken to test a transmission system which enables one to obtain good isolation between transmitter and receiver coils, and which also permits specimens to be mounted in a strain-free fashion. A hollow box is used as a sample instead of the conventional single slab. Using this system a survey of transmission size effects in gallium single crystals was made.

After the completion of this study, it was learned that Druyvesteyn and Smets[11] employed a similar technique to observe size effects in tin crystals.

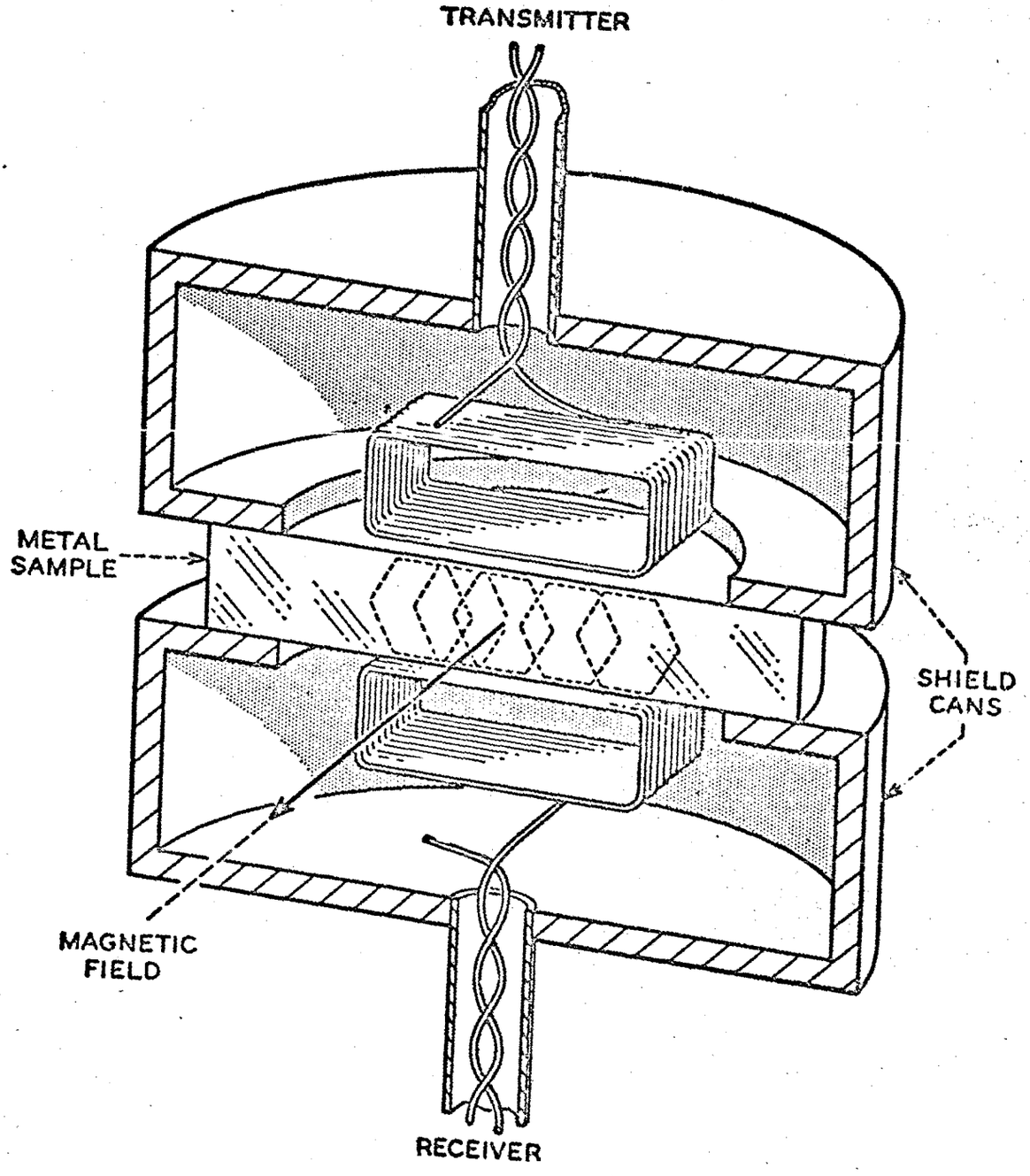

Fig 1-1 Experimental Arrangement Developed by Grimes for Observation of Transmission Through a Metal Slab

Chapter 2

RADIO FREQUENCY SIZE EFFECTS

2.1 The Gantmakher Effect

If a thin flat single metallic crystal is immersed in a uniform magnetic field H, and is placed within a coil carrying a radio frequency current of angular frequency ω, high enough so that $\delta << d$, where d is the sample thickness, and yet low enough so that $\omega << \omega_c = \frac{eH}{m^*c}$, where ω_c is the cyclotron frequency then the electrons may complete many cyclotron orbits before the applied electric field changes appreciably in time. When the magnetic field, H, is applied parallel to the surface (see Fig. 2-1, page 13), the electrons will move along helices having axes parallel to the surface. The major part of the electron orbit will be contained deep inside the metal where there is no high frequency field (since $\delta << d$). The penetration of the electromagnetic field inside the metal is due to electrons that "carry away" the high frequency field from the skin layer and then reproduce it within the volume of the metal. The electron interacts most intensely with the electromagnetic field on those sections of the trajectory where it moves along the electric field, that is, parallel to the surface of the metal at those regions such that $v_z = 0$*. The retardation of the field can be neglected, since the velocity of the electron, v ($\approx 10^8$ cm/sec), is usually much

---

*We use the notation that z is parallel to the normal to the surface of the metal.

larger than the characteristic phase velocity, $\omega\delta$ ($\approx 10^3$ for 1 mhz radiation and $\delta \approx 10^{-4}$ cm), of the wave. The points $v_z = 0$ on the electron trajectory and the corresponding points on the orbits in k-space are called effective points. Since, in a magnetic field the velocity vector, $\vec{v}$, changes on the trajectory, there are a large number of effective points in real space. When the electron moves along the effective section of the trajectory in the skin layer, it acquires a velocity increment $\Delta\vec{v}$. Consequently, it is the carrier of part of the skin current $\Delta\vec{j} = - e\Delta\vec{v}$, where e is the value of the electronic charge. It is clear that the vector $\Delta\vec{v}$ varies along the trajectory. At the next effective point, which is located deep inside the metal, the electron again moves parallel to the surface of the metal and produces increments to the velocity $\Delta\vec{v}$ and to the current $\Delta\vec{j}$. Hence, current and field peaks are produced inside the metal, and the distances between them are determined by the dimensions of the electron orbit.

If the magnetic field strength is such that the electrons have spatial orbits which just span the slab, current is carried from one side of the specimen to the other and a discontinuity or anomaly in the transmission occurs. It was this type of size effect anomaly in the surface impedance of thin plates of pure tin that was first observed by Gantmakher[8][12][13] in 1962. It should be noted that this is an effect of second order superimposed on a larger variation of the surface impedance with applied magnetic field.

In the presence of an applied magnetic field, $\vec{H}$, the carriers move in reciprocal space on the Fermi surface in planes perpendicular to the direction of the field. The projections of the real space orbits have the same shape but rotated by 90° about $\vec{H}$. The relationship between the dimension Δk of an orbit in reciprocal space and a dimension Δr on a corresponding real space orbit is[14]

$$\Delta k = \frac{eH}{\hbar c} \Delta r \qquad (1)$$

obtained by integrating the equation of motion for a charge e in a magnetic field $\vec{H}$ (the Lorentz force equation) over time. Experimentally one measures the magnetic field at which a discontinuity occurs in the transmission. The extremal diameter, Δk_{ext}, of the Fermi surface can then be obtained from,

$$\Delta k_{ext} = \frac{ed H_0}{\hbar c} = 0.15194 \times 10^8 H_0 d \quad cm^{-1}$$

where H_0 is measured in gauss, and d is measured in cm. From equation (1) it is clear that Gantmakher resonances can be used to measure dimensions of Fermi surfaces in a direction perpendicular to both the magnetic field and the normal to the metal surface. Because the skin depth is finite, there is a range of electrons having different values of $\vec{k}$ which contribute to a resonance. Hence, the resonance has a fractional width in magnetic field given approximately by[5],

$$\Delta H/H \approx \delta/d = 10^{-2}$$

for $\delta = 10^{-4}$ cm and $d = 10^{-2}$ cm.

It is this sharp variation in transmission or surface impedance which is called the Gantmakher effect or radio frequency size effect.

Gantmakher[12] also established that anomalies occurred not only when single extremal orbit diameters spanned the sample thickness, but also whenever multiples of such dimensions occurred. That is, if fundamental signals occur at magnetic field strengths H_1 and H_2 then other signals may also occur at magnetic field strengths $(nH_1 + mH_2)$ where n and m are integers.

It should be noted that the Gantmakher effect is a geometrical or spatial resonance dependent upon the thickness of the sample. This effect should not be confused with cyclotron resonances which are a temporal resonance occurring when the period of the electron orbit is a multiple of the period of the external driving field, that is which occur whenever $\omega = n\omega_c$, where n is an integer.

2.2 The Gantmakher-Kaner Effect

An important feature of the Gantmakher effect is the ability to generalize it to include arbitrary orientations of the magnetic field relative to the sample surface[5][15][16]. The electrons interacting with the electric field in the skin

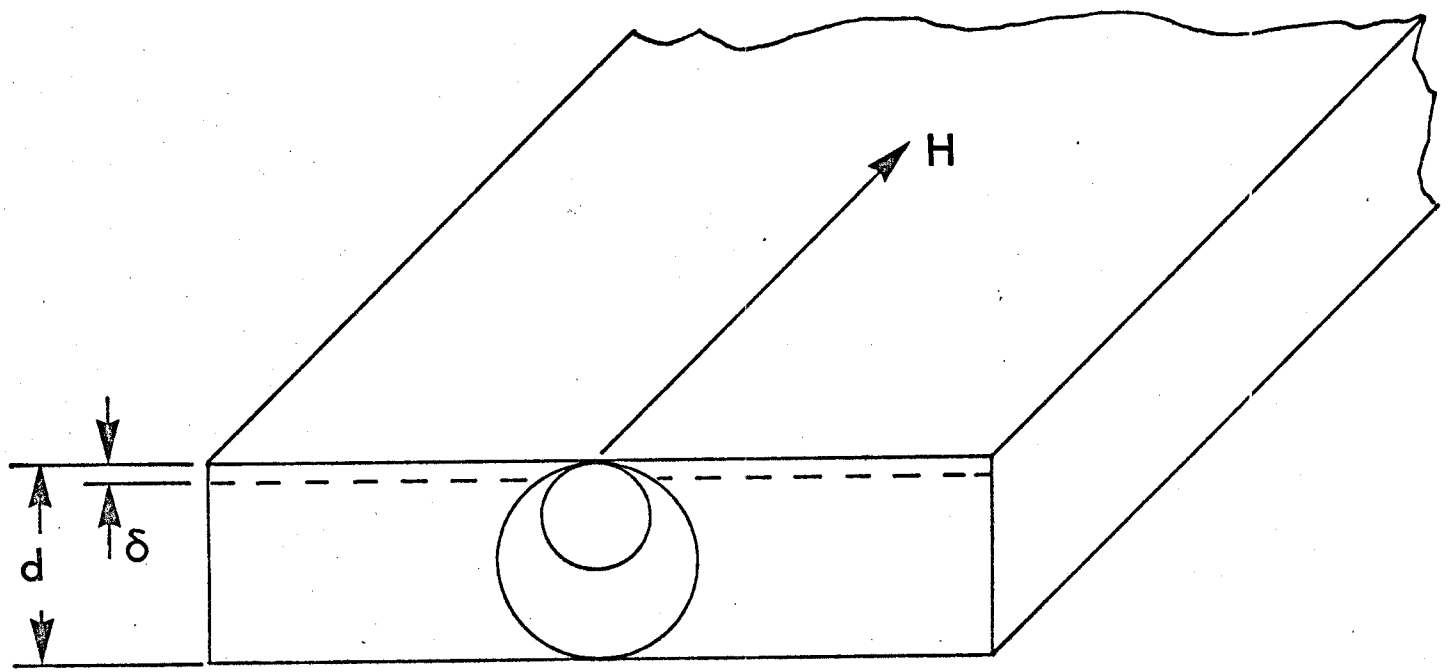

Conditions: $\ell > d$

$d \gg \delta$

$\omega \ll \omega_c = \frac{eH}{m^* c}$

Fig 2-1 Geometry for Observing the Gantmakher Effect

layer can carry the field to a large depth (of the order of ℓ) either along a chain of closed trajectories[5][17] or by drifting along the direction of the applied magnetic field, if the Fermi surface has elliptical limiting points or sections with an extremal value of $\partial A/\partial k_H$[15][16]. Here A is the area of intersection of the Fermi surface with the plane k_H = constant, and k_H is the projection of the electron wave vector on the magnetic field direction. The electric field variation along the z direction inside the metal can either be of the form of sharp spikes[5][15][17][18] or have a quasi-harmonic distribution[16][18][19]. The form of the distribution of the field inside the metal is determined by the character of the interaction of the electrons with the field. If the electron trajectory has places where the velocity is parallel to the surface of the metal, i.e. $v_z = 0$, then the interaction is effective and a system of sharp spikes of electric field and current are produced inside the metal. The distance between these spikes is determined by the characteristic dimensions of the electron trajectories in a magnetic field. However, if the trajectory has no points with $v_z = 0$, then the interaction is called ineffective and the electric field inside the metal has a quasi-harmonic form.

This latter case occurs when a static magnetic field is applied normal to the surface of the metallic slab. Gantmakher and Kaner[16] have shown for the case a non-ellipsoidal Fermi surface that the wave vector depends only on the spatial

periodicity, u, of the electron orbit, i.e. the displacement of the orbit center along the magnetic field during one cyclotron period. In other words, the interaction between the electron and the electromagnetic field is large only for that harmonic of the alternating field in the metal whose wavelength λ is equal to the displacement of the electron, u, in one cyclotron period. This dependence can be written,

$$k = \frac{2\pi}{u} = \frac{2\pi e H}{\hbar c}\left(\frac{\partial A}{\partial k_H}\right)^{-1}_{ext.} \qquad (2)$$

where the spatial period of the current or field distribution is determined by the extremal values $u = u_{ext}$. In addition to this effect due to electrons on helical trajectories, oscillations may also arise from electrons at elliptic limiting points*. In this case,

$$u_{ext} = v_F T_o \qquad \text{where } T_o = \frac{2\pi}{\omega_c}$$

$$\therefore u_{ext} = \frac{2\pi c \hbar}{e H \sqrt{K}} \qquad (3)$$

where K is the value of the Gaussian curvature of the Fermi surface at the limiting point, i.e. $K = \frac{1}{R_1 R_2}$ where R_1 and R_2 are the principal radii of curvature in k-space at the limiting point in question. In general, the elliptic limiting

---

* The limiting points of the Fermi surface are defined as the points of contact with tangent planes perpendicular to the magnetic field direction.

point effect is weaker in strength than that due to an extremal helical trajectory.

The oscillations periodic in magnetic field observed in transmission or in the surface impedance for the normal field geometry are generally referred to as the Gantmakher-Kaner effect.

In order to understand qualitatively how spatially periodic oscillations in the electric field distribution can arise, consider for simplicity, a transverse circularly polarized wave normally incident on the surface of a semi-infinite slab. The radio frequency electric field $\vec{E}_{\pm}(z)$ propagating in the positive z direction (along the normal direction) with time dependence $e^{-i\omega t}$, and the electric current in the metal $\vec{j}_{\pm}(z)$ both of which vary only in the z-direction, are related by Maxwell's equations,

$$\frac{d^2\vec{E}_{\pm}(z)}{dz^2} + \frac{\omega^2}{c^2}\vec{E}_{\pm}(z) = -\frac{4\pi i\omega}{c^2}\vec{j}_{\pm}(z)$$

where

$$E_{\pm}(z) = E_x(z) \pm i E_y(z)$$

For the case of an axially symmetric Fermi surface and specular reflection of the electrons from the surface of the metal, the distribution of the circularly polarized components of the electromagnetic field in the metal can be written[16],

$$E_{\pm}(z) = \frac{1}{\pi} E'_{\pm}(0) \int_0^{\infty} \frac{(e^{ikz} + e^{-ikz})\, dk}{k^2 - \frac{4\pi i \omega}{c^2} \sigma_{\pm}(k)} \qquad (4)$$

where $\vec{E}(z,t) = \vec{E}(z)\, e^{-i\omega t}$

$$E'_{\pm}(0) = \left. \frac{\partial E_{\pm}}{\partial z} \right|_{z=0}$$

and ω and k are the frequency and wave number of the electromagnetic wave, and

$$\sigma_{\pm}(k) = \sigma_{xx}(k) \mp i \sigma_{xy}(k)$$

where

$$j(k) = \sigma(k)\, E(k)$$

Here $\sigma_{\pm}(k)$, j(k), and E(k) are the Fourier transform coefficients.

Upon examination of equation (4) it can be seen that there are two types of contributions to the electric field. One is the contribution from the poles of the integrand in equation (4). These occur at,

$$k^2 = \frac{4\pi i \omega}{c^2} \sigma_{\pm}(k)$$

These poles correspond to modes of the electromagnetic field (sometimes called collective modes) which propagate if k is essentially real or which are damped if k has an appreciable imaginary part. The long wavelength propagating mode is called a helicon[20][21]. At shorter wavelengths there is also doppler shifted cyclotron resonance absorption[21][22].

The other contribution to the electric field is due to the presence of isolated branch points*[64] of the integrand. These isolated branch points in the Fourier transform of the conductivity, $\sigma_{\pm}(k)$, are due to contributions of electrons from those sections of Fermi surface where $u(k_H) = u_{ext}$. The branch points in $\sigma_{\pm}(k)$ can be regarded as giving rise to a long range oscillatory components of the electric field, when the integral is evaluated using a contour integration in the complex k-plane. These branch points are responsible for the Gantmakher-Kaner oscillations (sometimes called single particle modes). According to Gantmakher and Kaner[23] for the case of a single axially symmetric piece of Fermi surface and a magnetic field directed normal to the surface of the metal, i.e. only ineffective electrons are involved, the Fourier

---

* If a function, f(z), of a complex variable is multi-valued then a branch F(z) is any single-valued function in some domain at which every point in that domain takes on one and only one value of f(z). A branch cut, then, is a line or curve of points at which the branch function F(z) is not analytic, i.e. its derivative does not exist at that point. A branch point is a point such that if a complete circuit is made about it is necessary to cross a branch cut and therefore the function does not return to its original value.

transform of the conductivity, $\sigma_{\pm}(k)$, has a single branch point located near the real axis on the complex k-plane.

The following development illustrates more clearly the reason why oscillations in the surface impedance or transmission of a finite slab are observed given a periodic field distribution in a semi-infinite slab. The circularly polarized notation of $E_{\pm}$ that was used in equation (4) is again employed. For a periodic field distribution we can write,

$$E_x = E_o \exp\left[i(kz-\omega t)\right]$$

$$E_Y = -i E_o \exp\left[i(kz-\omega t)\right]$$

and $$E_{\pm} = E_x \pm i E_Y$$

It is clear that E_x and E_y are components of a vector of constant length E_0 rotating at an angular velocity ω in the x-y plane. This is illustrated in the following sketch. We shall call this wave E_+.

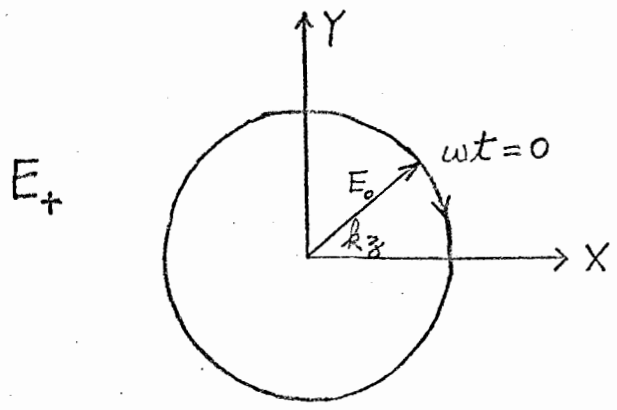

The electric vector rotates clockwise, and the angle made by E_+ with the x-axis at any time t is,

$$\theta_+ = kz - \omega t$$

An analogous sketch shows that for E_- the electric vector rotates anti-clockwise and the angle made by the electric vector with the x-axis at any time t is,

$$\theta_- = \omega t - kz$$

Now energy is extracted from the electric fields by electrons which at time t = 0 are at z and which are specified by an angle ϕ on the Fermi surface, as shown below.

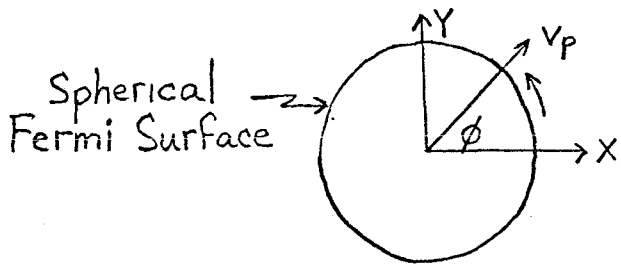

where v_p is the electron velocity in the x-y plane

Initially the electric field is directed along the x-axis. At a time t both the angle the electric field vector makes with the x-axis and the angle the electron makes with the x-axis will be changed. At time t the electron is at $(z'-z) = v_z t$. For the E_+ polarization of the electric field the angle with respect to the x-axis is now,

$$\theta_+ = k(z-z') - \omega t = kv_z t - \omega t$$

During this time t, the angle the electron velocity makes with the x-axis is altered by $\omega_c t$. For a charge carrier with a negative charge the angle on the Fermi surface of the electron is

$$\alpha_+ = \phi - \omega_c t$$

The amount of energy picked up by the electron from the electric field can be written[14],

$$\Delta E = -e v_p E_o \int_{-\infty}^{o} \exp(t/\tau) \cos\beta \, dt$$

where β is the angle between the electric vector and the electron vector. But this angle is,

$$\beta_+ = (kv_z t - \omega t) + (\phi - \omega_c t)$$
$$= \phi - (\omega + \omega_c - kv_z)t$$
$$= \phi - \Omega_+ t$$

where $\Omega_+ = \omega + \omega_c - kv_z$

Analogously, for the E_- polarization,

$$\beta_- = \phi - \Omega_- t$$

where $\Omega_- = \omega - \omega_c - kv_z$

$\because \alpha_- = \phi + \omega_c t$ and $\beta_- = \alpha_- - \theta_-$

Therefore, for the energy picked up by the electron from the electric fields we obtain, changing t to -t in the integral,

$$\Delta E_{\pm} = -e v_p E_o \int_o^\infty \exp(-t/\tau)\cos(\phi - \Omega_{\pm} t)\,dt$$

$$= -e v_p E_o \int_o^\infty \exp(-t/\tau)\{\cos\phi\cos\Omega_{\pm}t + \sin\phi \cdot \sin\Omega_{\pm}t\}\,dt$$

$$= \frac{-e v_p E_o \tau (\cos\phi + \Omega_{\pm}\tau\sin\phi)}{(1+\Omega_{\pm}^2\tau^2)}$$

We may now evaluate the contribution to the current using the relation[14],

$$\vec{j}(\vec{r},t) = \frac{-2e}{(2\pi)^3\hbar}\int_{F.S.} \Delta E\,\frac{\vec{v}}{|\vec{v}|}\,dS$$

where dS is an element of surface area on the Fermi surface in k-space. For a slice of Fermi surface in the k_z direction, as shown below,

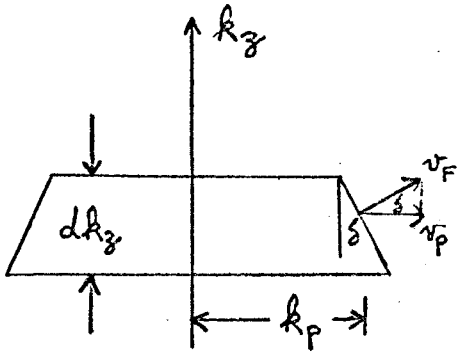

$$dS = d\phi\, k_p \frac{dk_z}{\cos\delta} = d\phi\,\frac{k_p\,dk_z}{v_p}\,v_F$$

and $$\vec{j}(\vec{r},t) = \frac{-2e}{(2\pi)^3\hbar}\int_{k_z}\frac{k_p}{v_p}\,dk_z\int_o^{2\pi} v_F\,\Delta E\,d\phi\,\frac{\vec{v}}{|\vec{v}|}$$

$$\therefore j_x = \frac{-2e}{(2\pi)^3 \hbar} \int_{k_z} dk_z \frac{k_p}{v_p} \int_0^{2\pi} v_p \cos\phi \, \Delta E_\pm \, d\phi$$

$$\because \int_0^{2\pi} \cos\phi \, \Delta E \, d\phi = -\pi e v_p E_0 \tau \,/ (1 + \Omega_\pm^2 \tau^2)$$

$$\therefore dj_{\pm x} = \frac{2\pi e^2 k_p v_p \tau E_0 \, dk_z}{(2\pi)^3 \hbar \, (1 + \Omega_\pm^2 \tau^2)}$$

Similarly,

$$j_{\pm y} = -\frac{2e}{(2\pi)^3 \hbar} \int_{k_z} k_p \, dk_z \int_0^{2\pi} \sin\phi \, \Delta E_\pm \, d\phi$$

and $$dj_{\pm y} = \frac{2\pi e^2 k_p v_p \tau E_0 \Omega_\pm \tau \, dk_z}{(2\pi)^3 \hbar \, (1 + \Omega_\pm^2 \tau^2)}$$

Consquently, $$\frac{dj_n}{E_0} = \frac{2\pi e^2 v_p \tau k_p \, dk_z}{(2\pi)^3 \hbar \sqrt{1 + \Omega_\pm^2 \tau^2}}$$

and $$\gamma_\pm = \tan^{-1}(\Omega_\pm \tau)$$

where $\gamma_\pm$ is the angle between $\vec{E}_0$ and $\vec{j}_{\pm x}$.

In the Gantmakher-Kaner effect a particular slice on the Fermi surface is picked out because for this slice $\Omega_\pm \tau \to 0$ and the current becomes rather large. This determines a particular value for k. For $E_\pm$ and $\Omega_\pm = 0$

$$k v_z = \omega \pm \omega_c$$

$$\text{i.e.} \quad |k| = \left| \frac{\omega \pm \omega_c}{v_z} \right|$$

For this value of k then, σ is increased by $\Delta\sigma$ which is real, and this particular component of the electric field is enhanced over the other components.

Now the amplitude of the field, E(k), varies as,

$$E(k) \propto \cos kz \; e^{-i\omega t}$$

This is because the waves for +k and -k interfere to give a standing wave. Therefore, one expects the long range part of the electric field which is due to the Gantmakher-Kaner effect to vary as

$$\cos kz = \cos\left(\frac{\omega \pm \omega_c}{v_z}\right) z$$

For the case of a finite slab of thickness d, effectively one measures the electric field at d so one expects

$$\Delta T \approx \cos kd = \cos\left(\frac{\omega \pm \omega_c}{v_z}\right) d$$

When both polarizations are excited simultaneously one gets an amplitude which goes like

$$\Delta T \propto \cos\left(\frac{\omega+\omega_c}{v_z}\right) d + \cos\left(\frac{\omega-\omega_c}{v_z}\right) d$$

$$= 2\cos\left(\frac{\omega d}{v_z}\right) \cos\left(\frac{\omega_c}{v_z} d\right)$$

Therefore, the period of the transmission oscillations is given by,

$$\frac{\omega_c d}{v_z} = 2\pi n$$

$$\text{i.e. } d/n = v_z T_o = 2\pi v_z m^* c/eH_o$$

These oscillations will be periodic in magnetic field.* For extremal helical trajectories, from equation (2),

$$\Delta H = \frac{\hbar c}{ed}\left(\frac{\partial A}{\partial k_H}\right)_{ext}$$

while for elliptic limiting points, from equation (3),

$$\Delta H = \frac{2\pi\hbar c}{ed\sqrt{K}}$$

The amplitude of this oscillatory component of E(z) vanishes both in the limit $H \to 0$ and $H \to \infty$. This result can be seen by examining the behaviour of the Fourier components of the conductivity $\sigma_{\pm}(k)$ and the electric field E(k). For a piece of Fermi surface which is singly-connected and is axially-symmetric with respect to the Oz axis, then for a single slice of Fermi surface of thickness dk_z, the conductivity can be written,

$$\sigma_{\pm}(k) \propto \left[1 + i\{kl - (\omega \pm \omega_c)\tau\}\right]^{-1}$$

---

* The effect vanishes when $\omega d/v_z = \pi/2$ or $\omega = \pi v_z/2d$. For $v_z = 10^8$ cm/sec and $d = 10^{-2}$ cm, $f = v_z/4d = 2.5 \times 10^9$ hz.

The actual conductivity is more complicated because one must sum over all such slices so that,

$$\sigma(k) \propto F\left[1 + i\{k\ell - (\omega \pm \omega_c)\tau\}\right]^{-1}$$

When the condition $k\ell = \omega_c\tau$ is fulfilled, and if $\omega_c\tau \gg 1$ the conductivity becomes very large. However, for $\omega_c\tau \ll 1$ the condition $k\ell = \omega_c\tau$ obviously has a negligible effect on the electric field, since near resonance ($k\ell \pm \omega_c\tau$) is in any case negligibly small with respect to 1. Physically, $u_{ext} = \frac{2\pi v_f}{\omega_c}$, so that if $\omega_c\tau$ is small then $\frac{u_{ext}}{\ell} \gg 1$ and the electrons which carry the energy are attenuated very strongly compared to u_{ext}. One should keep in mind that the electrons of helical pitch u are coupled strongly only to E(k) for $k = \frac{2\pi}{u}$.

Now as the magnetic field strength is increased one obtains the condition,

$$\frac{u_{ext}}{\ell} = \frac{2\pi}{\omega_c\tau} \longrightarrow 0$$

Therefore, at large magnetic field when the wave vector, k, becomes large, u_{ext} becomes small.

We now examine the behaviour of the Fourier components of the electric field, From Maxwell's equation,

$$\frac{d^2E}{dz^2} + \frac{\omega^2 E}{c^2} = -\frac{4\pi i \omega \tau_0 E}{c^2}$$

one can obtain E(k). At radio frequencies, one finds that for u_{ext} small, i.e. $u_{ext} << \delta$ or $k >> 1/\delta$, the amplitude of E(k) is sufficiently small that the electrons do not pick up much energy from the electric field. Consquently, one expects the oscillation amplitude to vanish at sufficiently high magnetic fields. As a result one expects the amplitude of that part of the surface impedance of a finite slab or the transmission through a finite slab, which is oscillatory in the applied magnetic field to vanish both for small and for large values of the magnetic field.*

---

* The decrease in amplitude in the high field limit is expected to be slower than in the limit $H \to 0$.

It is important to note at this point that according to the Gantmakher-Kaner theory[16], the period of oscillation for an axially symmetric piece of Fermi surface should not be dependent upon the polarization of the electric field. However, the amplitude of the oscillations and cut-off fields may change since $\sigma(k)$ and hence the skin depth is in general orientation dependent.

According to Falk, Gerson, and Carolan[24], the amplitude of the Gantmakher-Kaner oscillations depends upon the following factors.

1) Is there a point p_0 where $|v_z|$ or more precisely $|\frac{\partial A}{\partial k_H}|$ has a local maximum?
2) Is the maximum $|\frac{\partial A}{\partial k_H}|$ an extremum? That is, does $\frac{\partial^2 A}{\partial k_H^2} = 0$ as opposed to the case in which $\frac{\partial A}{\partial k_H}$ becomes maximal because it is increasing and p_z terminates at p_0 (as for an elliptic limiting point)?
3) Does $A(p_0) = 0$?
4) Does $|p_z|$ terminate at p_0?

From a study based upon various models they concluded that the strongest branch point singularity in the conductivity $\sigma(k,\omega)$ was the square root. This occurred when there was a concentration of electron orbits with almost the same $\frac{\partial A}{\partial k_H}$, i.e. $\frac{\partial^2 A}{\partial k_H^2} = 0$, at a point of finite cross-section $\{A(p_0) = 0\}$, that is, when there were enough electrons with orbits in the vicinity of p_0 to give a large contribution to the conductivity. Therefore one expects Gantmakher-Kaner oscillations to be strongest when

there is a large group of electrons at a point of finite cross-sections such that $\frac{\partial A}{\partial k_H}$ is an extremum.

2.3 Line Shapes

Attempts to explain in detail the line shapes of the many singularities of the radio frequency size effect have been made by Kaner and Fal'ko[25] for the case of unilateral excitation upon a metal with a spherical Fermi surface. Experiments have been performed by Koch and Wagner[26] on potassium and the experimental lines compared with the line shapes calculated from the Kaner-Fal'ko theory. By numerically evaluating the relevant expressions which determine the derivative with respect to magnetic field of both the surface resistance, $\frac{\partial R}{\partial H}$, and surface reactance, $\frac{\partial X}{\partial H}$, instead of using the Kaner-Fal'ko approximations, they report that the theory and experiment are "sufficiently in agreement to allow a meaningful comparison".

More recently Juras[27] has attempted to solve self-consistently the complete boundary value problem of the radio frequency size effect for a number of simple Fermi surfaces and for different modes of excitation of the sample by the external radio frequency field. A comparison was then made between the theoretical field derivatives of the surface impedance and those experimentally observed in potassium by Koch and Wagner[28]. This comparison was only qualitative

since the ratio $\frac{\ell}{d}$ was approximately $\frac{1}{3}$ experimentally but equal to 1 theoretically. This seemingly small difference in the ratio of the mean free path to the specimen thickness reduces the line amplitudes of the surface impedance by a large factor. Nevertheless, the qualitative similarity in the line shapes between theory and experiment is good not only for the primary singularity but also for the second harmonic as well.

It should be emphasized that Juras' calculation assumes $\omega\tau \approx 0$ and therefore does not include the possibility of an electron orbit encountering a change in phase of the electric field while passing many times through the skin layer.

Experimentally, Gantmakher and Tsoi[29] have noticed line shapes (in potassium) which look approximately like those calculated by Juras when the condition $\ell \approx d$ is satisfied. However, when the sample thickness is increased such that $\ell < d$, a distinct change in line shape is observed.

Although the above theories qualitatively explain the dependence of line shape on the mean free path, they do not handle the condition $\ell < d$. The behaviour of the size effect line for this case has not been studied and consequently requires additional investigation.

Cochran[30] has suggested that the line shapes of transmission signals are related to the line shapes of surface impedance signals. For transmission into a box he proposes that,

$$\Delta T = -\Delta\delta/2a$$

where $\Delta\delta$ is the change in the skin depth, and a is the width of the transmission cavity, and ΔT is the change in transmission. Since $\Delta\delta$ is related to the surface impedance, a comparison between transmission line shapes and the line shapes predicted by Juras can be made.

Chapter 3

TRANSMISSION THROUGH A SLAB

3.1 Transmission Ratio Coefficient

A simple and elegant method for investigating Gantmakher size effects will now be presented. This is the transmission of electromagnetic radiation through a thin metallic plate.

Let the specimen of thickness d, form one side of a rectangular cavity as illustrated in Fig. 3-1. The other three sides are assumed to be infinitely thick or of such thickness that no radiation effectively passes through them. It can be shown[30] that for this geometry the transmission ratio coefficient, T_c, can be written

$$T_c = \frac{H_i}{H_o} \approx \frac{i\lambda}{2\pi a} G_x(d)$$

where H_i is the magnetic field inside the cavity, H_0 is the alternating magnetic field outside the cavity, "a" is the width of the transmission cavity, λ is the free space wavelength of the radiation, and $G_x(z)$ is the component of the electric field in the slab along the direction x, generated by a radio frequency magnetic field of unit strength applied at the surface $z = 0$. This expression explicitly indicates that the transmission ratio is a quantity proportional to the electric field distribution in the metal at $z = d$.

This relationship indicates in general terms what quantities are measured. The following development evaluates the

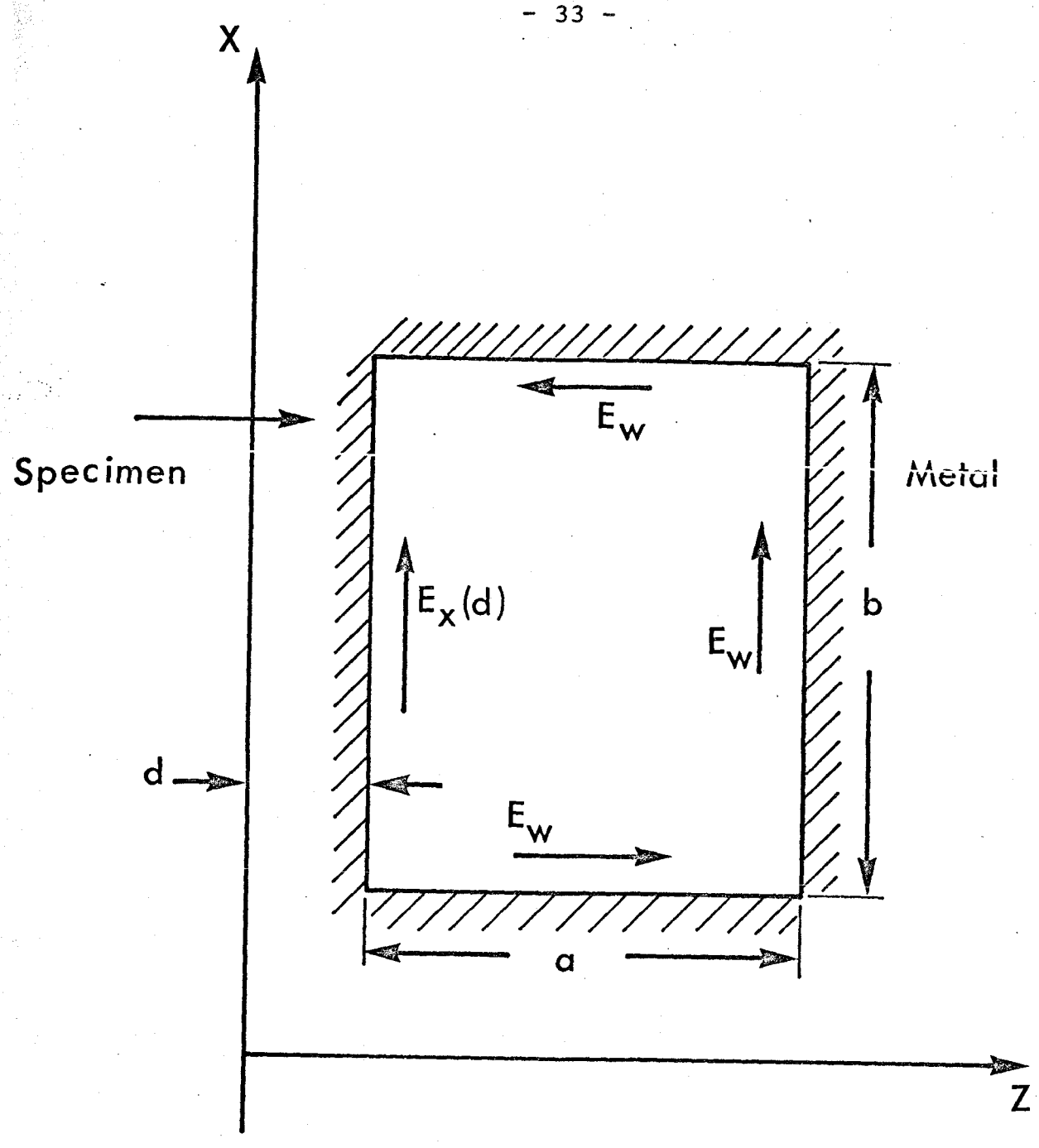

Fig 3-1 A Rectangular Cavity of Dimensions a x b cm Surrounded by Metal Walls. The Specimen, thickness d cm, Forms One of the Walls of the Cavity

transmission ratio, T_c, in terms of measurable experimental quantities for the classical case in which $\vec{j} = \sigma\vec{E}$, where σ is the d.c. conductivity of the metal.

Taking the time variation of the magnetic field to be $e^{-i\omega t}$, Maxwell's equations can be written,

$$\text{curl}\ \vec{E} = -\frac{\mu}{c}\frac{\partial H}{\partial t}$$

$$\text{curl}\ \vec{H} = \frac{4\pi\vec{j}}{c} + \frac{1}{c}\frac{\partial E}{\partial t}$$

where μ is the permeability and $\vec{j}$ is the current density. Let us apply these equations to the rectangular box of Fig. 3-1. Taking $\vec{H}$ to be a function of z only, being polarized along y, and $\vec{E}$ to be a function of z only, being polarized along x,

$$\text{curl}\ \vec{H} = -\frac{\partial H_y}{\partial z}\,\hat{i}$$

$$\text{curl}\ \vec{E} = \frac{\partial E_x}{\partial z}\,\hat{j}$$

$$\therefore \frac{\partial E_x}{\partial z} = -\frac{\mu}{c}\frac{\partial H_y}{\partial t} = \frac{i\omega\mu}{c}H_y = \frac{i\omega\mu}{c}H_o$$

$$-\frac{\partial H_y}{\partial z} = \frac{4\pi\sigma}{c}E_x - \frac{i\omega}{c}E_x$$

Since $\omega \ll 4\pi\sigma$

$$\therefore \frac{\partial H_y}{\partial z} = -\frac{4\pi\sigma}{c}E_x$$

But $$\frac{\partial^2 E_x}{\partial z^2} = \frac{i\omega\mu}{c}\frac{\partial H_y}{\partial z} = -\frac{i\omega\mu}{c}\frac{4\pi\tau}{c}E_x = -\frac{4\pi i\omega\mu\tau}{c^2}E_x$$

In the thin wall of the box (Fig. 3-1) the electric field will be of the form

$$E_x(z) = Ae^{ikz} + Be^{-ikz}$$

where $$k = \sqrt{\frac{2\pi\omega\mu\tau}{c^2}}(1+i) = k_0(1+i)$$

$$\therefore H_y(z) = \frac{c}{i\omega\mu}\frac{\partial E_x}{\partial z} = \frac{ck}{\omega\mu}\left(Ae^{ikz} - Be^{-ikz}\right)$$

The constants A and B are found from the boundary conditions. At the inside metal-vacuum interface the electric field must satisfy the general Maxwell equation,

$$\int_C \vec{E}\cdot d\vec{S} = -\frac{\mu}{c}\frac{d\Phi}{dt}$$

where Φ is the flux through the closed curve C, around the inside of the cavity. In the infinitely thick sides $\frac{E_i}{H_i} = \frac{\mu\omega}{ck}$, where E_i is the electric field on the inside of the cavity, and H_i is the magnetic field on the inside of the cavity*.

---

* H_i in the cavity is uniform since we assume $\frac{a}{\lambda} << 1$.

$$\therefore \frac{\mu\omega}{ck} H_i (b+2a) - b(Ae^{ikd} + Be^{-ikd}) = -\frac{\mu}{c}\frac{d}{dt}(ab\,H)$$

$$= -\frac{i\omega\mu}{c} ab\, H_i$$

$$\therefore Ae^{ikd} + Be^{-ikd} = \frac{\mu\omega}{ck} H_i \left(1 + \frac{2a}{b} - iak\right) = \frac{\mu\omega}{ck} H_i \Delta$$

where $\Delta = 1 + \frac{2a}{b} - iak$

But $Ae^{ikd} - Be^{-ikd} = \frac{\mu\omega}{ck} H_i$

$$\therefore \frac{Ae^{ikd} + Be^{-ikd}}{Ae^{ikd} - Be^{-ikd}} = \Delta$$

$$\therefore \frac{A}{B} = -e^{-2ikd}\frac{(1+\Delta)}{(1-\Delta)}$$

Now $H_o = \frac{ck}{\mu\omega}(A-B)$

and $H_i = \frac{ck}{\mu\omega}(Ae^{ikd} - Be^{-ikd})$

$$\therefore T_c = \frac{H_i}{H_o} = \frac{Ae^{ikd} - Be^{-ikd}}{A-B}$$

$$= \frac{1}{\cos kd - \Delta i \sin kd}$$

For large $k_0 d$, which is the case in our experiments,

$$T_c = \frac{2e^{ikd}}{1+\Delta}$$

Also, for ka >> 1, which is the case in our experiments, then

$1 + \Delta \approx -ika$

$$\therefore T_c \approx \frac{2ie^{ikd}}{ka} = \frac{i\lambda}{2\pi a} G_x(d)$$

This is the expression obtained by Cochran[30]. This formula, which is in error by less than 1% for $k_0 d \geq 3$ can be used to evaluate the transmission ratio coefficient in terms of measurable quantities. It must be emphasized that the above development is only valid for the local case $\ell << \delta$.

This expression for the transmission ratio will be compared with experiment in order to check the calibration of the apparatus.

3.2 Transmission Amplitude for the Gantmakher Geometry

In our experimental geometry a unilateral mode of excitation is employed. Consider now the following sketch.

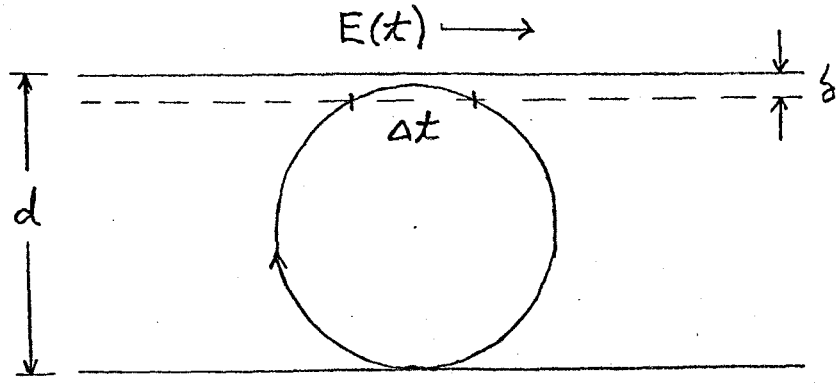

An electron making a pass through the skin layer at time t changes its velocity by $\frac{eE(t)\Delta t}{m^*}$, where Δt is the transit time (see above), m^* if the effective mass, and $E(t) = E(0)e^{-i\omega t}$ is the electric field at the surface. The probability of the electron making n such passes will be $\exp(\frac{-2\pi n}{\omega_c \tau})$, where τ is the mean collision time, and ω_c is the cyclotron frequency of the electron. For a circular orbit this probability can be written as $\exp(\frac{-n\pi d}{\ell})$. Now after the nth pass the electron will be in a field given by $E(t)\exp(\frac{-2\pi i\omega n}{\omega_c})$. This represents the phase change of the electric field during the time required for the passage of the particle.

For an electron initially in the skin layer, that part of the electric field which is generated by the carriers which contribute to a Gantmakher resonance at the back side of the slab, can be expressed as,

$$\Delta E(d) \propto E(t)\exp\left(\frac{-\pi d}{2\ell}\right) + E(t)\exp\left(\frac{-3\pi d}{2\ell}\right)\exp\left(\frac{-2\pi i\omega}{\omega_c}\right) + E(t)\exp\left(\frac{-5\pi d}{2\ell}\right)\exp\left(\frac{-4\pi i\omega}{\omega_c}\right) + \cdots$$

$$\therefore \frac{\Delta E(d)}{E(t)} \propto \frac{\exp\left(\frac{-\pi d}{2\ell}\right)}{1 - \exp\left(\frac{-\pi d}{\ell}\right)\exp\left(\frac{-2\pi i\omega}{\omega_c}\right)}$$

For $\frac{\omega}{\omega_c} = \alpha$, the above equation can be written,

$$S_o = \frac{\Delta E(d)}{E(t)} \propto \frac{\exp\left(-\frac{\pi d}{2\ell}\right)}{1 - \exp\left(-\frac{\pi d}{\ell}\right)\exp\left(-2\pi i\alpha\right)} \qquad (1)$$

Since the transmission experiment measures a quantity proportional to $\Delta E(d)$ the amplitude of the signal observed depends on ω, d, and ℓ. Figures 3-2 and 3-3 show the frequency dependence of the Gantmakher amplitude factor S_0 while Fig. 3-4 and Fig. 3-5 illustrate the real and imaginary parts of the Gantmakher resonances factor respectively, as functions of the mean free path. Fig. 3-6 and Fig. 3-7 illustrate the real and imaginary parts respectively of the Gantmakher factor multiplied by a phase factor $e^{i\pi/3}$. Fig. 3-8 illustrates the mean free path dependence of the absolute value of the Gantmakher amplitude factor while Fig. 3-9 illustrates the mean free path dependence of the phase of the Gantmakher amplitude factor.

The frequency dependence of the Gantmakher amplitude factor can be illustrated by the following development. From equation (1), and for $\omega_c\tau >> 1$ and $\frac{d}{\ell} << 1$

$$S_o \propto \frac{1}{1 - \left(1 - \frac{\pi d}{\ell} + \ldots\right)\left(\cos 2\pi\alpha - i \sin 2\pi\alpha\right)}$$

since $\exp\left(-\pi d/2\ell\right) \approx 1$

It is readily seen that the real part of this expression will be a maximum for $\alpha = 0, 1, 2, \ldots$ and a minimum for $\alpha = \frac{1}{2}, \frac{3}{2}, \ldots$ The behaviour of the real and imaginary parts of S_0 is shown

in Fig. 3-3.

In our experiments $\omega \approx 10^7$/sec. Taking $\tau \approx 10^{-9}$ sec we find $\omega\tau << 1$. Therefore, we are working in the regime indicated in Fig. 3-2. For this experimental geometry in which the magnetic field is accurately parallel to the sample surface, it is well known that Azbel'-Kaner cyclotron resonance will occur for $\omega = n\omega_c$. Fig. 3-3 not only indicates a maximum transmission corresponding to the cyclotron resonance condition but also for $\omega << \omega_c$. Consequently, the radio frequency size effect, which satisfies the condition $\omega << \omega_c$, is related to the 0th order Azbel'-Kaner cyclotron resonance.

Since many of our experiments are performed in the regime $\omega << \omega_c$ and $d/\ell << 1$, it is interesting to consider this case separately. We can write equation (1) as,

$$S_o \propto \frac{1}{1-\left(1-\frac{\pi d}{\ell}+\ldots\right)\left(1-2\pi i\frac{\omega}{\omega_c}+\ldots\right)}$$

$$\therefore\ S_o \propto \frac{1}{\frac{\pi d}{\ell}+\frac{2\pi i\omega}{\omega_c}}$$

For a circular orbit $v_f = R\omega_c$ and at a Gantmakher resonance $R = \frac{d}{z}$ so $d = \frac{2v_F}{\omega_c}$

$$\therefore\ S_o \propto \frac{1}{\frac{2\pi}{\omega_c\tau}+\frac{2\pi i\omega}{\omega_c}}$$

$$= \frac{\omega_c\tau\,(1-i\omega\tau)}{2\pi\,(1+\omega^2\tau^2)}$$

From this expression it is seen that at $\omega\tau = 1$ the amplitude $|S_0|$ drops to $\frac{1}{\sqrt{2}}$ the value which it has in the limit $\omega\tau << 1$. Therefore, by adjusting the frequency of the electromagnetic radiation until the amplitude of a characteristic anomaly falls to $\frac{1}{\sqrt{2}}$ of its previous value, one can determine the mean collision time, τ, for this group of electrons.

It is important to note at this point that both the real and imaginary parts of the electric field at the surface will be carried across the slab. In the process of traversing the slab each part (real and imaginary) will undergo a phase shift, ϕ, such that each component will have a real and imaginary part. Therefore, it is reasonable to expect that the shape of the signal transmitted, which represents the electric field at z=d in the metal, will be somewhat different from the electric field distribution at the surface of the slab.

For this reason, a calculation of line shapes is not as simple as simply multiplying Juras' calculation by our S_0 factor. One must also take into account this phase factor, ϕ. According to Haberland and Shiffman[31] this phase factor, ϕ, is approximately 60°. The effect of this phase factor on the Gantmakher amplitude factor is shown in Fig. 3-6 and Fig. 3-7.

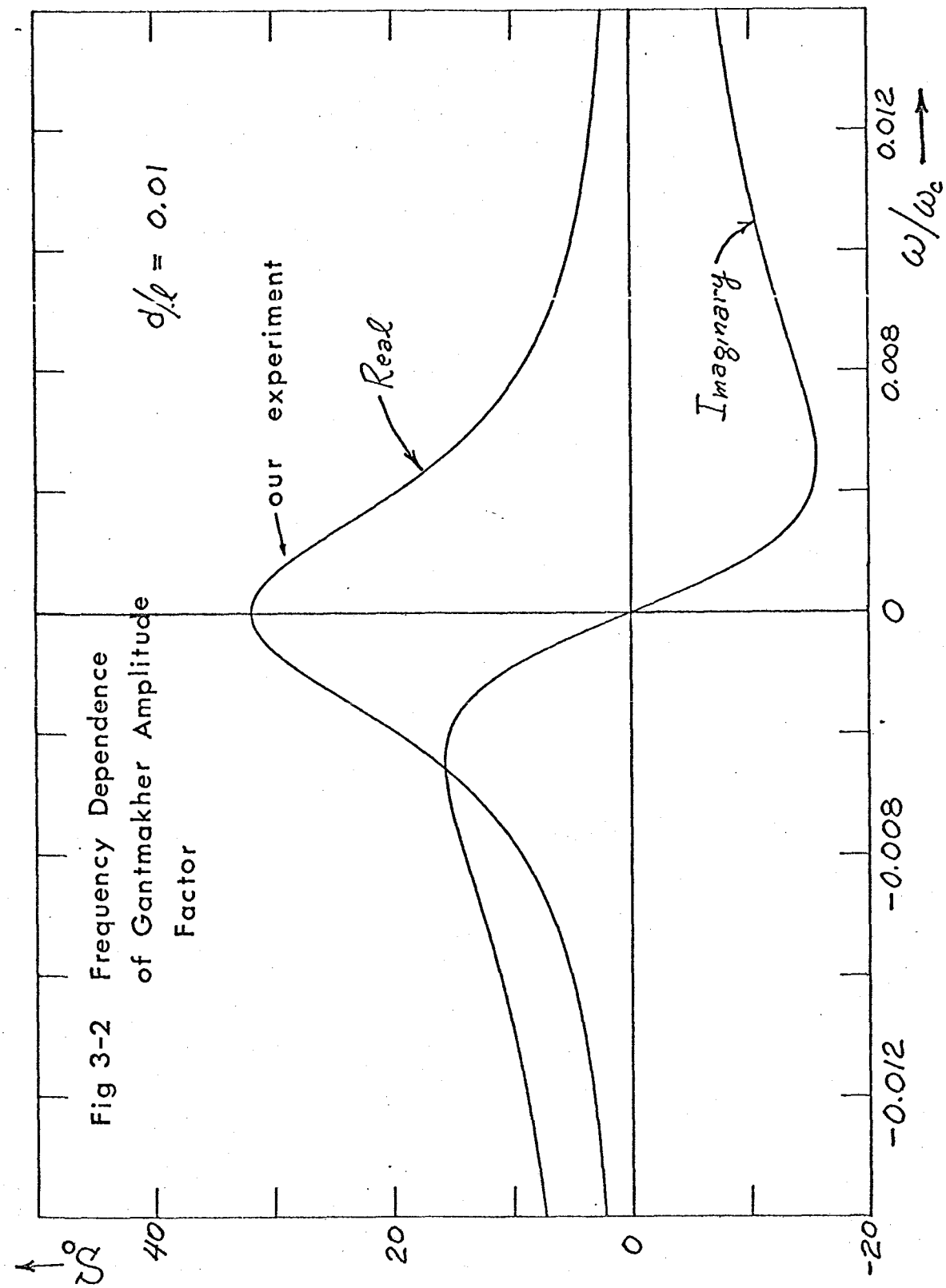

Fig 3-2 Frequency Dependence of Gantmakher Amplitude Factor

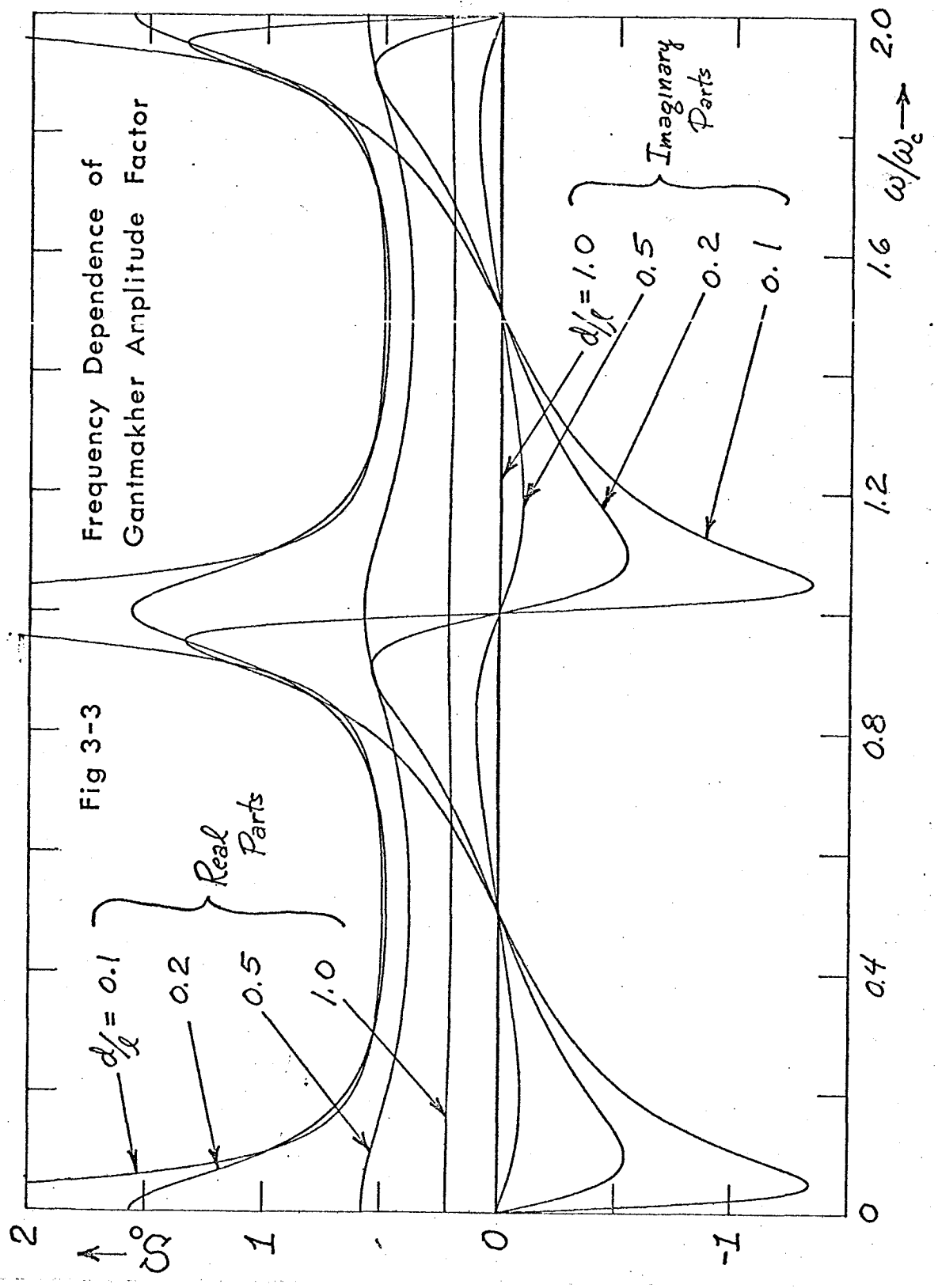
Frequency Dependence of
Gantmakher Amplitude Factor
Fig 3-3
Real Parts
Imaginary Parts
d/ℓ = 0.1
0.2
0.5
1.0
d/ℓ = 1.0
0.5
0.2
0.1
A
2
1
0
-1
0
0.4
0.8
1.2
1.6
2.0
ω/ω_c →

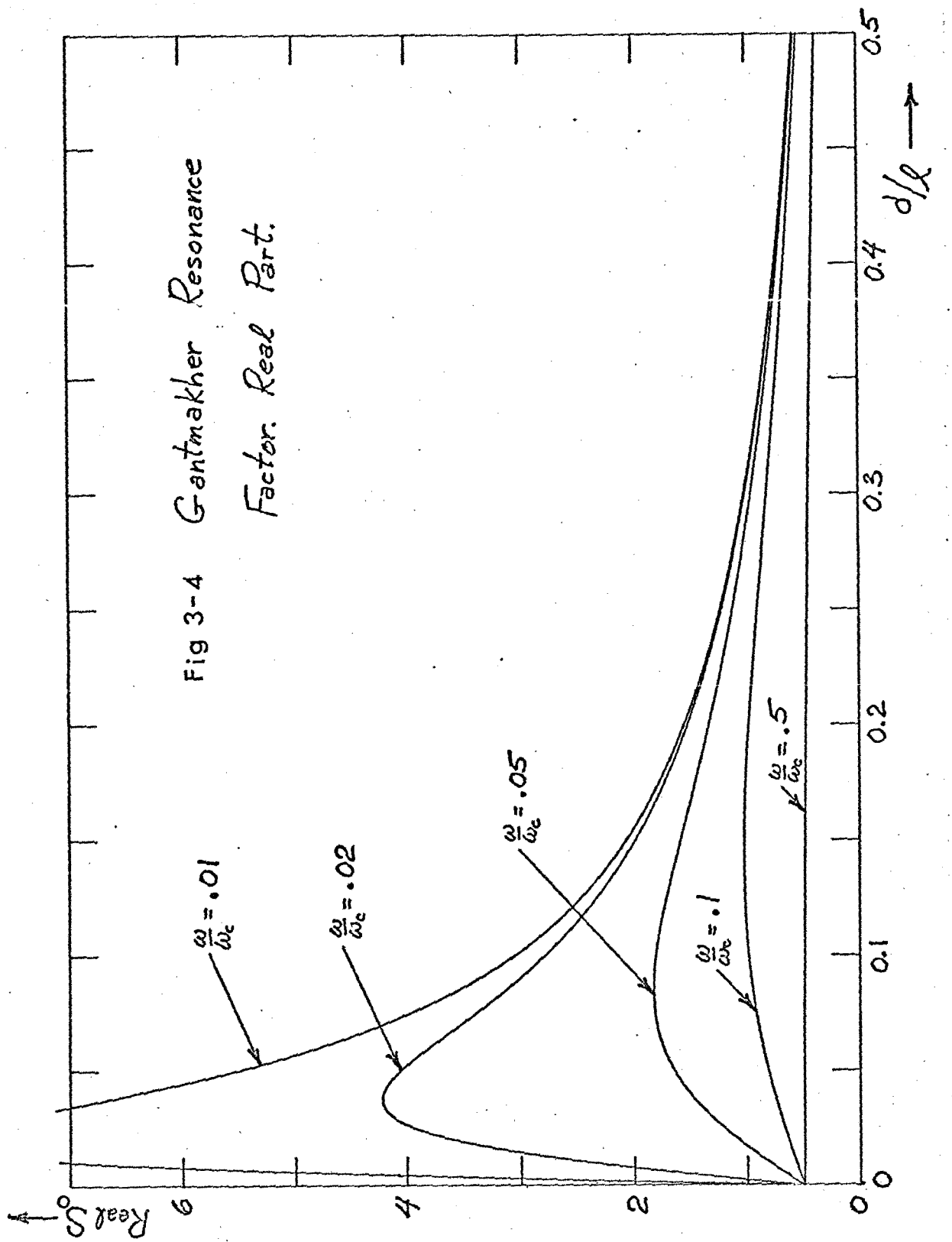

Fig 3-4 Gantmakher Resonance Factor. Real Part.

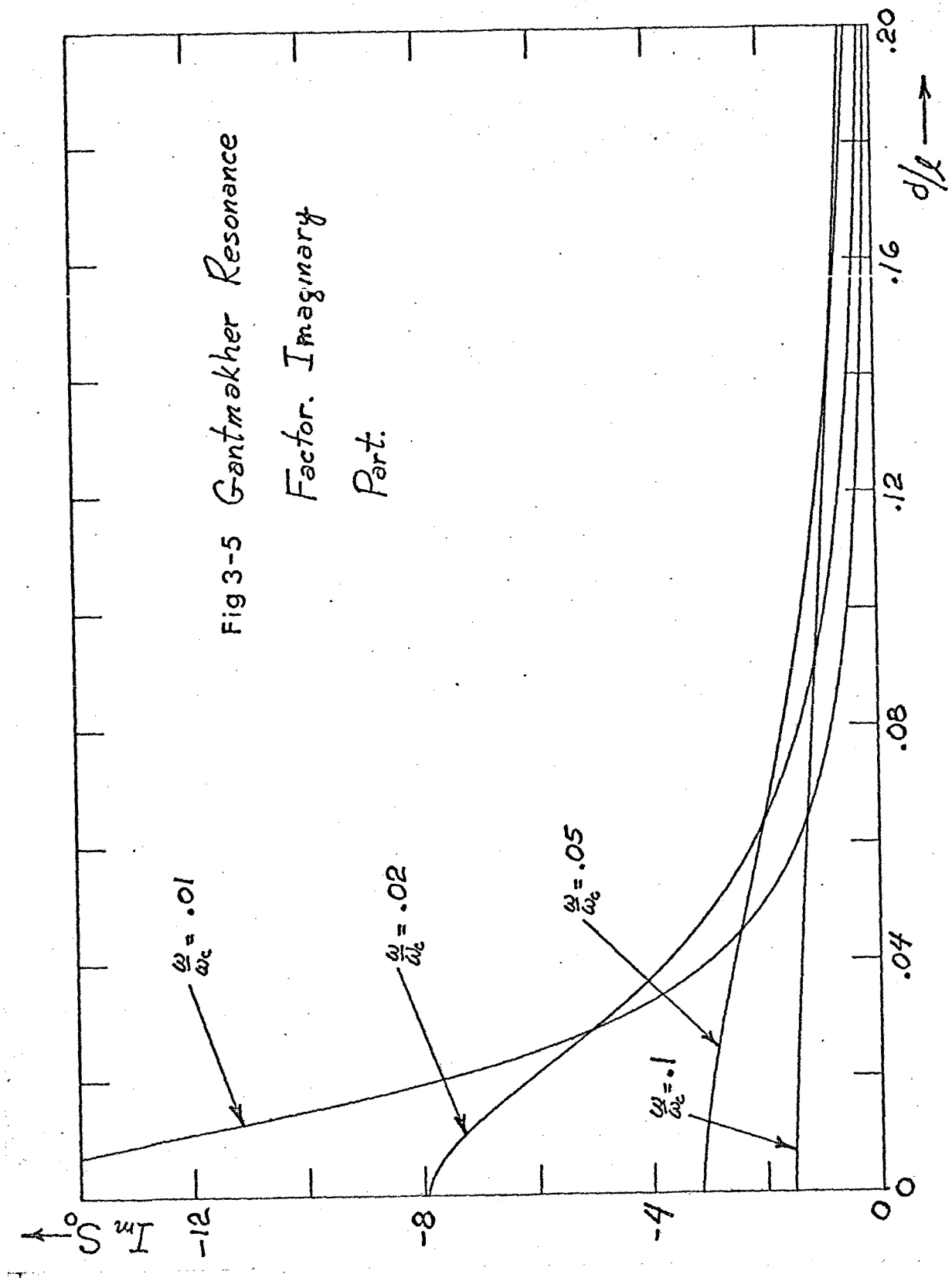

Fig 3-5 Gantmakher Resonance Factor. Imaginary Part.

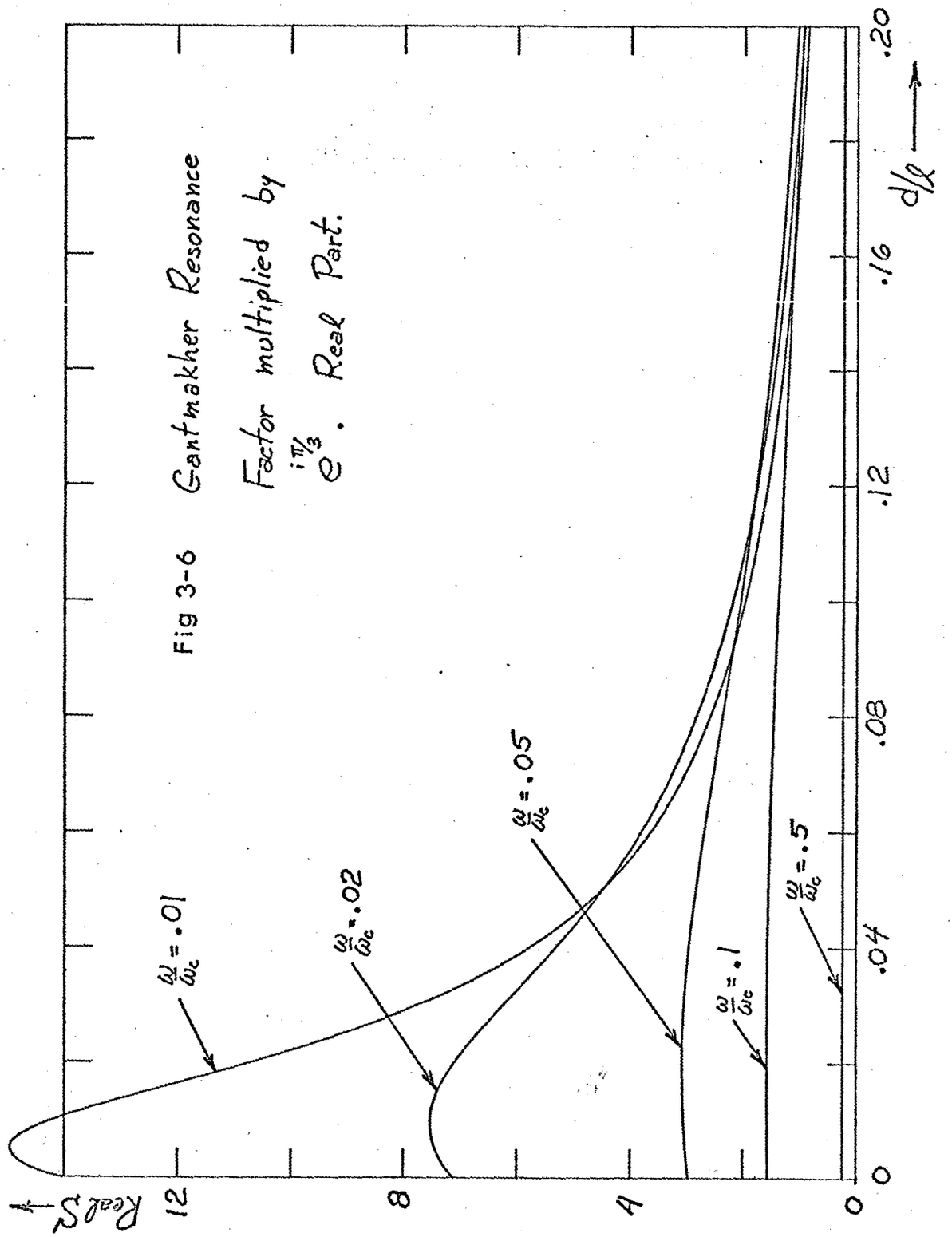

Fig 3-6 Gantmakher Resonance Factor multiplied by $e^{i\pi/3}$. Real Part.

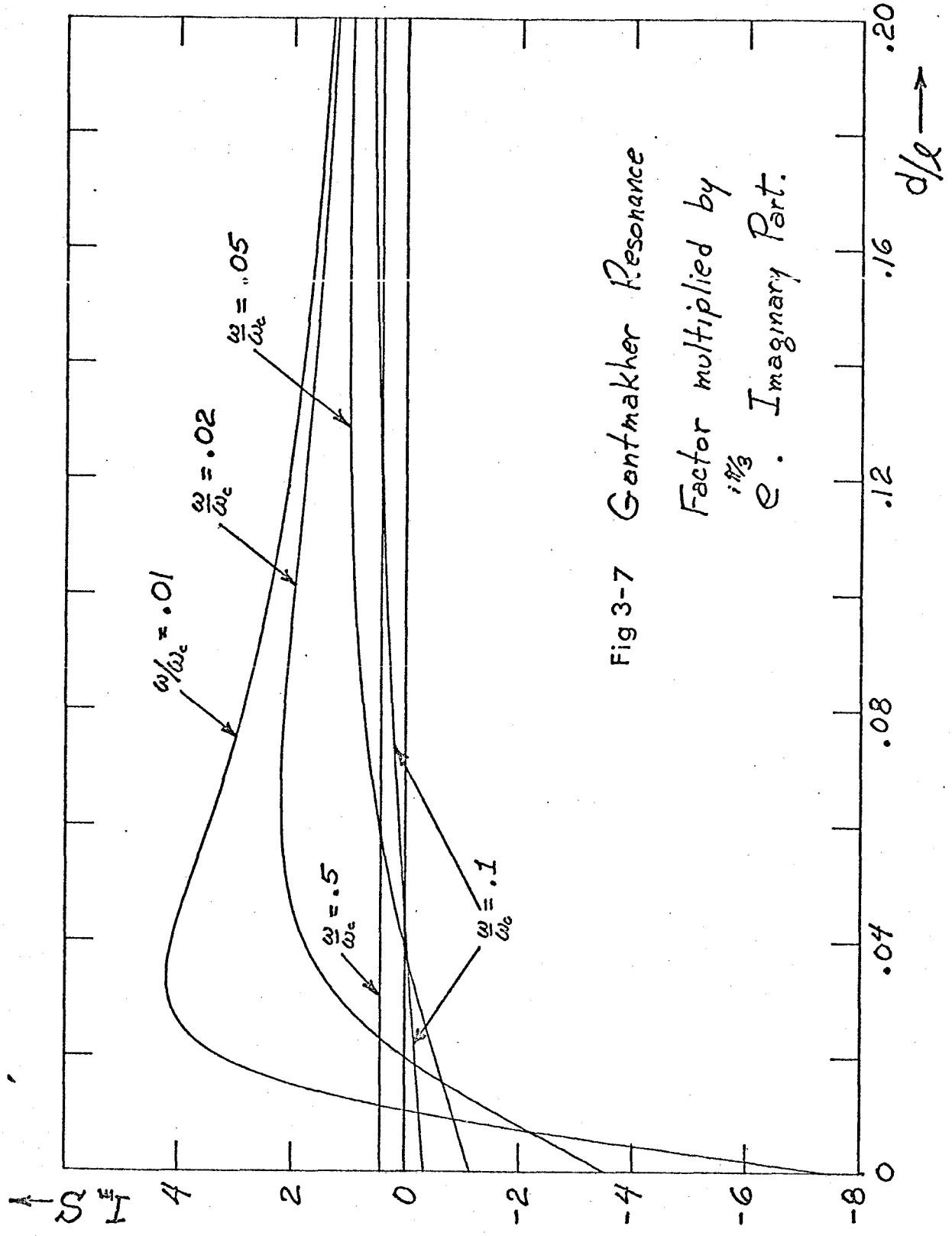

Fig 3-7 Gentmakher Resonance Factor multiplied by $i^{4/3}$ e. Imaginary Part.

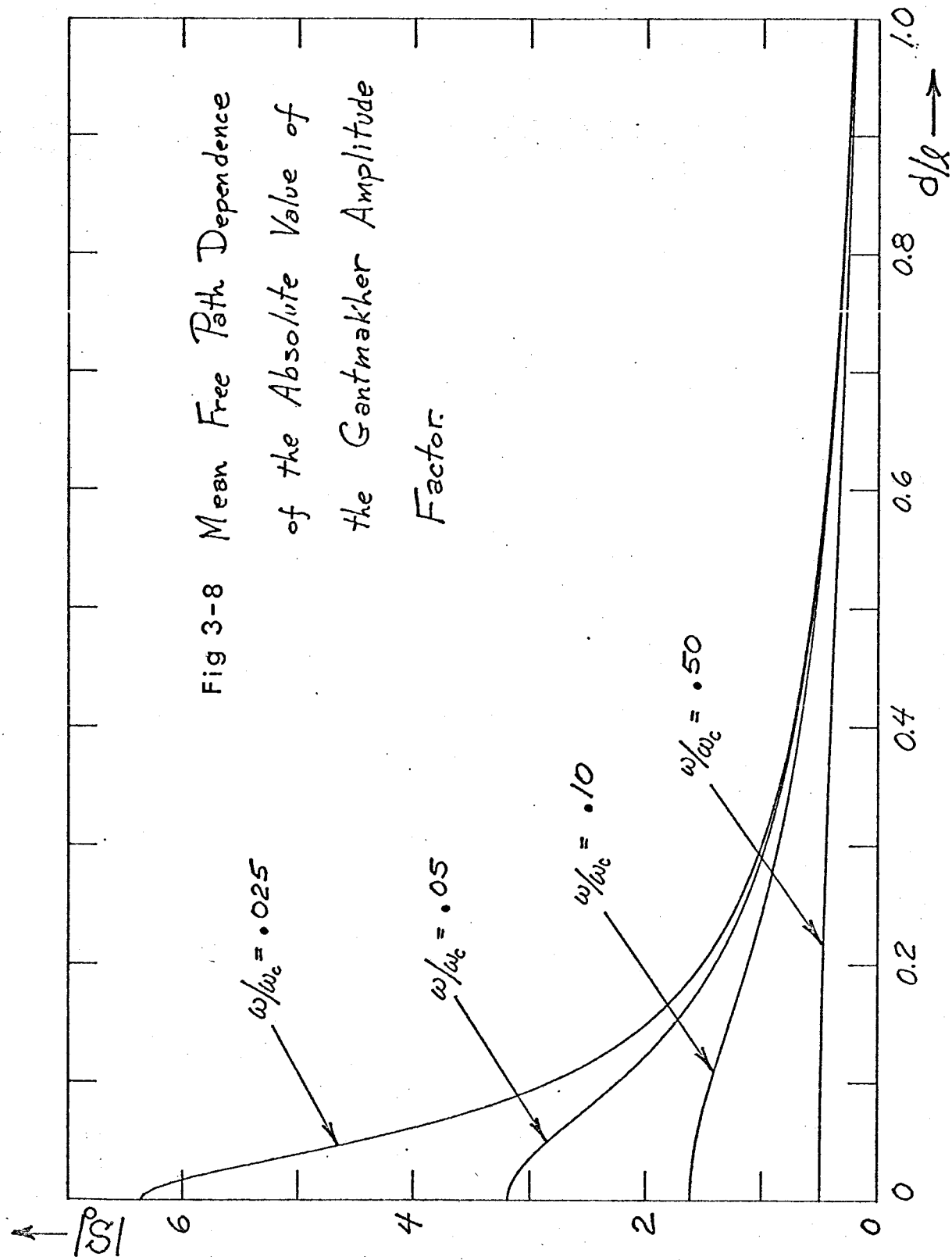

Fig 3-8 Mean Free Path Dependence of the Absolute Value of the Gantmakher Amplitude Factor.

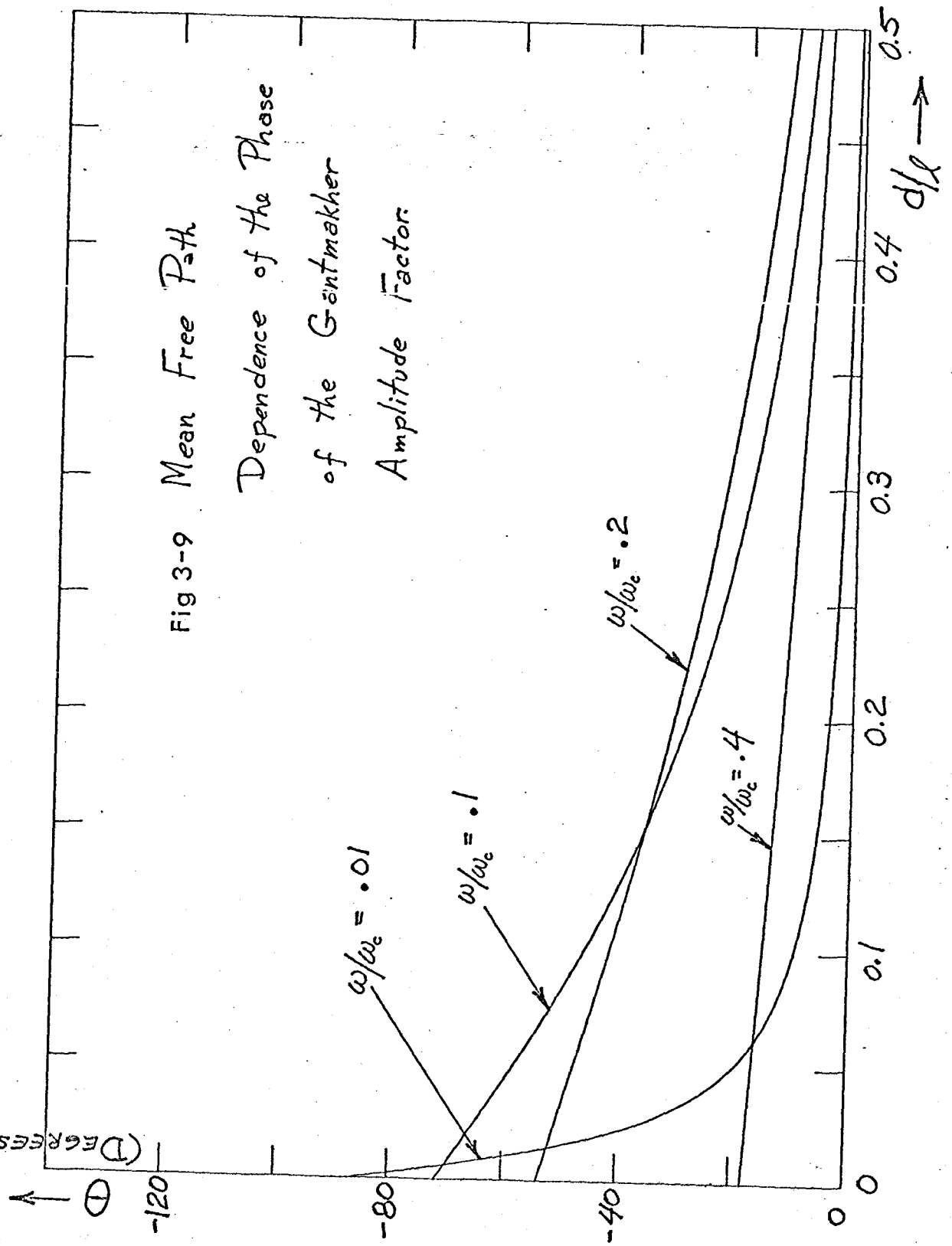

Fig 3-9 Mean Free Path Dependence of the Phase of the Gantmakher Amplitude Factor

3.3 Relation Between Transmission Anomalies and Surface Impedance Anomalies

It was stated in section 2.3 that the change in surface resistance, ΔR, and the change in surface reactance, ΔX, could be related to the change in transmission, ΔT. According to Cochran[30] one might expect

$$\Delta\delta = -\frac{2ic}{\omega}\,\Delta G_x(d) \qquad (2)$$

where $\delta = \delta_x + i\delta_R$ is the skin depth and $G_x(z)$ is the component of the electric field in the slab along the direction X, generated by a unit radio frequency magnetic field, H_y, applied at the surface $z = 0$. The surface resistance, R, and surface reactance, X, are related to the skin depth in the following manner*,

$$Z = R - iX = -\frac{4\pi i\omega}{c^2}(\delta_x + i\delta_R)$$

Since the change in transmission, ΔT, is

$$\Delta T = \frac{i\lambda}{2\pi a}\,\Delta G_x(d) = \frac{ic}{\omega a}\,\Delta G_x(d)$$

then

$$\Delta T = -\Delta\delta/2a$$

Consequently, line shapes predicted for ΔX and ΔR should be

---

* The negative sign in $Z = R - iX$ is due to the time factor $e^{-i\omega t}$ instead of $e^{i\omega t}$ which is used in conventional circuit theory.

directly related to transmission line shapes.

$$\text{Real } \Delta T = -\frac{\Delta\delta_X}{2a} = -\frac{c^2}{8\pi a\omega}\Delta X$$

$$\text{Im } \Delta T = -\frac{\Delta\delta_R}{2a} = -\frac{c^2}{8\pi a\omega}\Delta R$$

Thus it is possible to check Cochran's hypothesis, equation (2), by comparing the amplitude of a transmission anomaly with that of a surface impedance anomaly.

Chapter 4

PHYSICAL PROPERTIES OF GALLIUM AND ITS FERMI SURFACE

Gallium is a compensated metal[32] which has a base-centered orthorhombic crystal structure. There are 8 atoms per unit cell[33] although the primitive cell* contains only 4[34]. The melting point of gallium is 29.8°C. The superconducting transition temperature, T_c, is 1.1°K. The lattice constants at T = 2.35°K are[35],

$$a = 4.5151 \text{ Å}$$

$$b = 4.4881 \text{ Å}$$

$$c = 7.6318 \text{ Å}$$

From these constants one can construct a Wigner-Seitz unit cell which has the form of a right hexagonal cylinder. The boundaries of the Brillouin zone in reciprocal space are at,

$$k_x = 2\pi/a = 1.3916 \times 10^8 \text{ cm}^{-1}$$

$$k_y = 2\pi/b = 1.4003 \times 10^8 \text{ cm}^{-1}$$

$$k_z = 2\pi/c = 0.8232 \times 10^8 \text{ cm}^{-1}$$

---

* A unit cell is any cell that will cover all space under the action of the crystal translation operations. A primitive cell is a minimum volume unit cell.

One corner of the cell is at $k_x = k_y = k_z = 0$. The Brillouin zone is shown in Fig. 4-1.

Gallium has a complicated Fermi surface comprised of many separate sheets, some of which are very complex. There exists a large body of experimental data including magnetoresistance measurements[32][36], de Haas-van Alphen measurements[37][38], radio frequency size effect measurements[6][39][40], magnetoacoustic effect measurements[41][42][43][44], cyclotron resonance measurements[45][46][47][48], and d.c. size effect measurements[49]. However, the shape of the Fermi surfaces of most of these bands is not well established. Because of the complexity of these surfaces and the approximations involved in the Fermi surface model calculations* comparison of theoretical[50][51] and experimental results is very difficult.

Most recently Reed[52] has derived a model for the gallium Fermi surface using a local semi-empirical pseudopotential calculation without spin-orbit effects. From this calculation Reed obtained six closed electron sheets, one closed hole sheet, and a large multiply-connected hole sheet. Pictures taken from a model of Reed's Fermi surface constructed by R. Douglas at McMaster University, are shown in Figs. 4-2, 4-3, 4-4, and 4-5. A comparison of Reed's results with existing data gives good agreement with the larger pieces. Recent

---

* Models based on single-orthogonalized-plane wave (OPW) and augmented-plane-wave (APW) calculations.

work by Cook and Datars[53], using an induced torque method, are in excellent agreement with Reed's multiply-connected hole sheet.

Reed mentions that all of the Fermi surface pieces which appear in his calculation can be found in the data but notes that the data suggests that one or more very small pieces may have been missed.

In summary, it appears that Reed's recent calculation presents the best picture of the gallium Fermi surface to date. It has determined the number of Fermi surface pieces as well as their approximate sizes and shapes. An attempt will be made to compare aspects of our experimental data with this model. We shall also discuss the results of Munarin, Marcus, and Bloomfield[36] with respect to our data, as well as comparing our Gantmakher resonance data to those obtained by Haberland, Cochran, and Shiffman[40] and to those obtained by Fukumoto and Strandberg[39].

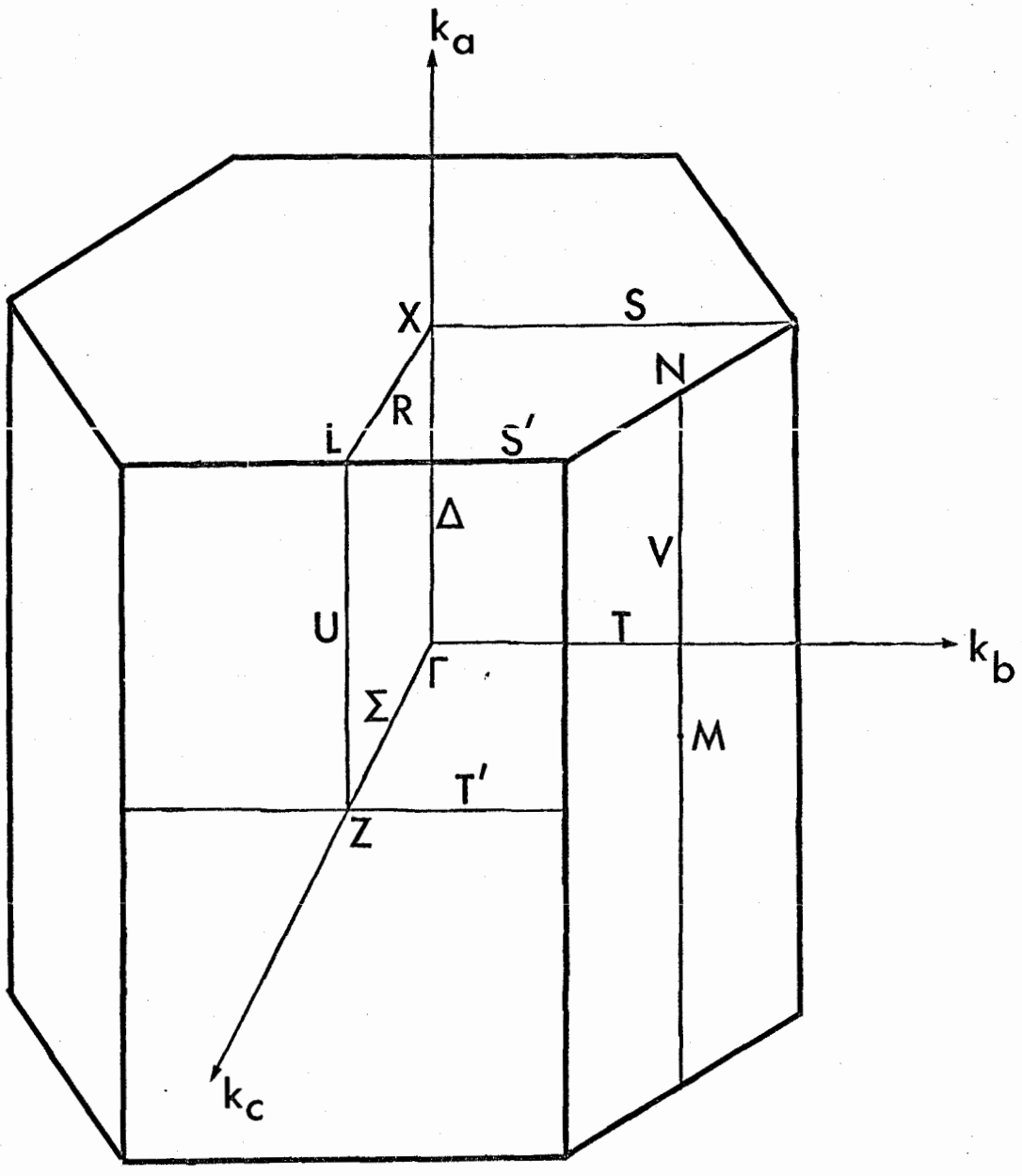

Fig 4-1. Brillouin Zone for Gallium

Fig 4-2. Model of the Gallium Fermi Surface

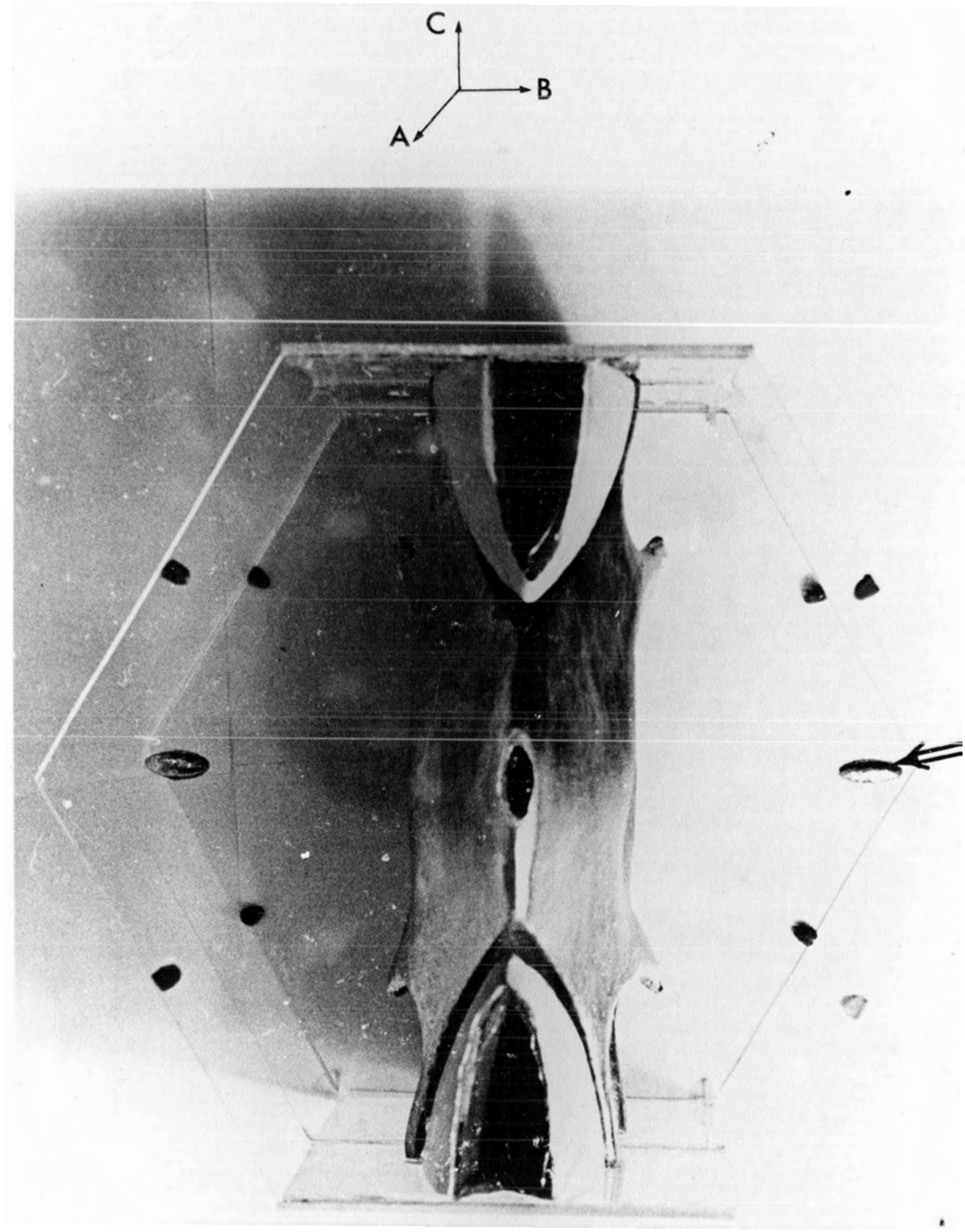

Fig 4-3. Model of the Gallium Fermi Surface

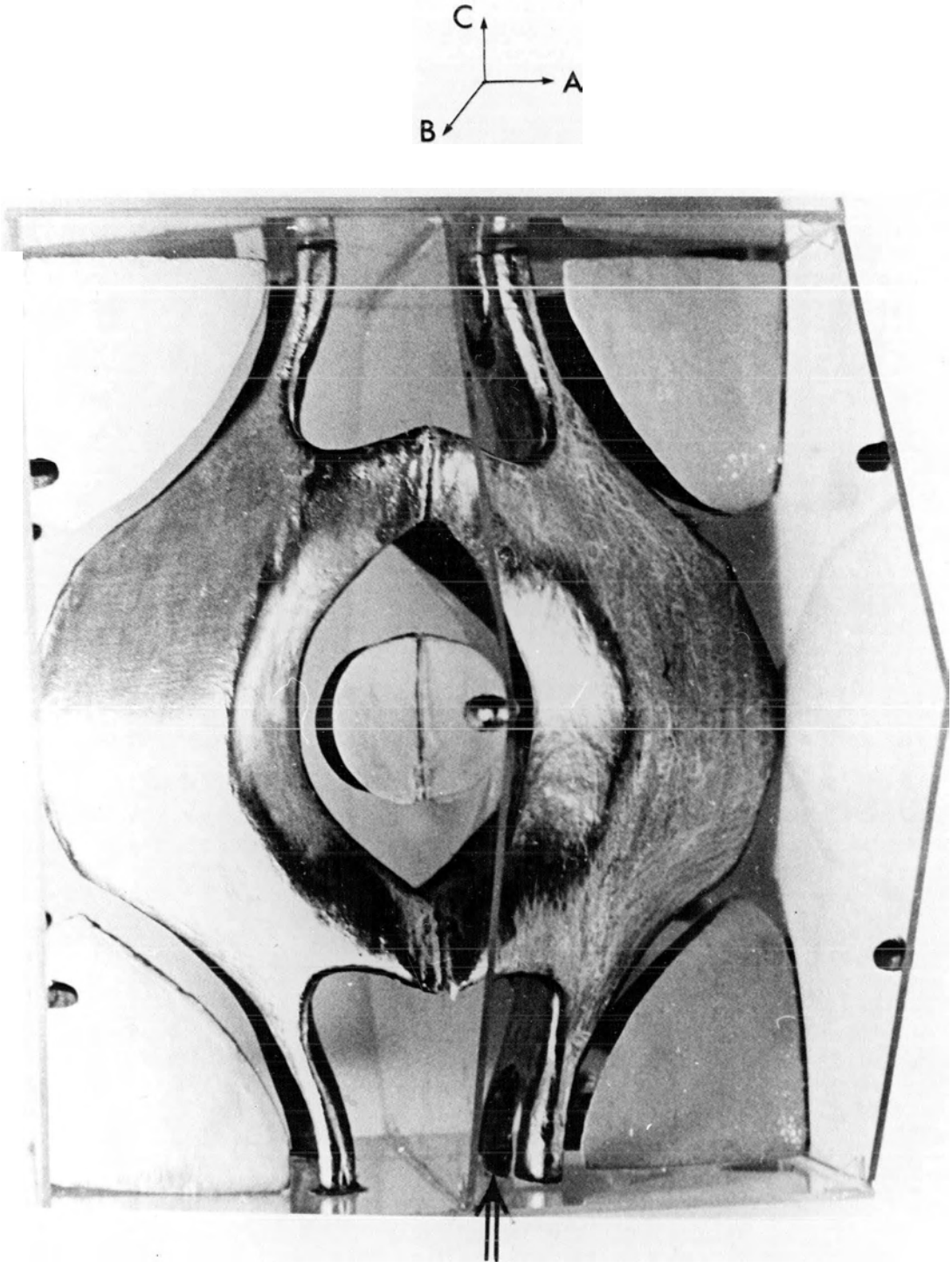

Fig 4-4. Model of the Gallium Fermi Surface

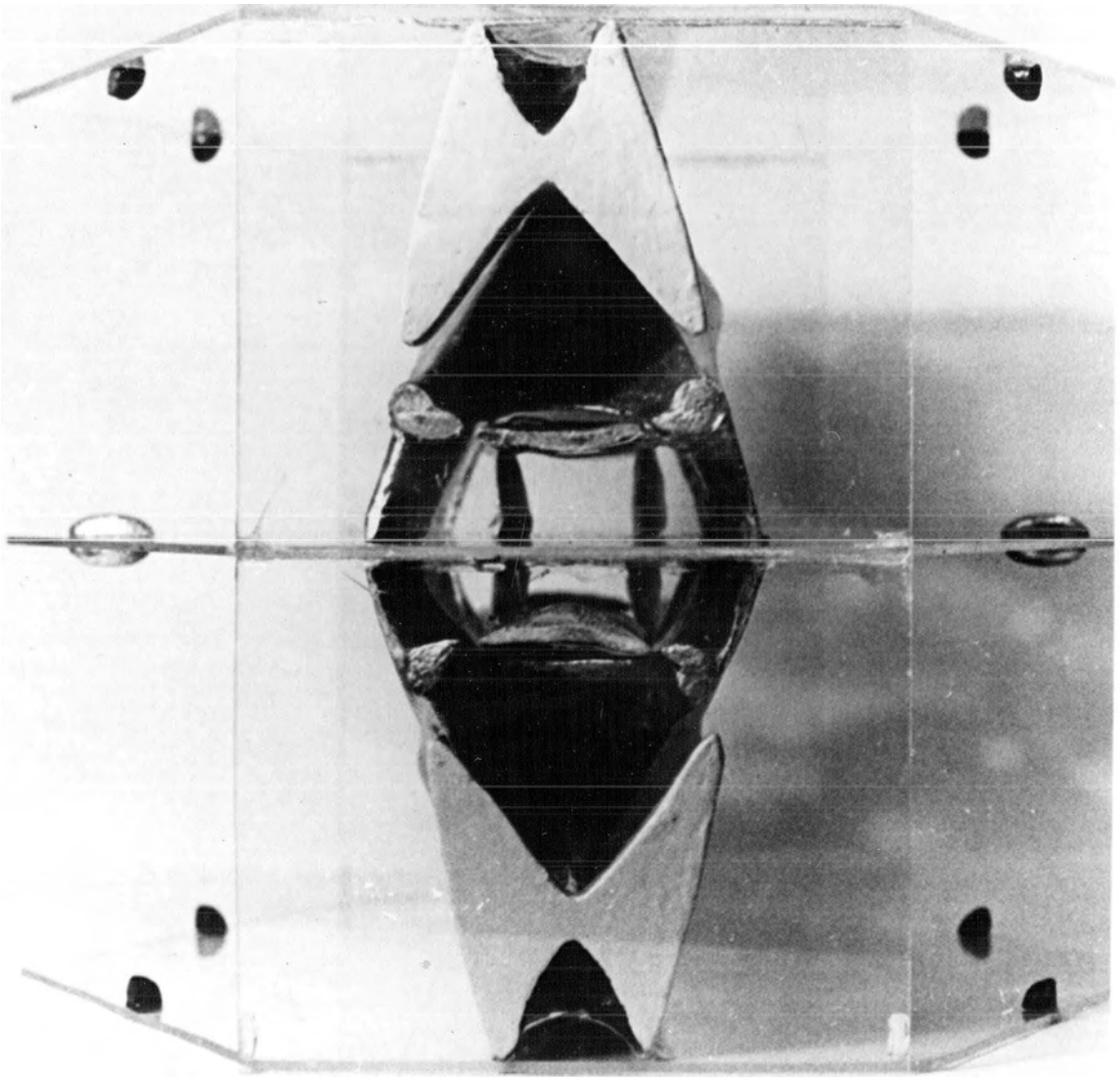

Fig 4-5. Model of the Gallium Fermi Surface

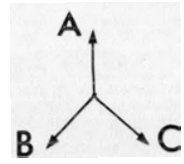

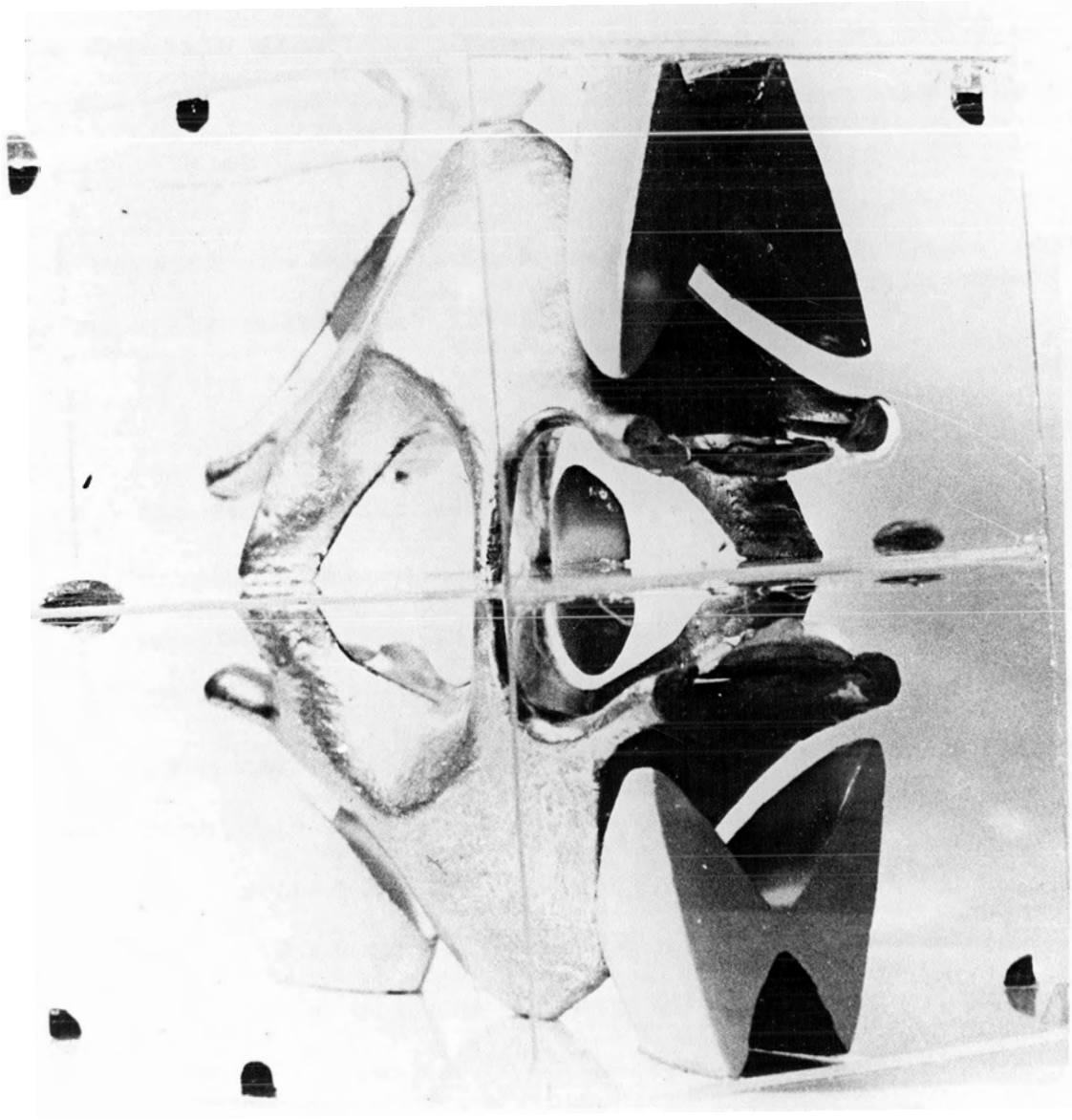

Chapter 5

EXPERIMENTAL

5.1 Specimen Geometry

Gallium single crystals in the shape of rectangular slabs were used. The slab thickness was 0.038 cm for most of the crystals examined. Thicknesses of 0.076 cm and 0.114 cm were also used. The length and width of the crystals were 3.18 cm and 0.95 cm respectively.

A crystal was mounted on a rectangular metal trough using three separate methods as illustrated in Fig. 5-1.

a) In the first method complete single crystals cavities were grown from the melt, that is, the thin slab and the thick walls were a continuous piece of single crystal gallium (Fig. 5-1A). The three thick walls had thicknesses of approximately 0.16 cm.

b) It was found that the thick sides transmitted appreciable radiation to the interior of the box. To overcome this difficulty the thick sides were electroplated with copper on the outside to a thickness of approximately 0.05 cm (Fig. 5-1C). This plating was accomplished by placing the crystal in a bath of copper sulphate solution to which had been added alum and sulphuric acid*. By continually rotating the specimen

---

* The actual recipe used was, 1800 g. of copper sulphate; 108 g. of potassium alum; 279 c.c. of sulphuric acid; and 9 liters of distilled water.

Fig 5-1. SPECIMEN CONFIGURATIONS

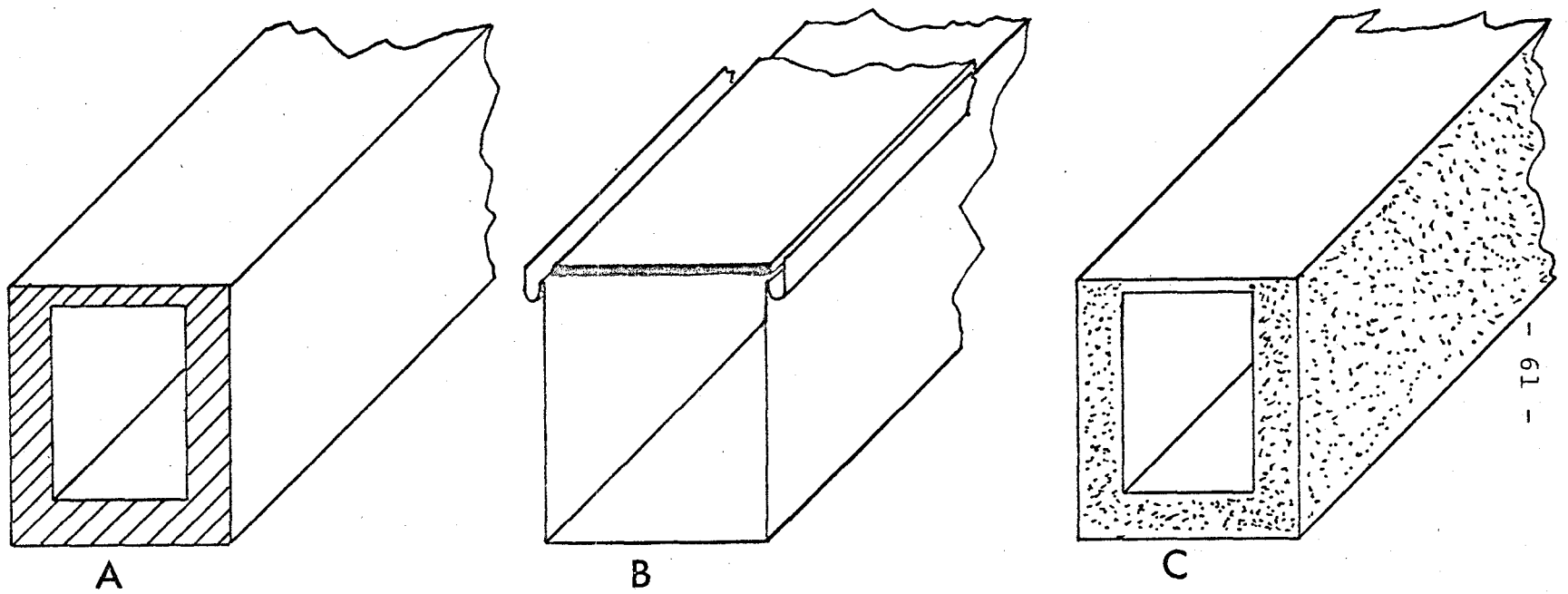

A

Single crystal of Gallium

B

Gallium Slab Mounted on Copper Trough

C

Solid Gallium Crystal with Exterior of Three Thick Sides Electroplated with Copper

an even deposition of copper was obtained. Layers of nail polish were applied to those areas of the crystal which were to be kept copper-free. The nail polish was subsequently dissolved in acetone. In too large a number of instances the copper plating was found to make relatively poor contact with the gallium crystal so that the radio frequency currents were not shorted out by the layer of copper.

c) Thus, it was necessary to proceed to the method of specimen mounting illustrated in Fig. 5-1B. In this case the gallium crystal was soldered to a rectangular trough made of high purity polycrystalline copper. The copper trough had a thickness of approximately 0.012 cm. This thickness was adequate to ensure that the transmission of 2 Mhz radiation through the copper sides was negligible at 4.2°K. On the other hand the copper walls were not so thick as to induce appreciable stresses in the gallium crystals upon cooling. As an added precaution pure gallium was used as the solder and the copper trough was annealed before the crystal was attached to it.

5.2 Experimental Arrangement

5.2.1 Coil System

The crystals were mounted on a rectangular sample holder (central specimen mounting post of Fig. 5-2). A smaller

circular post, upon which was wound a pickup coil, could be moved along the length of the sample holder by means of a micrometer screw located at the top of the cryostat. This adjustable cylindrical coil was set near the center of the crystal by locating the position of minimum transmission. The diameter of the secondary or pickup coil was 0.32 cm while its length was approximately 1.1 cm. A total of 145 turns of #40 gauge copper wire were wound over the 1.1 cm length. The secondary coil, when attached to the amplifiers via approximately 7 ft. of coaxial cable, was tuned to a frequency of 1.74 Mhz at liquid helium temperatures. The quality factor Q, of the coil at 4.2°K was 100.

A primary or transmitting coil was wound on a cylindrical mount which was then fitted over the specimen (see Fig. 5-2). The cylindrical primary coil had a diameter of 1.64 cm and a length of approximately 2.2 cm. A total of 87 turns of #36 gauge copper wire were wound over the 2.2 cm length. The resonant frequency of the primary coil at liquid helium temperatures when it was attached to the signal generator via approximately 7 ft. of coaxial cable, was 1.74 Mhz. The quality factor, Q, of this coil at 4.2°K was approximately 50.

The mounting post and framework for the primary and secondary coils were made of celoron, a substance similar to micarta, a resin-bonded cloth laminate.

To minimize the electrostatic coupling between the primary

Fig 5-2

Specimen Holder

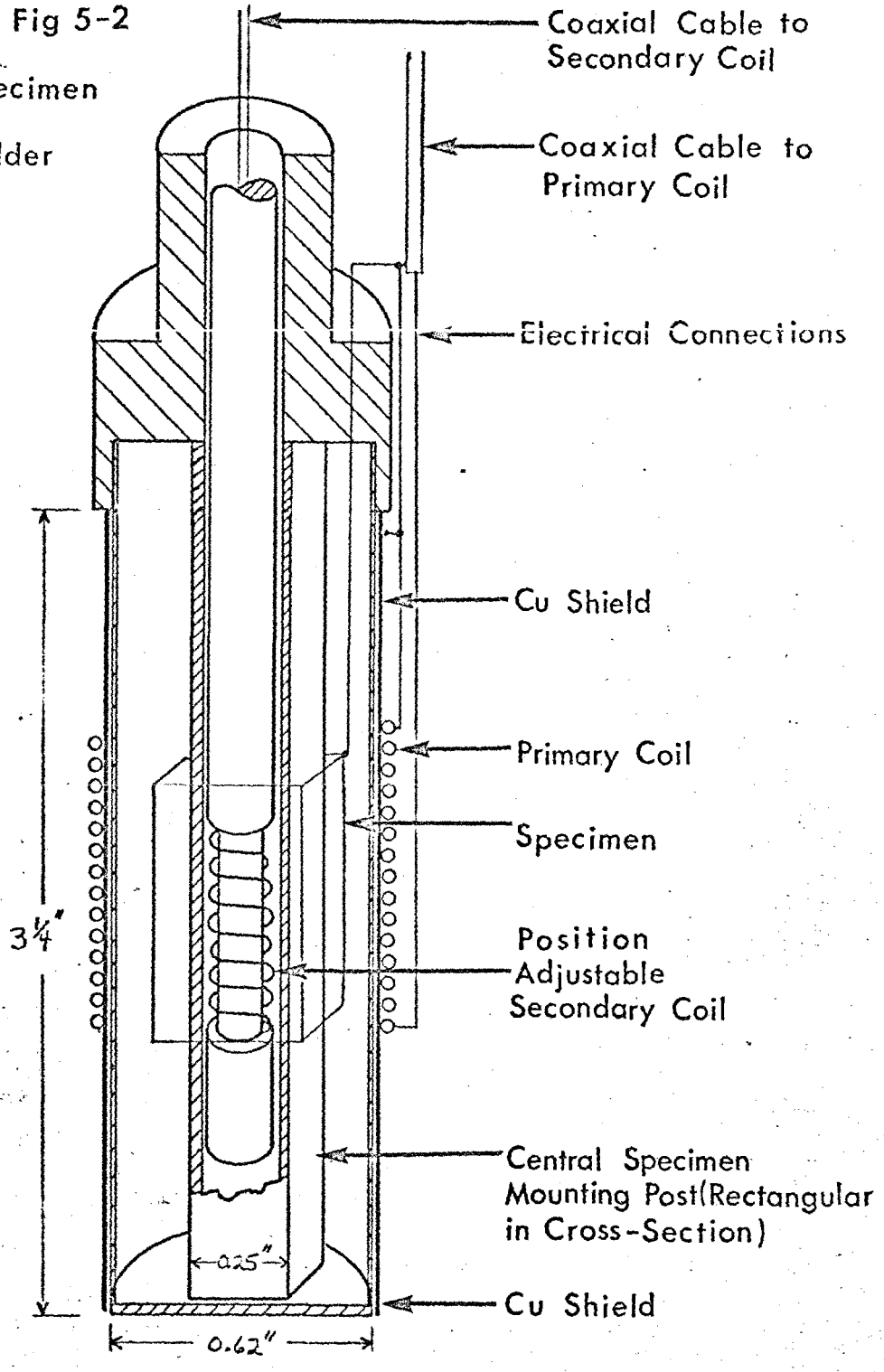

and secondary circuits, a cylindrical copper shield of length 8.25 cm was placed between the primary and secondary coils (see copper shield of Fig. 5-2). The charging currents due to electrostatic induction could then flow mainly in the shield, and the interior of the shield constituted a nearly field free enclosure despite the voltage drop along the primary coil.

5.2.2 Dewar System and Magnetic Field Generator

The experimental configuration as illustrated in Fig. 5-2, was suspended from Cupro-nickel tubing inside a conventional glass double dewar system. It was found necessary to remove the silver film from the tails of the dewars because eddy currents induced in them provided a coupling between the coils and therefore degraded the degree of isolation which could be obtained between primary and secondary coils.

A solenoid, 6.0 cm in diameter and 10.0 cm in length, was wound upon the outside of the nitrogen dewar tail such that the specimen was located at the center of the coil system. This solenoid, having 76 turns of 0.206 cm O.D. water cooled copper tubing produced a steady magnetic field along the length and parallel to the surface of the specimen. The solenoid had a coil constant of 8.2 gauss/amp and was capable of producing a maximum magnetic field of approximately 300 gauss. The field was calculated to be uniform to within ± 3% over the length of the specimen.

Fields perpendicular to the axis of the specimen assembly were provided by a large water cooled Helmholtz pair capable of generating a maximum field of 1100 gauss. This Helmholtz pair had a coil constant of 10.65 gauss/amp. The field homogeneity for these coils was measured to be ± 0.04% over the length of the specimen. The Helmholtz pair could be rotated about a vertical axis and therefore, could be used to provide a magnetic field whose orientation varied from normal to the plane of the specimen to parallel with the specimen width. Current for both these coils was supplied from a 100 ampere current regulated power supply manufactured by Spectromagnetic Industries Ltd. (Model 6003).

The earth's magnetic field was compensated to within 0.05 gauss by means of two mutually perpendicular pairs of Helmholtz coils which contained the magnetic field generators described above (see Fig. 5-4).

5.2.3 Alignment and Calibration of Magnetic Field

The location of the plane of the specimen surface and consequently, the location of the orientation of the crystallographic axes with respect to the magnetic field, was determined using the symmetry of the transmission versus field diagrams with respect to angle of field oreintation setting. This, of course, could only be done using the big Helmholtz coils. It should be noted that in all the specimens used to align the field, the principle axes of gallium lay in the

planes of the specimen surfaces. Hence, the location of one axis direction was sufficient to align the crystal. Using this method, the field could be aligned to within 0.5° of a principle axis.

The solenoid employed to produce a vertical magnetic field, was calibrated to 1% by means of a Bell gaussmeter (Model 620). The Helmholtz pair was calibrated by means of a nuclear magnetic resonance signal produced by protons (presumably protons in the celoron specimen holder). At a frequency of 1.74 Mhz this nuclear magnetic resonance occurred at 408.5 gauss. This calibration standard provided a field accuracy equivalent to that of the frequency accuracy (approximately 0.2%). Examples of proton resonance signals are indicated in Fig. 6-62, 6-63, etc. and 5-9.

5.2.4 Control and Measurement of Temperature

Temperatures between 4.2°K and 1.2°K were obtained by pumping on the helium bath by means of a Stokes' mechanical pump. The temperature was monitored by means of a $\frac{1}{10}$ watt Ohmite carbon resistor which had a resistance (including the lead wires) of 107 ohms at room temperature. The resistance of the carbon resistor at low temperatures was measured by means of a simple 33 cycle Wheatstone bridge (see Fig. 5-3). In order to measure temperature the carbon resistor was calibrated against the vapour pressure of liquid helium. The vapour pressure of the bath was measured using a mercury

Fig 5-3. Resistance Measuring Circuit

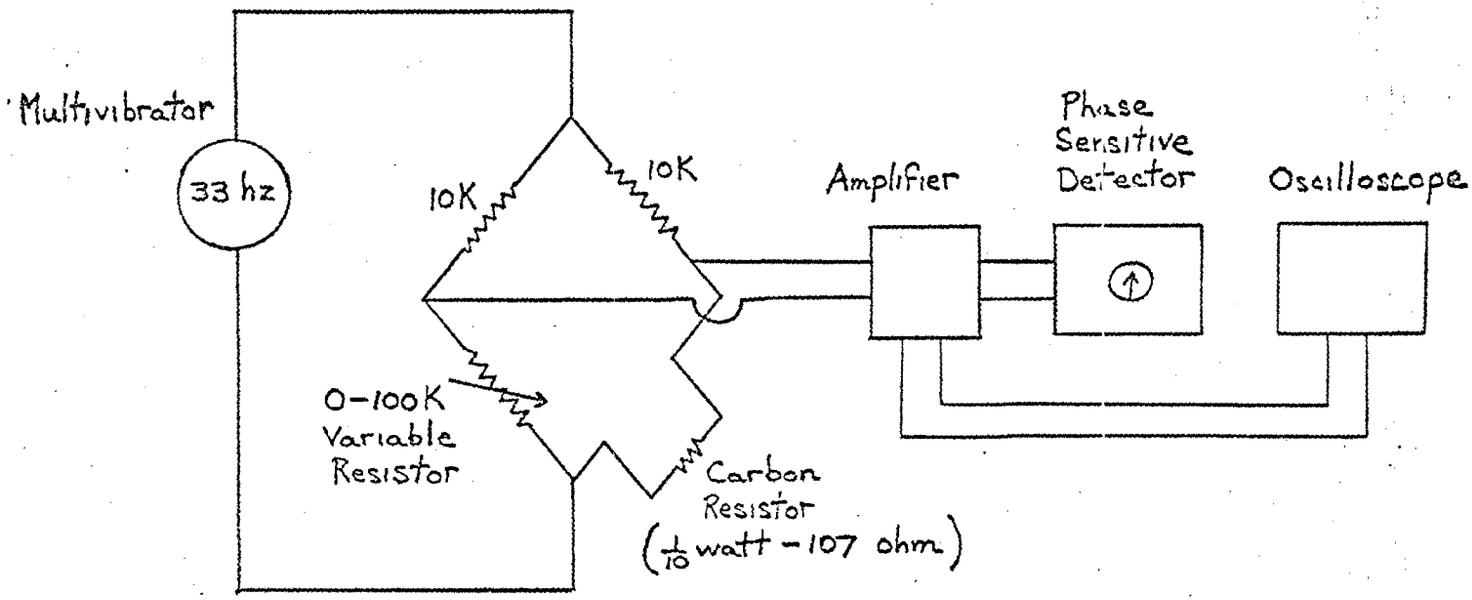

manometer for pressures down to about 20 mm. An oil manometer was then used to measure pressures below 20 mm. of mercury. The vapour pressures were converted to temperature using the T-58 scale[54]. No corrections were made to account for the hydrostatic head of liquid helium because temperatures were required with an accuracy of only ± 0.01°K.

Temperatures could be held within ± 0.05°K by adjusting the pumping valve but this was not critical since the position of a Gantmakher or Gantmakher-Kaner size effect does not change with temperature. The amplitudes of these resonances however, do depend upon temperature.

5.2.5 Signal Detection

The electronic equipment used in this experiment was very simple. A block diagram of the experimental configuration is given in Fig. 5-4. Details of manufactured electronic equipment are presented in Table 5-1, while circuit diagrams of equipment that was constructed are given in Figs. 5-5, 5-6, and 5-7.

A 1.74 Mhz signal was applied to the primary coil, which was placed around a gallium crystal, from a Tektronix signal generator. The signal generator was placed in an enclosure made from 35 mil thick copper. This enclosure was found to be necessary in order to shield the apparatus from direct radiation from the oscillator. The signal transmitted through

Fig 5-4. EXPERIMENTAL CONFIGURATION

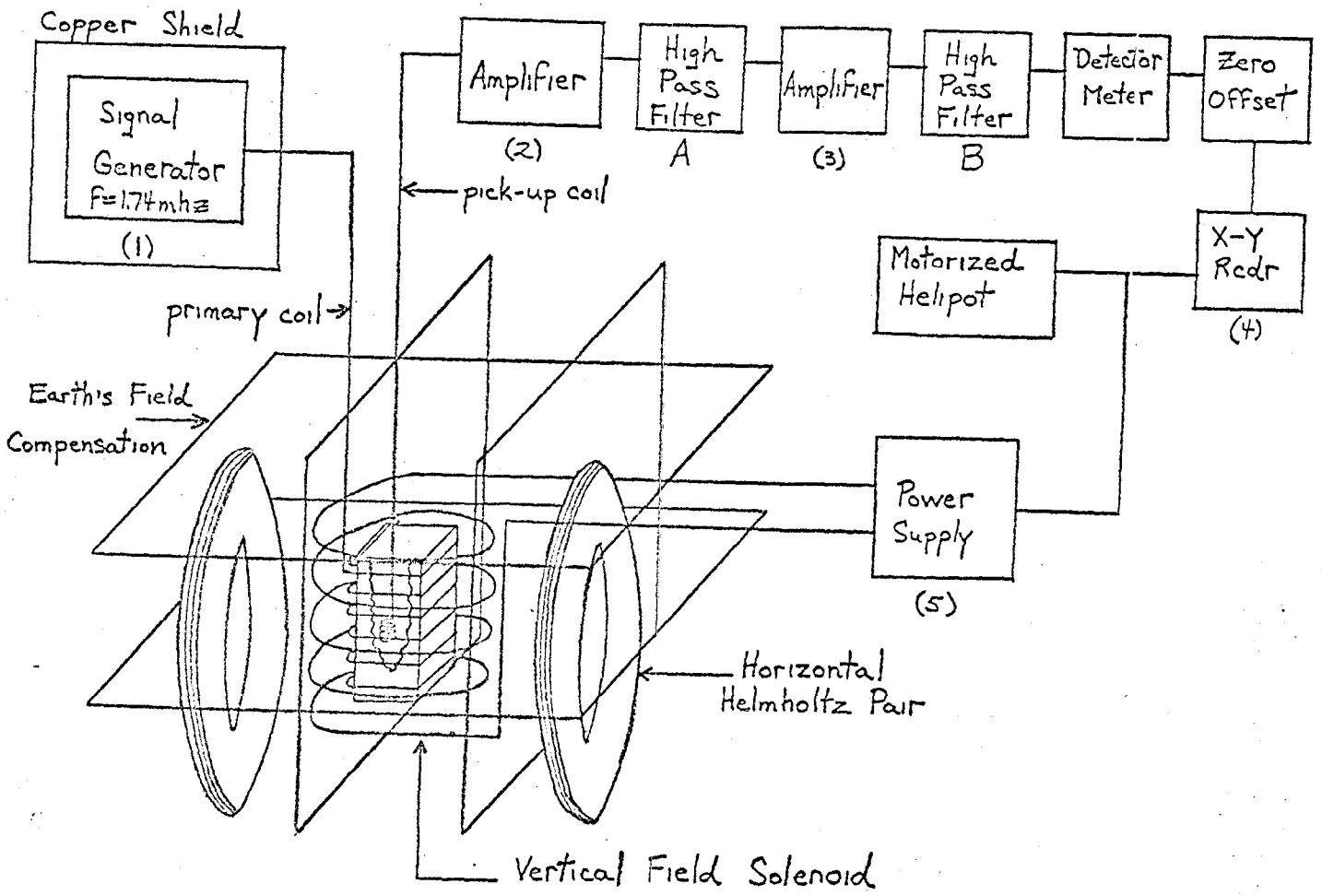

Table 5-1

Electronic Equipment

(1) Tektronix constant amplitude signal generator - Type 191
- operates between 350 khz and 100 Mhz and also at 50 khz
- maximum output of 5.0 v into 50 Ω load
- when load impedance very large (i.e. open circuit) maximum output is 10.0 v

(Tektronix Ltd., Beaverton, Oregon)

(2) Tektronix amplifier - Type 1121
- provides a gain from 100X to 0.2X
- frequency response from 5 hz to 17 Mhz

(Tektronix Ltd., Beaverton, Oregon)

(3) Hewlett Packard general purpose amplifier - Type 465A
- provides a gain of 10X or 100X with 50 Ω load
- frequency response from 50 hz to 1 Mhz

(Hewlett Packard, Palo Alto, California)

(4) Moseley 7005 AM X-Y recorder
- single pen type
- sensitivity from 0.4 mv/cm to 4 v/cm

(Hewlett Packard, Palo Alto, California)

(5) Spectromagnetic current regulated power supply - Model 6003
- maximum current of 100 amp

(Spectromagnetic Industries, Hayward, California)

Fig 5-5

High Pass Filters

(A)

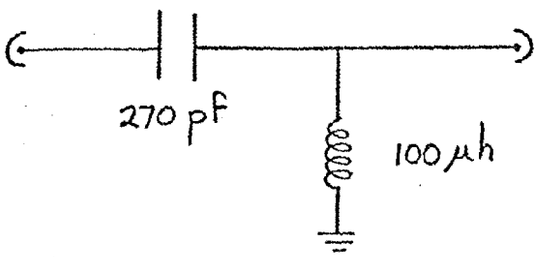

(B)

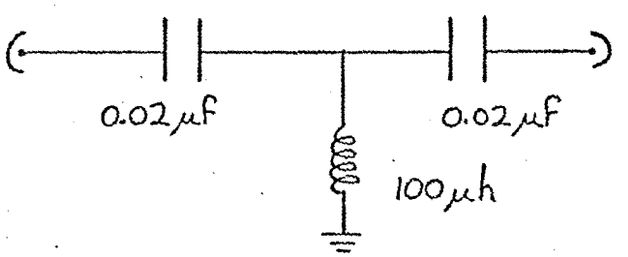

Fig 5-6. Detector Unit

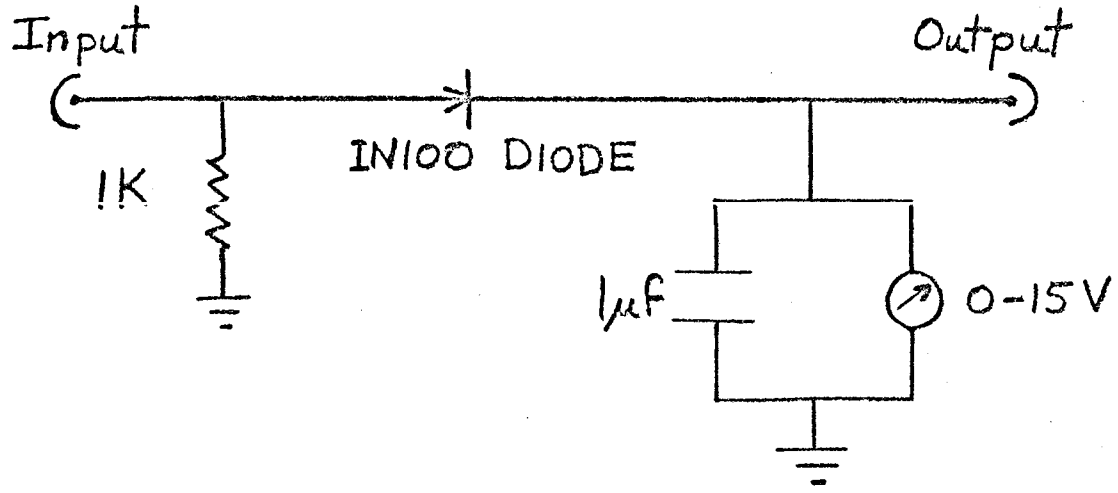

Zero Offset

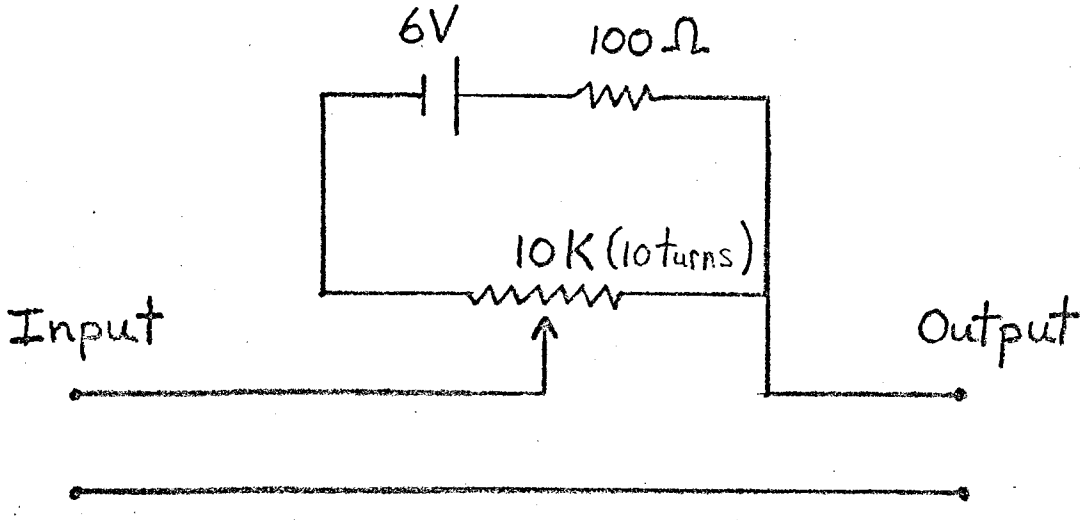

Fig 5-7. Motorized Helipot

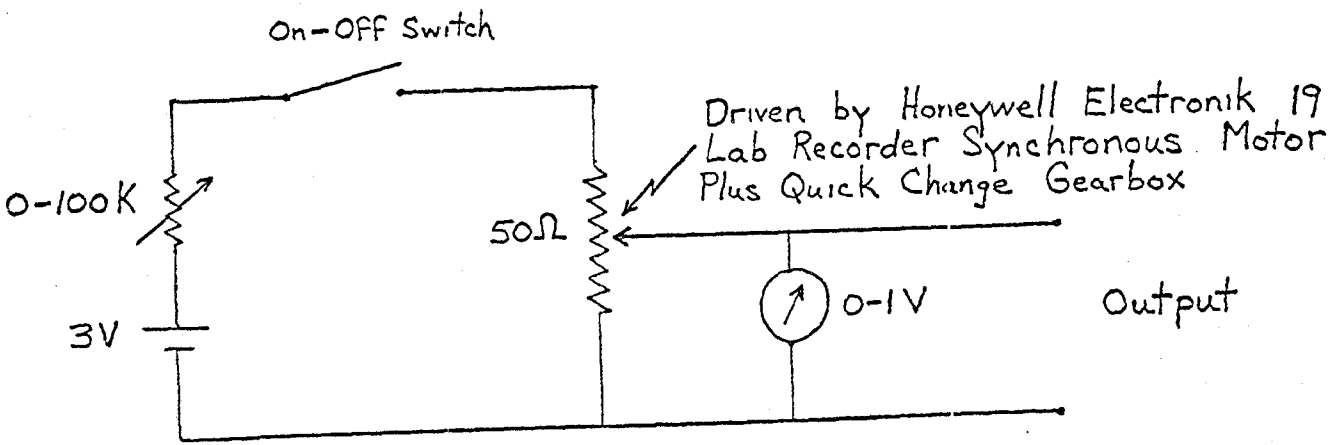

the specimen was then received by a pickup coil, amplified by means of wideband amplifiers*, filtered**, rectified, and plotted on an X-Y recorder as a function of magnetic field strength. Care was taken to ensure that all the electronic equipment was grounded to a single "quiet ground" point. The grounds of the primary and secondary coils were connected to the copper enclosure containing the signal generator.

An important aspect of the apparatus was the use of a tuned secondary coil. It was tuned to 1.74 Mhz at 4.2°K. The fact that it was tuned enabled one to use the quality factor, Q, of the coil to obtain a gain of 100 (at helium temperatures) in signal to noise of the small transmitted signal. In a typical experiment the signal of interest was much smaller than the background signal due to direct pickup of the field generated by the primary coil leaking around the ends of the specimen. Generally the apparatus was driven at such a level that the voltage through the detector meter was of the order of several volts. Since transmitted signals of the order of millivolts were observed on the X-Y recorder, the background signal was approximately 100 to 1000 times larger than the transmitted signal. As a result, this background signal had to be bucked out by means of the circuit

---

* At 1.74 Mhz the Hewlett Packard wideband amplifier no longer had a gain of 10X or 100X but rather 8.8X or 88X.

** High pass filter A was found to be only 82% efficient, i.e. passed 82% of the voltage, while filter B was 100% efficient at 1.74 Mhz.

illustrated in Fig. 5-6. (See zero offset).

The minimum detectable voltage was approximately 0.14 μv referred to the input of the 1st amplifier. This corresponds to a change in transmitted field, ΔH_i, of 1.1×10^{-9} gauss. The quality factor, Q, of the secondary coil has been included in this figure (see Section 5-3 equation (2)). Since the driving field used was 1.06 gauss, this gives $\Delta T_{min} \approx 10^{-9}$*. The limitation on the sensitivity of the system was found to be noise in the amplifiers. Fig. 5-8 illustrates this conclusion. The lower trace is the noise level of a signal fed directly from the signal generator to the rectifier, then to the zero offset circuit where the signal was offset to the point where it could be ovserved on the most sensitive scale of the X-Y recorder (Y = 0.4 mv/cm scale). The upper trace is the noise level of a signal from the signal generator which has now passed through the amplifiers and high pass filters before being rectified and plotted on the X-Y recorder. The output of the signal generator has been adjusted so that the signal level through the rectifier is the same for both cases. It is clear that the amplifier

---

* Although, the minimum, ΔT_{min} is 10^{-9} in this apparatus, this represents transmission into a cavity. According to Cochran[30], if one were transmitting into a vacuum ΔT_{min} would be equivalent to,

$$\Delta T_{free} \approx \frac{2\pi a}{\lambda} \Delta T_{cavity}$$
$$= 3 \times 10^{-4} \Delta T_{cavity}$$
$$= 3 \times 10^{-13}$$

noise is 2 to 3 times larger than the signal generator noise.

As mentioned previously the signals that we detect are small compared to the background. From the following vector diagram it is clear that we measure that part of the transmitted signal which is in phase with the background signal.

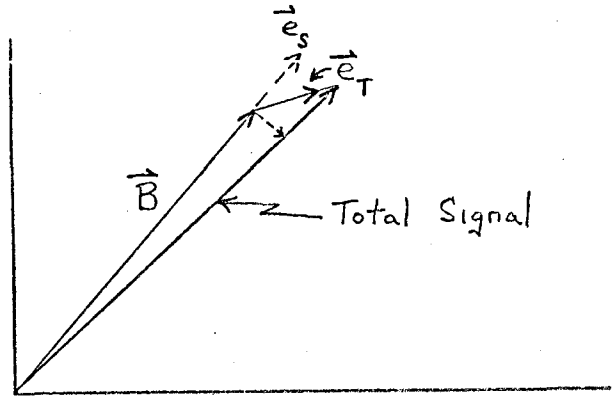

Here $\vec{B}$ represents the magnitude of the background signal and $\vec{e}_T$ the magnitude of the transmitted signal. Clearly, after $\vec{B}$ is bucked out of the total signal then the resultant signal is approximately that component of the transmitted signal, $\vec{e}_s$, which is in phase with the background signal $\vec{B}$.

Furthermore, from transformer theory one expects the background signal, B, to be a signal which is in phase with the applied radio frequency magnetic field. We therefore expect to measure a transmitted signal component which is in phase with the applied radio frequency magnetic field. The following experiment was performed to verify this conclusion.

A comparison was made between the phase of the pickup signal, corrected for phase shifts through the amplifiers, and the phase of the signal generator voltage. It was found that these two voltages were approximately 77° out of phase. This phase difference depended critically on the tuning of the oscillatory frequency to the resonant center frequency of the secondary coil. The accuracy of the phase shift measurement was approximately ± 15°. Consequently, one can say that these voltages were approximately 90° out of phase. Thus, the background or reference signal was found to be approximately in phase with the driving radio frequency magnetic field, as expected. Hence, we detect the real part of the transmitted signal.

In section 5.3 an "experimental" expression for the transmission ratio coefficient, T_c, is obtained. This expression is entirely real in form. Cochran's[30] expression for the transmission is,

$$T_c \approx \frac{i\lambda}{2\pi a} G_x(d) = \frac{i\lambda}{2\pi a} H(0)\, E_x(d)$$

where H(0) is the magnetic field at the surface of the specimen, λ is the free space wavelength, "a" is the cavity width, and $E_x(d)$ is the electric field at the inside of the cavity. Since our experiment measures the real part of T_c, then the signal observed represents the imaginary part of $E_x(d)$.

Fig 5-8 Comparison of Noise Level in the Signal Generator to that in the Amplifiers

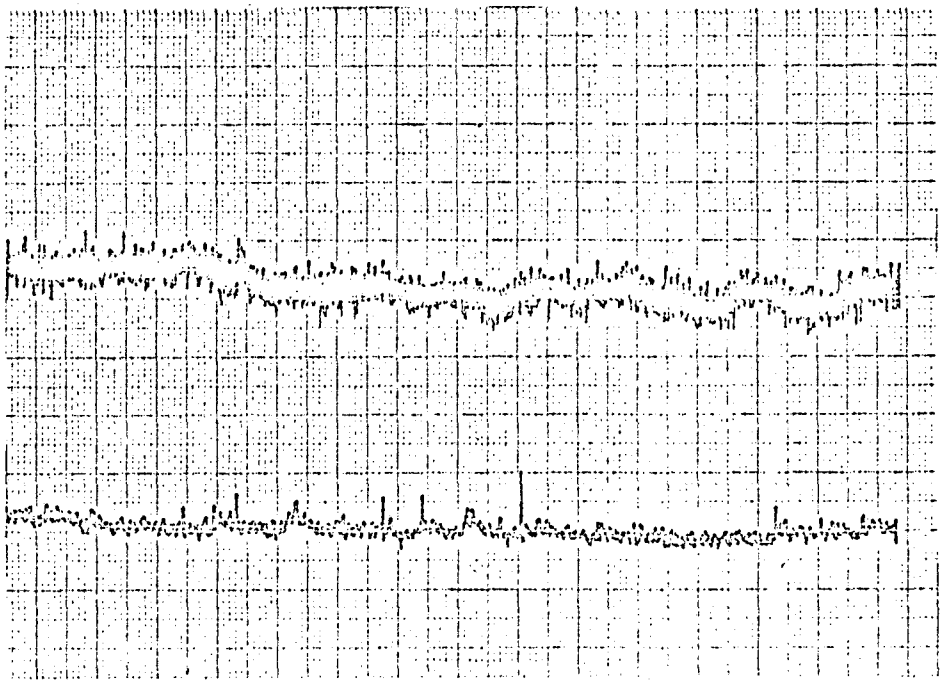

Arbitrary Scale

A

Signal after passed through amplifiers

B

Signal direct from signal generator

Signal level adjusted to give the same d.c. output level as for case A above

It can further be stated that the signal observed is in phase with the surface reactance. This can be easily seen if one recalls that the surface reactance, X, is defined to be due to that part of the magnetic flux contained in the skin layer which is in phase with the driving radio frequency magnetic field.

5.3 Calibration of the Transmission Ratio Coefficient

In section 3.1 an expression for the transmission ratio coefficient, T_c, was obtained. This expression, which was valid only in the classical limit, where $\vec{j} = \sigma\vec{E}$, was written,

$$T_c = \frac{2e^{ikd}}{1+\Delta}$$

$$\text{where} \quad \Delta = 1 + 2a/b - ika$$

where "a" and "b" is the width and the length of the cavity respectively and "k" is the wave vector. This coefficient can be evaluated if the resistivity of the sample is known.

The quantities that are measured experimentally are (1) the current and voltage applied to the primary coil, and (2) the voltage detected at the output terminals of the secondary coil. The field developed by the primary coil, H_o. at its center can be written,

$$H_o = \frac{4\pi}{10} \frac{V_p}{L\omega} n_p \cos\theta \qquad (1)$$

where L is the inductance of the primary coil in henrys, V_p is the applied voltage from the oscillator in volts, n_p is the number of turns per centimeter of the primary coil, and θ is the angle indicated in the following sketch.

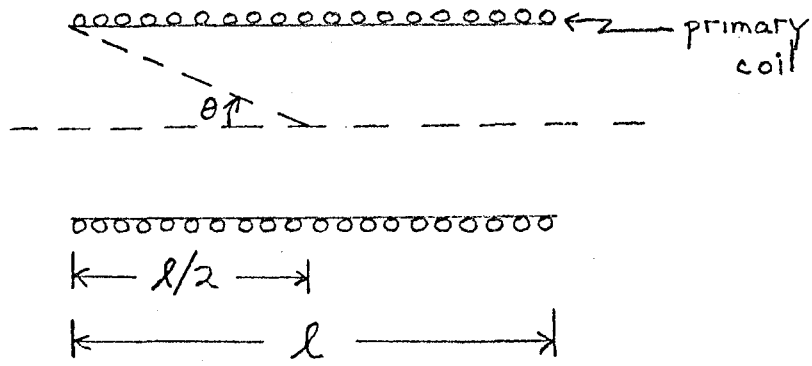

The equation for the magnetic field at the center of a thin solenoid has been used to obtain equation (1). The signal from the secondary coil is due to the time rate of change of flux through the turns of the coil. The actual tuned circuit consists of the inductance of the secondary coil shunted by the coaxial cable capacitance (approximately 200 pf) plus the amplifier input capacitance (approximately 10 pf). This is illustrated in the following sketch.

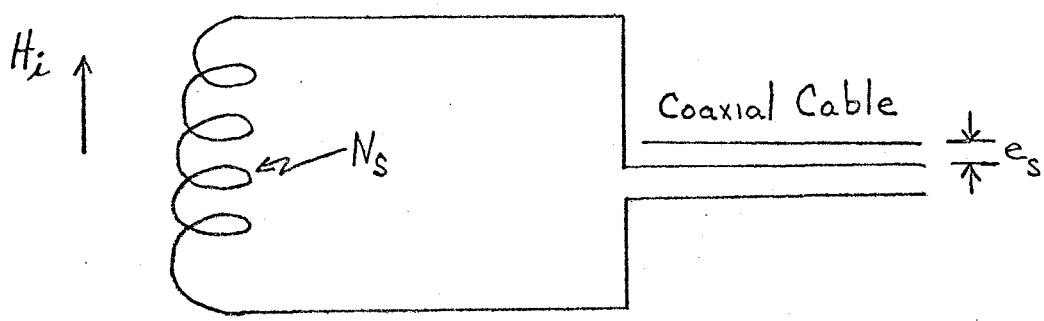

We can therefore, write the pickup signal, e_s, as,

$$e_s = Q_s N_s 10^{-8} \frac{d\phi}{dt} = Q_s N_s A_s \omega_o H_i 10^{-8}$$

where Q_s is the quality factor of the coil, N_s is the number of turns on the coil, A_s is the cross-sectional area of the coil in cm^2, ω_0 is the resonant frequency of the secondary coil, and e_s is the voltage induced in the turns of the secondary coil. Hence, the transmitted field is given by,

$$H_i = \frac{10^8 e_s}{N_s A_s \omega_o Q_s} \qquad (2)$$

The transmission ratio can now be written,

$$T_c = \frac{H_i}{H_o} = \frac{10^9 L e_s}{4\pi N_s A_s Q_s V_p n_p \cos\theta}$$

This then, is the "experimentally" determined transmission ratio value.

The inductance of the primary coil was obtained from a plot of the impedance of the coil as a function of frequency. For a tank circuit the position of maximum impedance, Z_{max}, has a value equal to $Q_p L\omega$. Since the quality factor, Q_p, and the frequency, ω, are readily determined, the inductance can also be determined. It is important to note that the inductance depends upon whether or not a specimen has been mounted in the sample holder since the inductance is a measure of the flux contained in the primary coil. A hollow box

specimen excludes most of the flux from its interior under circumstances of interest to us. As a result, the primary inductance is reduced by the insertion of a specimen. It was this reduced value that was measured.

In order to calibrate the system a rectangular box made of 0.013 cm (5 mil) high purity polycrystalline copper was inserted as a specimen. The box was such that only 3 sides were actually 0.013 cm thick. The 4th side was silver soldered to the other three in a fashion indicated in the following sketch.

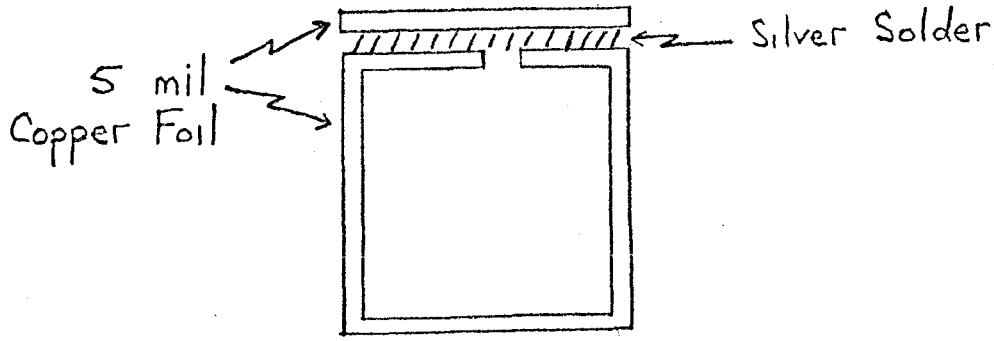

Copper Specimen Geometry

Effectively only 3 sides of the box transmit radiation. The transmission ratio was then calculated at room temperature and at liquid nitrogen temperatures using the "experimental expression",

$$T_c = \frac{10^9 L e_s}{4\pi N_s A_s Q_s V_p n_p \cos\theta}$$

and the "theoretical" expression which is valid in the classical limit,

$$T_c = 3\left\{\frac{2e^{ikd}}{2+\frac{2a}{b}-ika}\right\}$$

However, for our experiments ka $\approx$ 200 at room temperature and at a frequency of 1.74×10^6 hz.

$$\therefore\ T_c = 3\left\{\frac{2ie^{ikd}}{ka}\right\}$$

The "theoretical" expression has been multiplied by a factor 3 since 3 sides are effectively transmitting. The following parameters were used in the subsequent calculations.

$$\rho_{cu}(R.T.)^{(55)} = 1.7 \times 10^{-6}\ \Omega\ cm$$

$$\rho_{cu}(N_2)^{(55)} = 0.2 \times 10^{-6}\ \Omega\ cm$$

$$a = 0.7\ cm$$

$$N_s = 145$$

$$V_p = 10\ volts$$

$$Q_s(R.T.) = 20$$

$$Q_s(N_2) = 40$$

$$A_s = 0.08\ cm^2$$

$$n_p = 39.5$$

$$L(R.T.) = 3.5 \times 10^{-5} \text{ henrys}$$

$$L(N_2) = 3.4 \times 10^{-5} \text{ henrys}$$

$$\cos\theta = 0.79$$

Table 5-2 gives the results of these calculations.

It is clear that excellent agreement exists between the observed and theoretical transmission ratios. The signal at nitrogen temperatures is due in part to the leakage around the ends of the specimen. From the results of this simple experiment one can estimate a value for the degree of isolation between the primary and secondary coils. The value is,

$$\frac{H_i}{H_o}\,(\text{leakage}) \approx (7.8 - 4.8) \times 10^{-6} = 3.0 \times 10^{-6}$$

The above copper box was used as a specimen in a test made at liquid helium temperatures to determine if transmission through a passive specimen varied with magnetic field. The results of this experiment are shown in Fig. 5-9. At 4.2°K the skin depth, δ, of the polycrystalline copper is approximately 1 mil. Therefore, the expected "theoretical" transmission ratio through the copper walls is approximately

Temperature	Experimental Transmission Ratio	Theoretical Transmission Ratio
R.T	1.5×10^{-3}	1.6×10^{-3}
N_2	7.8×10^{-6}	4.8×10^{-6}

Table 5-2. Comparison of Theoretical and "Experimental" Transmission Ratios for a 5 mil Copper Box

Fig 5-9

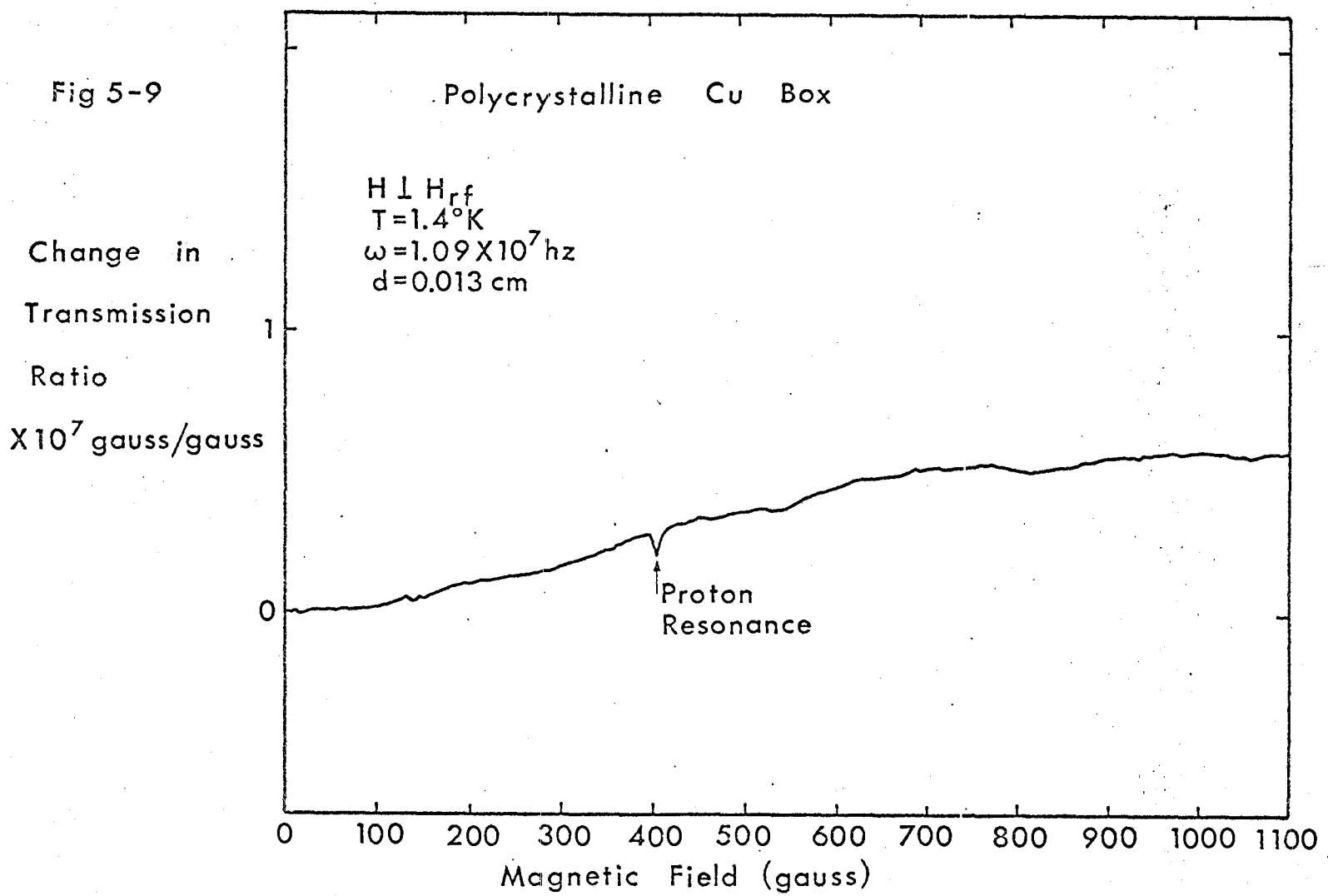
Polycrystalline Cu Box
H ⊥ H_rf
T=1.4°K
ω=1.09X10^7 hz
d=0.013 cm
Change in Transmission Ratio X10^7 gauss/gauss
1
0
Proton Resonance
0 100 200 300 400 500 600 700 800 900 1000 1100
Magnetic Field (gauss)

4×10^{-11}. Since the mean free path is so short in polycrystalline copper, one expects to see no variation with magnetic field in the transmission through the 5 mil thick walls. The increase in signal which is observed in Fig. 5-9 represents a change in transmission, ΔT, of approximately 5×10^{-8}. This small change is probably due to the change in primary inductance or in the secondary Q value. These parameters would only have to change by 1 part in 10^7 to give the observed change in signal level.

5.4 Preparation of Gallium Single Crystals

The gallium crystals were prepared from 99.9999% pure gallium supplied by Alcoa International Ltd., Toronto, Ontario, using a method similar to that described by Yaqub and Cochran[49]. The gallium, since it has a melting point of 29.8°C, was easily liquified and then injected, by means of a syringe, into a Plexiglass mould. The liquid quickly cooled below the melting point forming a super-cooled liquid. A seed crystal having the desired orientation was then brought into contact with the liquid in order to begin crystallization. The seed crystal had been mounted on a goniometer and aligned by means of Laue back reflection photographs. It was possible to align the crystallographic axes parallel to the specimen edges to within 1° of arc. X-ray photographs of typical crystal orientations, using Cu K-α radiation and a film to specimen distance of 3 cm are shown in Fig. 5-10. The notation used is indicated in the figures.

After the gallium had crystallized, the mould with the crystal was placed in a bath of isopropyl alcohol for several hours. The isopropyl alcohol had the effect of releasing the gallium crystal from the mould. Special care was taken to avoid scratching or bending the crystals. Crystals with mirror smooth surfaces were obtained in this way. The same procedure was followed both for specimens in the shape of slabs and specimens in the form of hollow boxes.

In the case of the hollow box crystals the center section around which the specimen was formed was constructed of five sections. A solid rectangular rod of Plexiglass formed the core. Four thin rectangular slabs of Plexiglass were then placed tightly about this central section. This geometry enabled one to pull out the center core after the gallium had crystallized. The thin rectangular slabs could then be removed from the inner walls of the crystal or if this proved difficult the thin slabs were dissolved away in acetone to avoid the risk of damaging the specimen.

Fig 5-10. Laue Back Reflection Photographs of Three Oriented Crystals

A_B Crystal

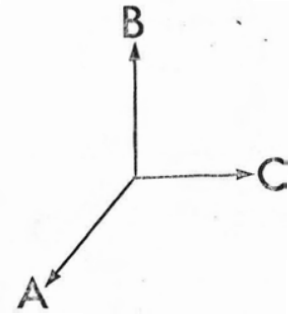

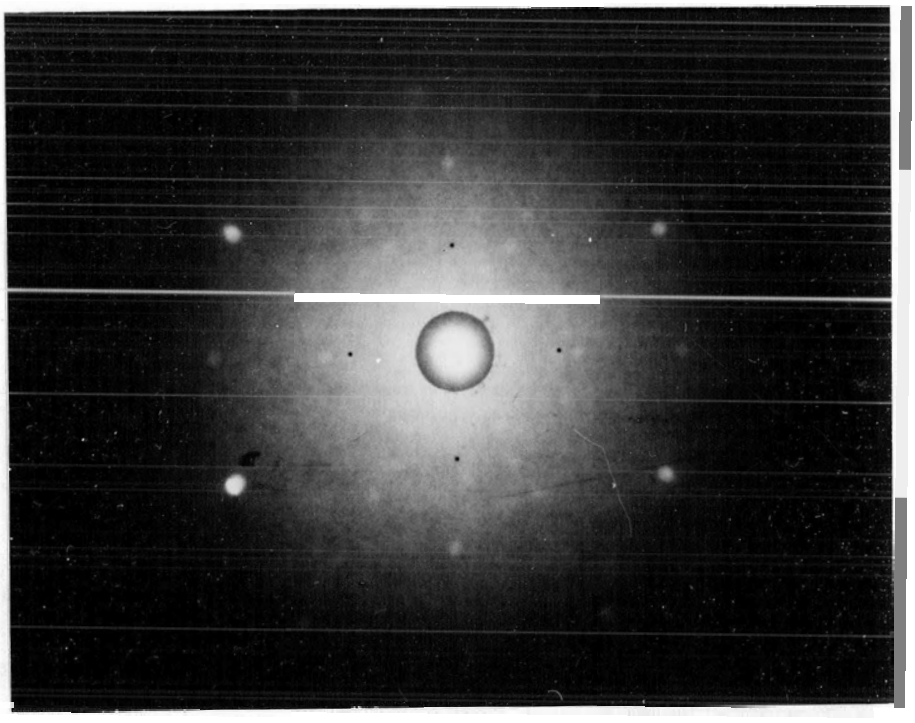

B_C Crystal

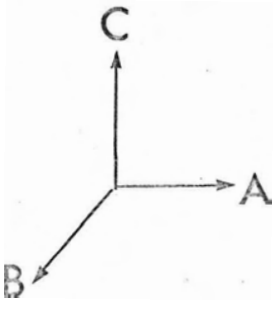

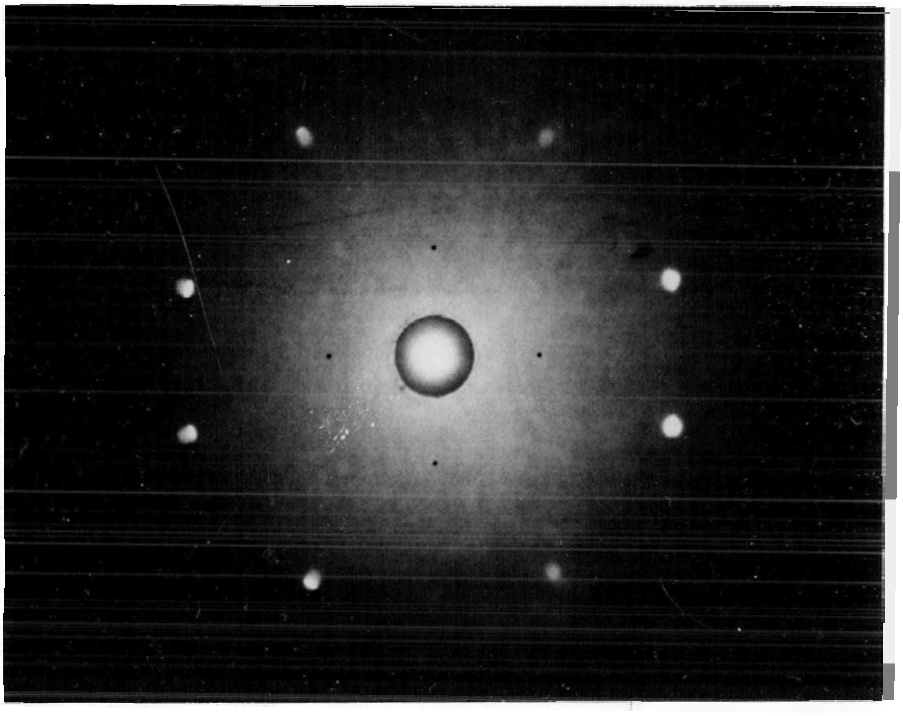

Fig 5-10 cont'd

C_B Crystal

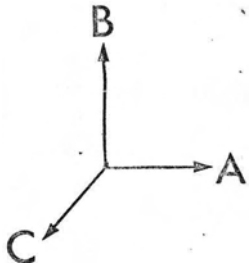

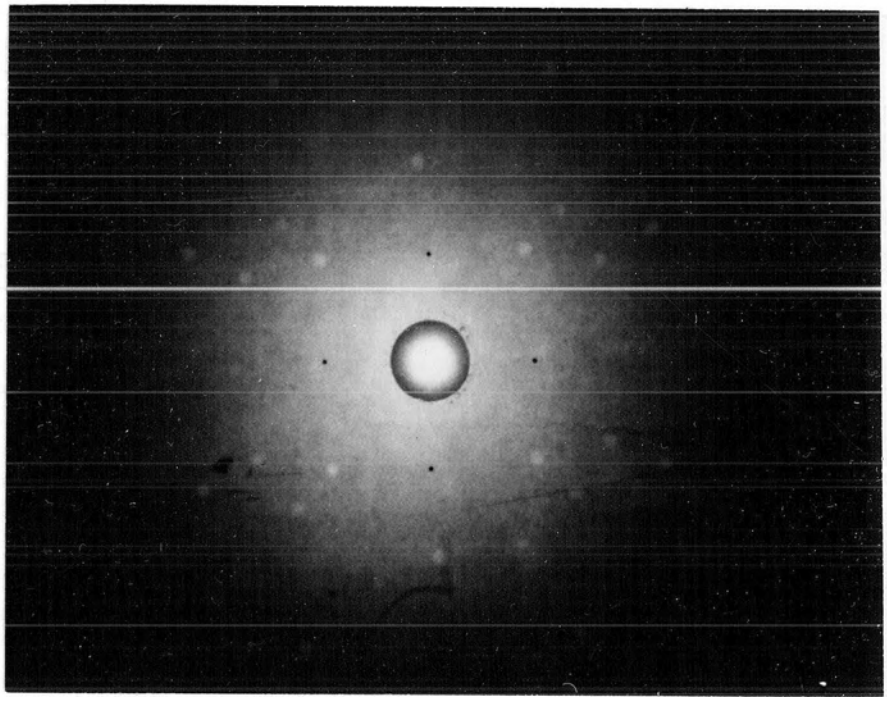

Chapter 6

EXPERIMENTAL RESULTS

6.1 Comments on Specimen Configuration

In discussing the results obtained using gallium single crystals, a notation for labelling each crystal unambiguously was established. A crystal labelled X_y indicates that the X-axis of the crystal is parallel to the normal to the surface of the slab, whereas, the Y-axis is along the length of the crystal. In our experimental arrangement the Y-axis was always parallel to the direction of the radio frequency magnetic field.

It was mentioned in section 5.1 that three specimen configurations were used to test the transmission technique. Briefly, these were,

a) a hollow box made of a continuous piece of single crystal gallium,

b) a box identical to the above except that the three thick sides were electroplated with copper,

c) a hollow box formed by soldering a rectangular slab of single crystal gallium to a rectangular trough made of high purity polycrystalline copper.

The first method, using a continuous piece of single crystal gallium, was found inappropriate for the following reason. Because of the long mean free path in high purity gallium at low temperatures (of the order of several centimeters),

transmission solely from the thin side was obscured by radiation penetrating the thick walls. Penetration of the radio frequency radiation occurred even though the thicknesses of these sides were approximately four times that of the thin side.

An attempt was made to eliminate transmission through the thick sides of the box by electroplating them with copper of a sufficient thickness to shield the gallium from the radio frequency radiation. By comparison with data taken using the third method, it was found that perfect shielding for all magnetic field orientations was not always possible even though the gallium surfaces were clean and a freshly prepared copper sulphate solution was used. The copper did not always short out the radio frequency currents flowing in the gallium because of the resistance between the gallium and the copper layers.

The third method, whereby gallium slabs were soldered to a three-sided copper trough, provided the desired unambiguous transmission versus magnetic field curves. As mentioned in section 5.3, there were no peaks in transmission which could be attributed to the copper trough. The following figures, except where noted otherwise, illustrate the results obtained using this method of mounting the crystals.

It was noticed during the experimental investigation

that certain crystal orientations had a tendency to crack when the crystal and copper trough were cooled to liquid nitrogen temperatures. These crystals had the C-axis perpendicular to the slab surface (called C crystals). An examination of X-ray photographs of the seam between the copper and gallium revealed that the gallium solder puddle assumed an orientation different from that of the crystal. Since the coefficient of thermal expansion is quite different for various principle directions in gallium[35], stresses are created along the seam at low temperatures. Table 6-1 gives these coefficients for the temperature range 297°K to 78°K (reference Barrett[35]). These stresses were evidently large enough to cause the crystal to crack. To minimize this problem a technique was developed in which the gallium solder puddles along the trough edges were kept at a temperature just above the melting point. The crystal slab was then lowered onto the trough such that the solder puddle and crystal made intimate contact. Because of the latent heat of the rectangular slab, the molten pools of gallium solidified, taking the orientation of the slab without destroying the specimen.

6.2 Magnetic Field Parallel to the Slab Surface and Parallel to the Radio Frequency Magnetic Field

When the static magnetic field is applied parallel to the sample surface and parallel to the radio frequency

AXIS DIRECTION	Mean Coefficient of Thermal Expansion ($°K^{-1}$) α (297°K → 78°K)
a	-3.7×10^{-6}
b	-3.3×10^{-5}
c	-1.6×10^{-5}

Table 6-1. Coefficient of Thermal Expansion in the Temperature Range 297°K → 78°K

$$\alpha = \frac{\Delta L}{L_o \Delta T} \quad °K^{-1}$$

(reference Barrett[35])

magnetic field, Gantmakher resonances can occur (see section 2.1). The experimental results for this field geometry are given in Figures 6-1 to 6-22 (page 99). The change in transmission ratio has been plotted as a function of applied magnetic field strength.

These sharp changes in transmission are superimposed upon a variation due to the skin depth. To first order one might expect this background to be similar to that observed by Cochran and Shiffman[6].

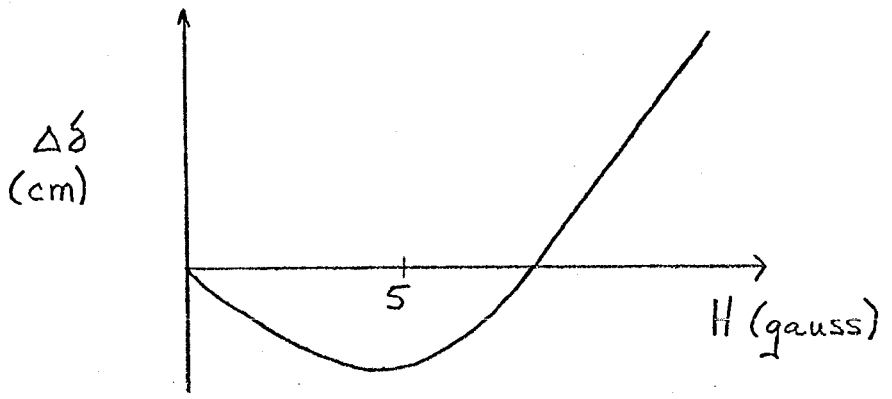

Indeed, this general behaviour of the background is noticed in all the crystals examined.

Fig. 6-6 and 6-8 have been included to illustrate the effect of re-examining a crystal after it has been stored in a jar of isopropyl alcohol in a refrigerator for a period of approximately 6 months. These results are to be compared with Fig. 6-5 and Fig. 6-7 which were obtained from the same crystal but taken after it had been freshly prepared. It is

clear that much detail has disappeared in the case of the refrigerated crystal.

Fig. 6-21 and 6-22 illustrate typical results obtained using a solid gallium box crystal whose thick sides have been electroplated with copper. These results are to be compared with Fig. 6-19 and 6-20 which are the results obtained using the standard method of mounting a rectangular slab on a rectangular copper trough (Note: the thicknesses of the crystals for these two cases are different). Although certain transmission features appear in the diagrams using both methods, it is clear that these methods do not give identical results.

Before proceeding further, it should be emphasized that this experiment does not measure the derivative of the transmitted signal but the signal itself. Most of the previous surface impedance measurements have used a modulation technique and therefore measure a derivative with respect to magnetic field. Consequently, a comparison of our results with this data will necessarily be indirect. Koch and Wagner[28] have demonstrated that for computation purposes the position in magnetic field of a transmission peak or Gantmakher resonance should be measured at the leading edge of a resonance derivative. This position, B_o, is illustrated in Fig. 6-23 (after Lyall[56]) which shows an example of a Gantmakher resonance in a gallium A_c crystal. It is also

customary to measure the width of a resonance line, ΔB_o, from peak to peak. Again, this convention is illustrated in Fig. 6-23. For comparison purposes then, a derivative of our direct signal was estimated and from this derivative, values of H_o and ΔH determined.

The lowest field Gantmakher resonances in A_B and A_C crystals have been observed by Cochran and Shiffman[6], Haberland, Cochran, and Shiffman[40], and Lyall[56]. A comparison of the position of the resonance in magnetic field and also of the line width of the resonance is presented in Tables 6-2 and 6-3. Since the position of a resonance in magnetic field will scale with the thickness of the specimen, we have computed the quantity $H_o d$. This value should be constant as predicted by the relation,

$$\Delta k_{ext} = 0.15194 \times 10^8 \, H_o d \quad cm^{-1}$$

With regard to the line width, it is known that the resonance will have a fractional width,

$$\frac{\Delta H}{H_o} \approx \frac{\delta}{d}$$

Therefore the quantity $\frac{\Delta H}{H_o} \frac{d}{\delta} \propto \frac{\Delta H}{H_o} d f^{1/3}$ should be constant. It is this latter quantity which has been used to compare line width data.

In section 2.1 it was shown how extremal dimensions of

Figures (6-1) to (6-22)

Transmission through gallium single crystals in which H_{rf} and the d.c. magnetic field are parallel. Note that the C_B crystal was twice as thick as the crystals used to obtain data for the other orientations.

$\underline{H_o \parallel H_{rf}}$

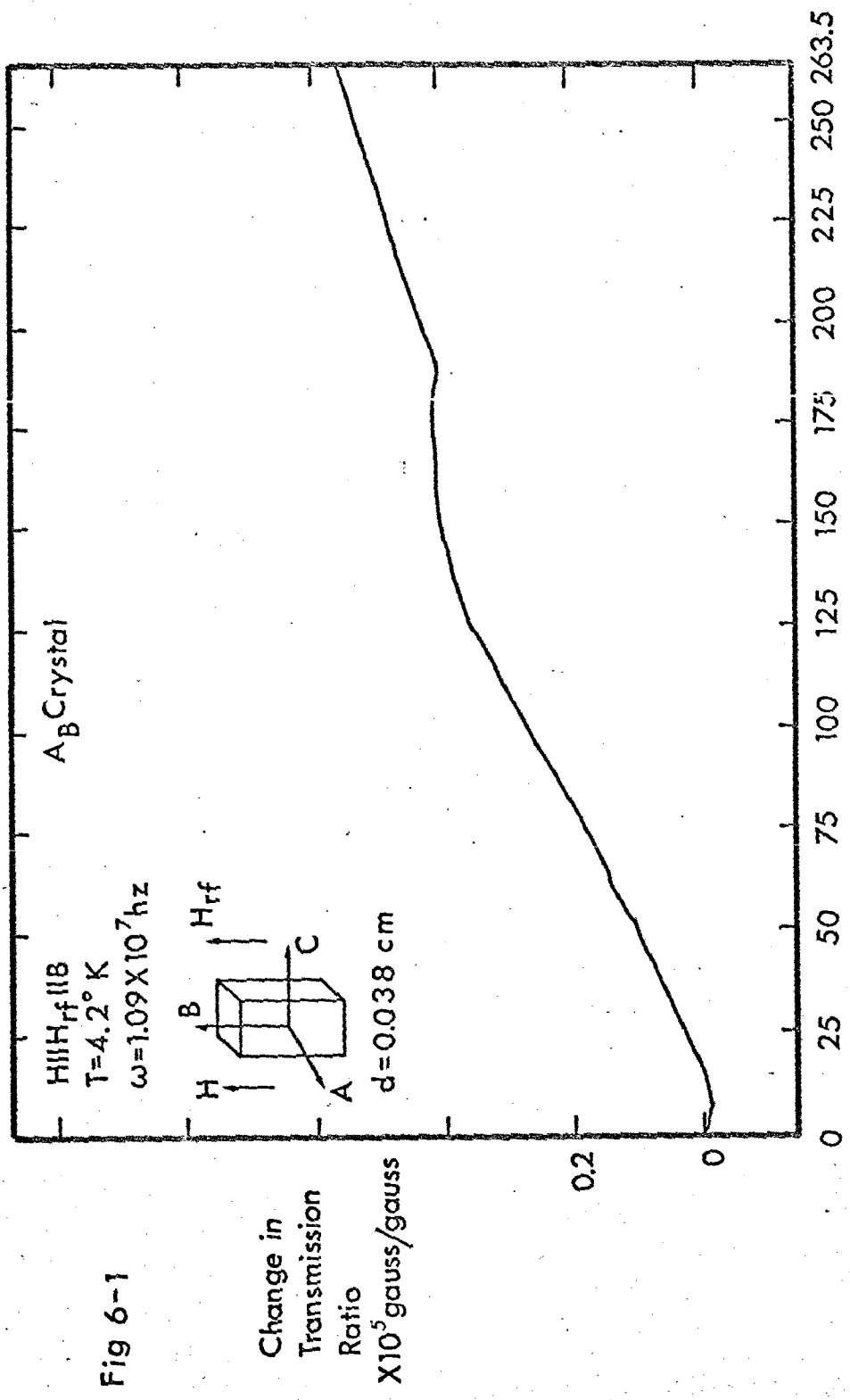
H||H_rf||B
T=4.2° K
ω=1.09X10^7 hz
A_B Crystal
H
H_rf
A
B
C
d=0.038 cm
Change in Transmission Ratio X10^5 gauss/gauss
0
0.2
0
25
50
75
100
125
150
175
200
225
250
263.5
Magnetic Field (gauss)

Fig 6-1

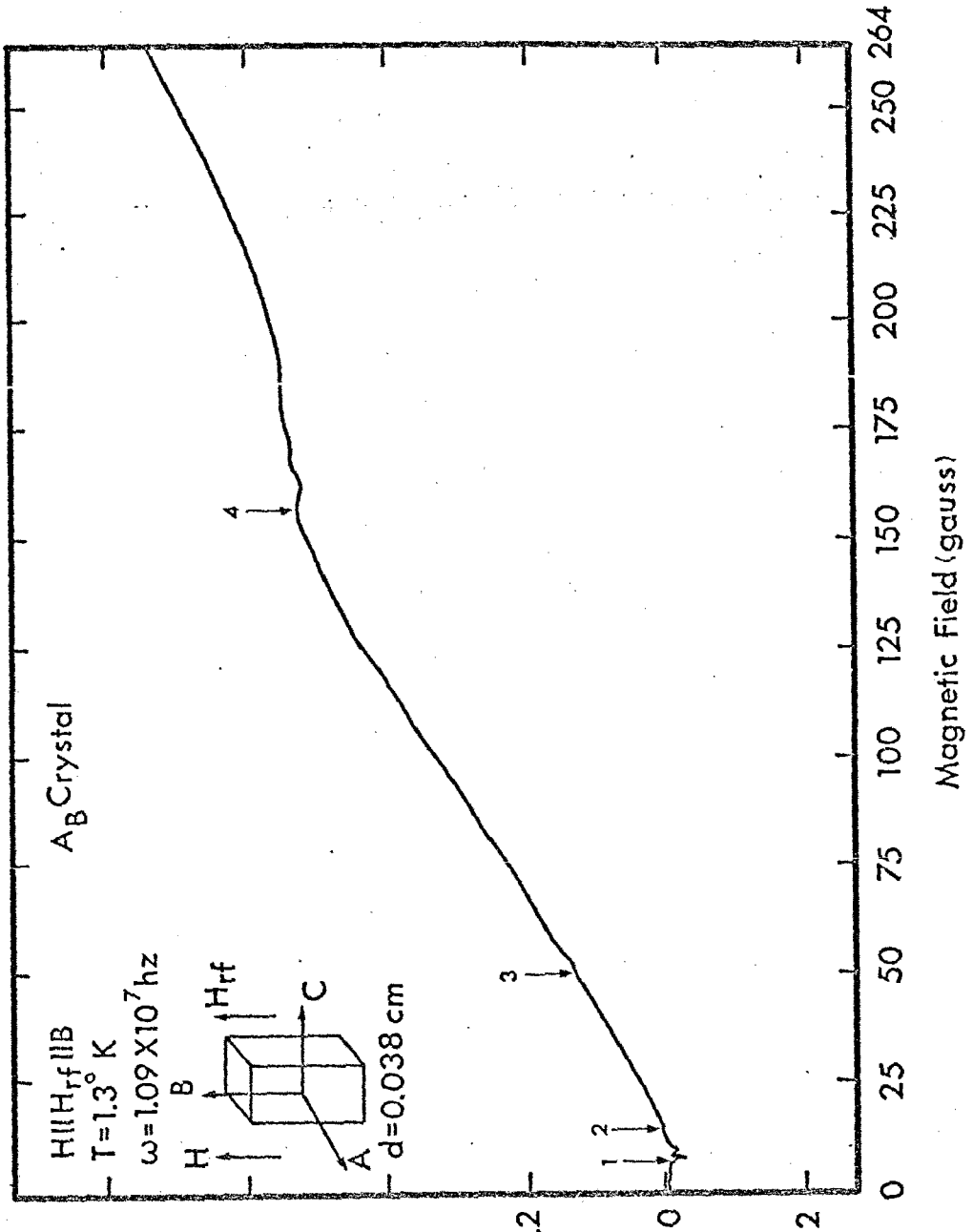
H||H_rf||B
T=1.3° K
ω=1.09 X10^7 hz
A_B Crystal
H
B
H_rf
C
A
d=0.038 cm
1
2
3
4
0.2
0
0.2
0
25
50
75
100
125
150
175
200
225
250
264
Magnetic Field (gauss)
Change in Transmission Ratio X10^5 gauss/gauss

Fig 6-2

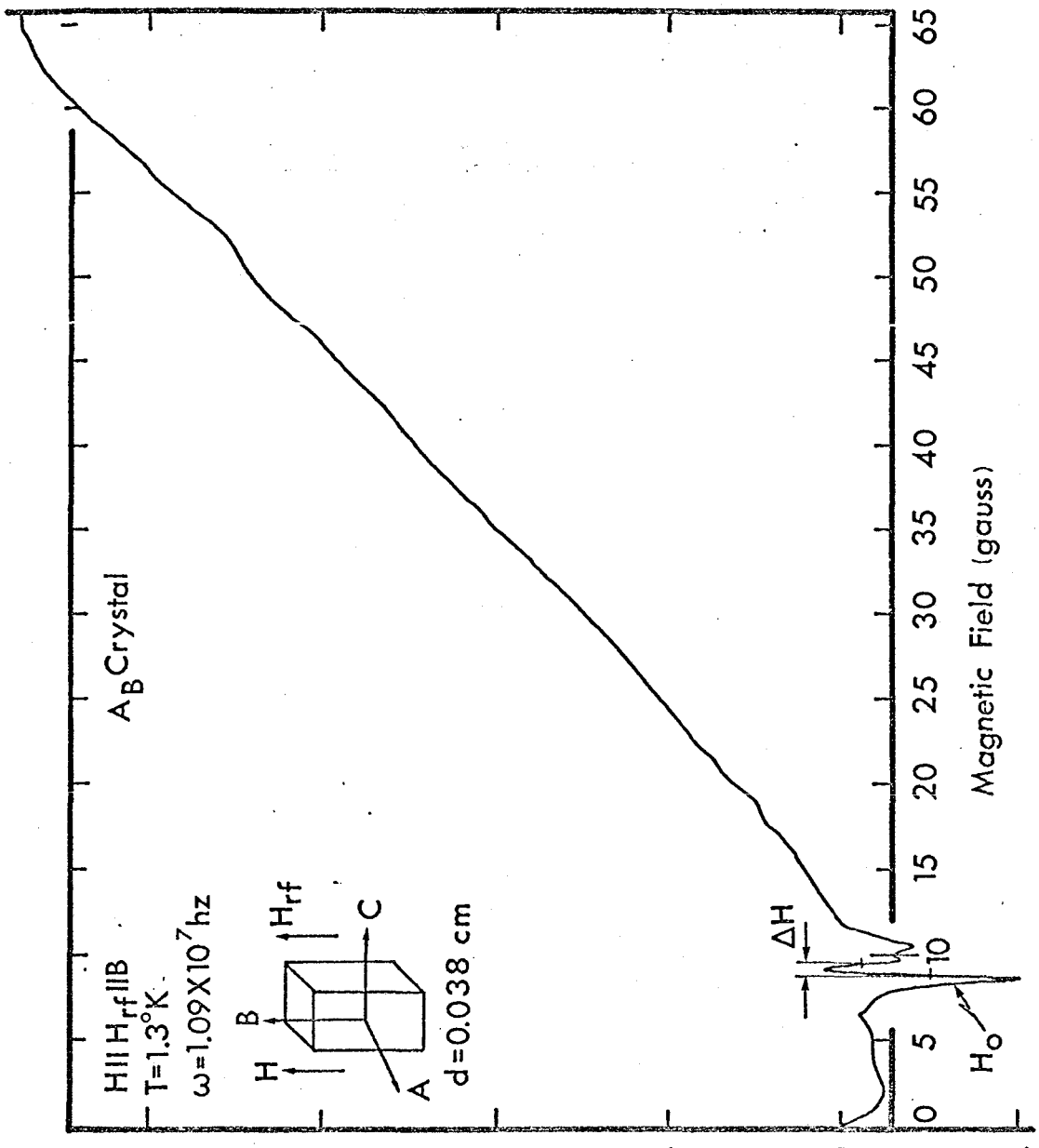
H II H_{rf} II B
T=1.3°K
ω=1.09X10⁷hz
A_B Crystal
H
B
H_{rf}
C
A
d=0.038 cm
ΔH
H_o
Change in Transmission Ratio X10⁶gauss/gauss
0.4
0
0.4
0
5
10
15
20
25
30
35
40
45
50
55
60
65
Magnetic Field (gauss)

Fig 6-3

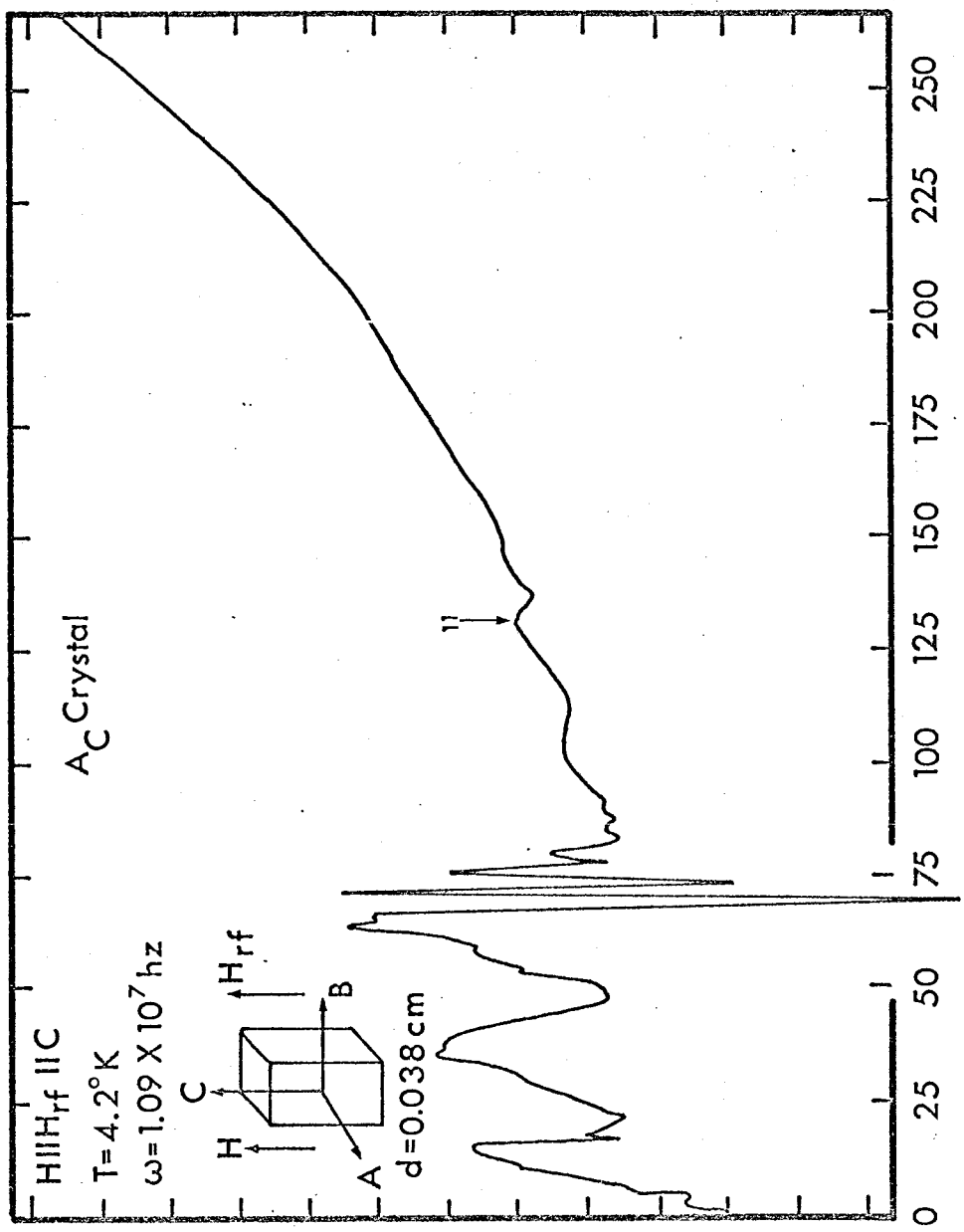
H||H$_{rf}$ ||C
T=4.2°K
ω=1.09 X 10^7 hz
A$_C$ Crystal
H
H$_{rf}$
C
B
A
d=0.038 cm
11
Change in Transmission Ratio X10^7 gauss/gauss
0.4
0
0.4
0
25
50
75
100
125
150
175
200
225
250
Magnetic Field (gauss)

Fig 6-4

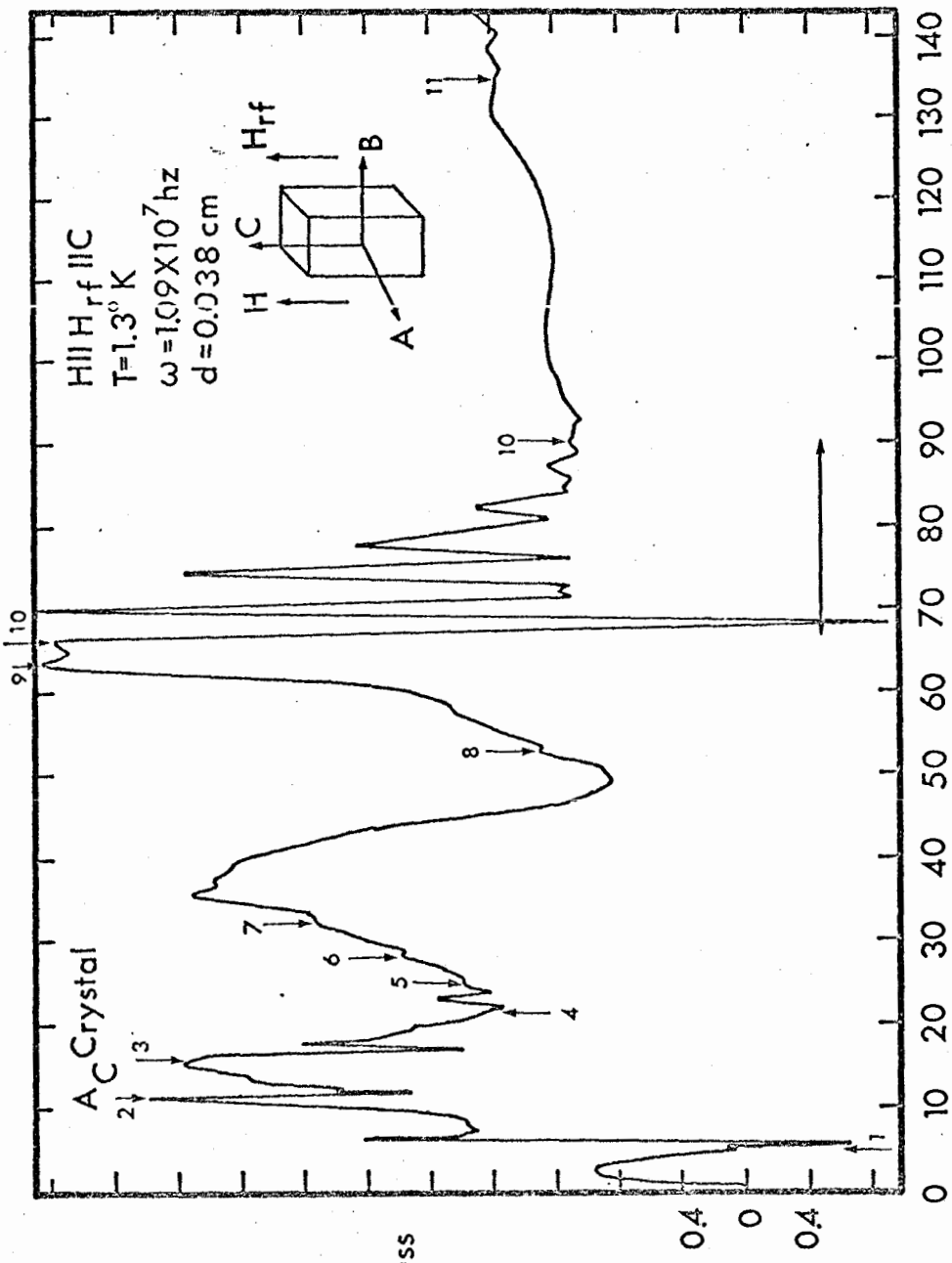
A_C Crystal
H∥H_rf⊥C
T=1.3° K
ω=1.09X10^7 hz
d=0.038 cm
H_rf
H
C
B
A
1
2
3
4
5
6
7
8
9
10
11
0
10
20
30
40
50
60
70
80
90
100
110
120
130
140
Magnetic Field (gauss)
0.4
0
0.4
Change in Transmission Ratio X10^7 gauss/gauss

Fig 6-5

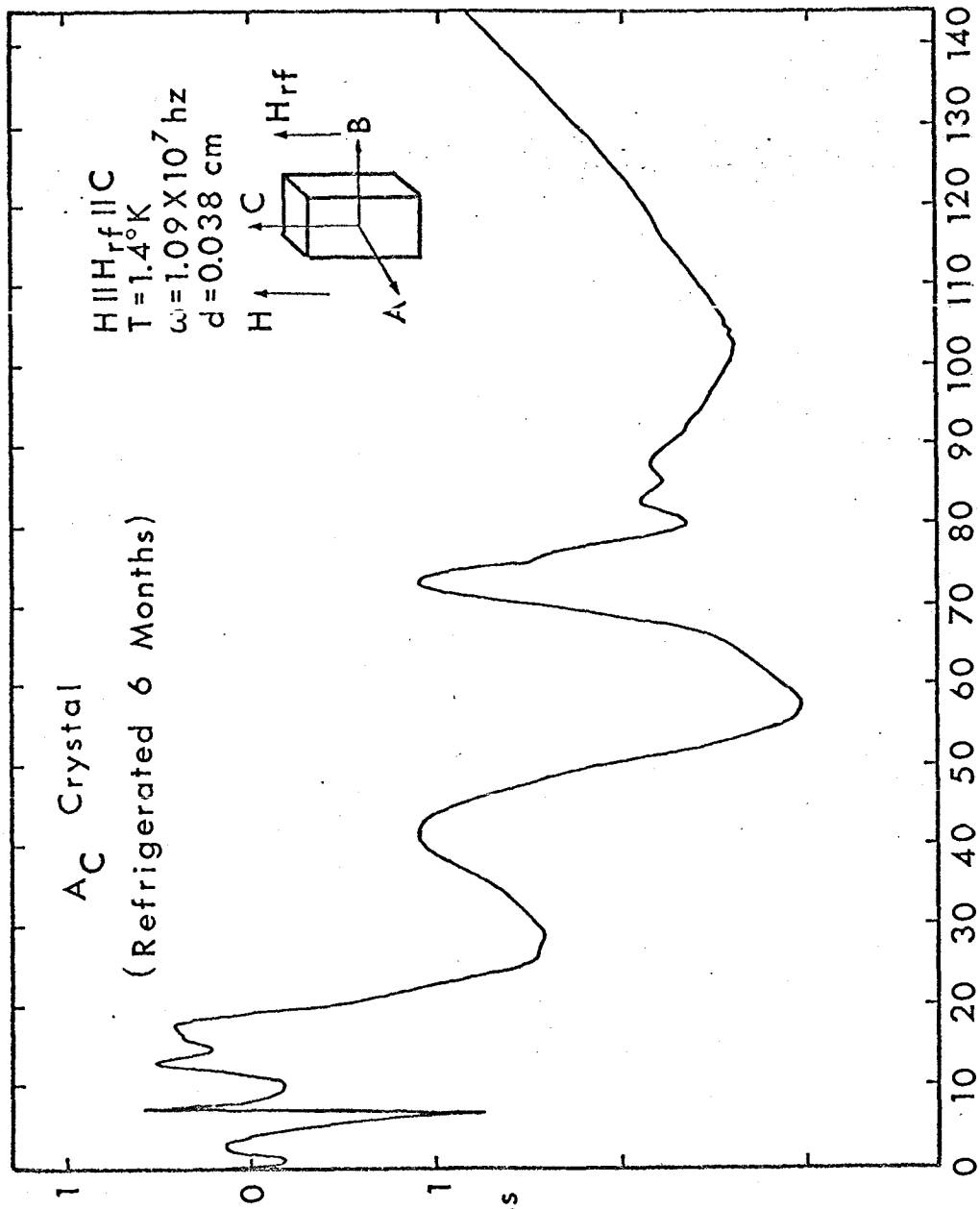
A_C Crystal
(Refrigerated 6 Months)
H||H_rf||C
T=1.4°K
ω=1.09X10^7 hz
d=0.038 cm
H
C
H_rf
B
A
1
0
1
0 10 20 30 40 50 60 70 80 90 100 110 120 130 140
Magnetic Field (gauss)
Change in Transmission Ratio X10^7 gauss/gauss

Fig 6-6

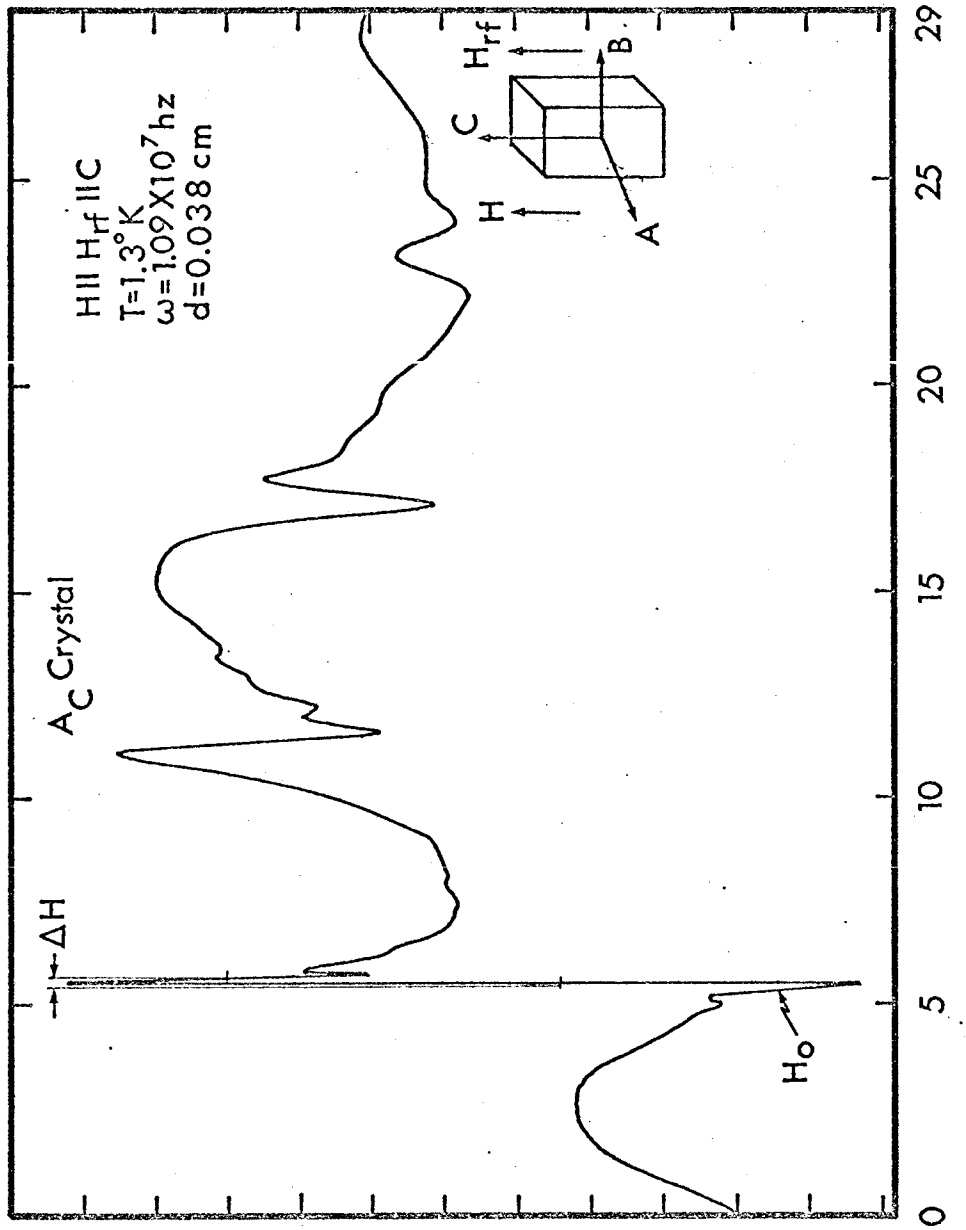
H ll H_{rf} llC
T=1.3°K
ω=1.09X10⁷hz
d=0.038 cm
A_C Crystal
-ΔH
H_o
H
C
H_{rf}
B
A
Change in Transmission Ratio X10⁷ gauss/gauss
0.4
0
0.4
0
5
10
15
20
25
29
Magnetic Field (gauss)

Fig 6-7

Fig 6-8

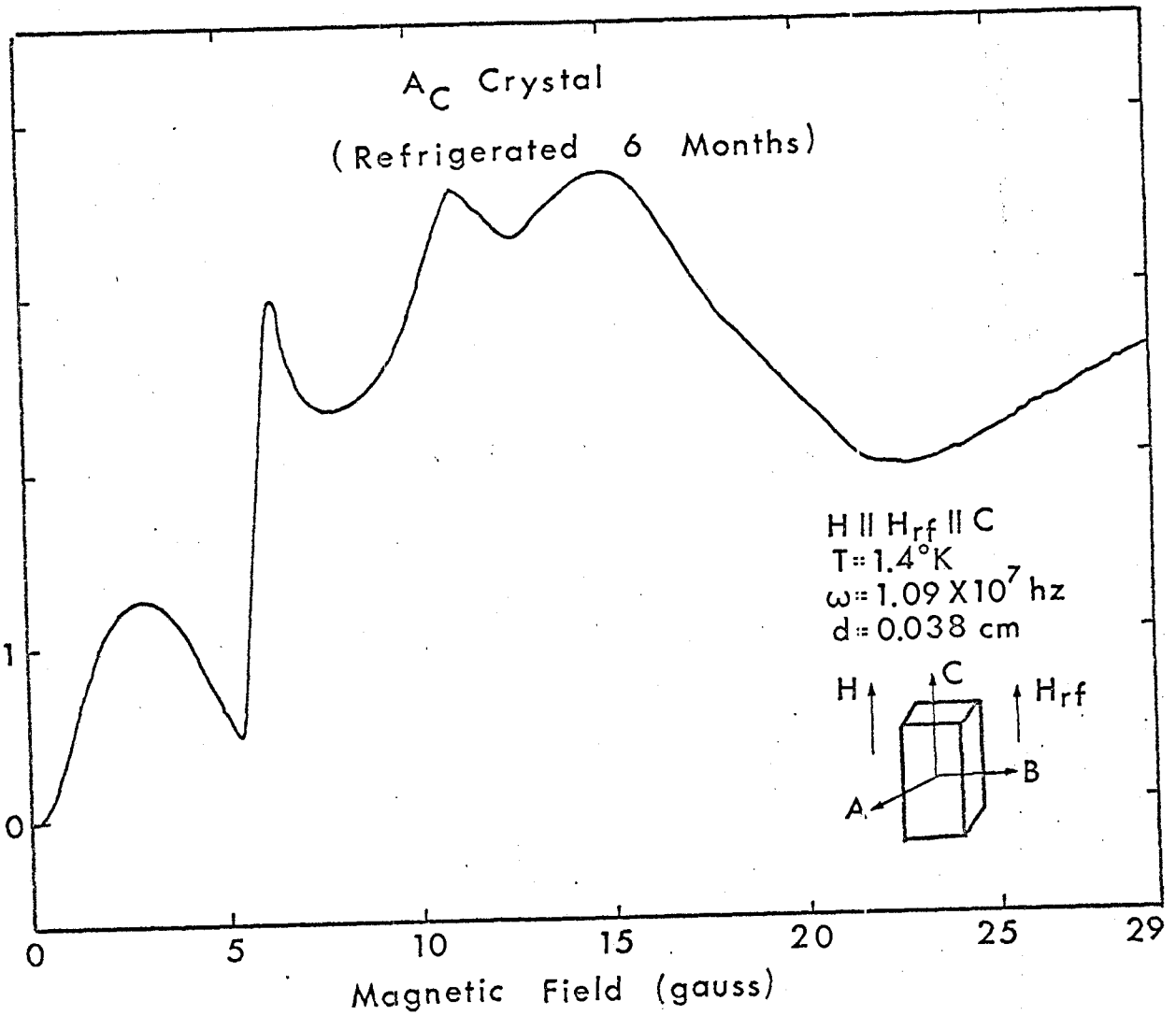
A_C Crystal
(Refrigerated 6 Months)
Change in Transmission Ratio
X 10^7 gauss/gauss
1
0
0
5
10
15
20
25
29
Magnetic Field (gauss)
H ∥ H_{rf} ∥ C
T = 1.4°K
ω = 1.09 X 10^7 hz
d = 0.038 cm
H
C
H_{rf}
B
A

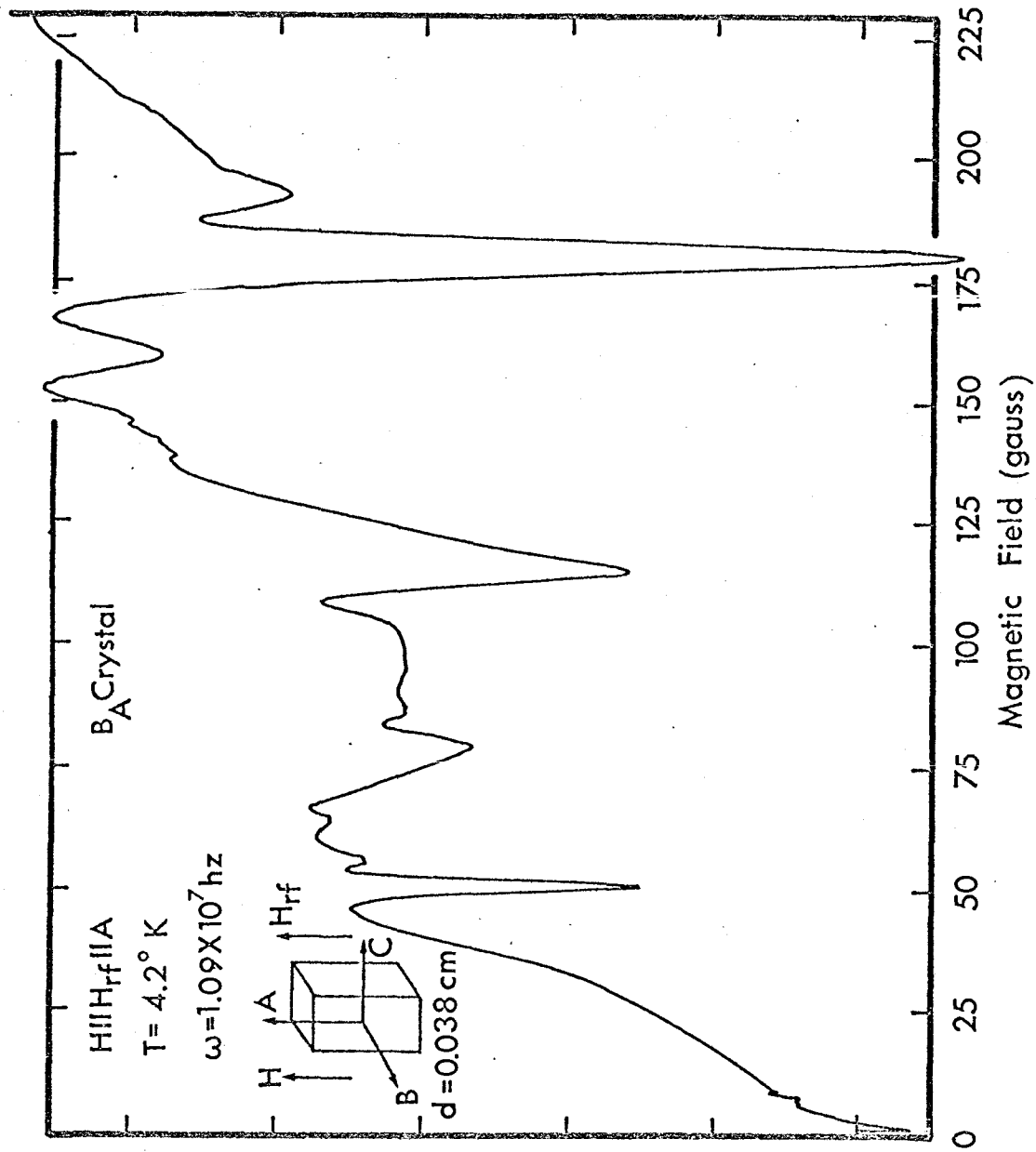
H∥H_rf∥A
T= 4.2° K
ω=1.09X10^7 hz
B_A Crystal
H
A
H_rf
C
B
d=0.038 cm
Change in Transmission Ratio X10^7 gauss/gauss
0.4
0
0
25
50
75
100
125
150
175
200
225
Magnetic Field (gauss)

Fig 6-9

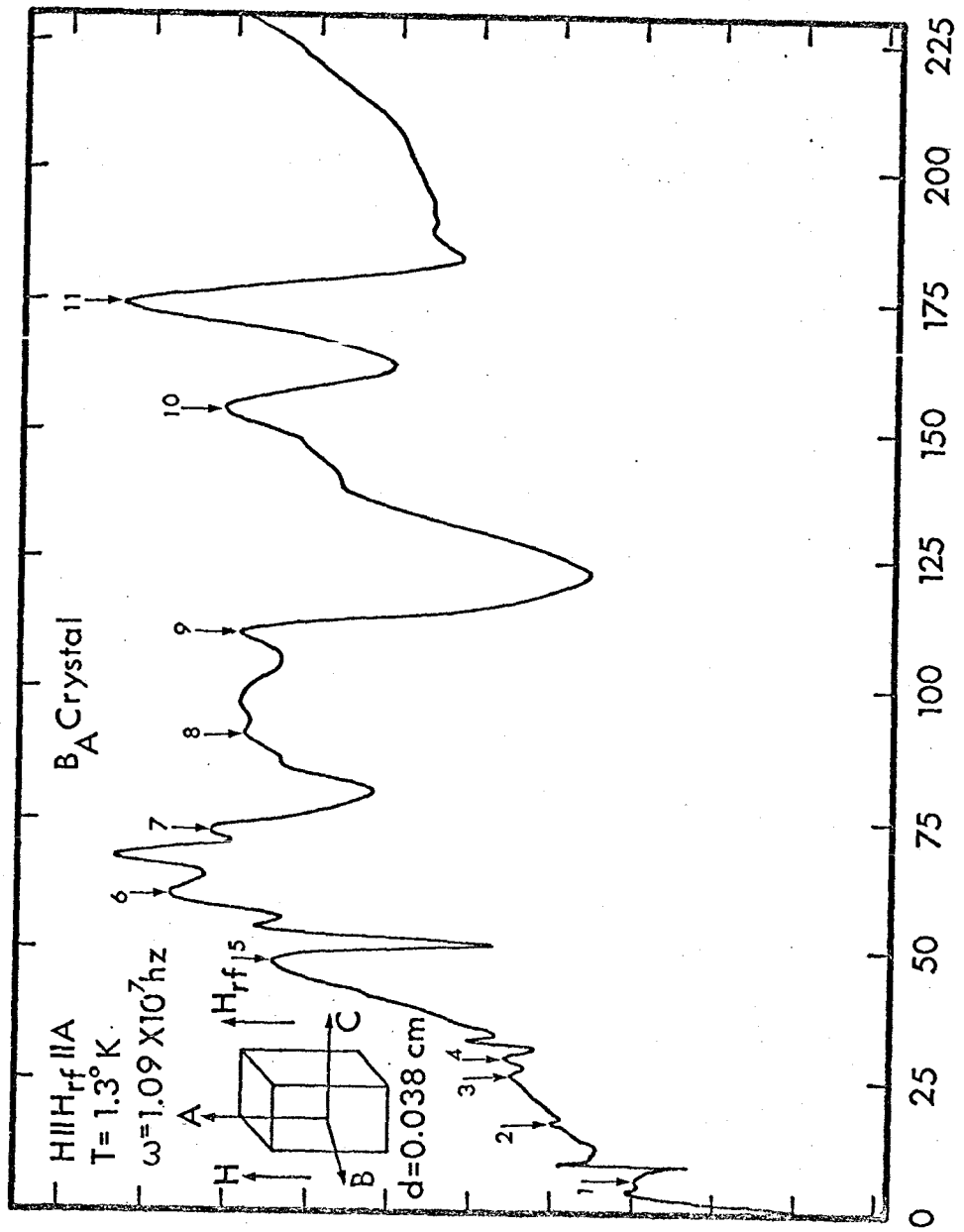
H∥H$_{rf}$∥A
T= 1.3° K
ω=1.09 X10^{7}hz
B$_A$Crystal
H$_{rf}$
A
B
C
H
d=0.038 cm
1
2
3
4
5
6
7
8
9
10
11
0.4
0
0.4
0
25
50
75
100
125
150
175
200
225
Change in Transmission Ratio X10^{7}gauss/gauss
Magnetic Field (gauss)

Fig 6-10

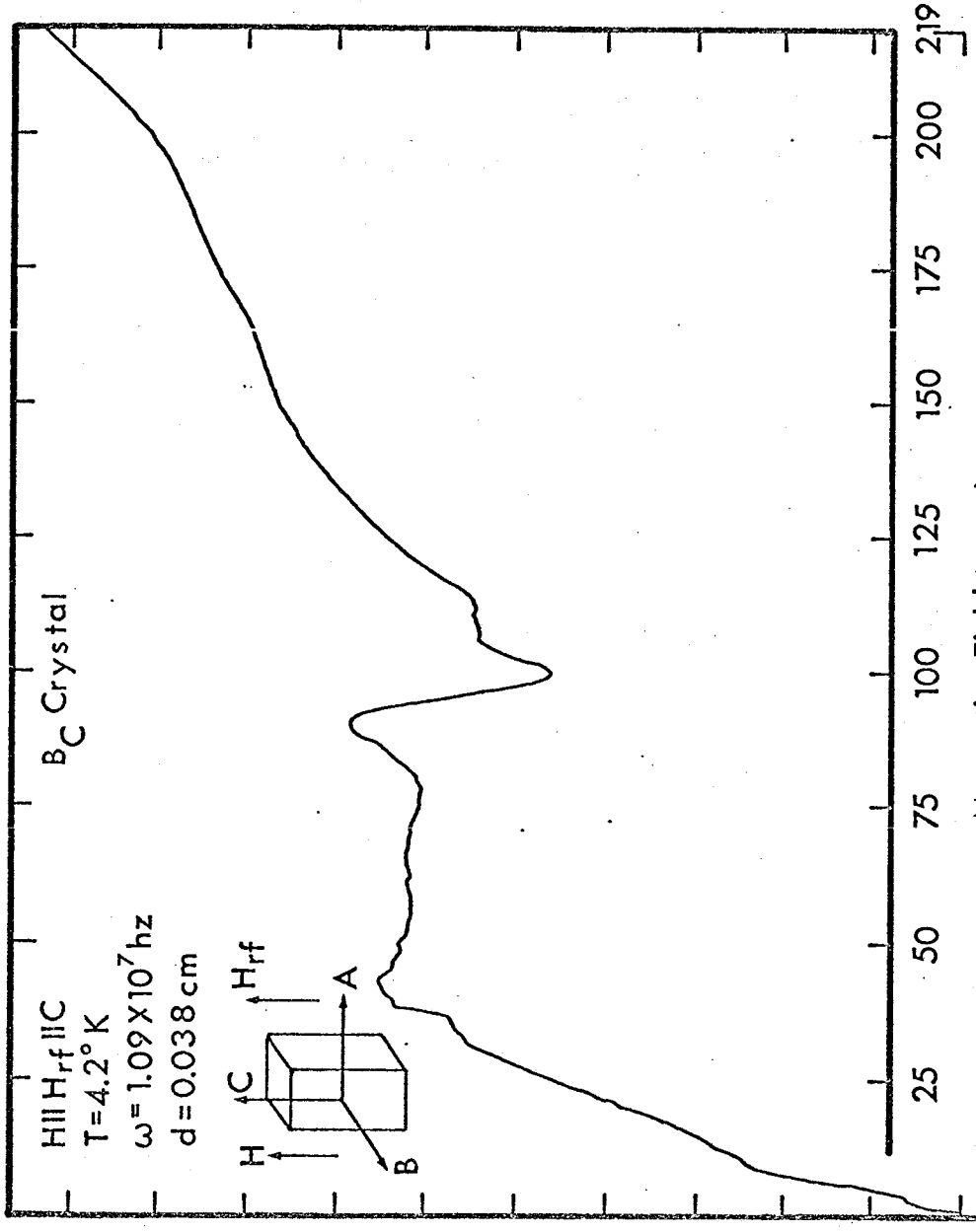
H∥H$_{rf}$∥C
T=4.2° K
ω= 1.09X10^{7}hz
d=0.038 cm
B$_C$ Crystal
H
C
H$_{rf}$
A
B
Change in Transmission Ratio X10^{7}gauss/gauss
0.4
0
0
25
50
75
100
125
150
175
200
219
Magnetic Field (gauss)

Fig 6-11

Fig 6-12

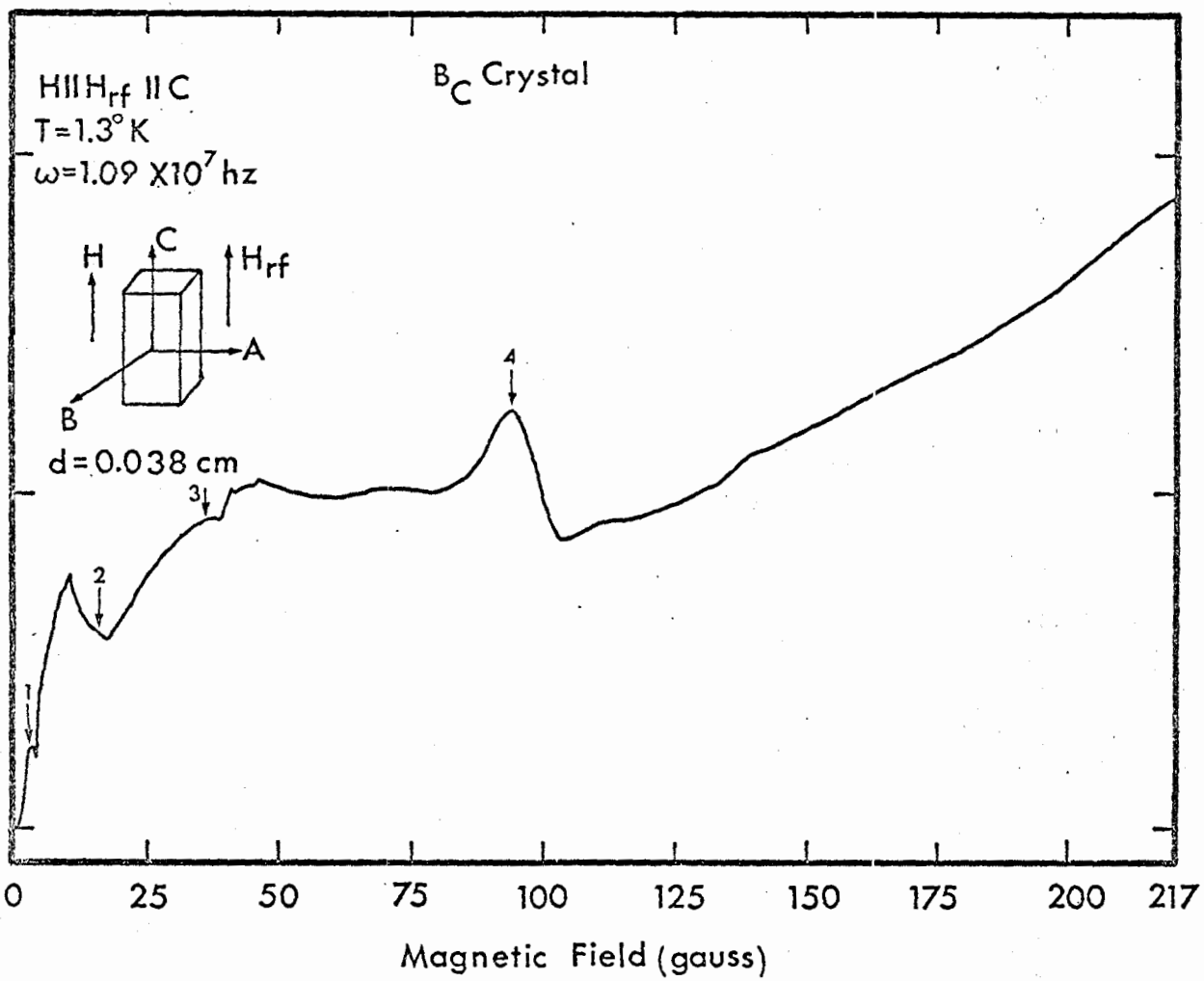
H||H_rf ||C
T=1.3° K
ω=1.09 X10^7 hz
B_C Crystal
H
C
H_rf
A
B
d=0.038 cm
Change in
Transmission
Ratio
X 10^6 gauss/gauss
0.4
0
1
2
3
4
0
25
50
75
100
125
150
175
200
217
Magnetic Field (gauss)

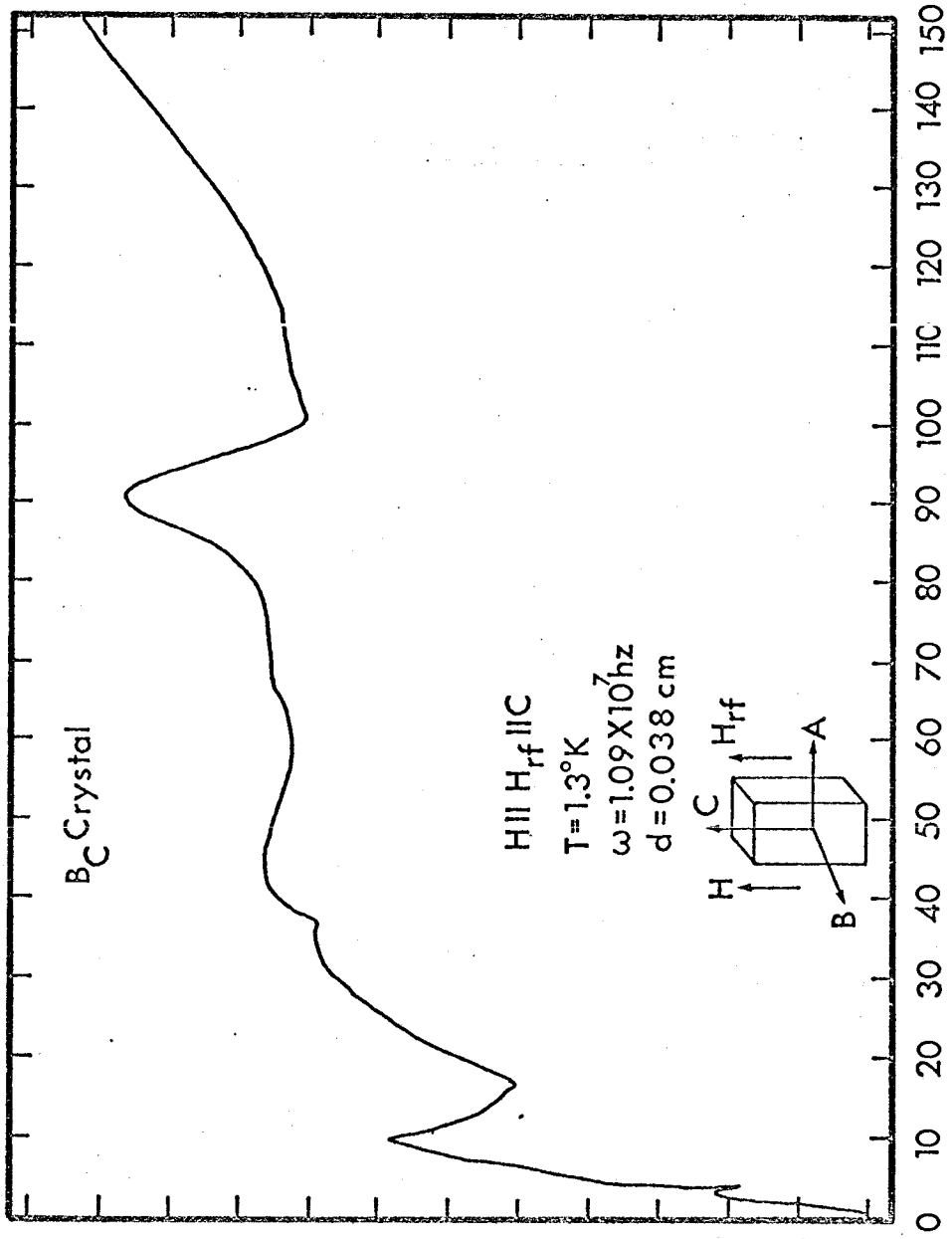
B_C Crystal
H II H_{rf} II C
T=1.3°K
ω=1.09X10⁷hz
d=0.038 cm
H
C
H_{rf}
A
B
0.4
0
0 10 20 30 40 50 60 70 80 90 100 110 120 130 140 150
Magnetic Field (gauss)
Change in Transmission Ratio X10⁷gauss/gauss

Fig 6-13

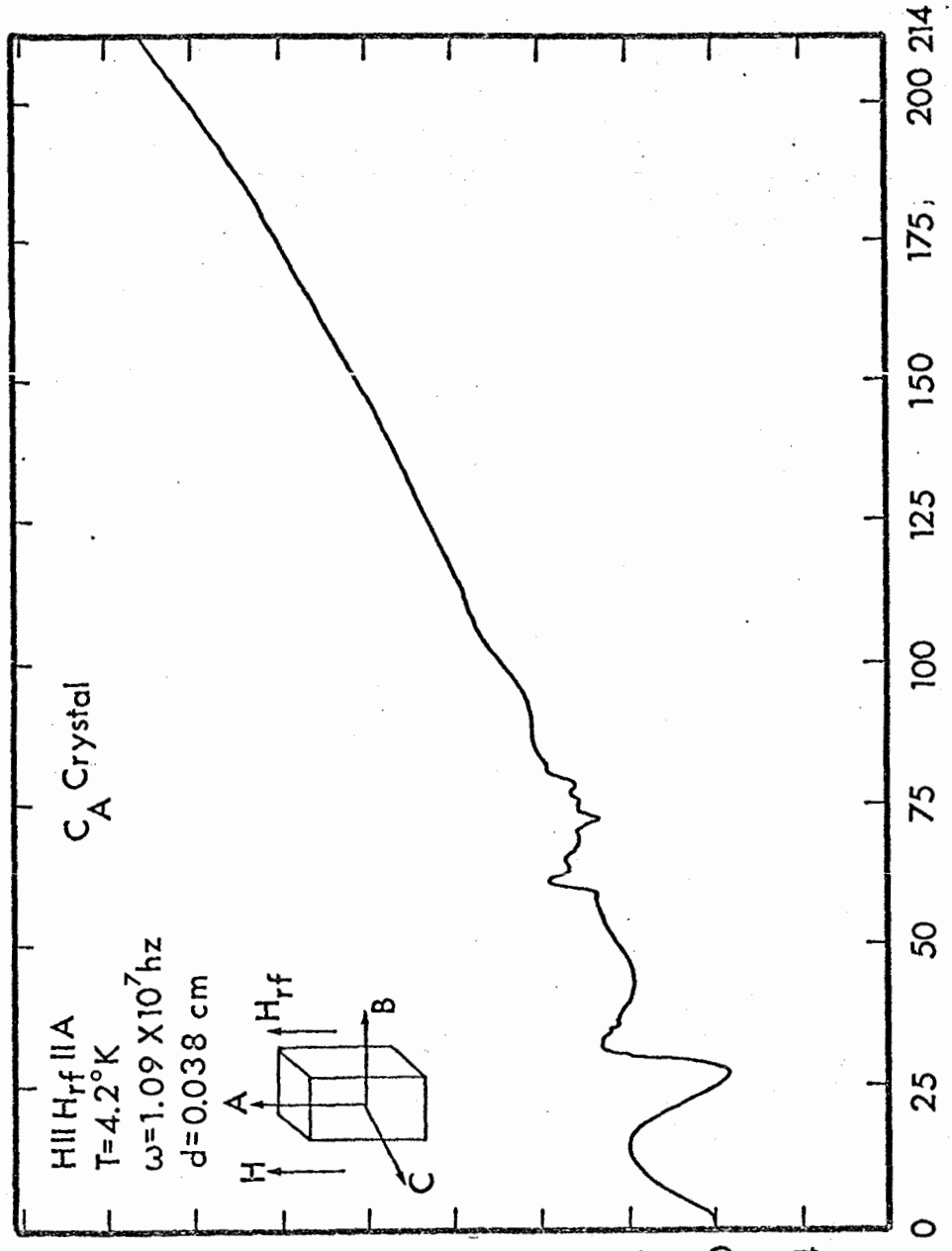
H∥ H_{rf} ∥A
T=4.2°K
ω=1.09 X10^{7}hz
d=0.038 cm
C_A Crystal
H
A
H_{rf}
B
C
Change in Transmission Ratio X10^{7}gauss/gauss
0.4
0
0.4
0
25
50
75
100
125
150
175
200 214
Magnetic Field (gauss)

Fig 6-14

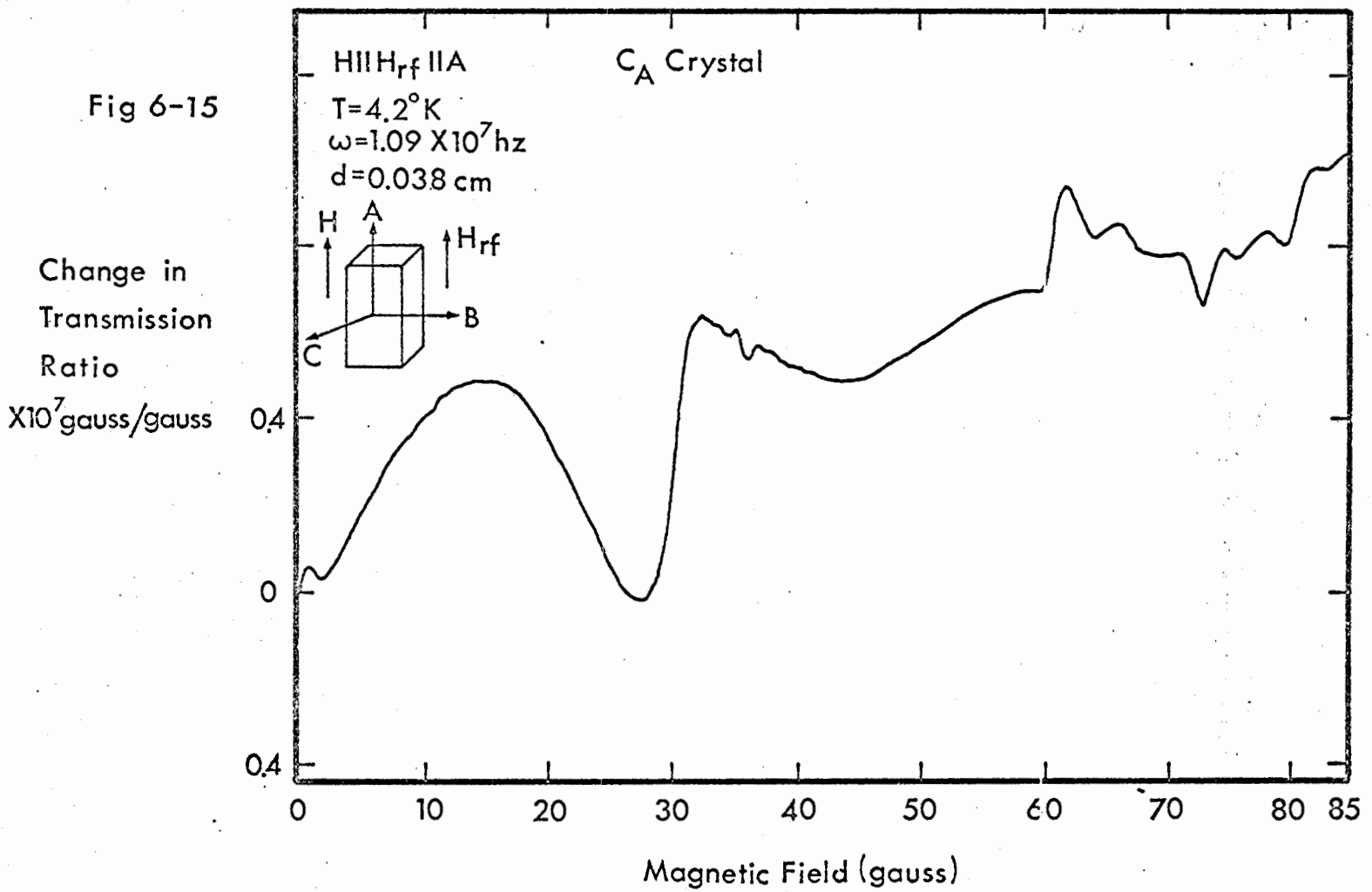
H ∥ H_{rf} ∥ A
C_A Crystal
T=4.2°K
ω=1.09 X10⁷hz
d=0.038 cm
H
A
H_{rf}
B
C
Change in Transmission Ratio X10⁷gauss/gauss
0.4
0
0.4
0
10
20
30
40
50
60
70
80
85
Magnetic Field (gauss)

Fig 6-15

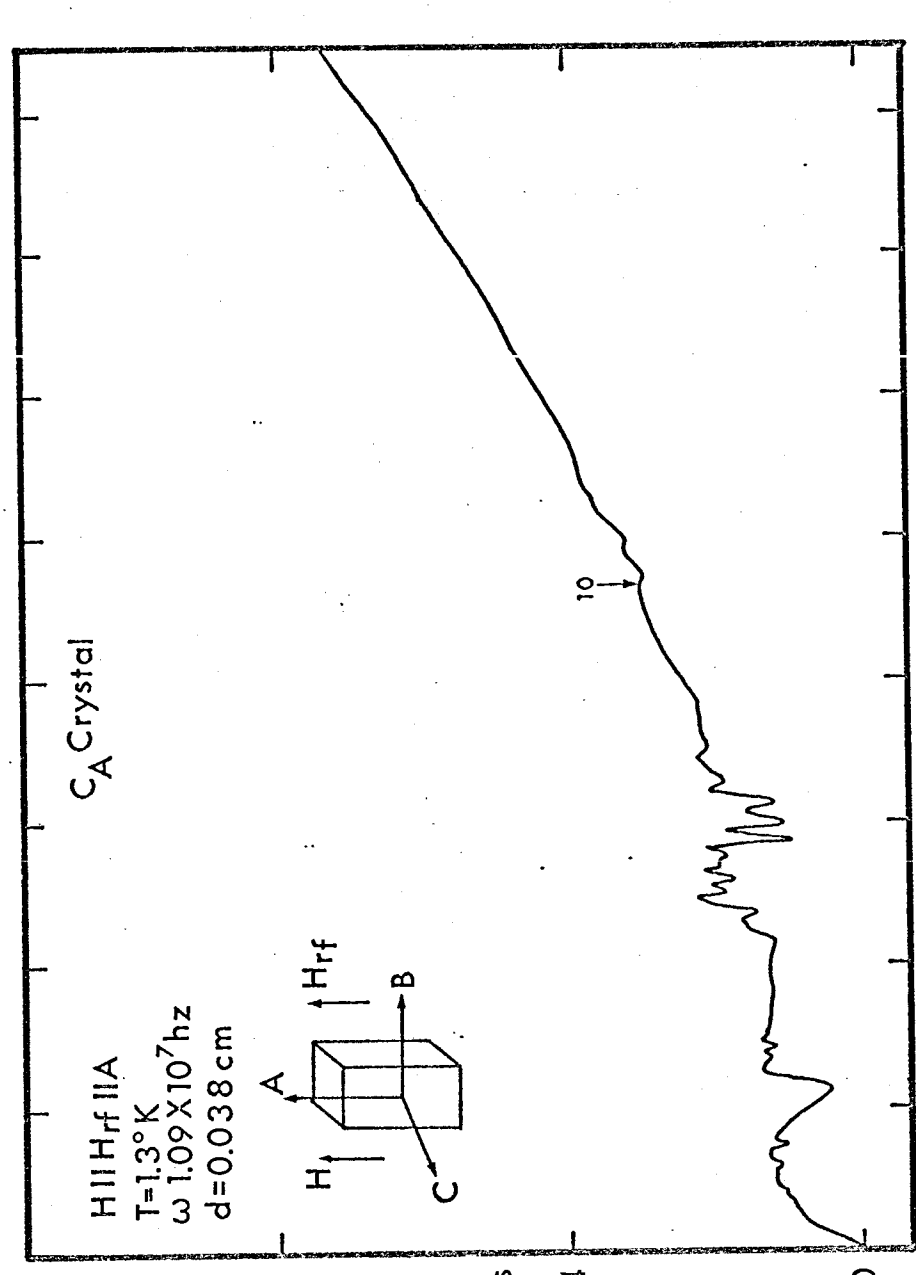
H∥Hrf ∥A
T=1.3°K
ω 1.09X10⁷hz
d=0.038cm
CA Crystal
A
Hrf
B
H
C
10
Change in Transmission Ratio X10⁶gauss/gauss
0.4
0
0
25
50
75
100
125
150
175
200 214
Magnetic Field (gauss)

Fig 6-16

Fig 6-17

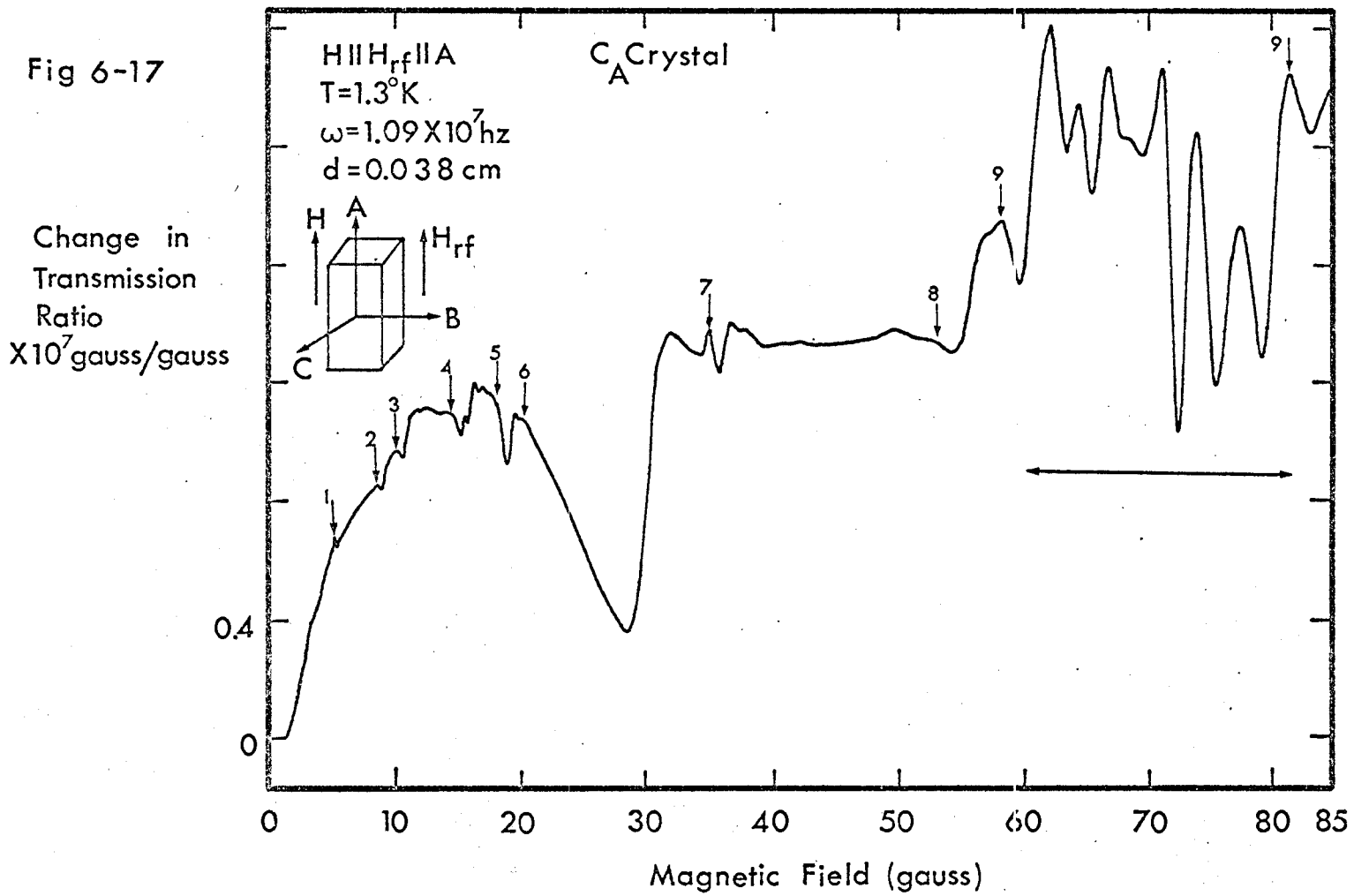
H∥H_rf∥A
C_A Crystal
T=1.3°K
ω=1.09X10^7 hz
d=0.038 cm
H
A
H_rf
B
C
Change in Transmission Ratio X10^7 gauss/gauss
0.4
0
0
10
20
30
40
50
60
70
80
85
Magnetic Field (gauss)
1
2
3
4
5
6
7
8
9
9

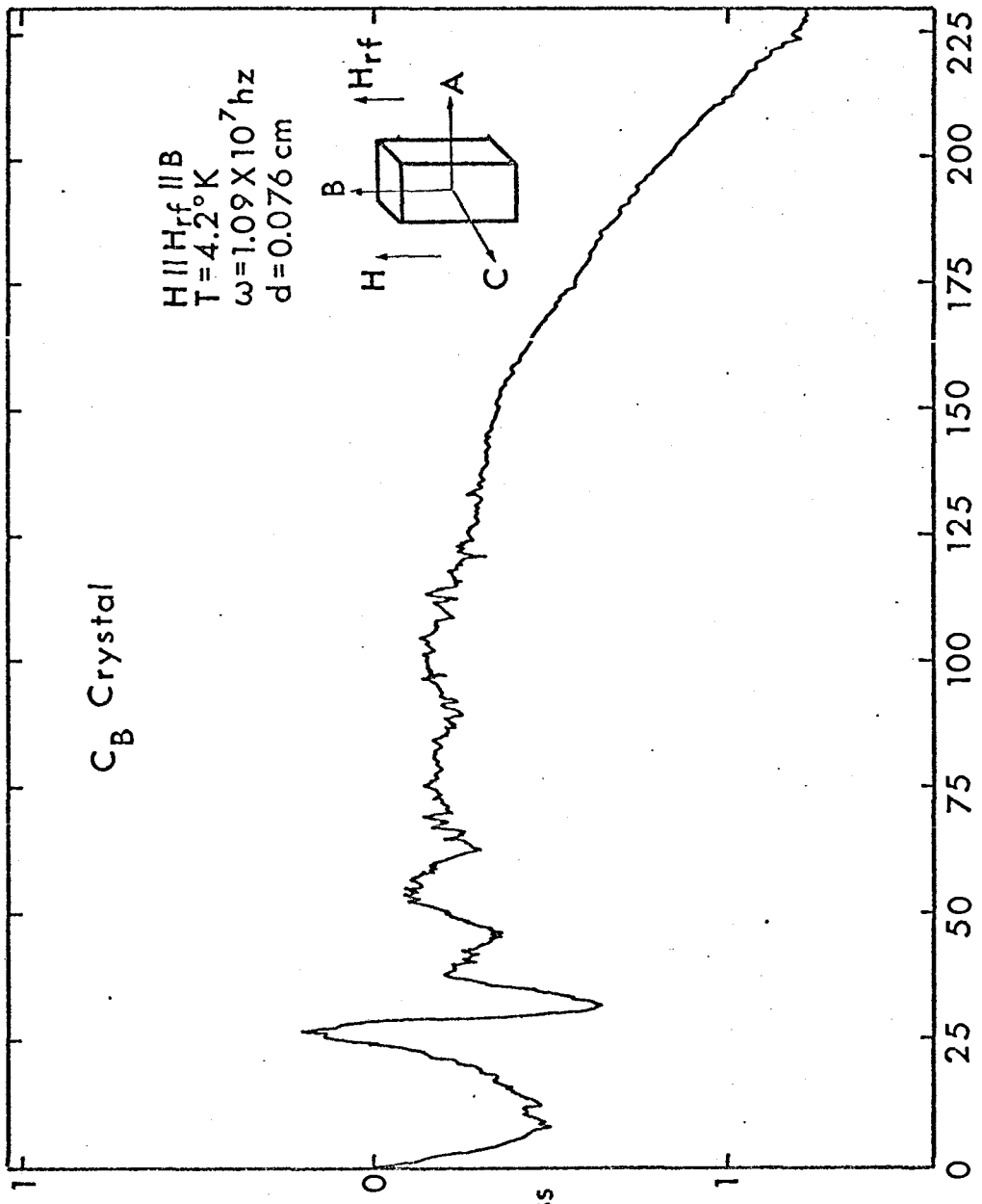
H ∥ Hrf ∥ B
T=4.2°K
ω=1.09X10^7 hz
d=0.076 cm
CB Crystal
H
B
Hrf
A
C
Change in Transmission Ratio X10^7 gauss/gauss
1
0
1
0
25
50
75
100
125
150
175
200
225
Magnetic Field (gauss)

Fig 6-18

Fig 6-19

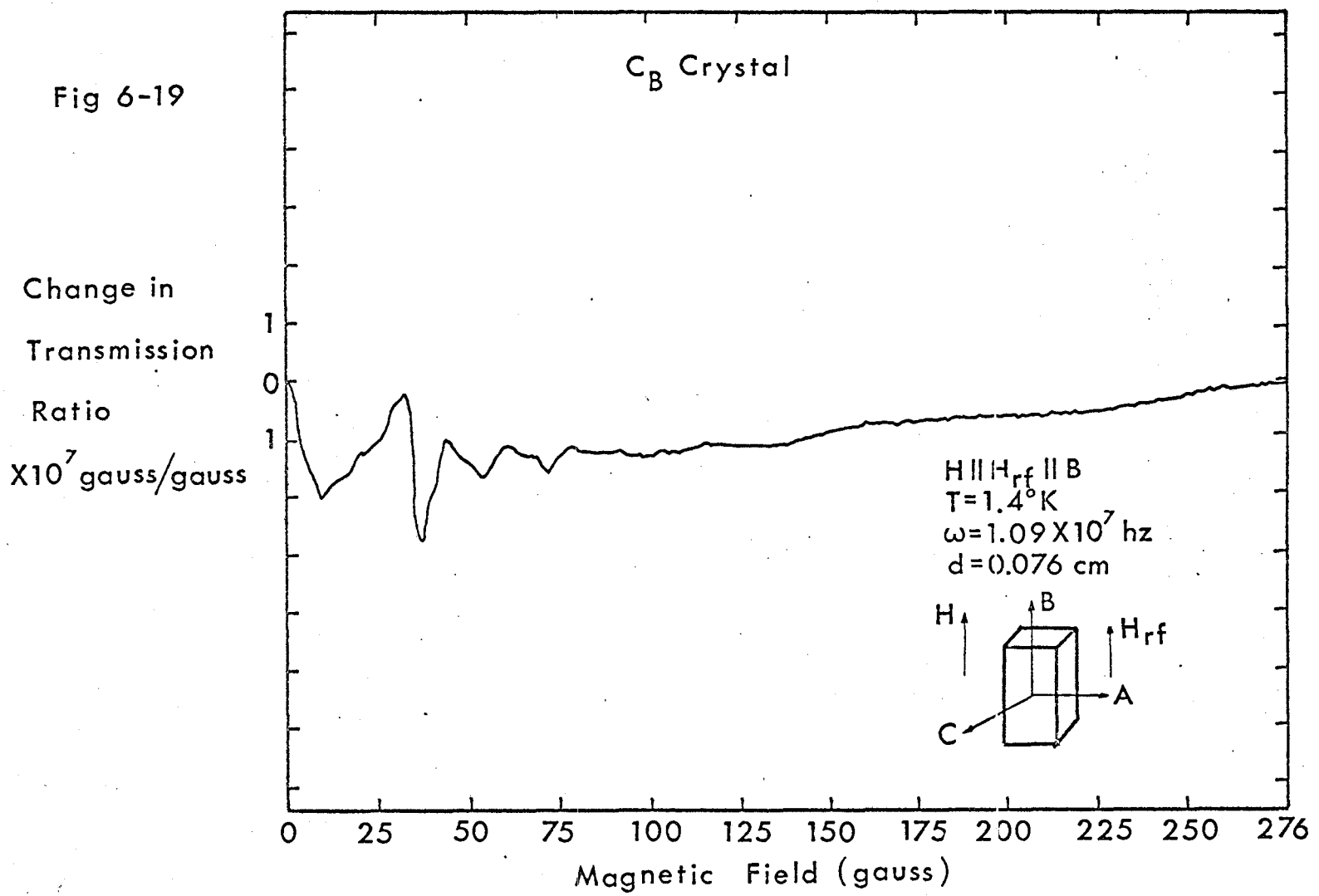
C_B Crystal
Change in
Transmission
Ratio
X10^7 gauss/gauss
1
0
1
H ∥ H_{rf} ∥ B
T = 1.4°K
ω = 1.09 X 10^7 hz
d = 0.076 cm
H
B
H_{rf}
A
C
0
25
50
75
100
125
150
175
200
225
250
276
Magnetic Field (gauss)

Fig 6-20

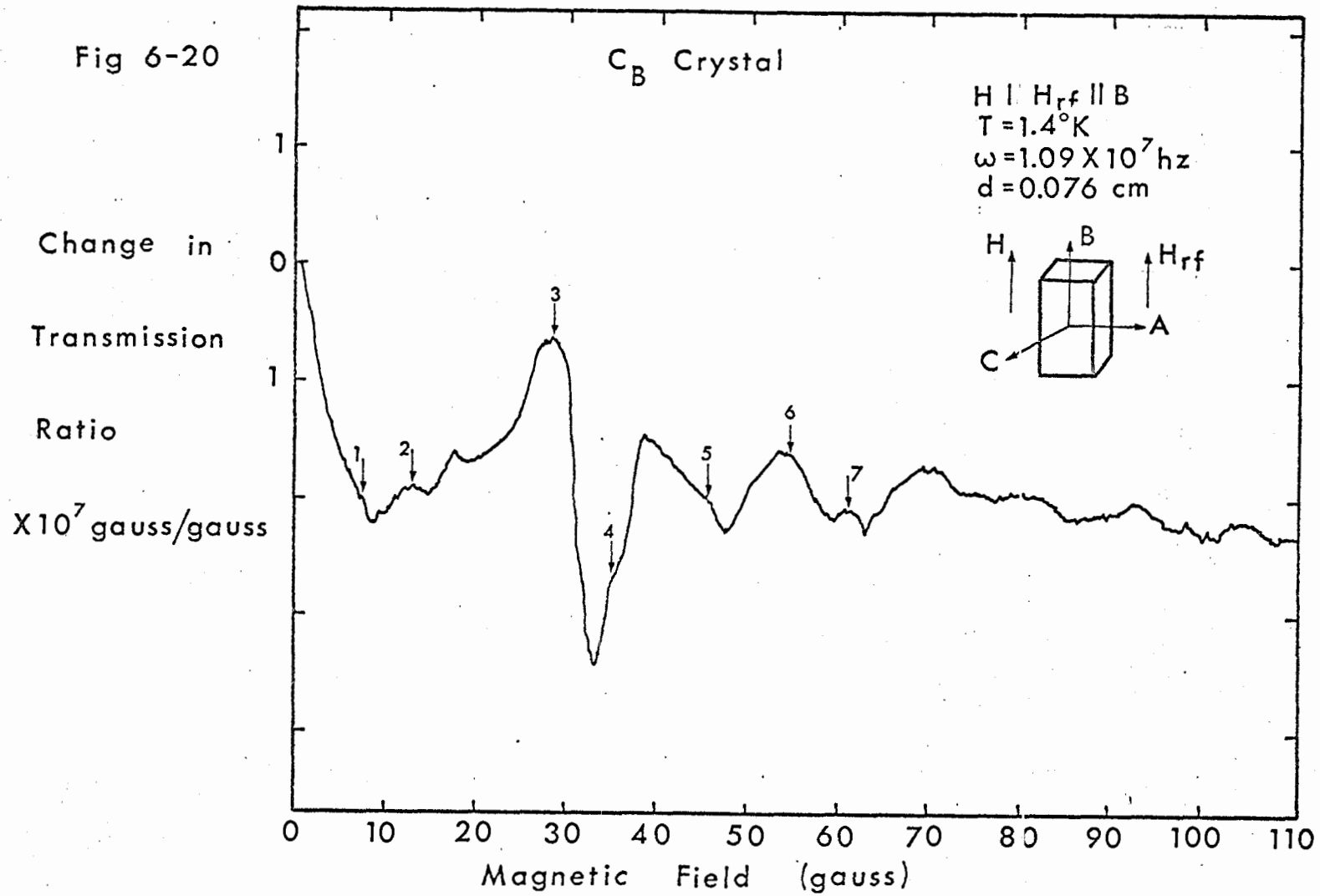
C_B Crystal
H ⊥ H_{rf} ∥ B
T = 1.4°K
ω = 1.09 X 10^7 hz
d = 0.076 cm
H
B
H_{rf}
A
C
Change in Transmission Ratio
X10^7 gauss/gauss
1
0
1
1
2
3
4
5
6
7
0
10
20
30
40
50
60
70
80
90
100
110
Magnetic Field (gauss)

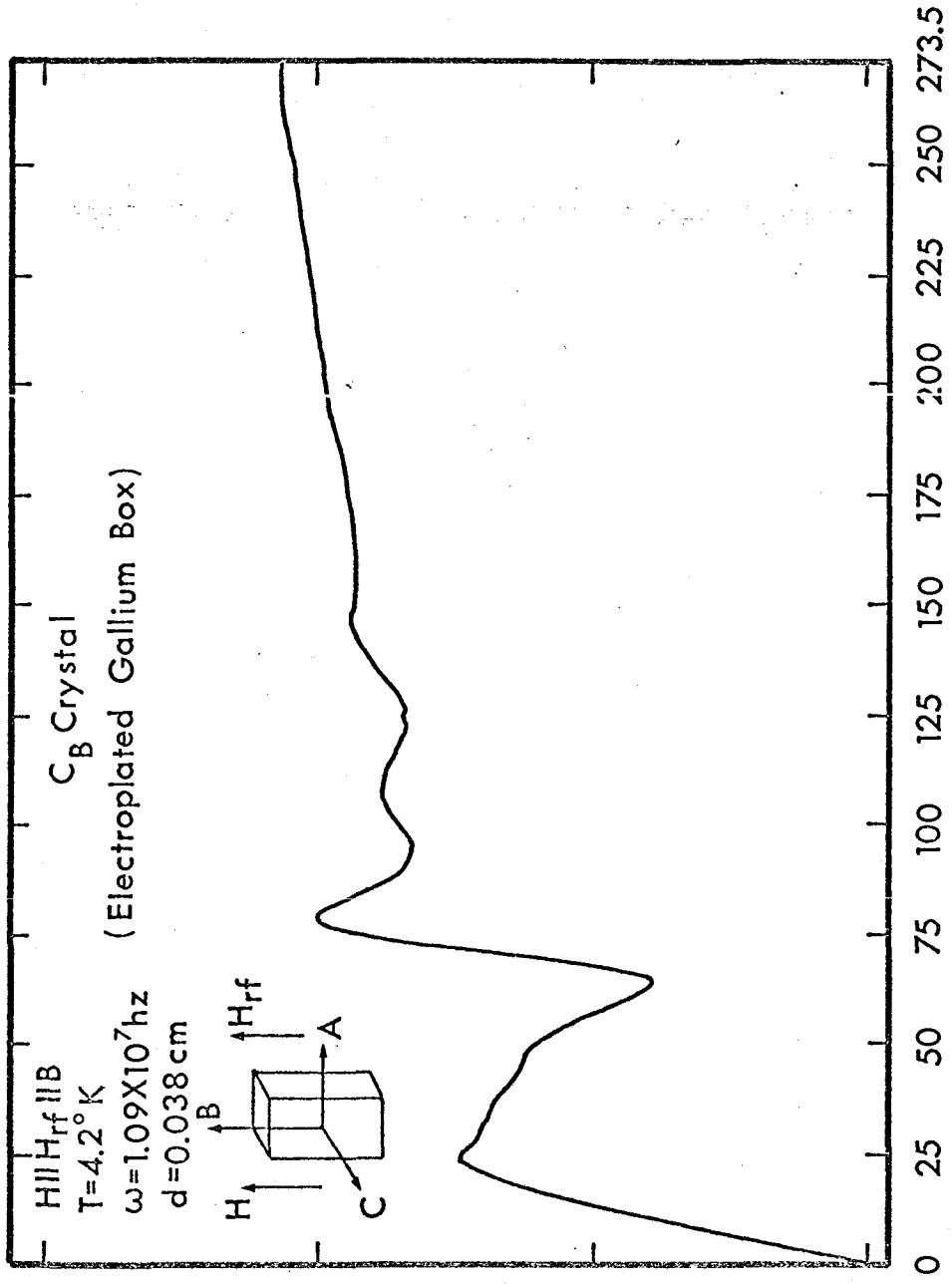
H∥H_rf ∥B
T=4.2° K
ω=1.09X10^7 hz
d=0.038 cm
C_B Crystal
(Electroplated Gallium Box)
H_rf
A
B
H
C
Change in Transmission Ratio X10^6 gauss/gauss
0.4
0
0
25
50
75
100
125
150
175
200
225
250
273.5
Magnetic Field (gauss)

Fig 6-21

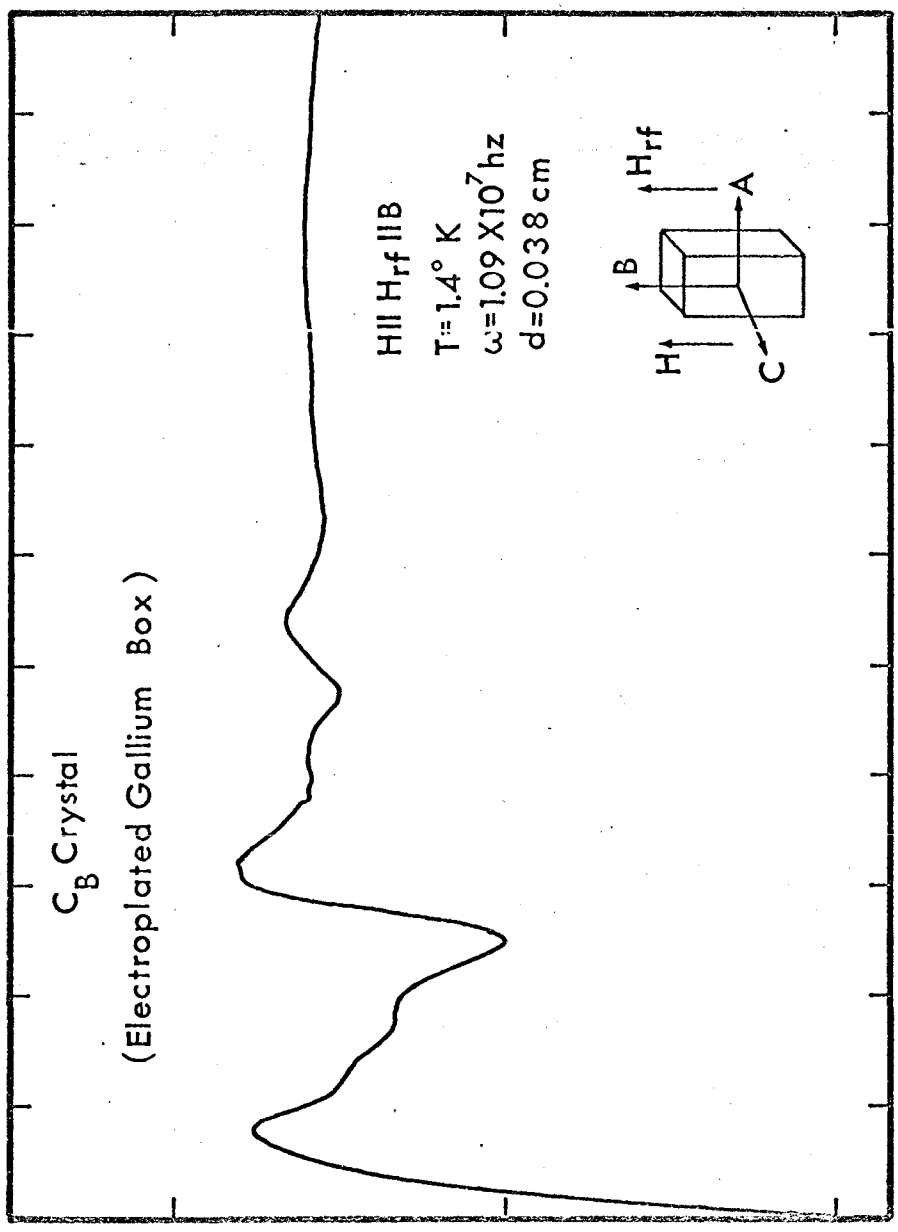
C_B Crystal
(Electroplated Gallium Box)
H|| H_{rf} ⊥B
T=1.4° K
ω=1.09 X10^{7}hz
d=0.038 cm
B
H_{rf}
A
H
C
Change in Transmission Ratio X10^{6}gauss/gauss
1
0
0 25 50 75 100 125 150 175 200 225 250 273.5
Magnetic Field (gauss)

Fig 6-22

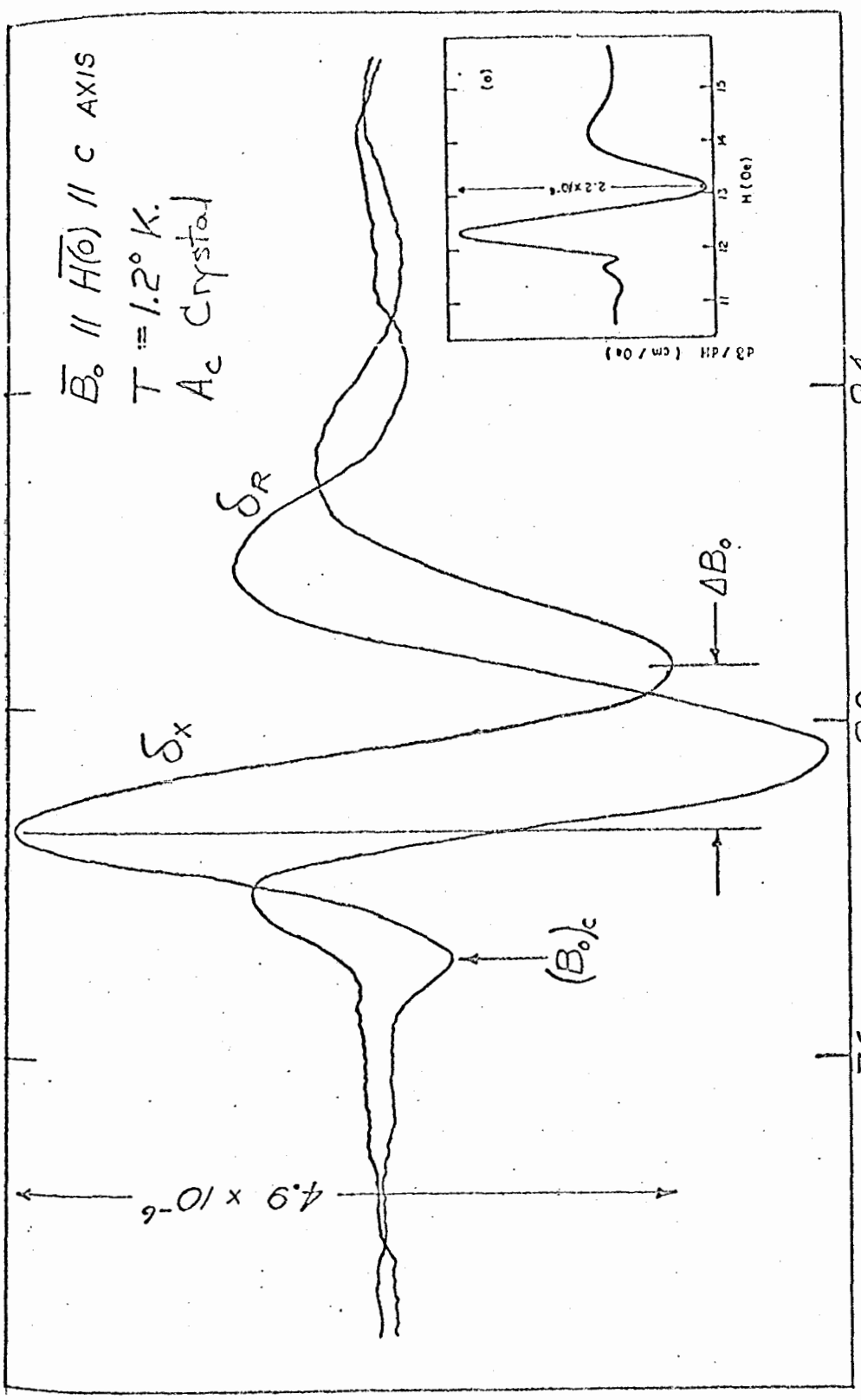

FIG. 6-23 RADIO-FREQUENCY SIZE-EFFECT RESONANCE IN GALLIUM.
INSET: SAME RESONANCE, REPORTED BY HAEBERLAND, ET. AL. (40)

Author	Crystal Thickness (cm)	$H_o d$ (gauss-cm)	f (Mhz)	$\frac{\Delta H \; d \; f^{1/3}}{H_o}$
This work	0.038	0.32	1.74	0.25
Cochran and Shiffman[6]	0.0394	0.324	2.0	0.16

Table 6-2. Comparison of Line Position and Line Width for the Lowest Field Gantmakher Resonance in A_B Crystals

Author	Crystal Thickness (cm)	$H_o d$ (gauss-cm)	f (Mhz)	$\frac{\Delta H \, d \, f^{1/3}}{H_o}$
This work	0.038	0.20	1.74	0.13
Cochran and Shiffman[6]	0.0394	0.2	2.0	--
Haberland et al[40]	0.017	0.20	1.0	0.12
Lyall[56]	0.0261	0.202	7.0	0.13

Table 6-3. Comparison of Line Position and Line Width for the Lowest Field Gantmakher Resonance in A_c Crystals

TABLE 6-4. Fermi Surface Dimensions as Deduced from Gantmakher Resonances

$$\Delta K = \frac{\Delta K_{ext}}{2} = \frac{0.15194 \times 10^8 \, H_0 d}{2} \text{ cm}^{-1}$$

Crystal	Direction along which ΔK is measured	Resonance Reference	ΔK(10^7 cm^{-1}) This work	Haberland et al.[39]	Strandberg Fukumoto[38]
A_B	C	Fig.6-2 (1)	0.2	0.21	
		(2)	0.5	0.46	
		(3)	1.5		
		(4)	4.5	4.7	4.8
				4.1	
A_C	B	Fig.6-5 (1)	0.14	0.13	
		(2)	0.32		
		(3)	0.46		
		(4)	0.6	0.6	
		(5)	0.75	0.72	
		(6)	0.84		
		(7)	0.95	1.0	
		(8)	1.5		
		(9)	1.85	1.8	1.8
		(10)	1.9→2.6		
		Fig.6-4, 6-5 (11)	3.9		
B_A	C	Fig.6-10 (1)	0.2	0.2	
		(2)	0.46		
		(3)	0.72	0.7	
		(4)	0.81		
		(5)	1.35		

Table 6-4 continued

B_A	C	Fig.6-10 (6)	1.7		
		(7)	2.1		
		(8)	2.6		
		(9)	3.2		
		(10)	4.4		
		(11)	5.0		4.8
B_C	A	Fig.6-12 (1)	0.08	0.09	
		(2)	0.43	0.58	
		(3)	1.0	0.8	
		(4)	2.5		2.5
C_A	B	Fig.6-17 (1)	0.14	0.09	
		(2)	0.25	0.21	
		(3)	0.29		
		(4)	0.42	0.4	
		(5)	0.52		
		(6)	0.58		
		(7)	1.0	0.9	0.9
		(8)	1.55	1.5	
		(9)	1.7→2.4		2.1
		Fig.6-16 (10)	3.4		
C_B	A	Fig.6-20 (1)	0.4	0.39	
		(2)	0.75		
		(3)	1.7	1.7	1.6
		(4)	2.0	2.0	
		(5)	2.6		
		(6)	3.1	3.0	
		(7)	3.6		
				0.05	
				0.13	

Fermi surface could be calipered from Gantmakher resonances. Since it is resonable to assume a center of symmetry for all pieces of the Fermi surface, the quantity

$$\Delta k = \frac{\Delta k_{ext}}{2} = \frac{0.15194 \times 10^{8} H_o d}{2} \ cm^{-1}$$

has been determined. Fermi surface dimensions corresponding to some of the most prominent features in the gallium crystals are presented in Table 6-4. Data obtained by Haberland et al[40] and by Fukumoto and Strandberg[39] are also given in this table. All the on-axis data of these above mentioned authors are shown. It should be noted that H_o was taken at the leading edge of the transmission anomalies. A derivative was not estimated. For comparison purposes, the dimension of the Brillouin zone in the A-B plane is,

$$\Delta k \approx 1.4 \times 10^{8} \ cm^{-1}$$

6.3 Magnetic Field Perpendicular to the Slab Surface and Perpendicular to the Radio Frequency Magnetic Field

In this magnetic field geometry it is possible to observe Gantmakher-Kaner resonances (see section 2.2). The experimental results are given in Figs. 6-24 to 6-50 (page 129). Again the change in transmission has been plotted as a function of applied magnetic field strength. Fig. 6-37 is included to show the effect of tilting the field 15° from

the normal direction in a B_c crystal.

Indeed, when the magnetic field was directed normal to the surface of the crystal, oscillations periodic in magnetic field were observed*. These Gantmakher-Kaner oscillations were observed in each gallium crystal studied. The periodic oscillations were usually superimposed on a non-monotonic background which tended to obscure the periodic transmission variations of small amplitude. In some cases several oscillations, each with a distinct period, could be observed in a given crystal.

---

*Similar oscillations, periodic in magnetic field, were first seen by Gantmakher and Kaner in tin crystals(16).

Figures (6-24) to (6-50)

Transmission through gallium single crystals versus applied magnetic field. The d.c. field is directed along the specimen normal. Note that the C_B crystal used was twice as thick as the other crystals.

$H_o \perp H_{rf}$; Normal to the plane

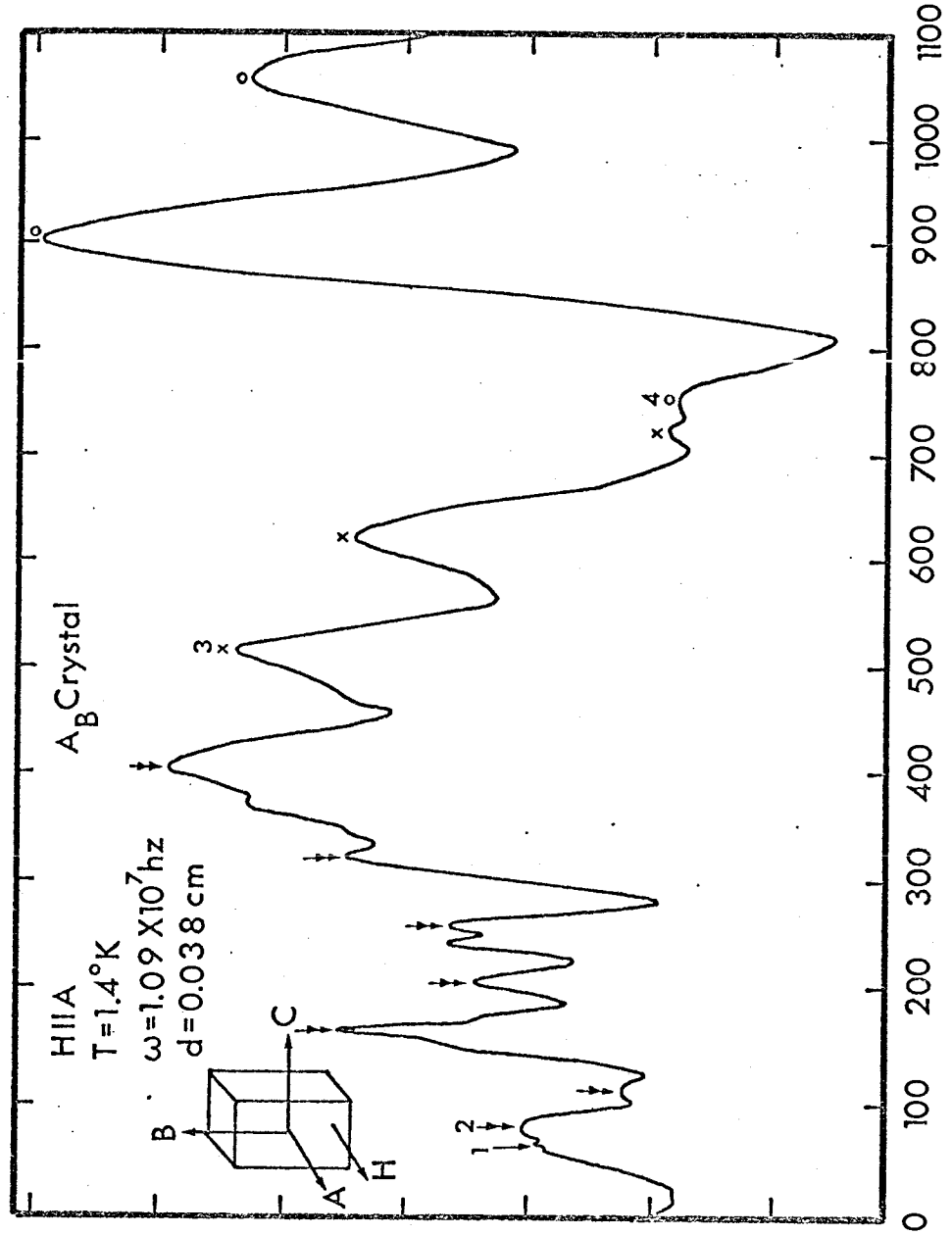
H||A
T=1.4°K
ω=1.09 X10⁷hz
d=0.038 cm
A_B Crystal
B
C
A
H
1
2
3
4
0.4
0
0.4
0
100
200
300
400
500
600
700
800
900
1000
1100
Magnetic Field (gauss)
Change in Transmission Ratio X10⁵ gauss/gauss

Fig 6-24

Fig 6-25

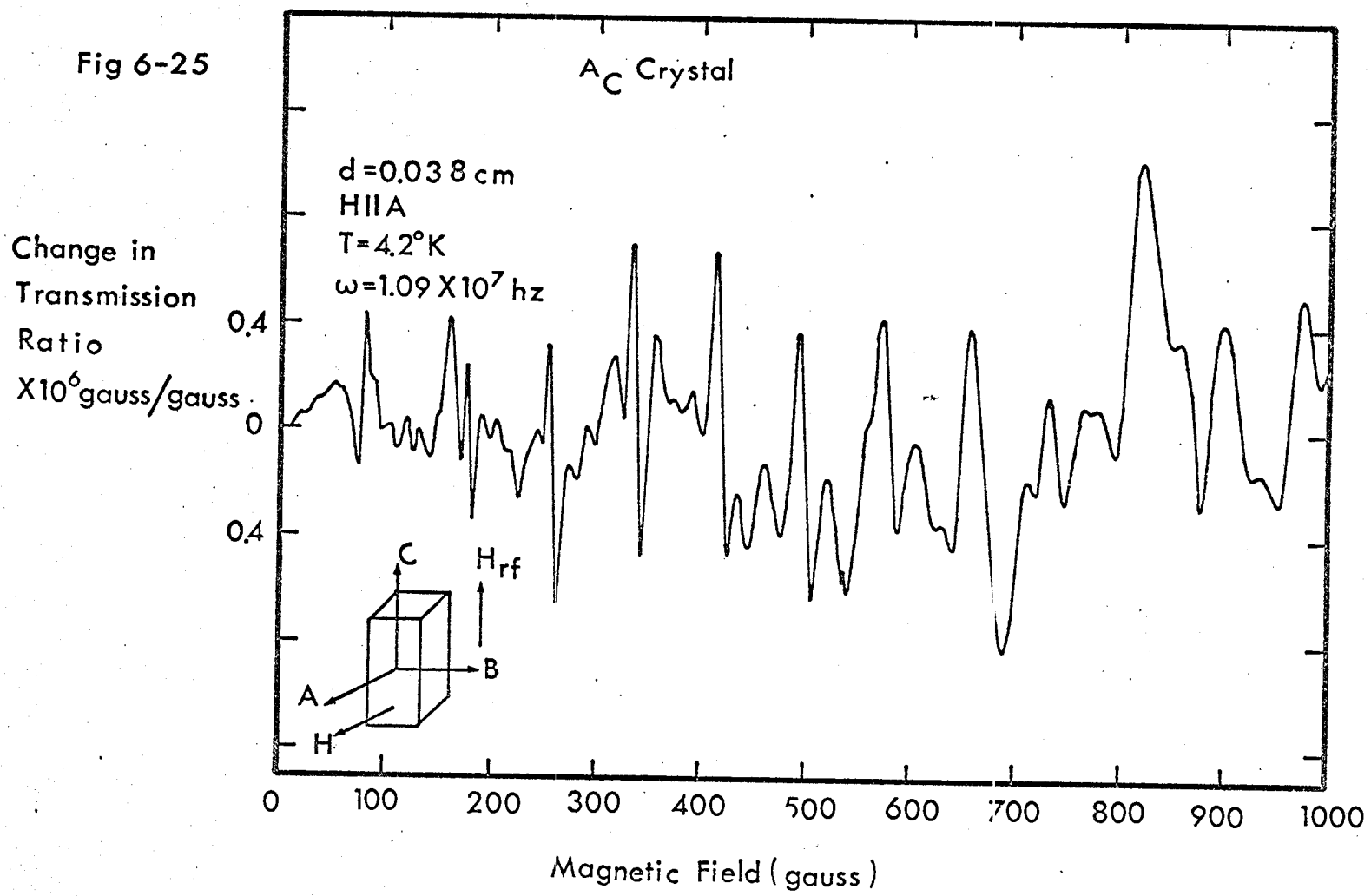
A_C Crystal
d=0.038 cm
HIIA
T=4.2°K
ω=1.09 X10^7 hz
Change in Transmission Ratio X10^6 gauss/gauss
0.4
0
0.4
C
H_rf
B
A
H
0
100
200
300
400
500
600
700
800
900
1000
Magnetic Field (gauss)

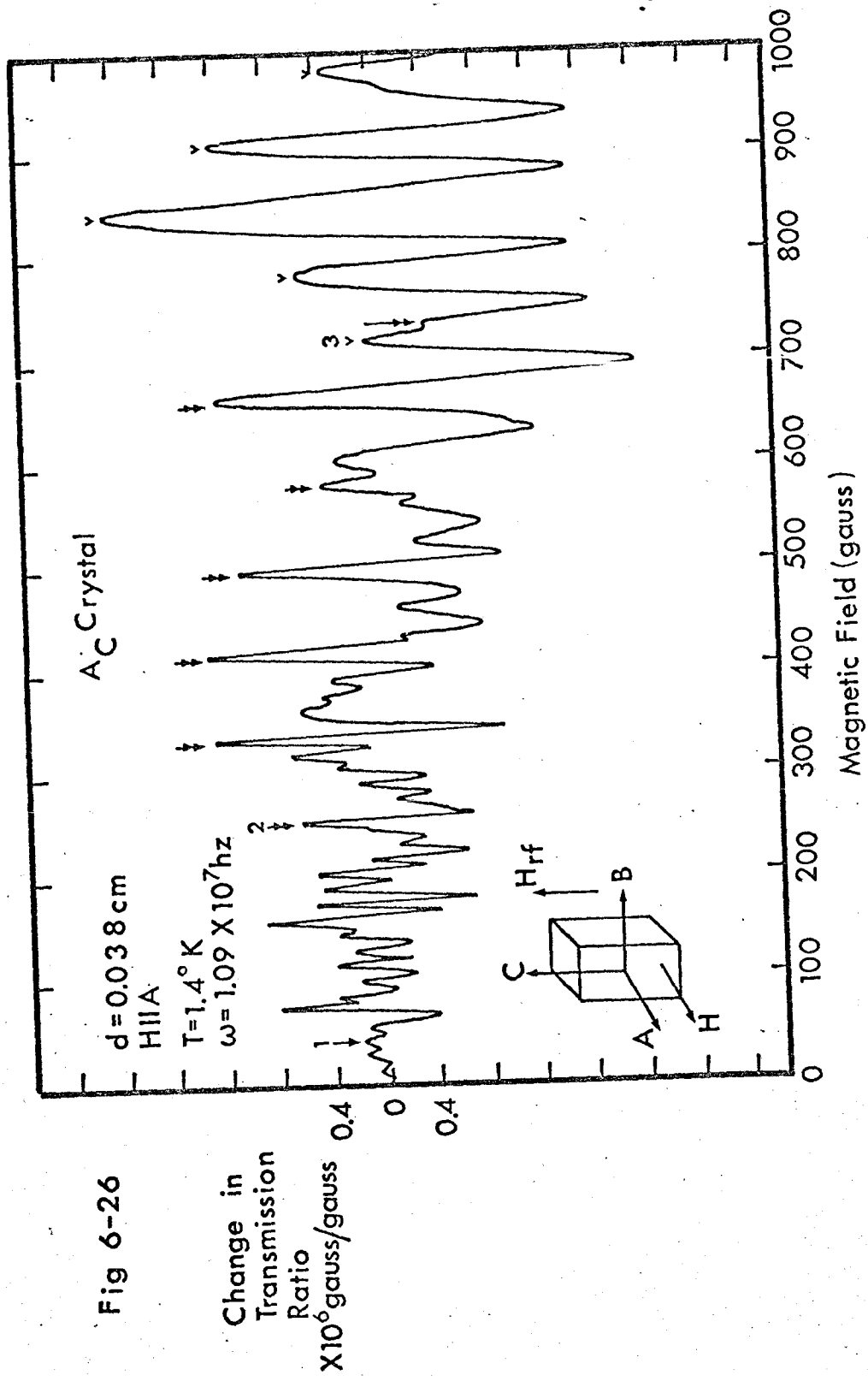
A_C Crystal
d=0.038 cm
H||A
T=1.4° K
ω= 1.09 X 10^7 hz
1
2
3
Change in Transmission Ratio X10^6 gauss/gauss
0.4
0
0.4
H_rf
B
C
A
H
0
100
200
300
400
500
600
700
800
900
1000
Magnetic Field (gauss)

Fig 6-26

Fig 6-27

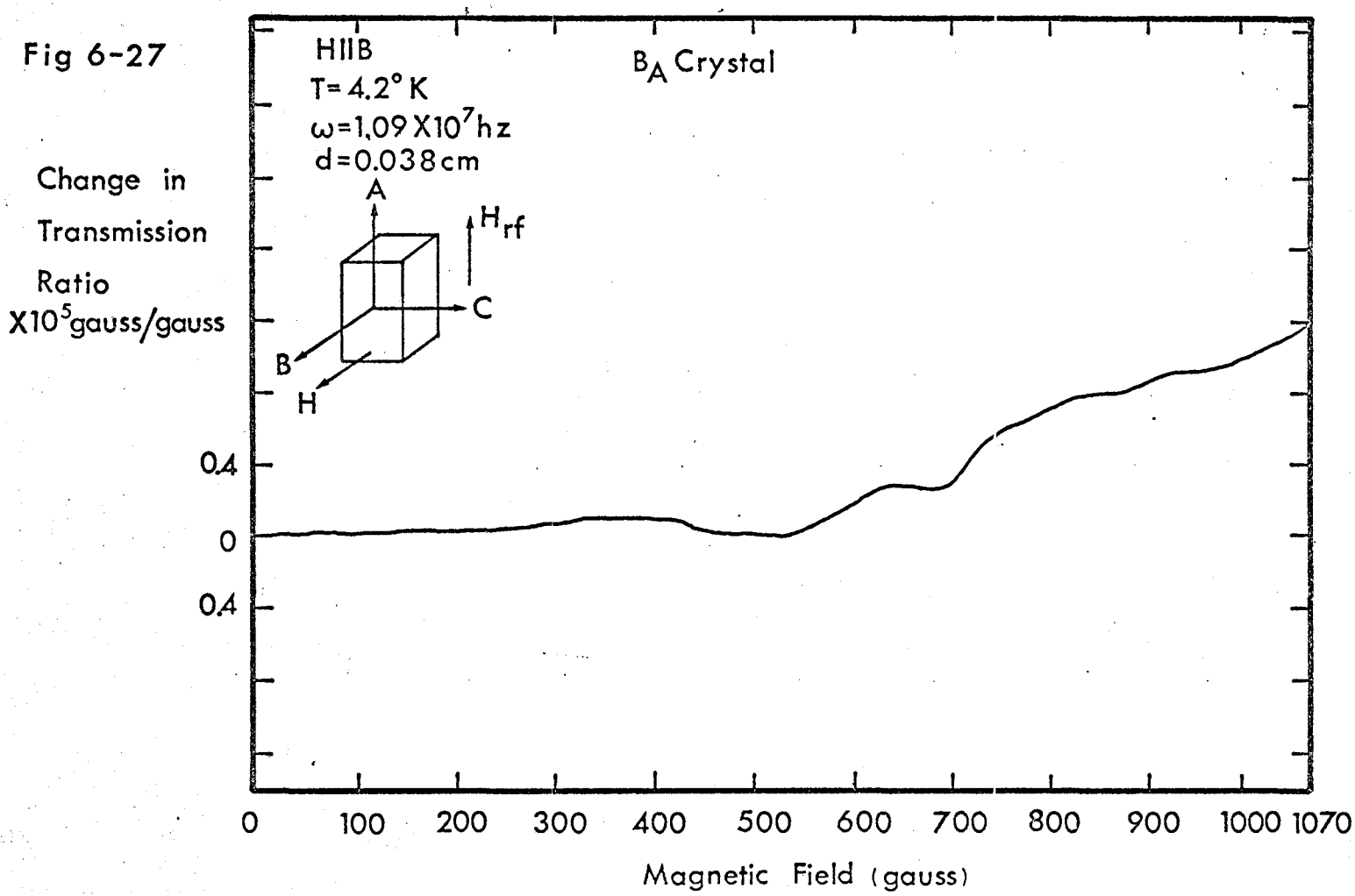
HIIB
T= 4.2° K
ω=1.09 X10^7 hz
d=0.038 cm
B_A Crystal
A
H_rf
C
B
H
Change in
Transmission
Ratio
X10^5 gauss/gauss
0.4
0
0.4
0
100
200
300
400
500
600
700
800
900
1000
1070
Magnetic Field (gauss)

Fig 6-28

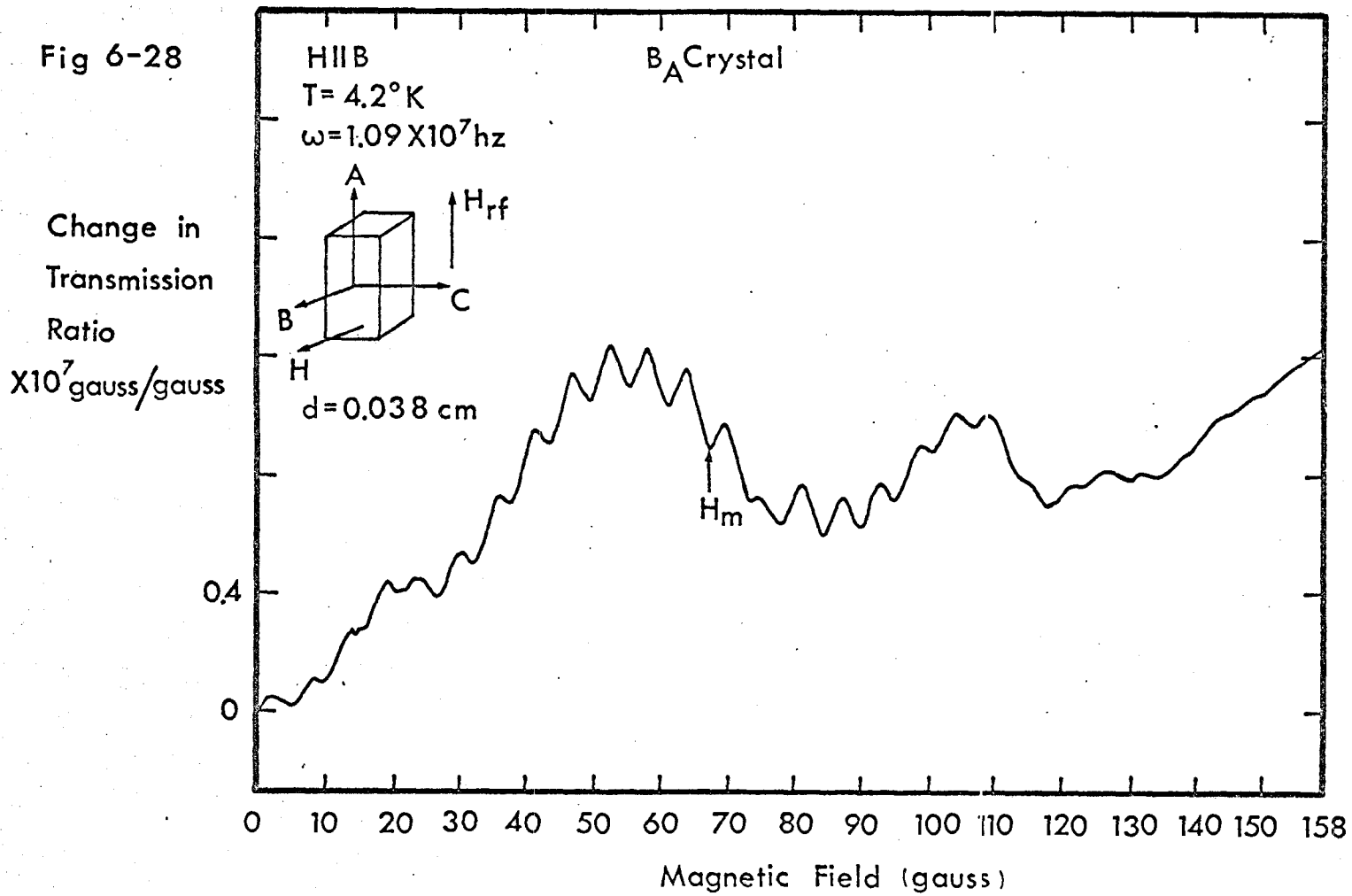
H II B
T= 4.2° K
ω=1.09 X10⁷hz
B_A Crystal
A
H_rf
B
C
H
d=0.038 cm
H_m
Change in
Transmission
Ratio
X10⁷gauss/gauss
0.4
0
0 10 20 30 40 50 60 70 80 90 100 110 120 130 140 150 158
Magnetic Field (gauss)

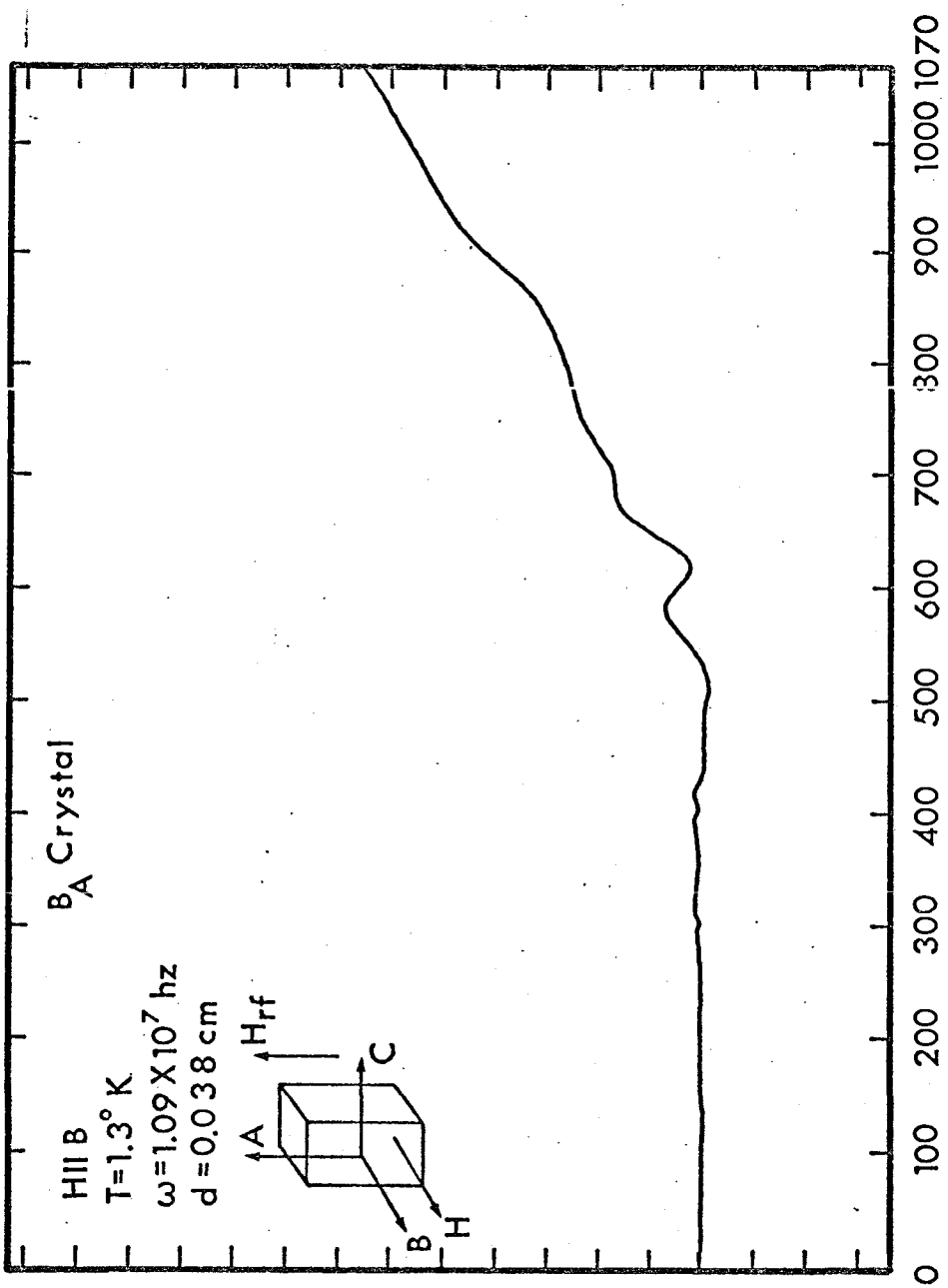
H⊥ B
T=1.3° K
ω=1.09 X 10^7 hz
d=0.038 cm
B_A Crystal
H_rf
A
C
B
H
Change in Transmission Ratio X10^5 gauss/gauss
0.4
0
0.4
0
100
200
300
400
500
600
700
800
900
1000
1070
Magnetic Field (gauss)

Fig 6-29

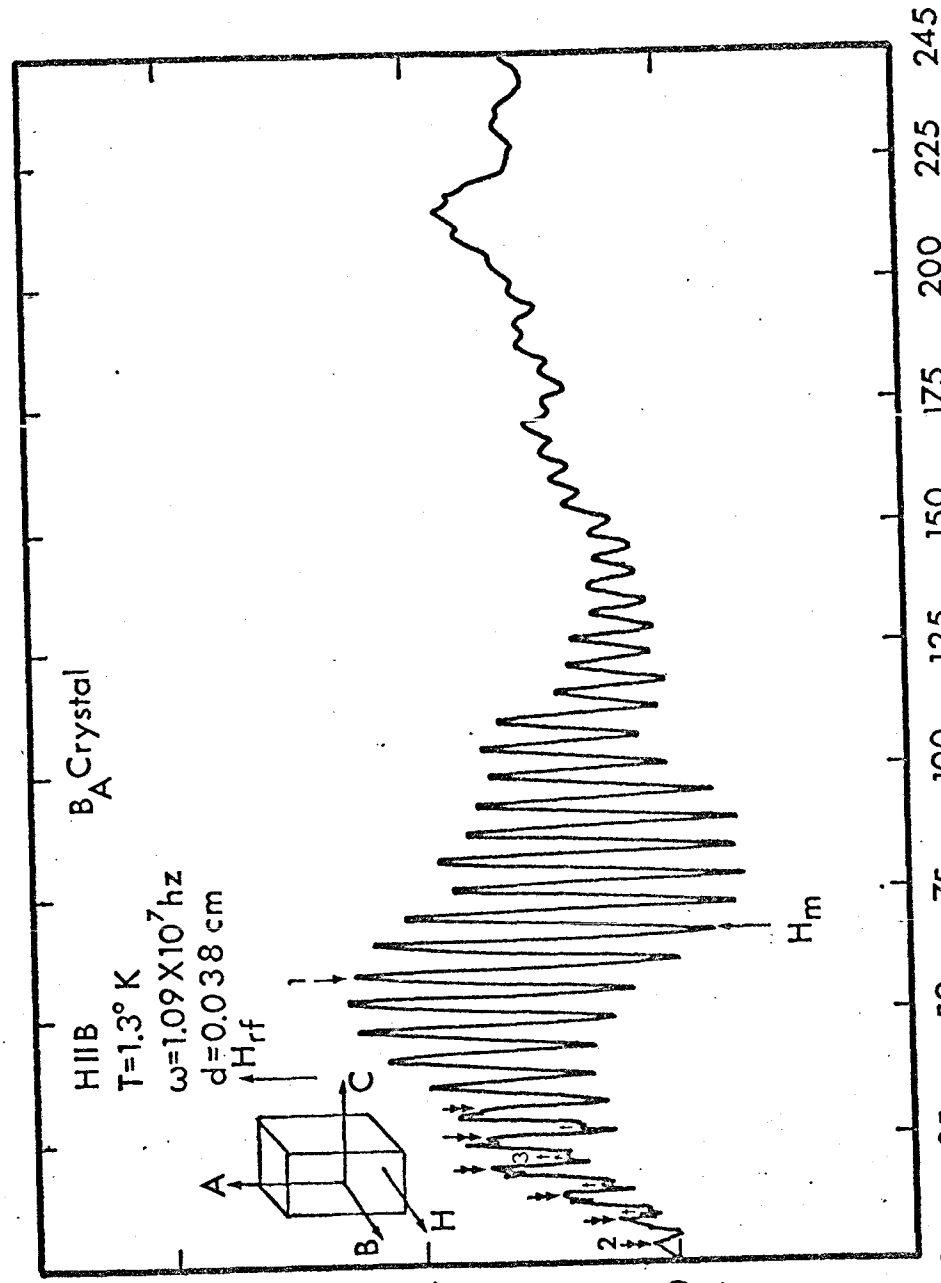
H⊥B
T=1.3° K
ω=1.09 X10⁷hz
d=0.038 cm
H_rf
B_A Crystal
A
B
C
H
1
2
3
H_m
Change in Transmission Ratio X10⁶gauss/gauss
0.4
0
0
25
50
75
100
125
150
175
200
225
245
Magnetic Field (gauss)

Fig 6-30

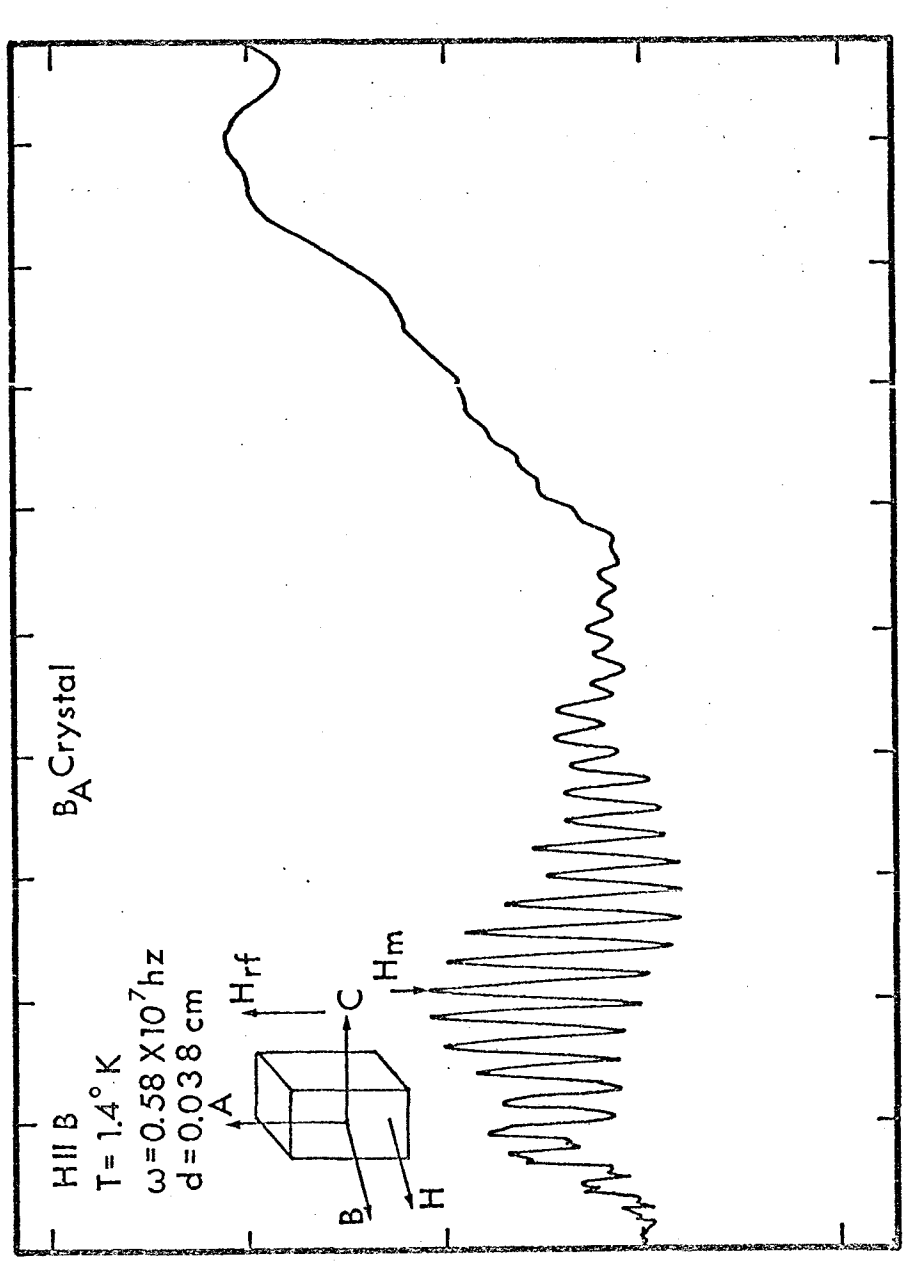
H II B
T= 1.4° K
ω=0.58 X10^7hz
d=0.038 cm
B_A Crystal
A
B
C
H
Hrf
Hm
Change in Transmission Ratio X 10^7 gauss/gauss
1
0
1
0
25
50
75
100
125
150
175
200
225
244
Magnetic Field (gauss)

Fig 6-31

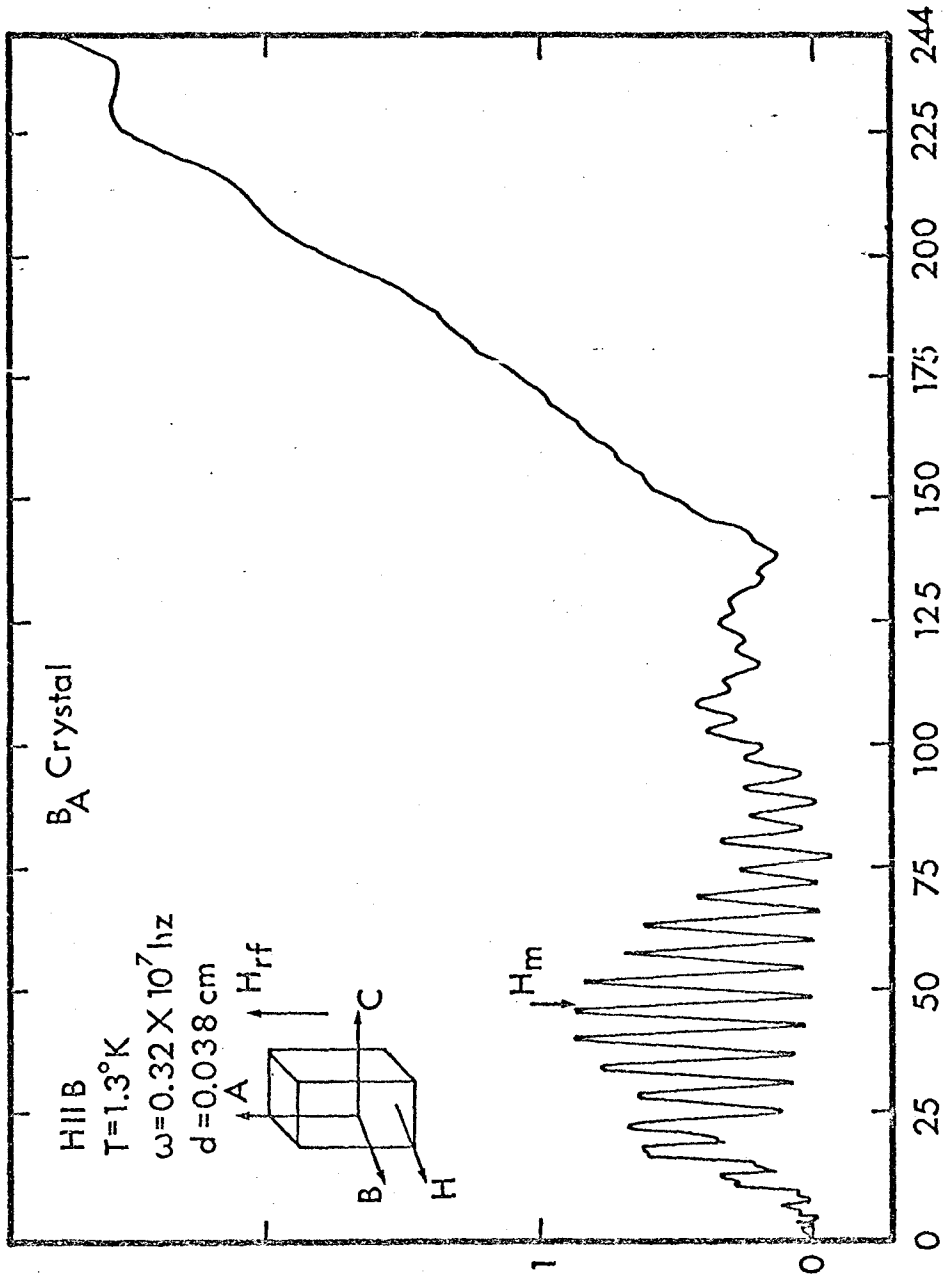
H II B
T=1.3°K
ω=0.32 X 10⁷ Hz
d=0.038 cm
A
H_rf
C
B
H
H_m
B_A Crystal
Change in Transmission Ratio X10⁷ gauss/gauss
1
0
0
25
50
75
100
125
150
175
200
225
244
Magnetic Field (gauss)

Fig 6-32

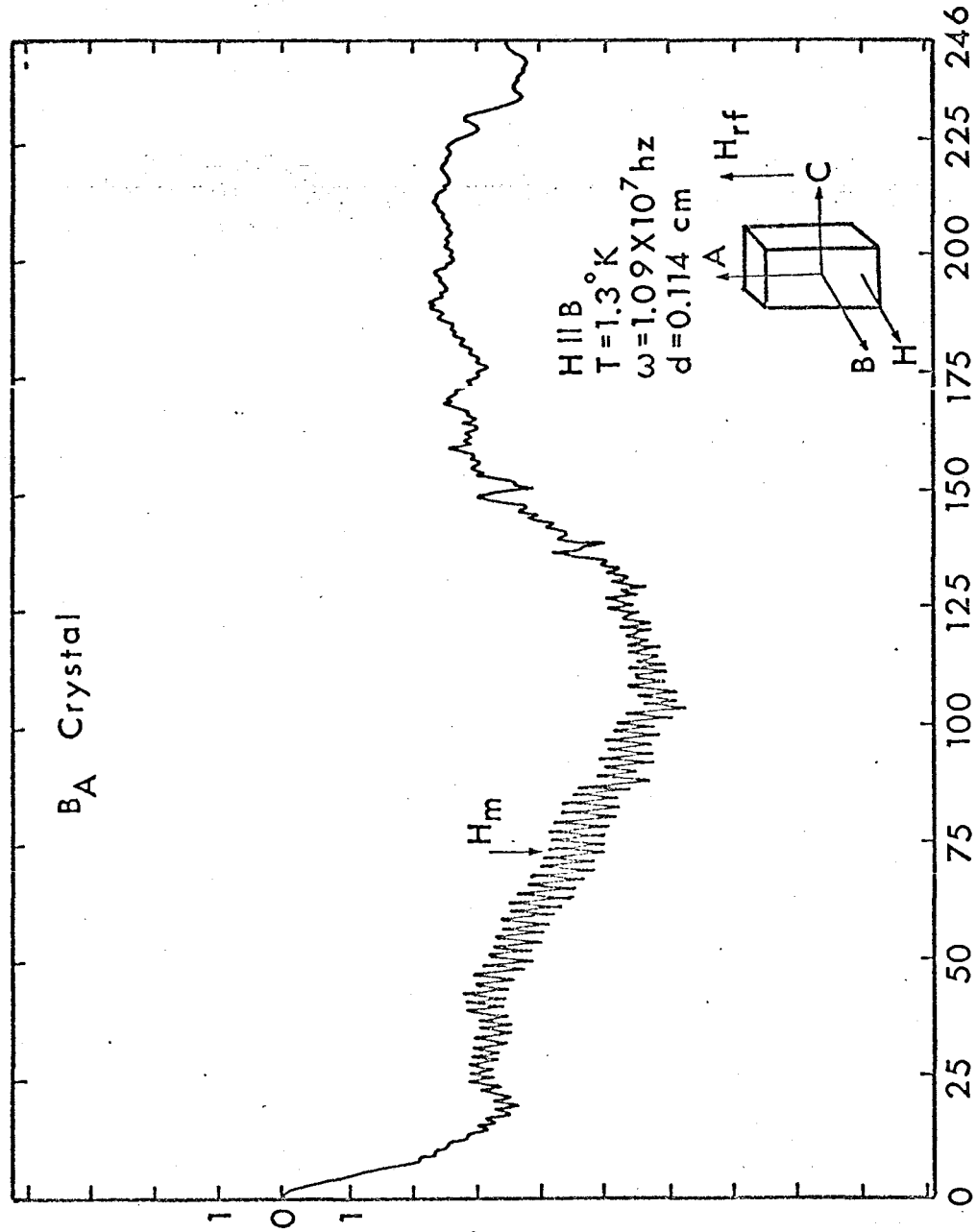
B_A Crystal
H_m
H ⊥ B
T=1.3°K
ω=1.09X10⁷hz
d=0.114 cm
A
H_{rf}
C
B
H
1
0
1
0
25
50
75
100
125
150
175
200
225
246
Change in Transmission Ratio X10⁷ gauss/gauss
Magnetic Field (gauss)

Fig 6-33

Fig 6-34

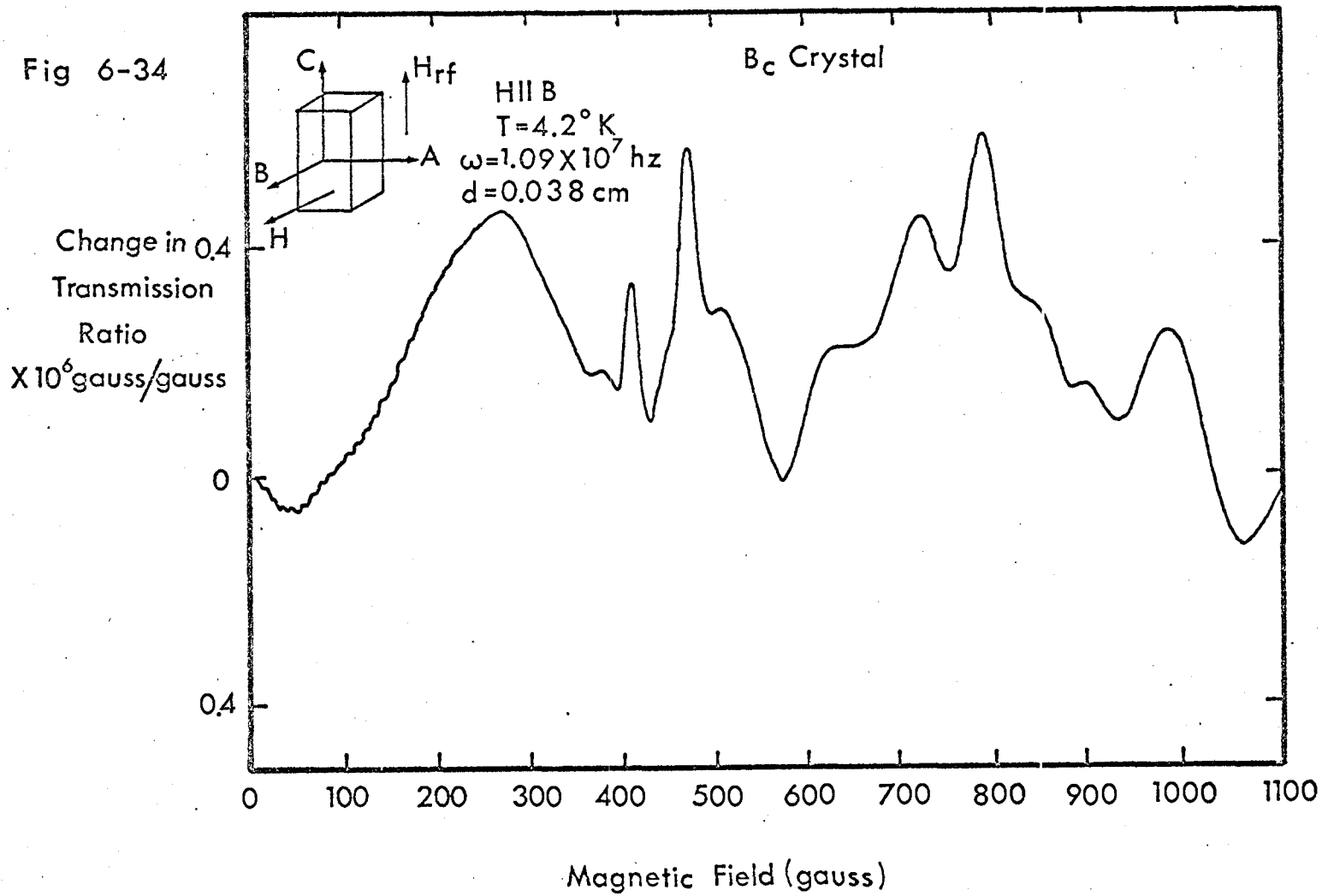
C
H_{rf}
H II B
T=4.2° K
ω=1.09X10⁷ hz
d=0.038 cm
A
B
H
B_c Crystal
Change in Transmission Ratio X10⁶gauss/gauss
0.4
0
0.4
0
100
200
300
400
500
600
700
800
900
1000
1100
Magnetic Field (gauss)

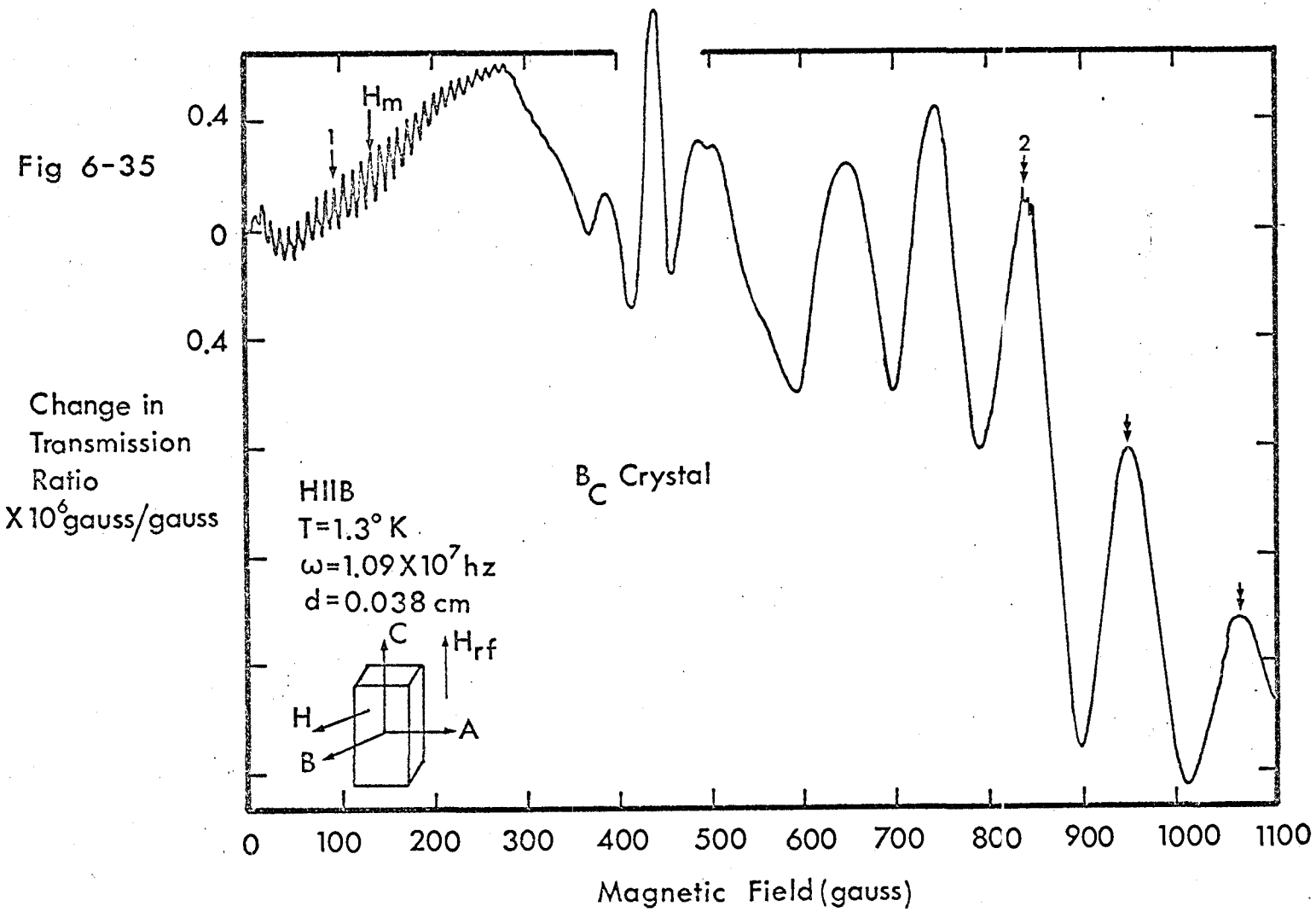
Fig 6-35
Change in Transmission Ratio X 10^6 gauss/gauss
0.4
0
0.4
Hm
1
2
H||B
T=1.3° K
ω=1.09X10^7 hz
d=0.038 cm
B_C Crystal
C
H_rf
H
A
B
0
100
200
300
400
500
600
700
800
900
1000
1100
Magnetic Field (gauss)

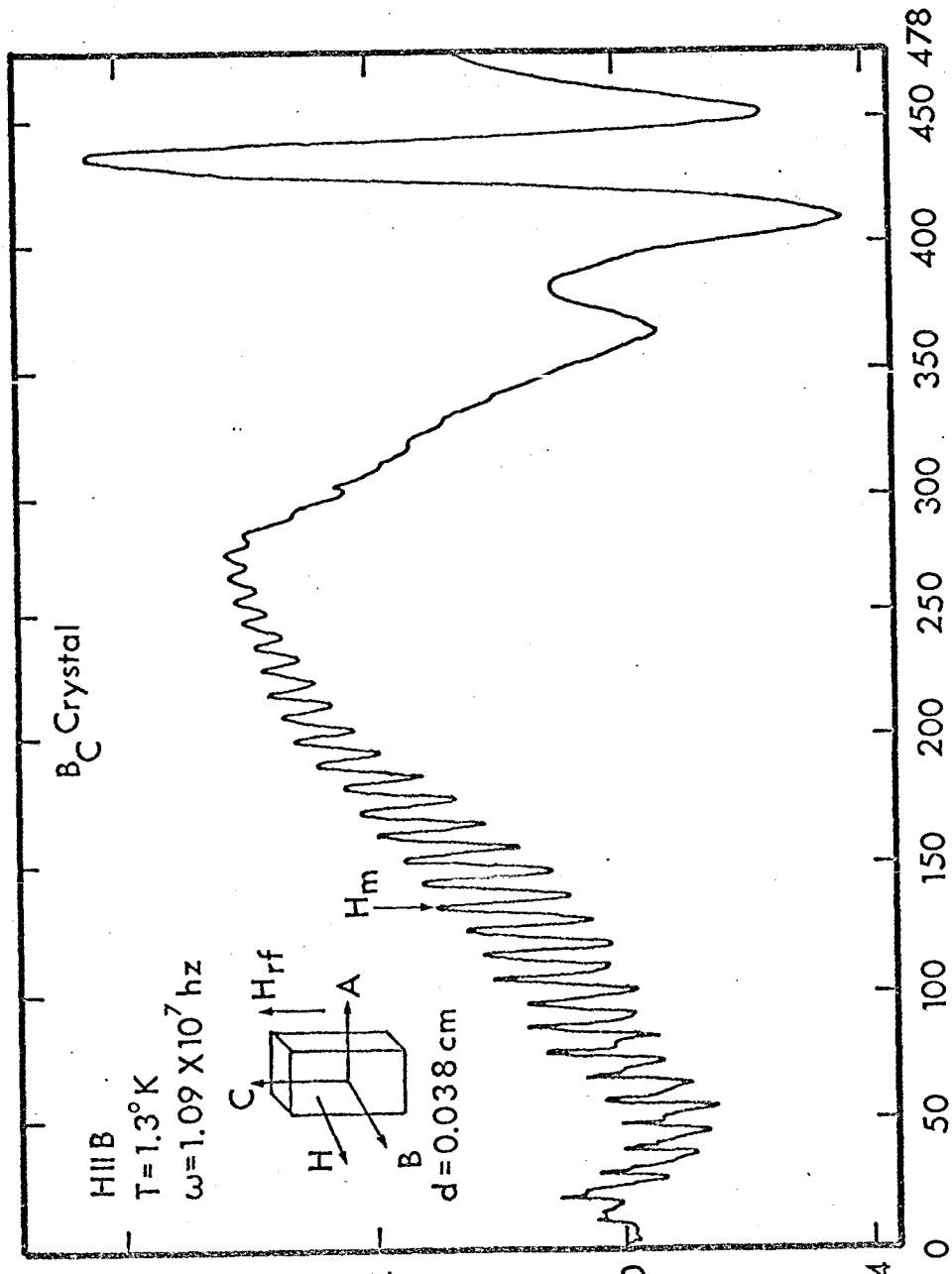
H II B
T = 1.3°K
ω = 1.09 X10^7 hz
B_C Crystal
H_m
H_rf
A
C
H
B
d = 0.038 cm
Change in Transmission Ratio X10^6 gauss/gauss
0.4
0
0.4
0
50
100
150
200
250
300
350
400
450
478
Magnetic Field (gauss)

Fig 6-36

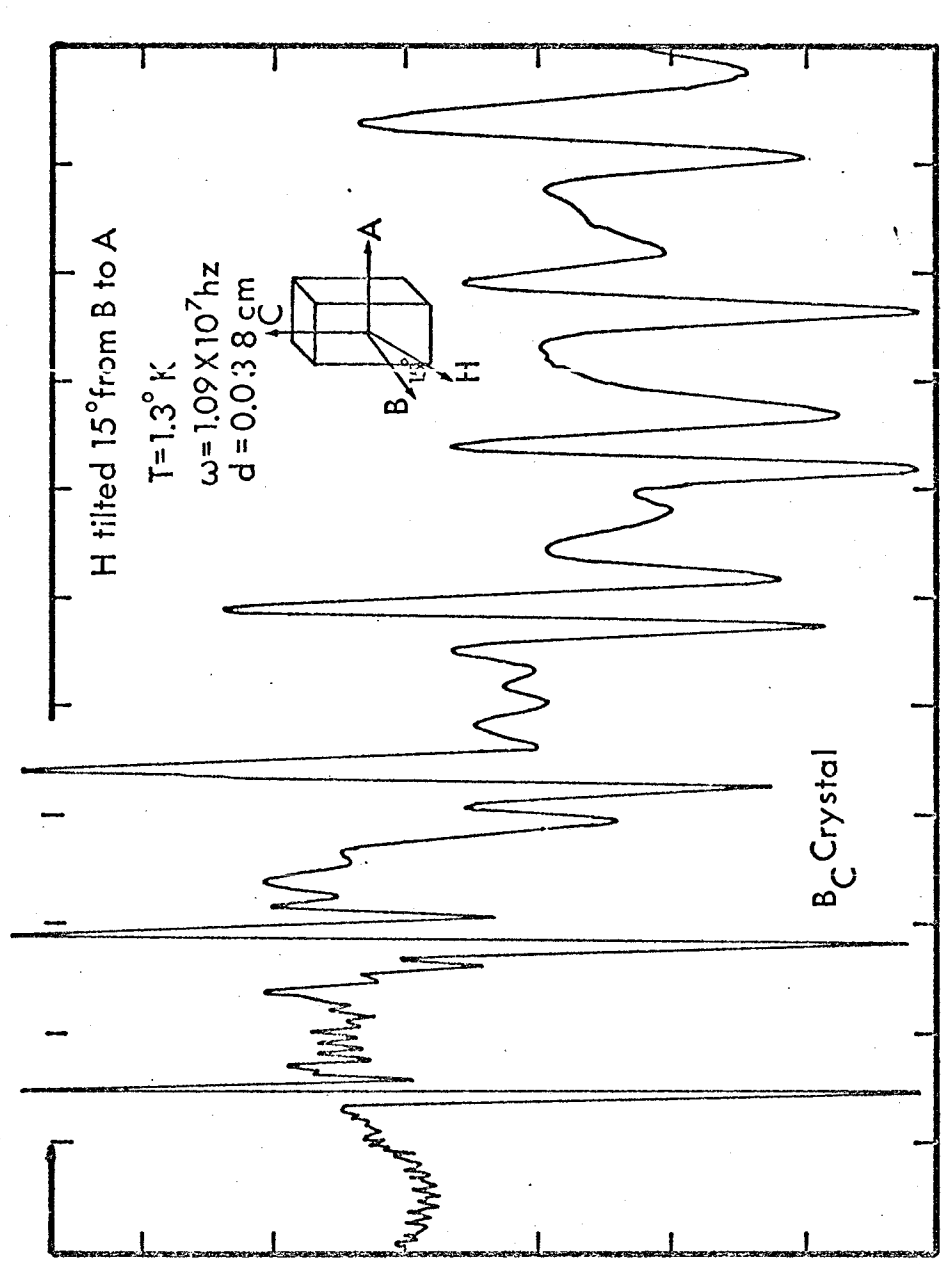
H tilted 15° from B to A
T=1.3° K
ω=1.09X10⁷hz
d=0.038 cm
C
A
B
H
B_C Crystal
0.4
0
0.4
Change in Transmission Ratio X10⁶gauss/gauss
0
100
200
300
400
500
600
700
800
900
1000
1100
Magnetic Field (gauss)

Fig 6-37

Fig 6-38

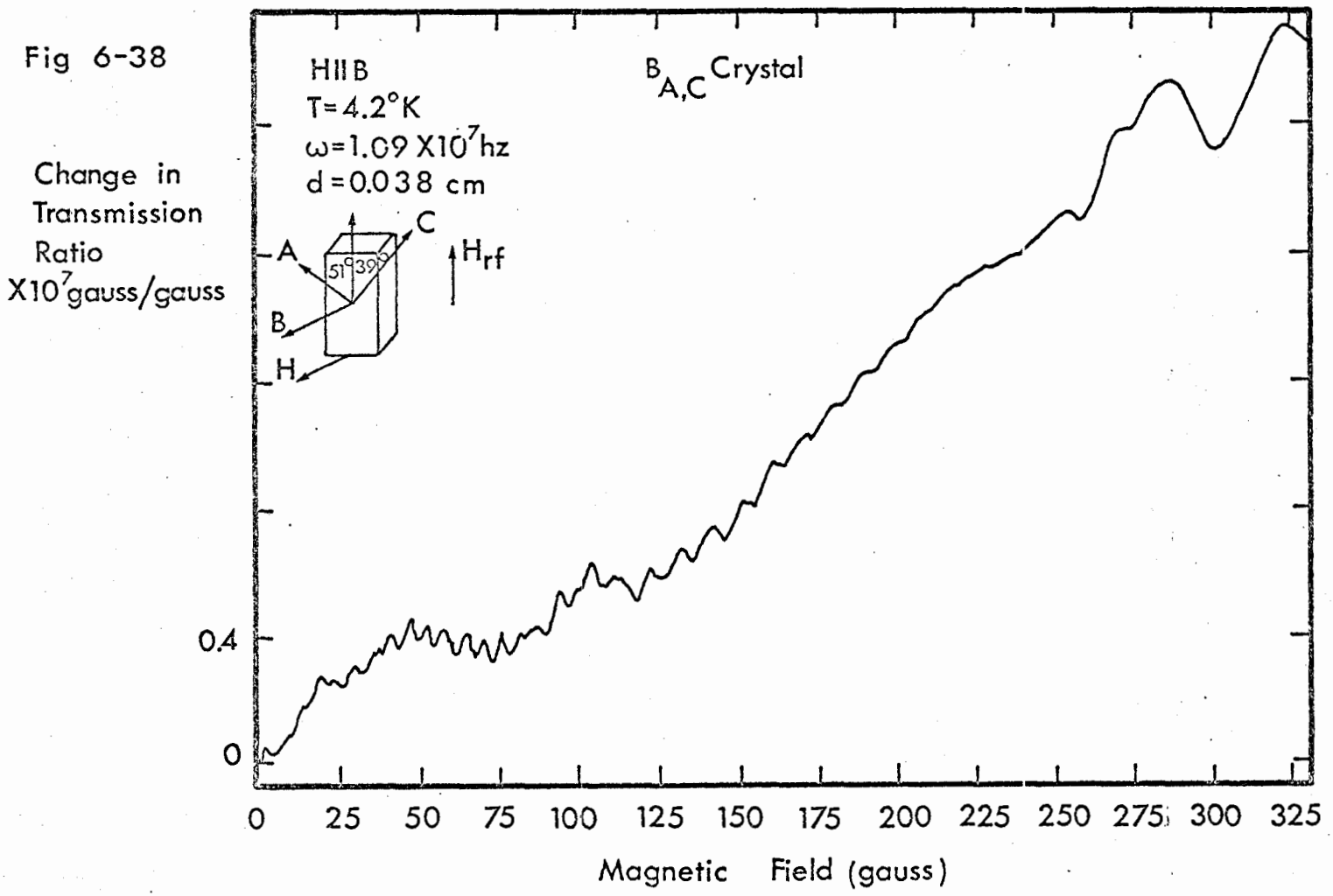
Change in
Transmission
Ratio
X10⁷gauss/gauss
H⊥B
T=4.2°K
ω=1.09 X10⁷hz
d=0.038 cm
B A,C Crystal
A
B
C
H
51°39'
H rf
0.4
0
0 25 50 75 100 125 150 175 200 225 250 275 300 325
Magnetic Field (gauss)

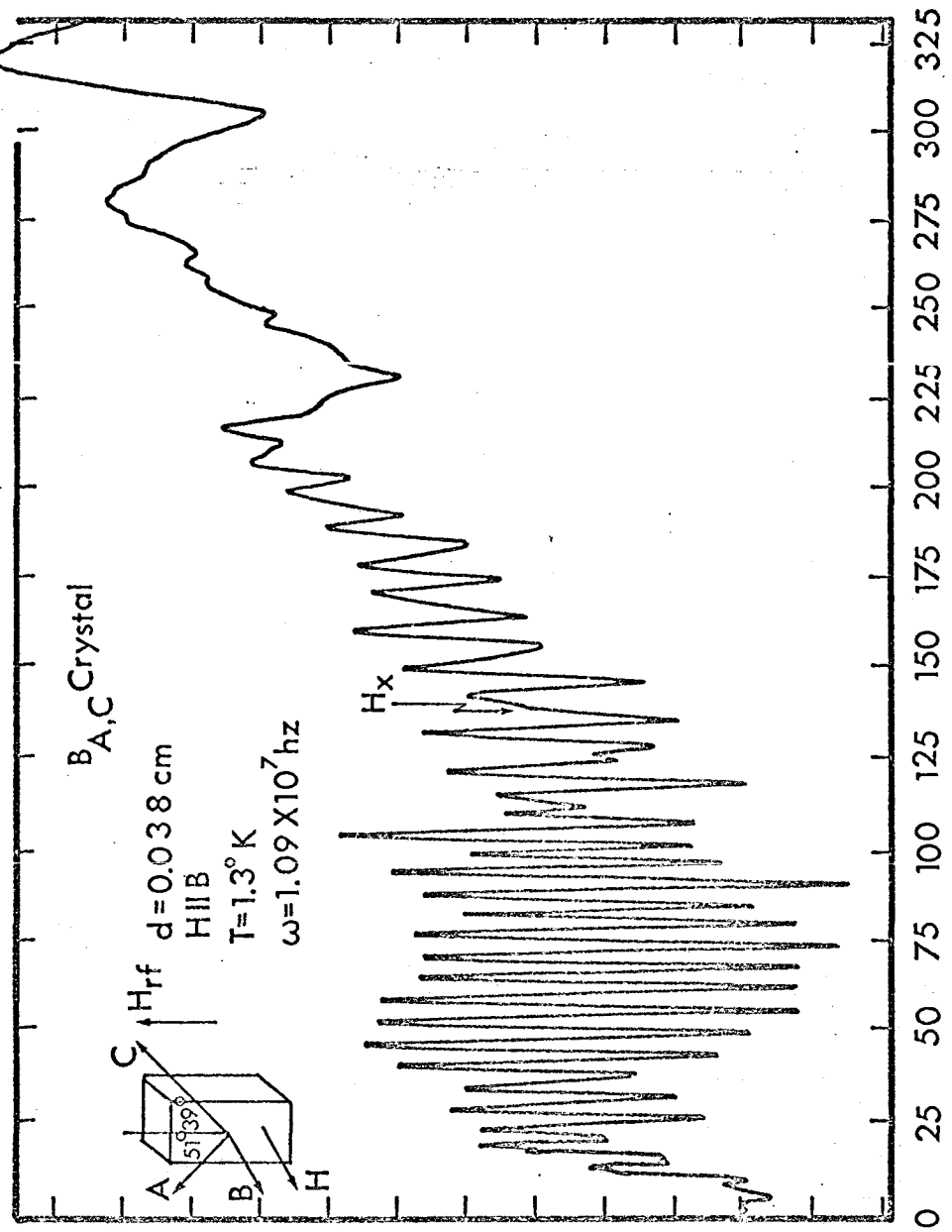
B A,C Crystal
d=0.038 cm
H II B
T=1.3° K
ω=1.09 X10⁷ hz
H_rf
H_x
C
A
B
H
51°39'
0.4
0
0.4
0 25 50 75 100 125 150 175 200 225 250 275 300 325
Magnetic Field (gauss)
Change in Transmission Ratio X10⁷ gauss/gauss

Fig 6-39

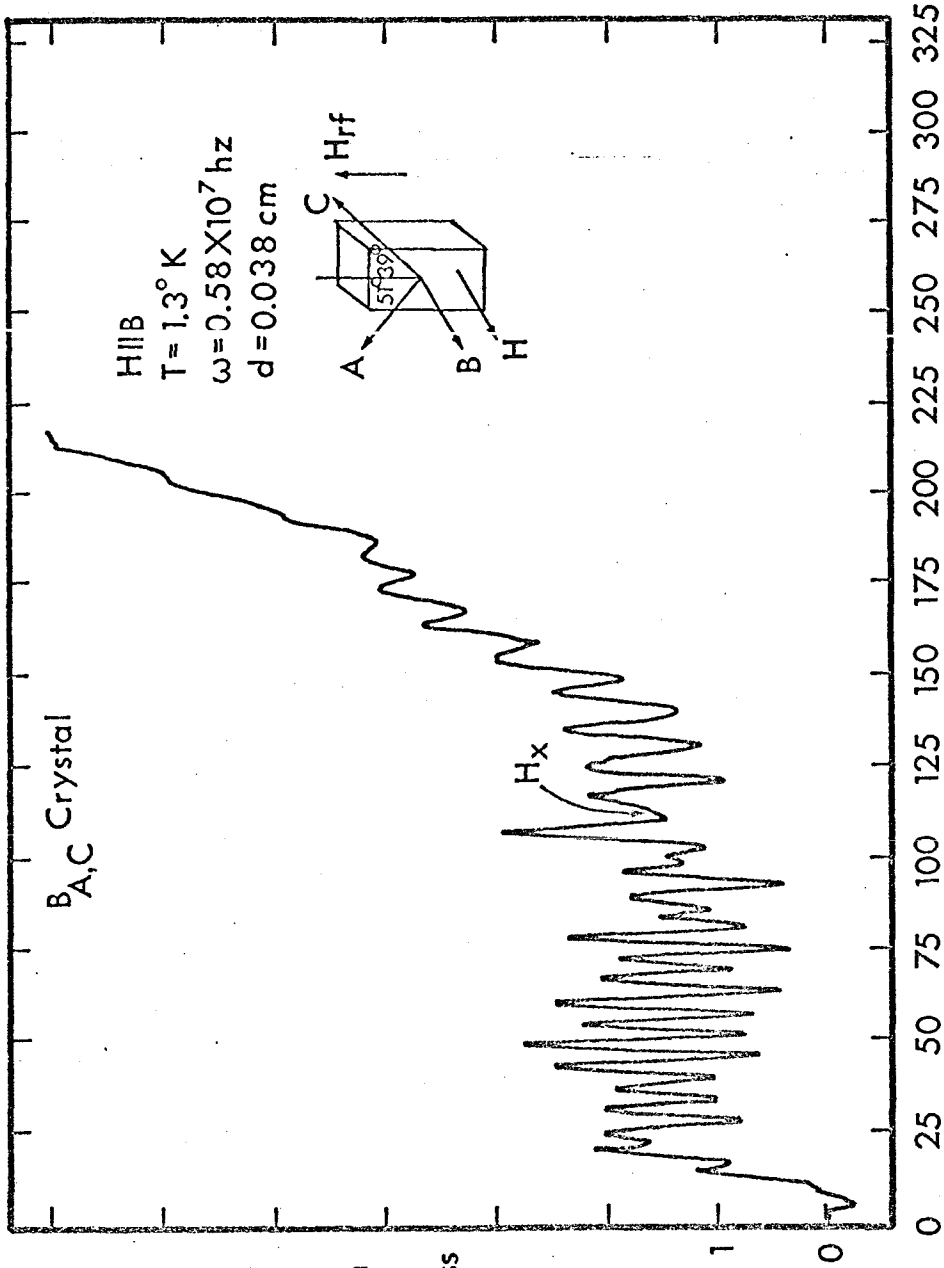
H⊥B
T= 1.3° K
ω=0.58X10⁷ hz
d=0.038 cm
C
Hrf
A
B
H
B A,C Crystal
Hx
Change in Transmission Ratio X10⁸ gauss/gauss
1
0
0 25 50 75 100 125 150 175 200 225 250 275 300 325
Magnetic Field (gauss)

Fig 6-40

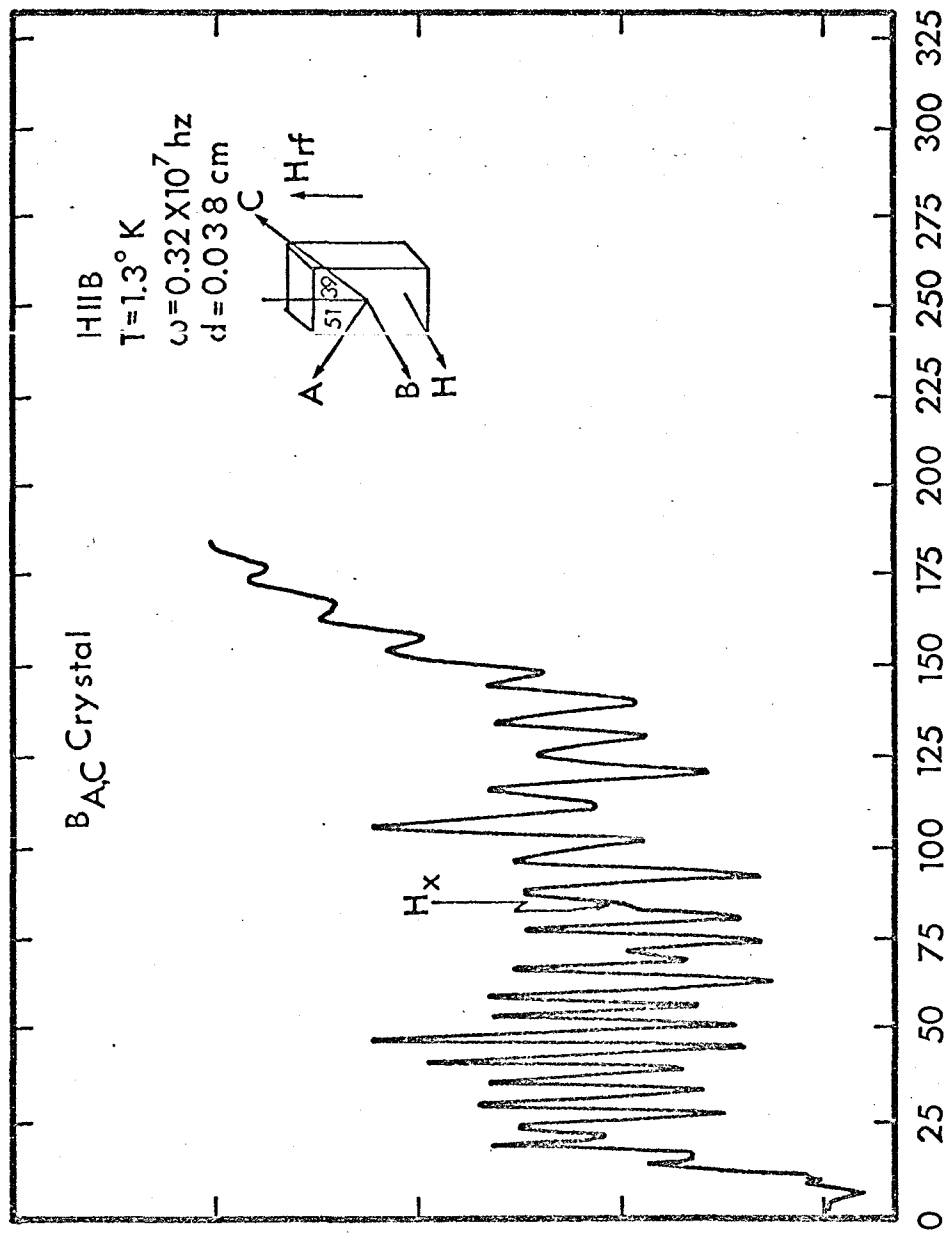
H||B
T=1.3° K
ω=0.32 X10^7 hz
d=0.038 cm
C
Hrf
A
B
H
51
39
B_A,C Crystal
Hx
Change in Transmission Ratio X10^8 gauss/gauss
1
0
0 25 50 75 100 125 150 175 200 225 250 275 300 325
Magnetic Field (gauss)

Fig 6-41

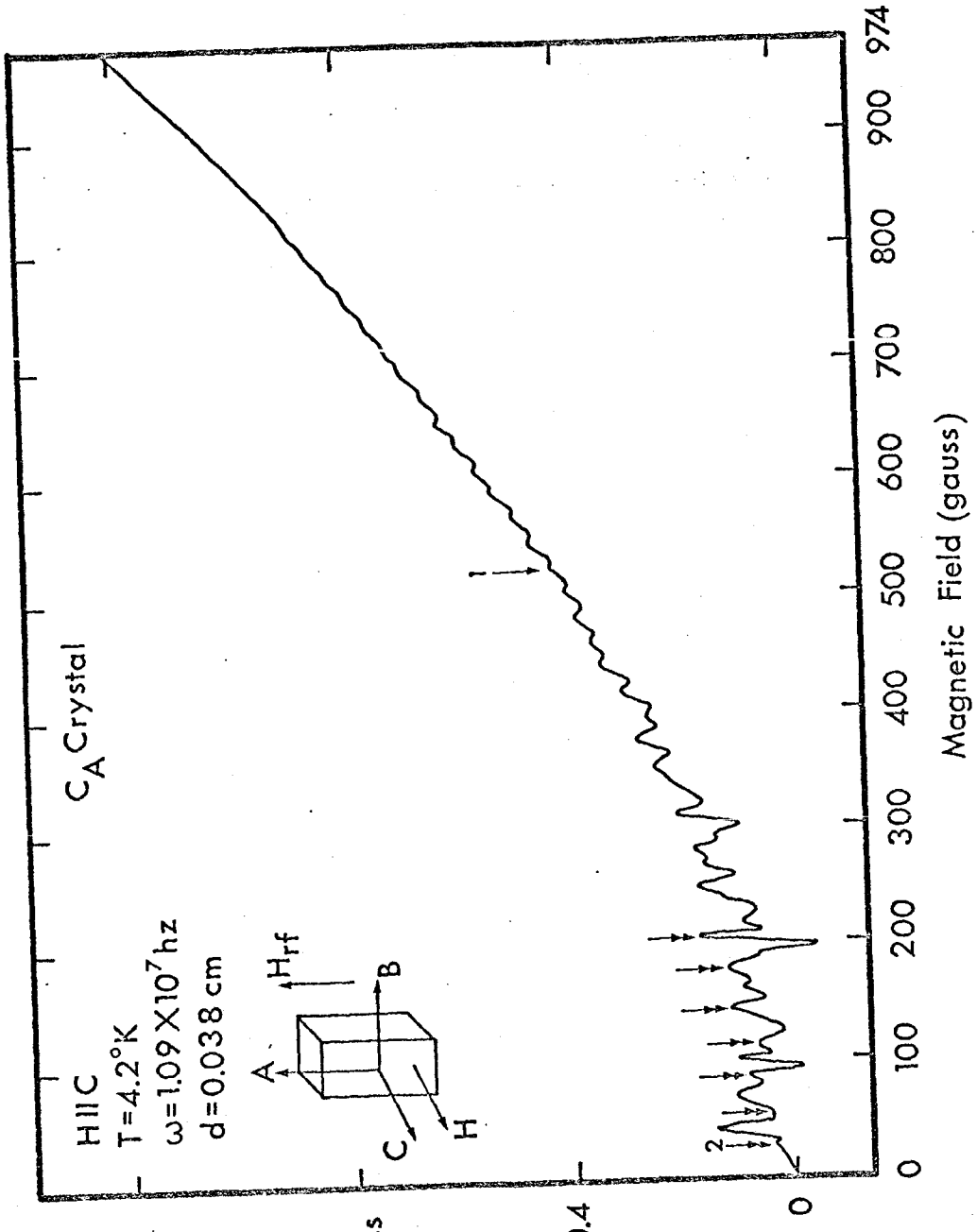
H⊥C
T=4.2°K
ω=1.09 X 10^7 hz
d=0.038 cm
C_A Crystal
A
H_rf
B
C
H
1
2
0
0.4
0
100
200
300
400
500
600
700
800
900
974
Magnetic Field (gauss)
Change in Transmission Ratio X10^6 gauss/gauss

Fig 6-42

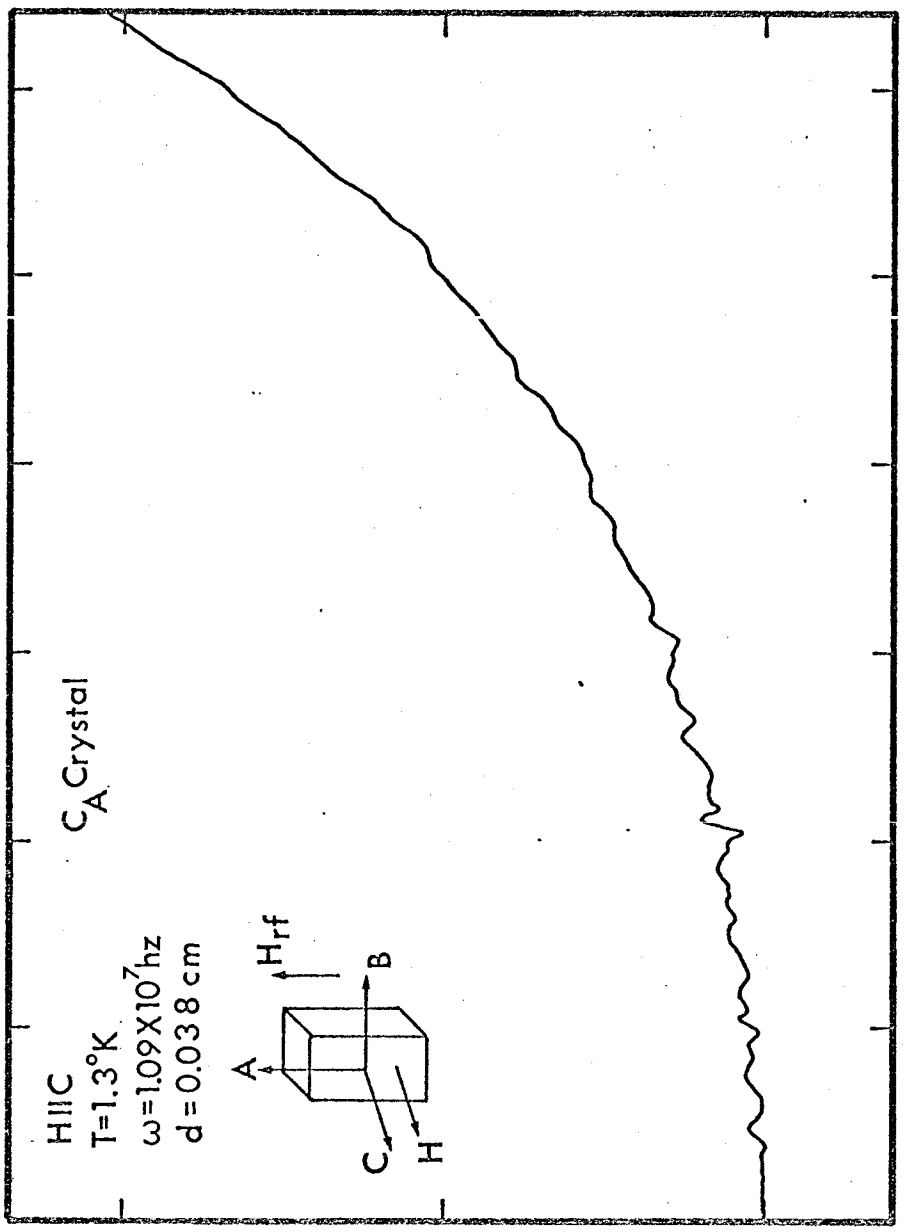
H⊥C
T=1.3°K
ω=1.09X10⁷hz
d=0.038 cm
C_A Crystal
A
B
C
H
H_rf
0.4
0
0
100
200
300
400
500
600
Magnetic Field (gauss)
Change in Transmission Ratio X10⁵gauss/gauss

Fig 6-43

Fig 6-44

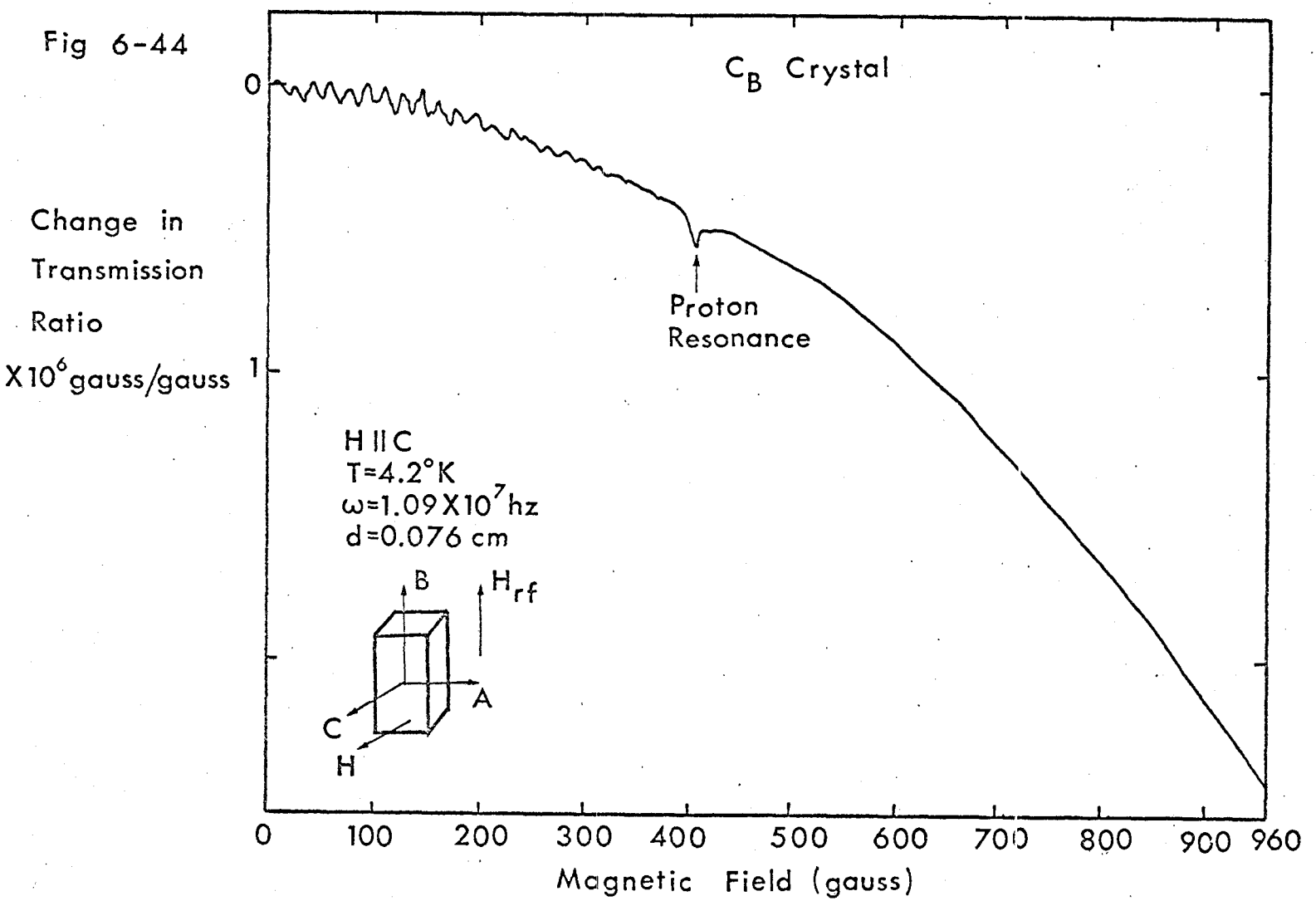
C_B Crystal
Change in Transmission Ratio $X10^6$ gauss/gauss
0
1
Proton Resonance
H ⊥ C
T=4.2°K
ω=1.09X10⁷hz
d=0.076 cm
B
H_{rf}
A
C
H
0
100
200
300
400
500
600
700
800
900
960
Magnetic Field (gauss)

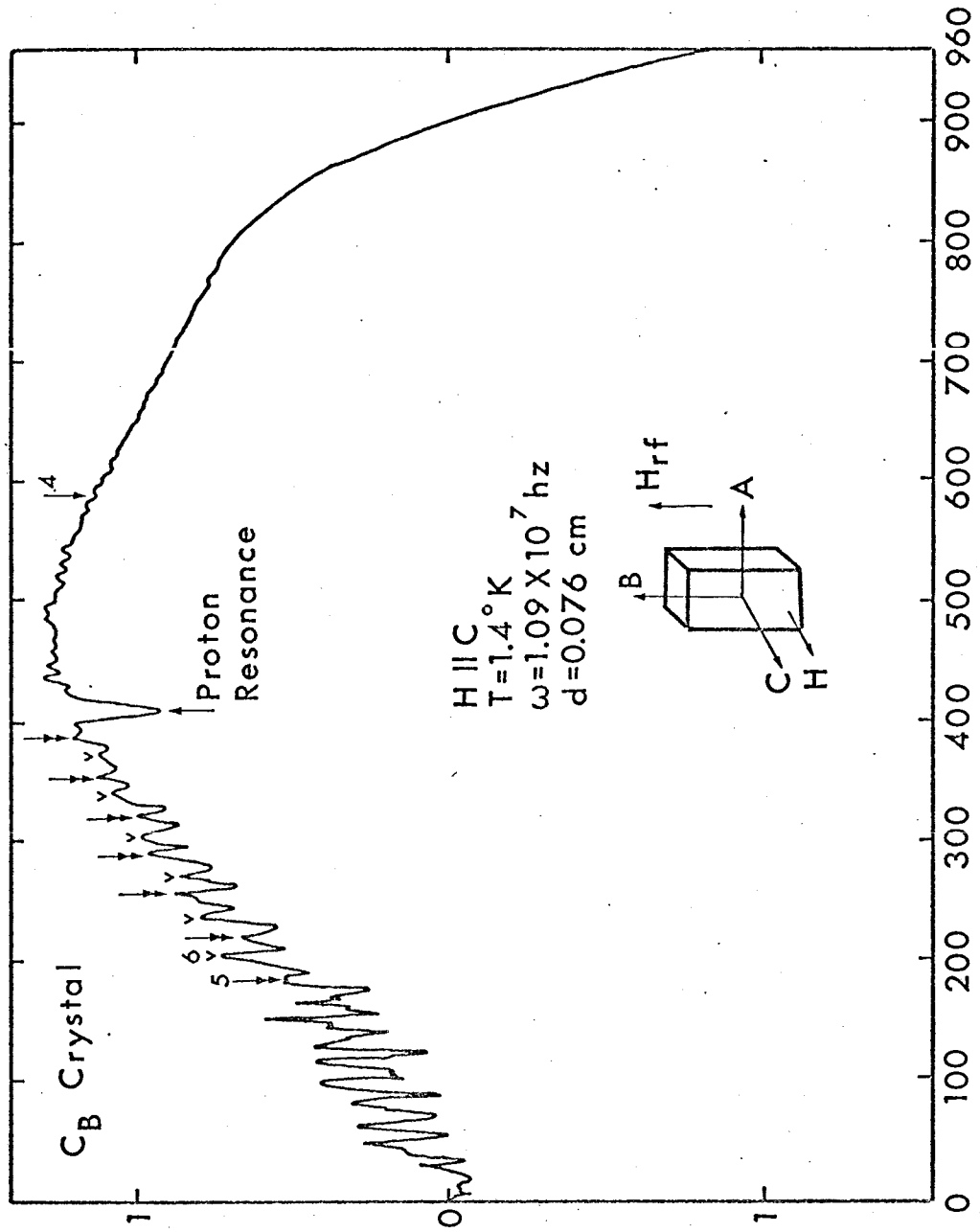
C_B Crystal
Proton Resonance
4
5
6
H ⊥ C
T=1.4° K
ω=1.09 X 10⁷ hz
d=0.076 cm
B
H_{rf}
A
C
H
1
0
1
0
100
200
300
400
500
600
700
800
900
960
Magnetic Field (gauss)
Change in Transmission Ratio X10⁶ gauss/gauss

Fig 6-45

Fig 6-46

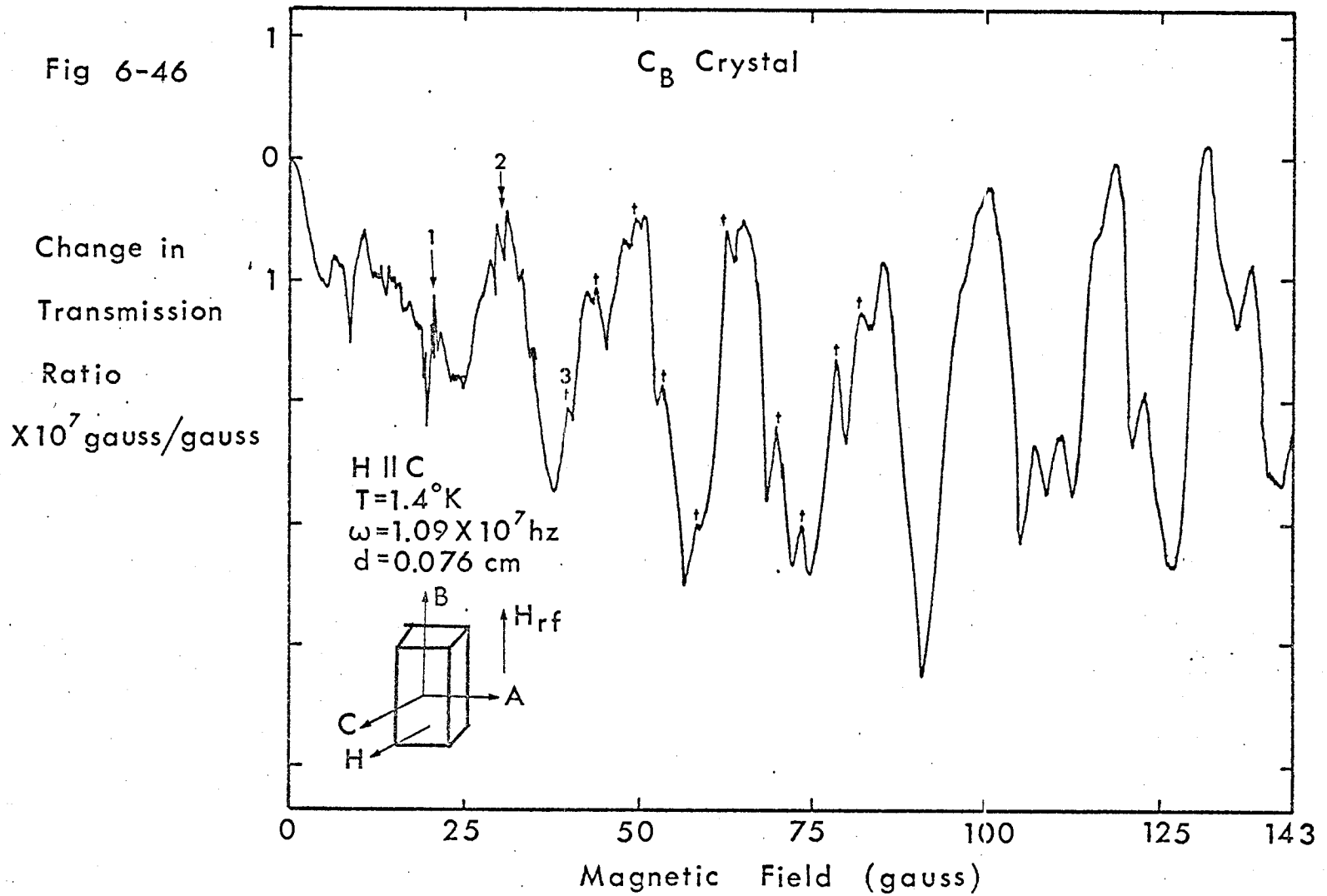
C_B Crystal
Change in Transmission Ratio X10^7 gauss/gauss
1
0
1
2
3
H ⊥ C
T=1.4°K
ω=1.09 X 10^7 hz
d=0.076 cm
B
H_{rf}
A
C
H
0
25
50
75
100
125
143
Magnetic Field (gauss)

Fig 6-47

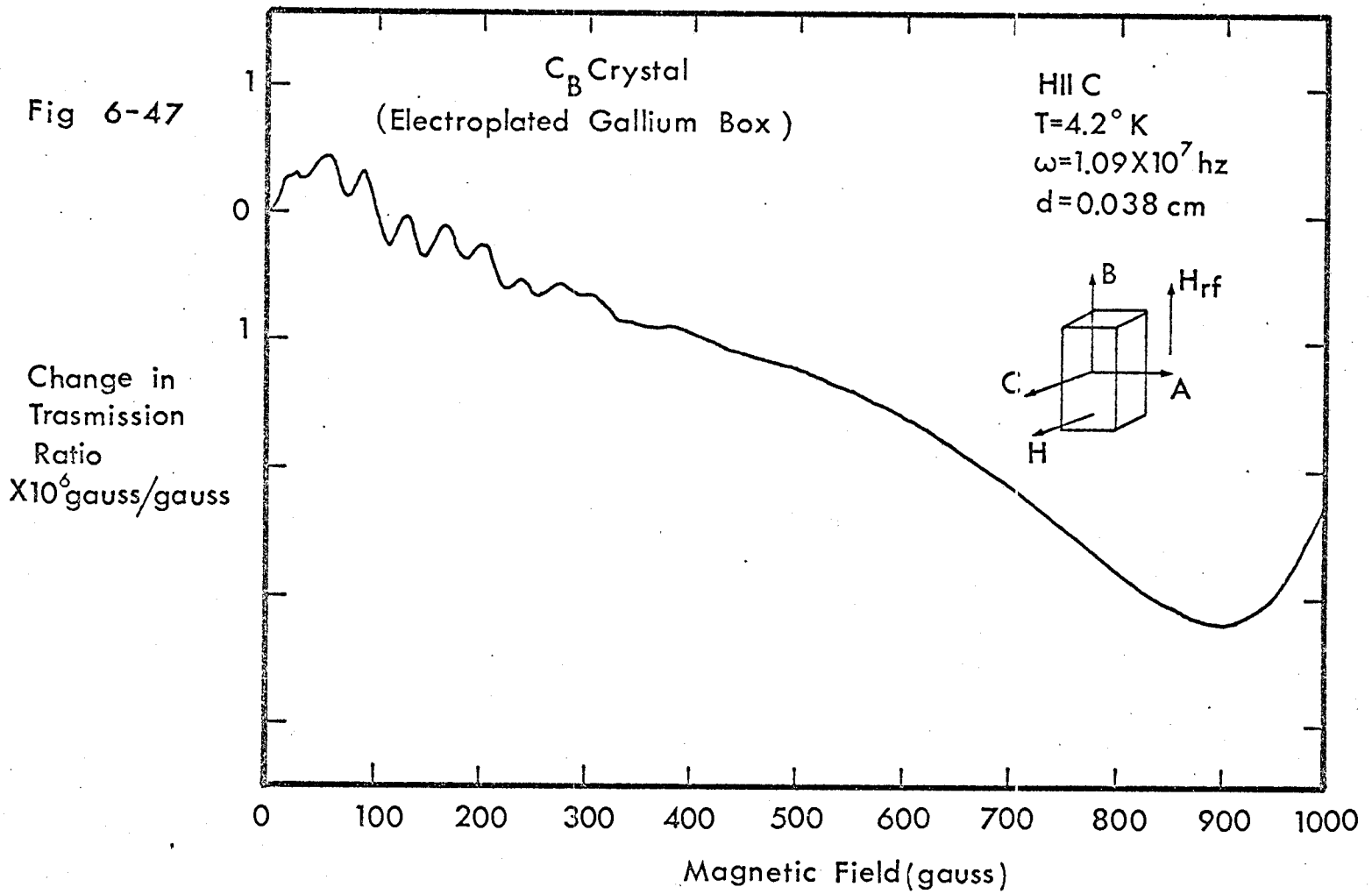
C_B Crystal
(Electroplated Gallium Box)
H‖ C
T=4.2° K
ω=1.09X10⁷ hz
d=0.038 cm
B
H_{rf}
C
A
H
1
0
1
Change in Trasmission Ratio X10⁶gauss/gauss
0
100
200
300
400
500
600
700
800
900
1000
Magnetic Field(gauss)

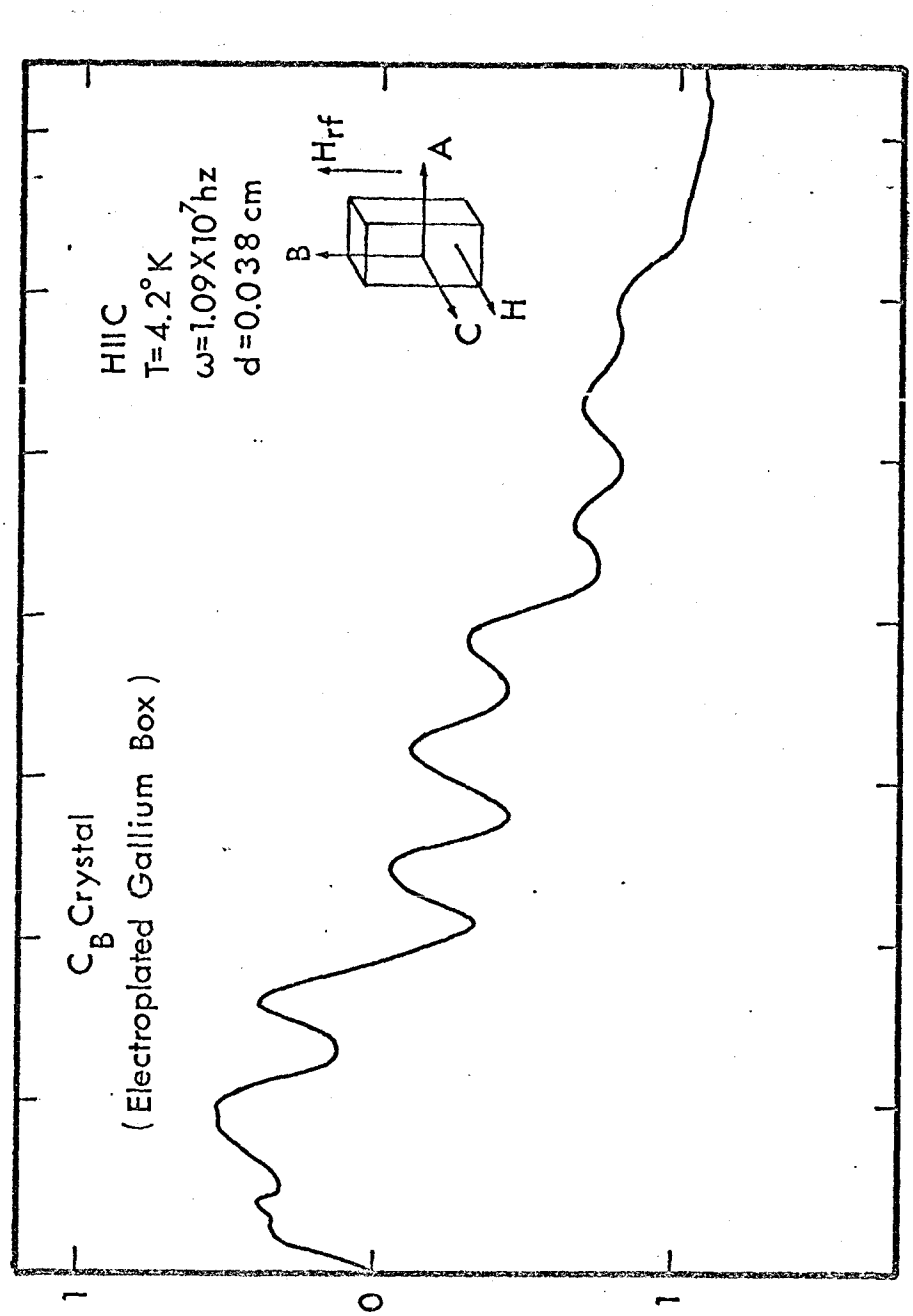
C_B Crystal
(Electroplated Gallium Box)
H⊥C
T=4.2°K
ω=1.09X10⁷hz
d=0.038 cm
H_{rf}
A
B
C
H
1
0
1
0
50
100
150
200
250
300
350
371.5
Magnetic Field (gauss)
Change in Transmission Ratio X10⁶gauss/gauss

Fig 6-48

Fig 6-49

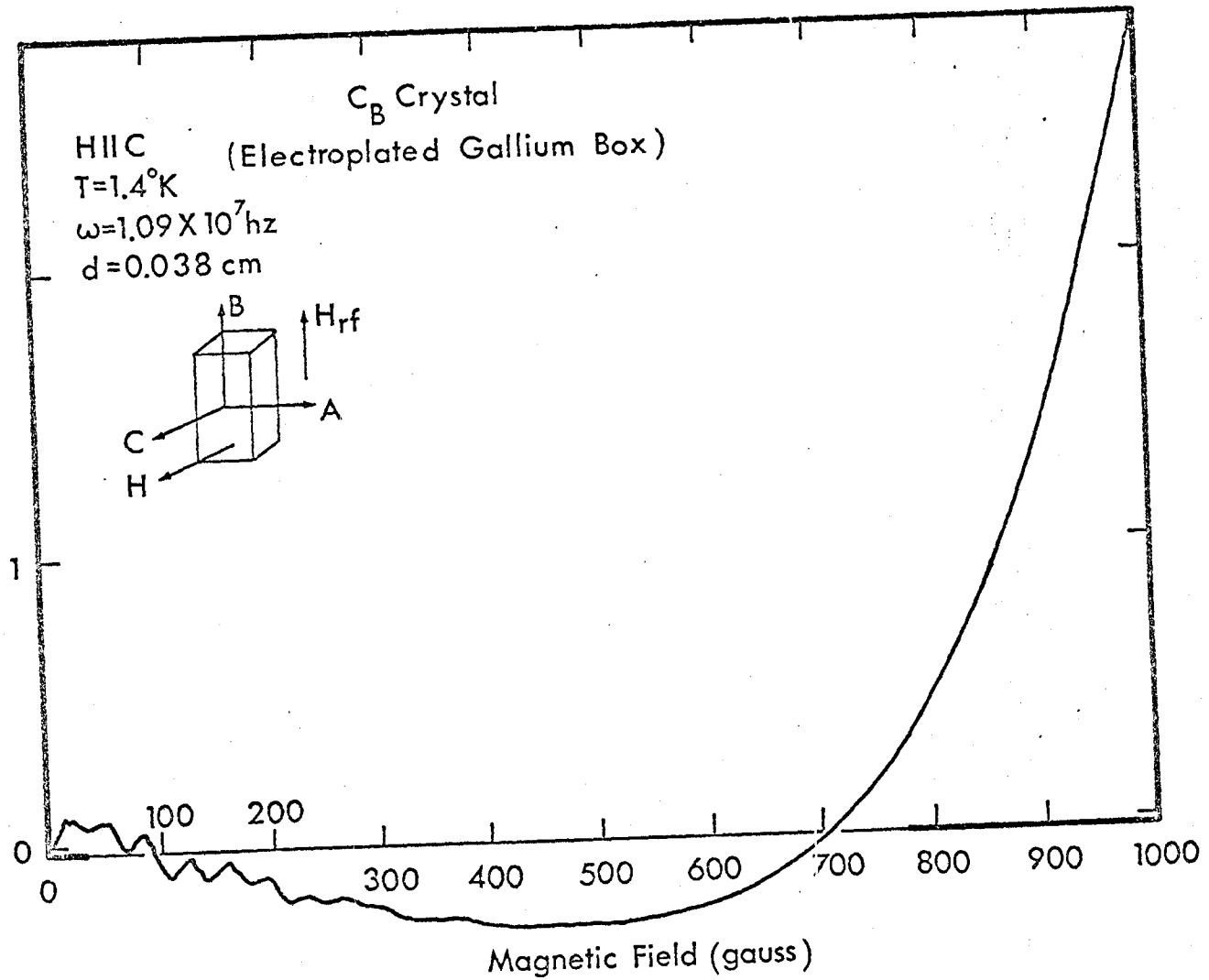
C_B Crystal
(Electroplated Gallium Box)
H II C
T=1.4°K
ω=1.09 X 10^7 hz
d=0.038 cm
B
H_{rf}
A
C
H
Change in Transmission Ratio X10^5 gauss/gauss
1
0
0
100
200
300
400
500
600
700
800
900
1000
Magnetic Field (gauss)

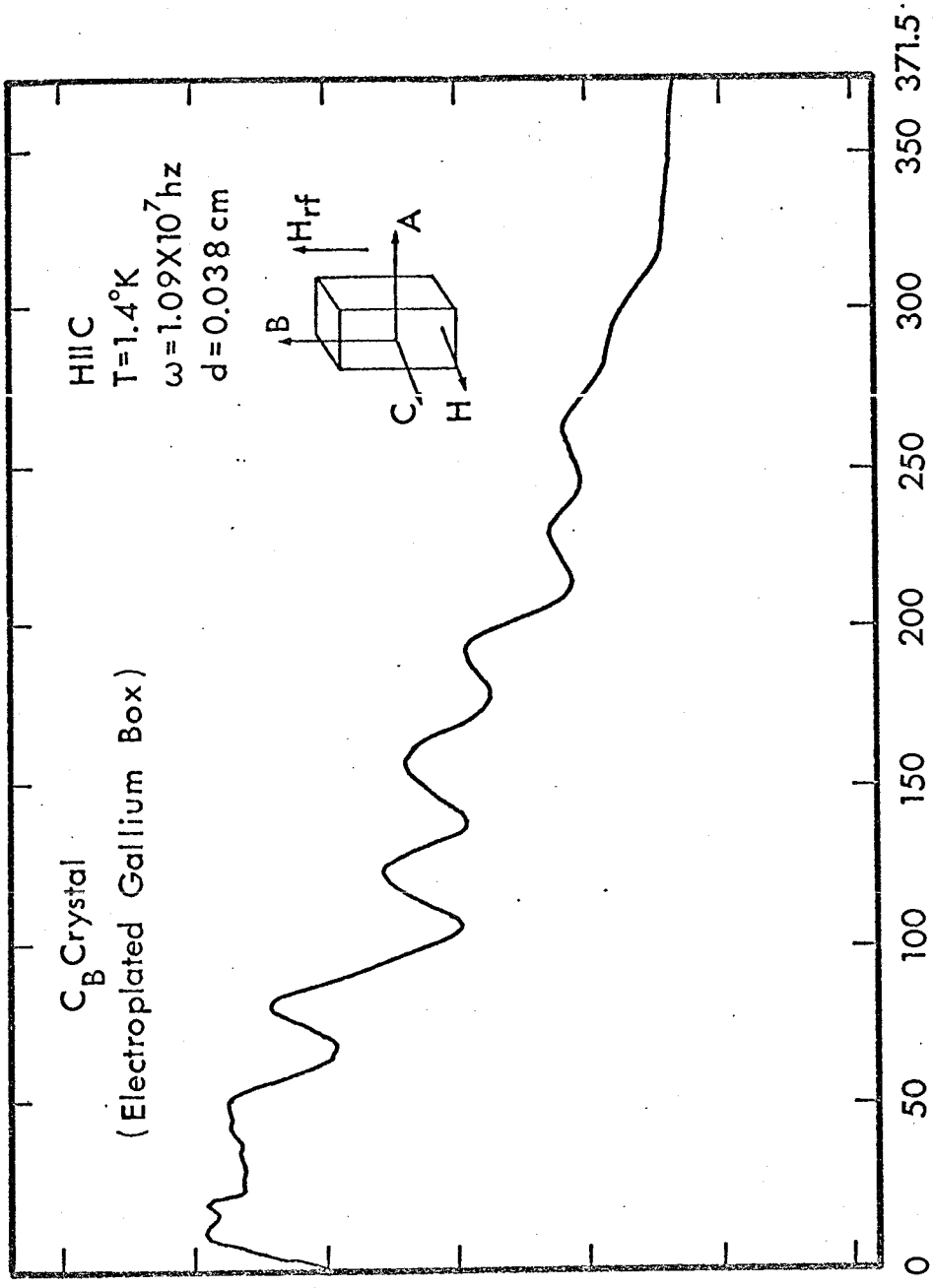
C_B Crystal
(Electroplated Gallium Box)
H⊥C
T=1.4°K
ω=1.09X10⁷hz
d=0.038 cm
H_{rf}
A
B
C
H
1
0
1
0
50
100
150
200
250
300
350
371.5
Magnetic Field (gauss)
Change in Transmission Ratio X10⁶gauss/gauss

Fig 6-50

TABLE 6-5. Gantmakher-Kaner Periods Observed in Gallium Crystals

Crystal	Thickness (cm)	Period Reference	Period (gauss) This Work	Period (gauss) Munarin et al.[36]*
A_B	0.038	Fig.6-24 (1)	7.35	
		(2)	59	
		(3)	103	
		(4)	147	222
A_C	0.038	Fig.6-26 (1)	14.8	
		(2)	83	135
		(3)	65	209
B_A	0.038	Fig.6-30 (1)	5.6	
		(2)	5.3	
		(3)	5.9	
B_C	0.038	Fig.6-35 (1)	9.5	
		(2)	120	
C_A	0.038	Fig.6-42 (1)	20.6	
		(2)	29.5	
C_B	0.076	Fig.6-46 (1)	0.7	
		(2)	1.35	
		(3)	4.0	
		Fig.6-45 (4)	11.7	
		(5)	35	
		(6)	32	

*periods adjusted to correspond to a crystal of our thickness.

Table 6-5 gives a summary of the Gantmakher-Kaner periods observed in gallium crystals. Only those periods which are reasonably clear are included*. For comparison purposes we have included periods seen by Munarin, Marcus, and Bloomfield[36] in magnetoresistance measurements. Oscillations in magnetoresistance are actually manifestations of oscillations in the conductivity. These oscillations in the conductivity, called Sondheimer oscillations, have a period given by,

$$\Delta H = \frac{2\pi m^* c \bar{v}_z}{ed \sec\theta} = \frac{\hbar c}{ed}\left(\frac{\partial A}{\partial k_H}\right)_{ext} \frac{1}{\sec\theta}$$

where m* is the effective mass of the electron, θ is the angle which the field makes with the sample normal, $\bar{v}_z$ is the projection of the electron velocity along H averaged over the orbit, and d is the specimen thickness. Since the period varies with specimen thickness, we have adjusted the periods seen by Munarin et al. in order that they correspond to a sample of our thickness.

The most clearly defined oscillations were observed in B_A and B_C crystals. These oscillations appear as the magnetic field is increased from zero, grow in amplitude until a maximum occurs, and then slowly decrease in amplitude until they

---

* Periods which were clear in the original transmission versus magnetic field recordings, but not necessarily obvious in these reproductions, are also included.

disappear at sufficiently large magnetic fields. The amplitude envelope of these oscillations is shown as a function of magnetic field in Fig. 6-51.

When a B_A crystal which was 3 times thicker than the standard thickness (0.114 cm versus 0.038 cm) was investigated, it was found that more oscillations occurred in the thicker crystal and that the amplitude envelope changed slightly in shape. A comparison of the envelope shape for these two B_A crystals of different thicknesses is shown in Fig. 6-52. The increase in the number of oscillations seen was found to be directly proportional to the increase in the specimen thickness. At a frequency of 1.74 Mhz, 39 fringes were seen in the 0.038 thick crystal whereas approximately 114 fringes were observed in the 0.114 cm thick crystal (117 if the number is extrapolated to zero magnetic field). See Fig. 6-33. The ratio of the crystal thicknesses was 3:1 and the ratio of the number of fringes observed in each case was approximately 2.9:1 (exactly 3:1 if 117 fringes is used for the thick crystal).

Because there is an envelope to the amplitude of the oscillations observed in B_A and B_C crystals, it is reasonable to characterize these oscillations by the field at which the amplitude is a maximum. We have called this field H_m. An investigation was made to determine if this field value, H_m, varied with radiation frequency. The results of this study

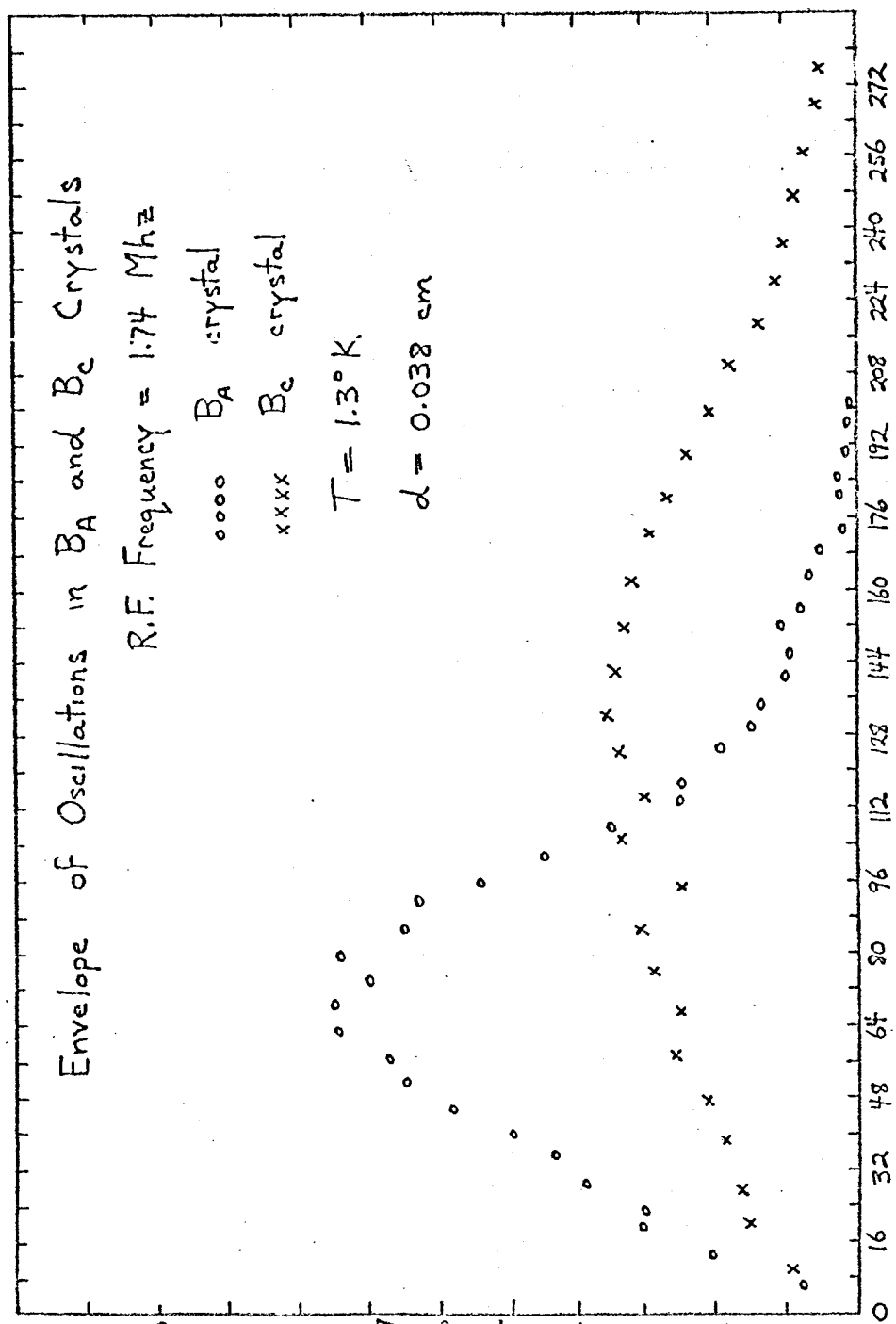
Envelope of Oscillations in B_A and B_c Crystals
R.F. Frequency = 1.74 Mhz
oooo B_A crystal
xxxx B_c crystal
T = 1.3° K
d = 0.038 cm
Transmission Units
Magnetic Field (gauss)
0 16 32 48 64 80 96 112 128 144 160 176 192 208 224 240 256 272
1 2 3 4 5 6 7 8 9 10 11

Fig 6-51

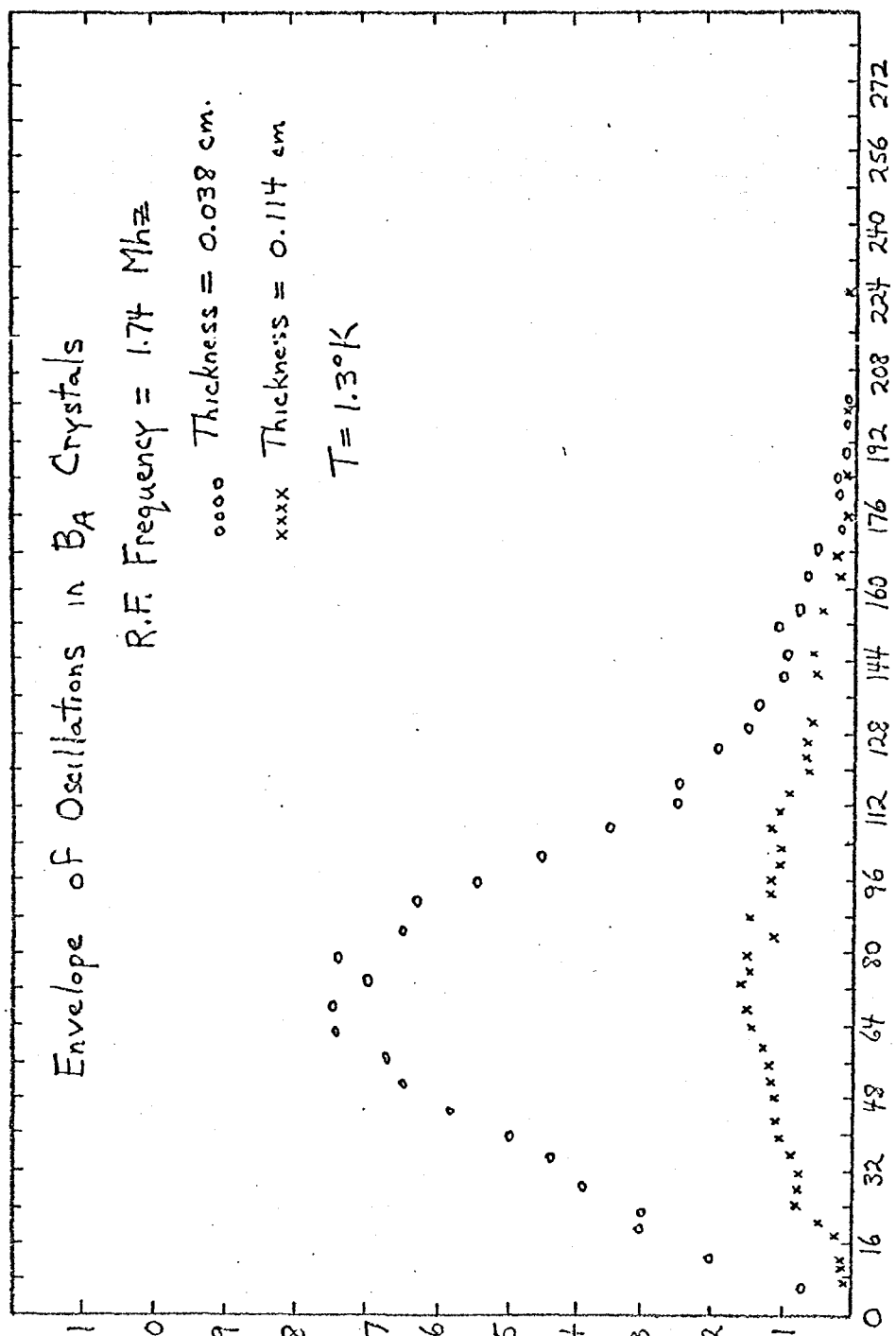
Envelope of Oscillations in B_A Crystals
R.F. Frequency = 1.74 Mhz
oooo Thickness = 0.038 cm.
xxxx Thickness = 0.114 cm.
T = 1.3°K
Transmission Units
Magnetic Field (gauss)
0
16
32
48
64
80
96
112
128
144
160
176
192
208
224
240
256
272
1
2
3
4
5
6
7
8
9
10
11

Fig 6-52

on a B_A crystal are given in Fig. 6-53. A frequency dependence is clearly indicated. The data appears to favour a $\omega^{1/3}$ dependence of H_m on frequency. We have chosen to plot H_m versus $\omega^{1/3}$ since the proportionality of H to $\omega^{1/3}$ (i.e. k to $\omega^{1/3}$) is characteristic of the anomalous skin effect. Similarly, we have plotted H_m as a function of $\omega^{2/5}$ because Falk et al[24] have suggested this dependence.

When the magentic field was tilted away from the normal direction but in a plane perpendicular to the radio frequency magnetic field, it was noticed that the period of the oscillations changed. Fig. 6-54 shows the variation of the period for the B_A oscillations with rotation of the magnetic field in the B, C plane.

Although the same Gantmakher-Kaner period did not appear in the B_A and B_C crystals, 5.6 ± 0.02 gauss for the B_A crystal and 9.5 ± 0.01 gauss for the B_C crystal, both periods appeared in a $B_{A,C}$ crystal. The notation for this $B_{A,C}$ crystal, means that the B-axis was normal to the surface of the sample (the A, C plane), but that the A-axis and C-axis were rotated such that neither axis was parallel to either the width or length of the crystal (see Fig. 6-38). At low fields the characteristic B_A oscillations predominated while at higher values of the magnetic field, oscillations characteristic of the B_C crystal predominated. We have called the field at which the oscillations change character the "crossover field", H_x.

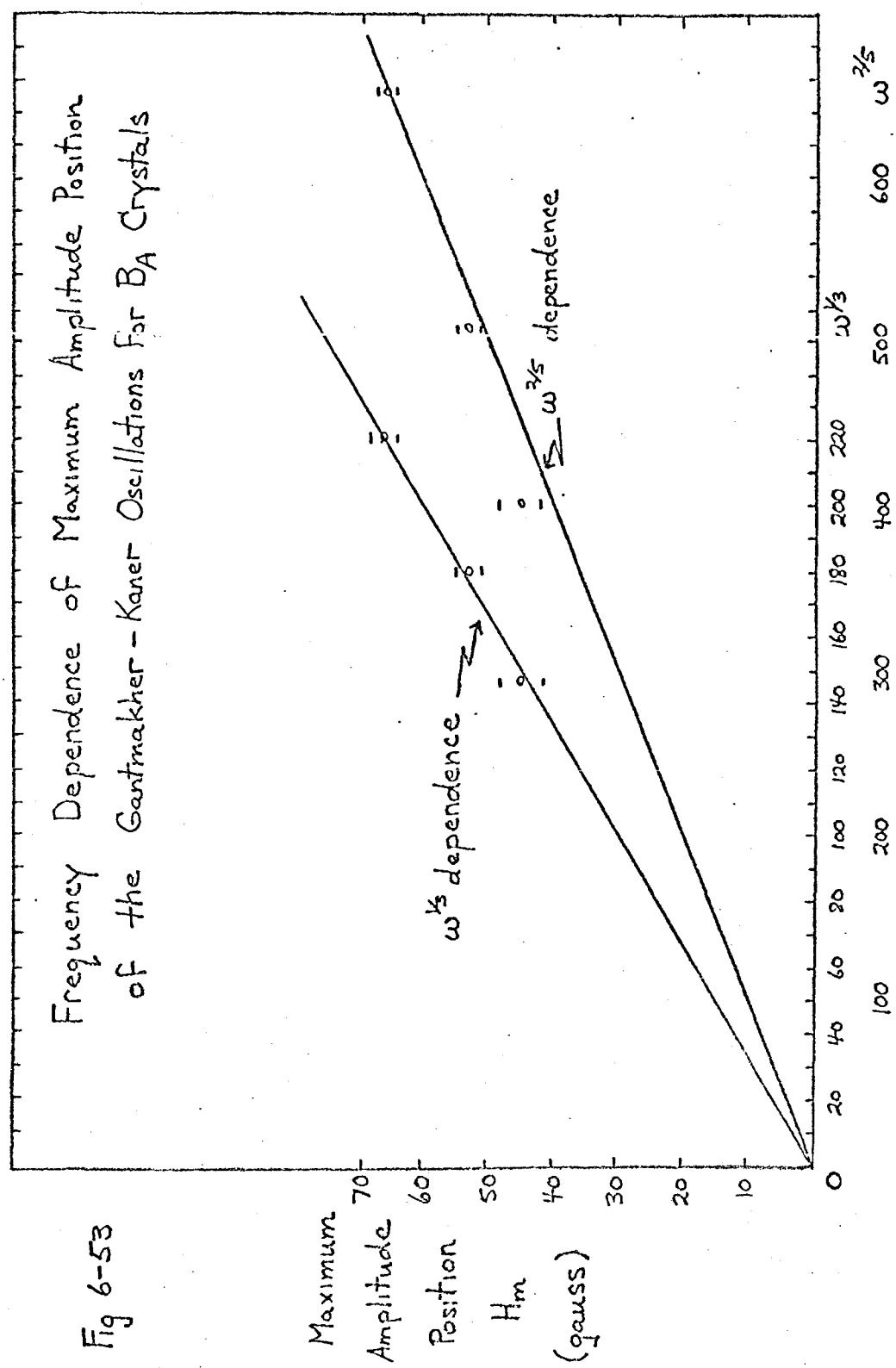
Frequency Dependence of Maximum Amplitude Position
of the Gantmakher - Kaner Oscillations For B_A Crystals
$\omega^{1/3}$ dependence
$\omega^{2/5}$ dependence
Maximum Amplitude Position H_m (gauss)
Frequency
$\omega^{1/3}$
$\omega^{2/5}$

Fig 6-53

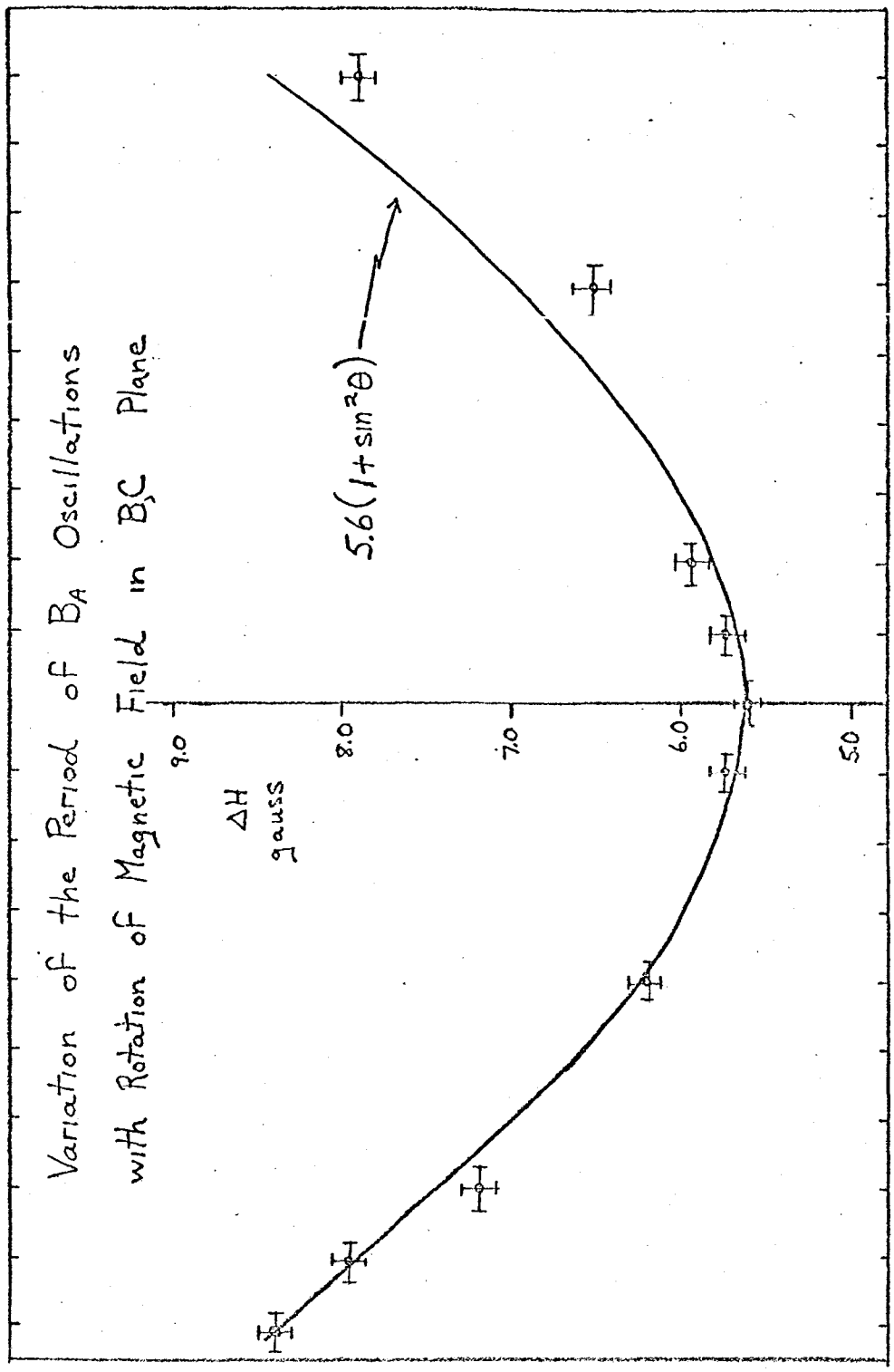
Variation of the Period of B_A Oscillations
with Rotation of Magnetic Field in BC Plane
$5.6(1+\sin^2\theta)$
ΔH
gauss
9.0
8.0
7.0
6.0
5.0
-45° -40° -35° -30° -25° -20° -15° -10° -5° 0° 5° 10° 15° 20° 25° 30° 35° 40° 45°
Angle of Rotation (counterclockwise positive)

Fig 6-54

H_x was found to be frequency dependent. The data, given in Fig. 6-55, appear to favour a $\omega^{2/5}$ dependence over the $\omega^{1/3}$ dependence.

Figs. 6-47 to 6-50 show the results obtained from an electroplated gallium box having a C_B orientation. These results are to be compared with the results obtained using the standard method whereby the crystal is soldered to a rectangular copper trough (Figs. 6-44 to 6-46). It is important to note that the crystals are of different thicknesses. It is clear that fundamental discrepancies exist in these two separate results.

Measurements of the amplitude of the Gantmakher-Kaner oscillations as a function of temperature were made in order to determine the temperature dependent part of the electron mean free path. These measurements were made on a $B_{A,C}$ crystal, and the amplitude measurement was made at the position of maximum amplitude of the oscillations characteristic of a B_A crystal. The results of this investigation are given in Fig. 6-56. Clearly a T^2 temperature dependence is indicated. The data can be fitted by the relation,

$$\frac{A(T)}{A(4.2^\circ K)} = 45 \exp(-0.216 T^2)$$

Fig 6-55

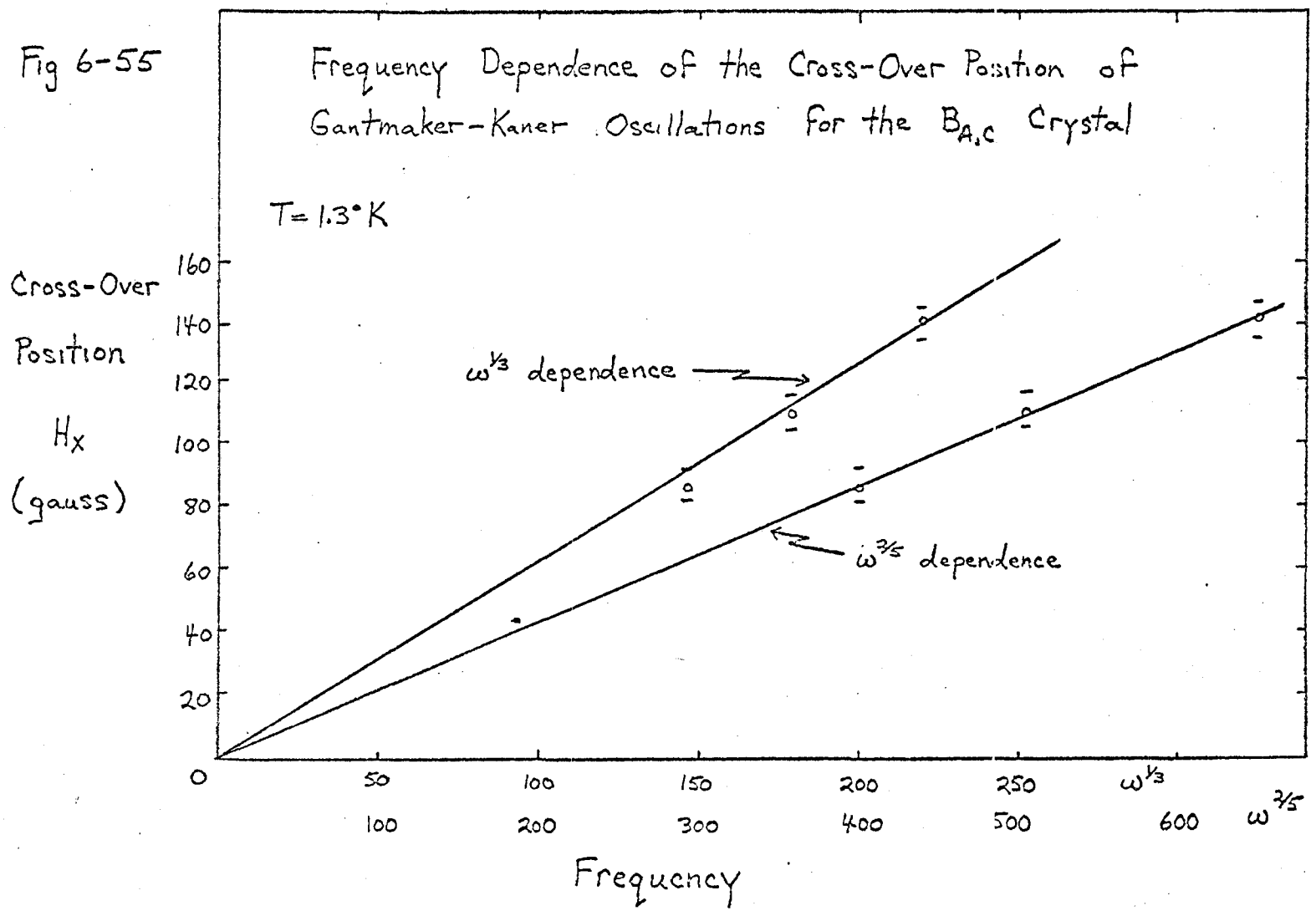
Frequency Dependence of the Cross-Over Position of Gantmaker-Kaner Oscillations for the $B_{A,C}$ Crystal
T = 1.3° K
Cross-Over Position H_x (gauss)
160
140
120
100
80
60
40
20
0
$\omega^{1/3}$ dependence
$\omega^{3/5}$ dependence
50
100
150
200
250
$\omega^{1/3}$
100
200
300
400
500
600
$\omega^{3/5}$
Frequency

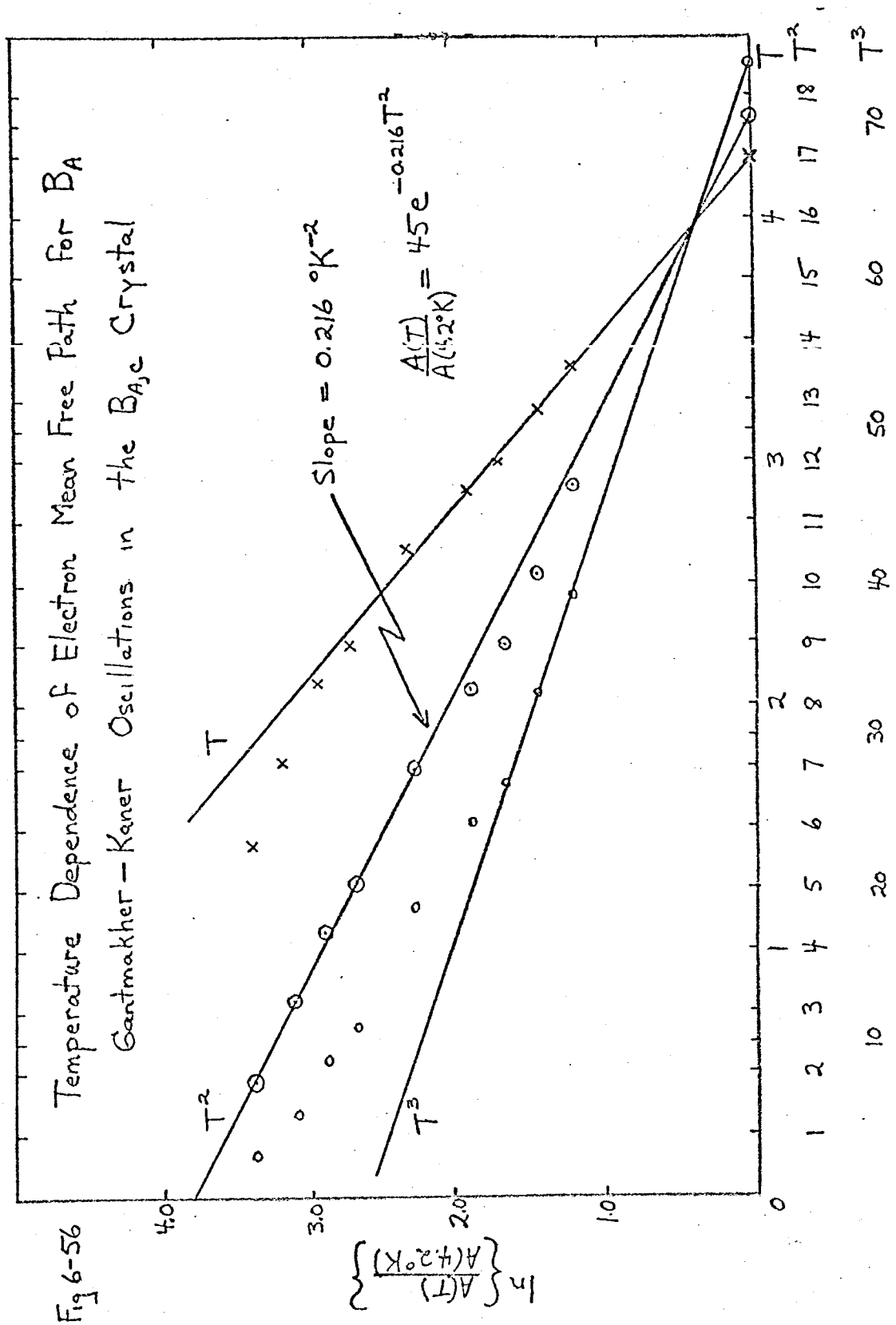
Temperature Dependence of Electron Mean Free Path for B_A
Gantmakher – Kaner Oscillations in the $B_{A,c}$ Crystal
Slope = 0.216 °K^{-2}
$\frac{A(T)}{A(4.2°K)} = 45e^{-0.216T^2}$
T
T^2
T^3
$\ln\left\{\frac{A(T)}{A(4.2°K)}\right\}$
4.0
3.0
2.0
1.0
0
1 2 3 4 5 6 7 8 9 10 11 12 13 14 15 16 17 18
10 20 30 40 50 60 70
1 2 3 4
T
T^2
T^3

Fig 6-56

6.4 Magnetic Field Parallel to Slab Surface But Perpendicular to the Radio Frequency Magnetic Field

In this experimental configuration one expects to see a minimum change in transmission ratio with magnetic field. The actual experimental results are given in Figs. 6-57 to 6-75. For several crystal orientations data has been included to show the effect of tilting the magnetic field several degrees into the surface of the metal (see Figs. 6-61, 6-66 and 6-68). Clearly, remarkable changes in transmission occur.

The data taken on the $B_{A,C}$ crystal has been included only for interest (Fig. 6-67 and Fig. 6-68). The data obtained from an electroplated gallium box specimen with a C_B orientation, again is included for purposes of comparison with data obtained from a similar crystal which was soldered to a rectangular copper trough. It is important to note the difference in thickness for these two crystals.

Figures (6-57) to (6-75)

Transmission through gallium single crystals as a function of d.c. magnetic field. The d.c. field is normal to the r.f. magnetic field but in the specimen plane. Note that the C_B crystal was twice as thick as the other specimens.

$H_0 \perp H_{rf}$, but in the specimen plane

Fig 6-57

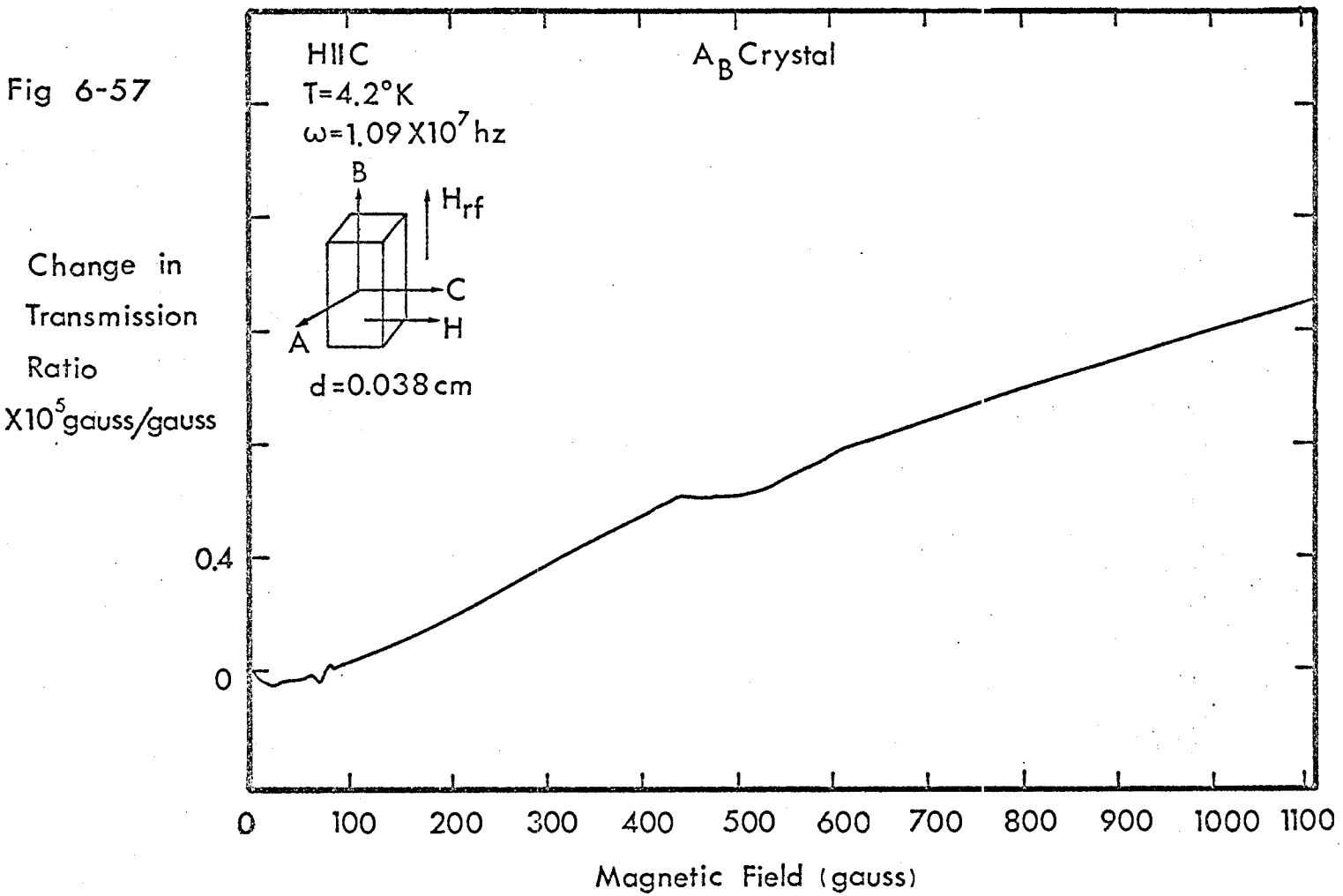
H⊥C
T=4.2°K
ω=1.09X10^7 hz
A_B Crystal
B
H_rf
C
H
A
d=0.038 cm
Change in Transmission Ratio X10^5 gauss/gauss
0.4
0
0
100
200
300
400
500
600
700
800
900
1000
1100
Magnetic Field (gauss)

Fig 6-58

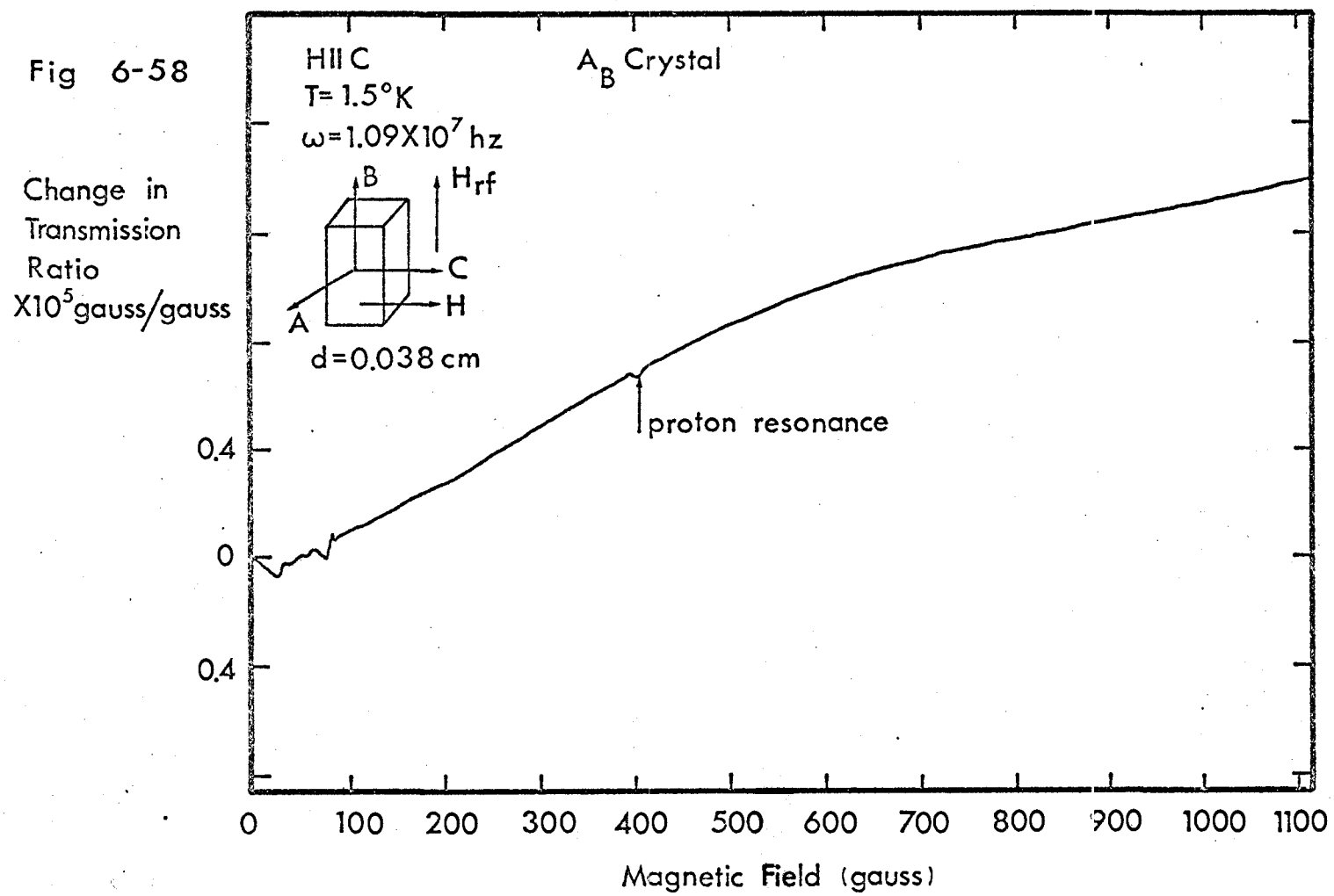
H II C
T= 1.5°K
ω=1.09X10^7 hz
A_B Crystal
B
H_rf
C
H
A
d=0.038 cm
proton resonance
Change in Transmission Ratio X10^5 gauss/gauss
0.4
0
0.4
0
100
200
300
400
500
600
700
800
900
1000
1100
Magnetic Field (gauss)

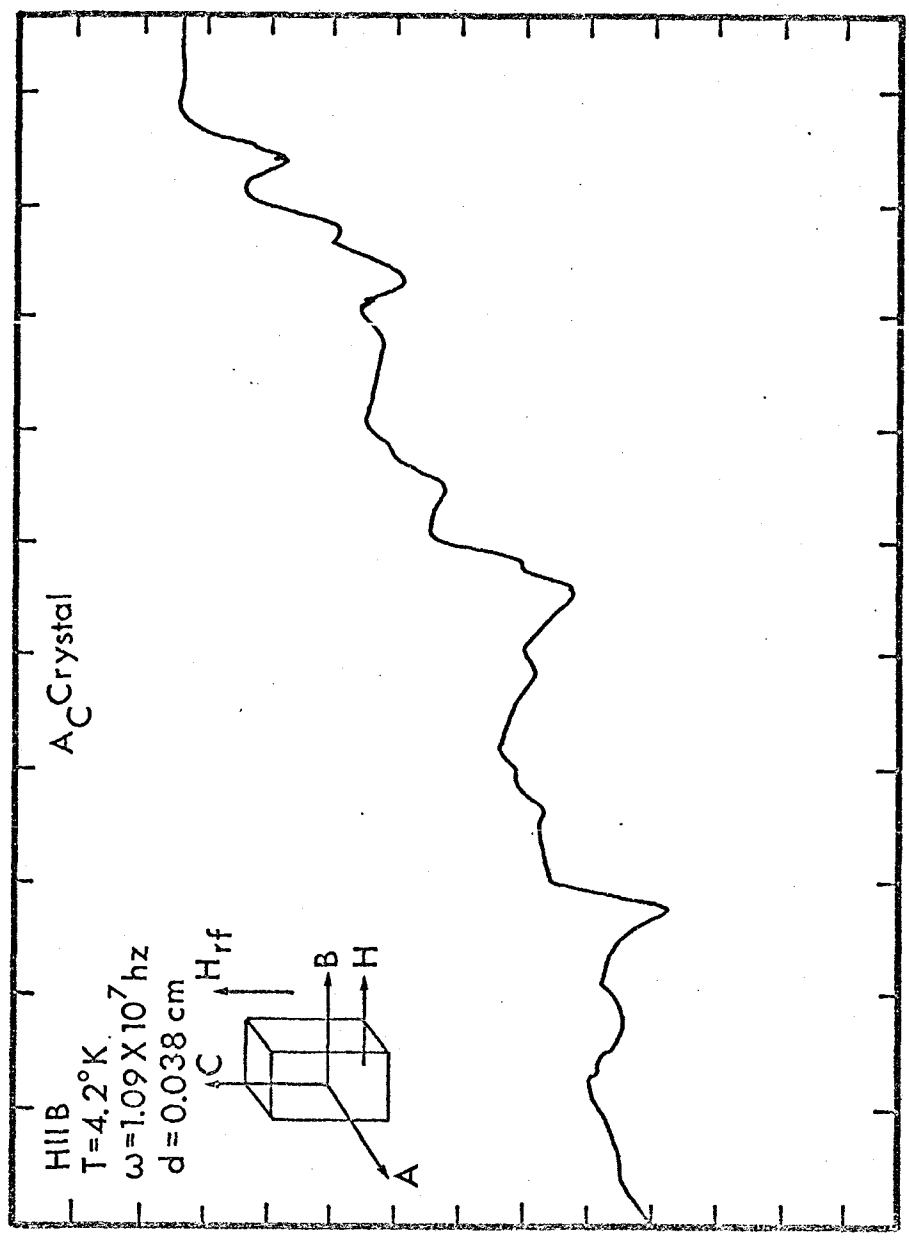
H⊥B
T=4.2°K.
ω=1.09 X 10^7 hz
d=0.038 cm
A_C Crystal
H_rf
C
B
H
A
Change in Transmission Ratio X10^7 gauss/gauss
0.4
0
0.4
0
100
200
300
400
500
600
700
800
900
1000
Magnetic Field (gauss)

Fig 6-59

Fig 6-60

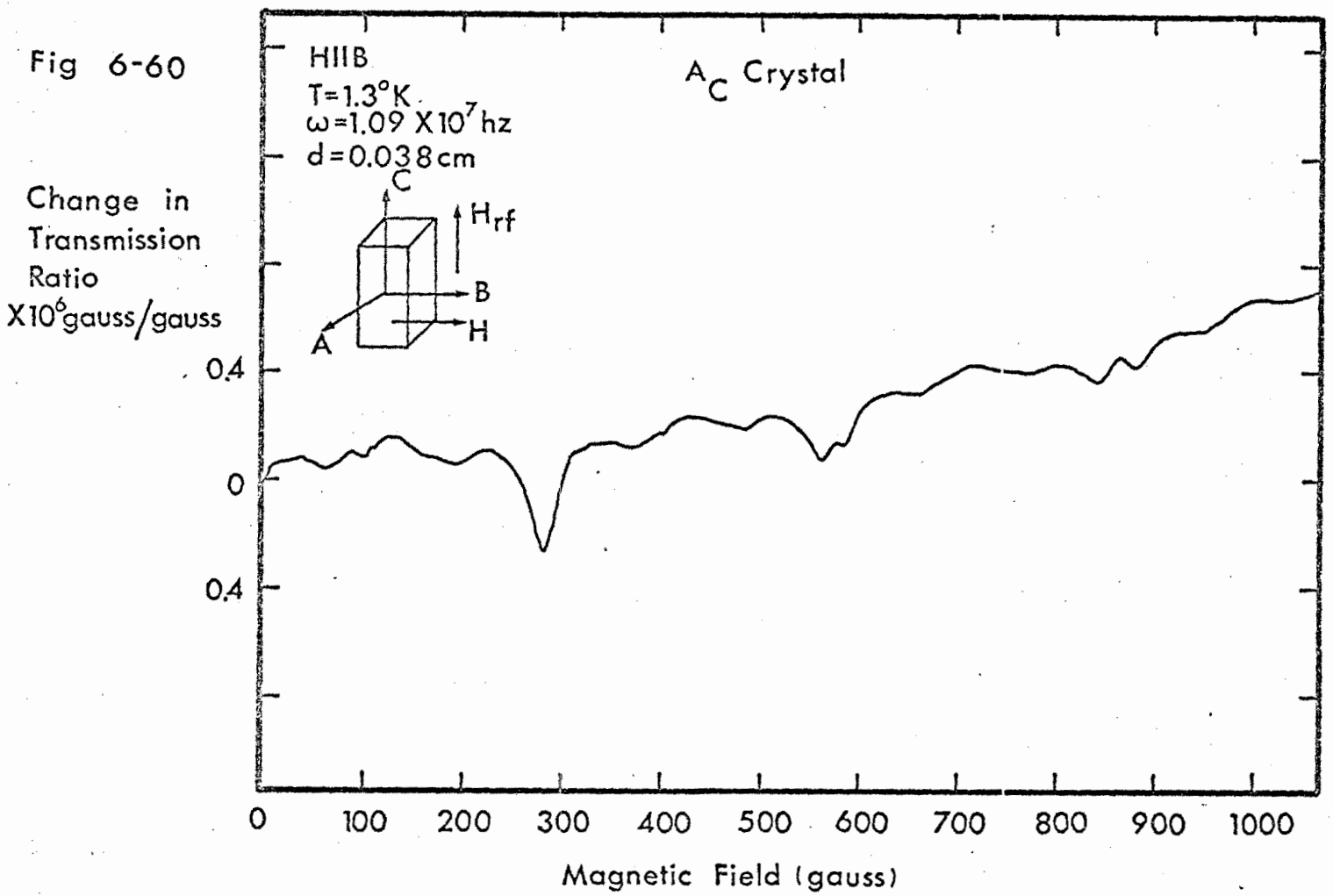
H⊥B
T=1.3°K
ω=1.09 X10^7 hz
d=0.038 cm
A_C Crystal
C
H_rf
B
H
A
Change in Transmission Ratio X10^6 gauss/gauss
0.4
0
0.4
0
100
200
300
400
500
600
700
800
900
1000
Magnetic Field (gauss)

Fig 6-61

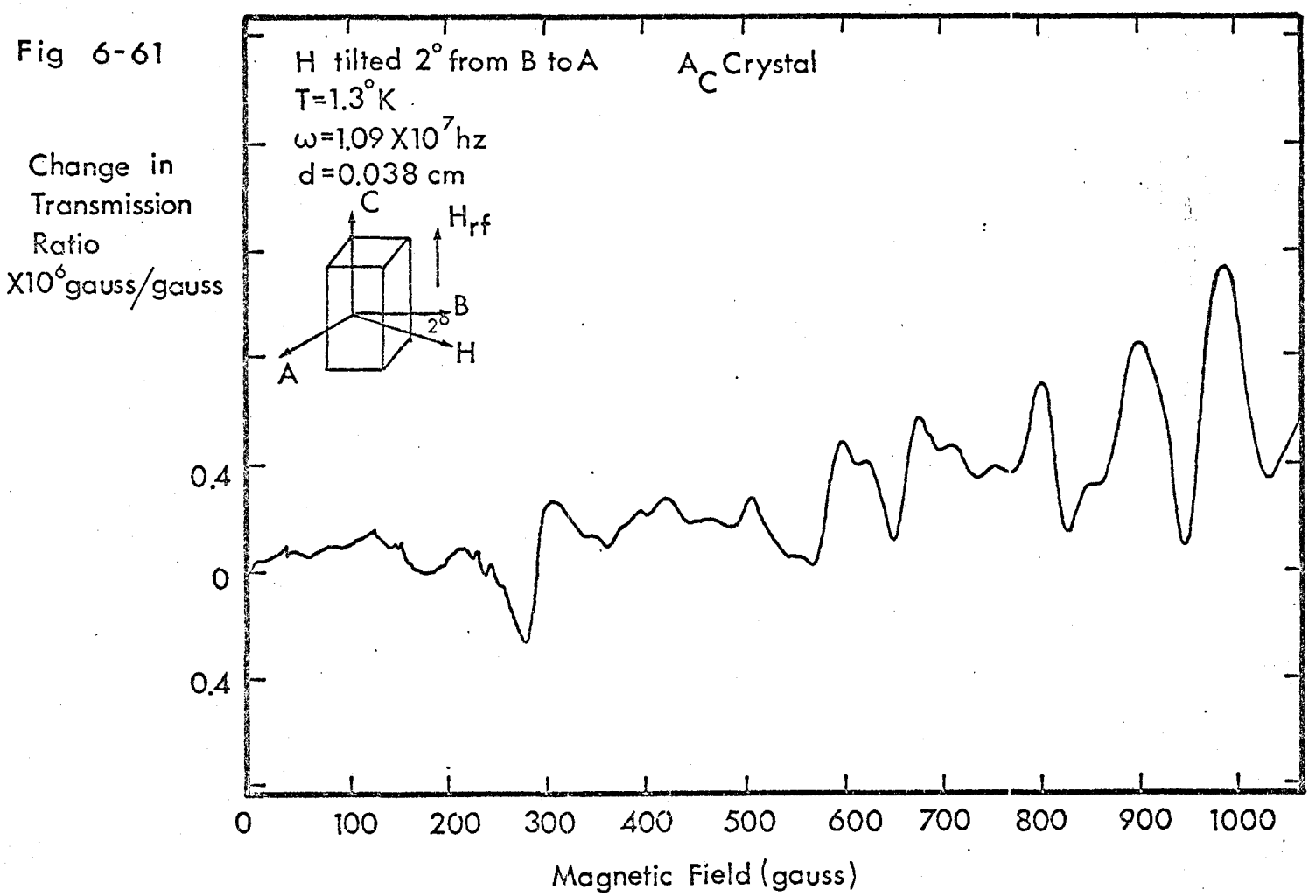
H tilted 2° from B to A
A_C Crystal
T=1.3°K
ω=1.09 X10^7 hz
d=0.038 cm
C
H_rf
B
2°
H
A
Change in Transmission Ratio X10^6 gauss/gauss
0.4
0
0.4
0
100
200
300
400
500
600
700
800
900
1000
Magnetic Field (gauss)

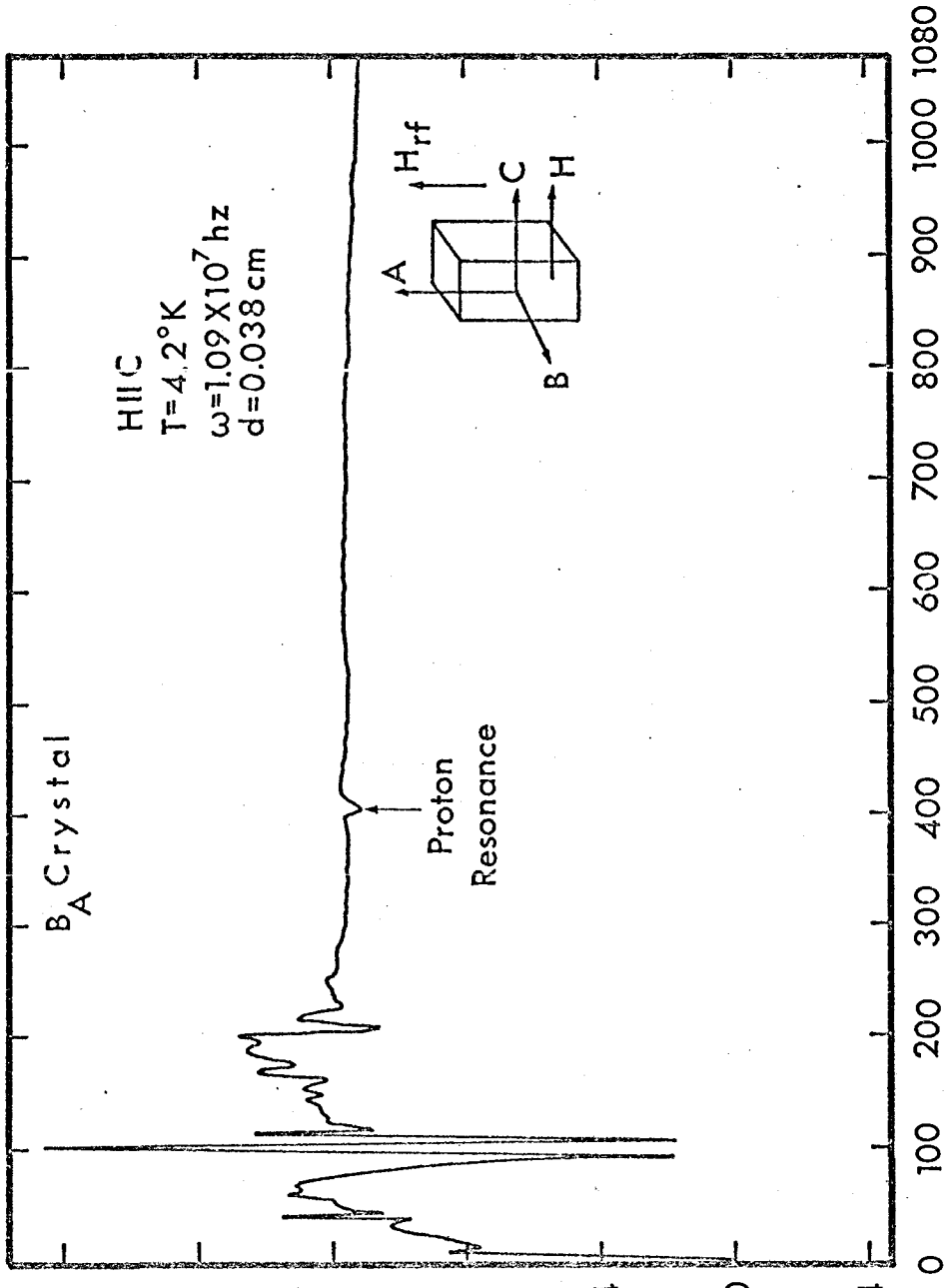
H||C
T=4.2°K
ω=1.09X10^7 hz
d=0.038 cm
B_A Crystal
Proton
Resonance
A
H_rf
C
H
B
Change in
Transmission
Ratio
X10^7 gauss/gauss
0.4
0
0.4
0
100
200
300
400
500
600
700
800
900
1000
1080
Magnetic Field (gauss)

Fig 6-62

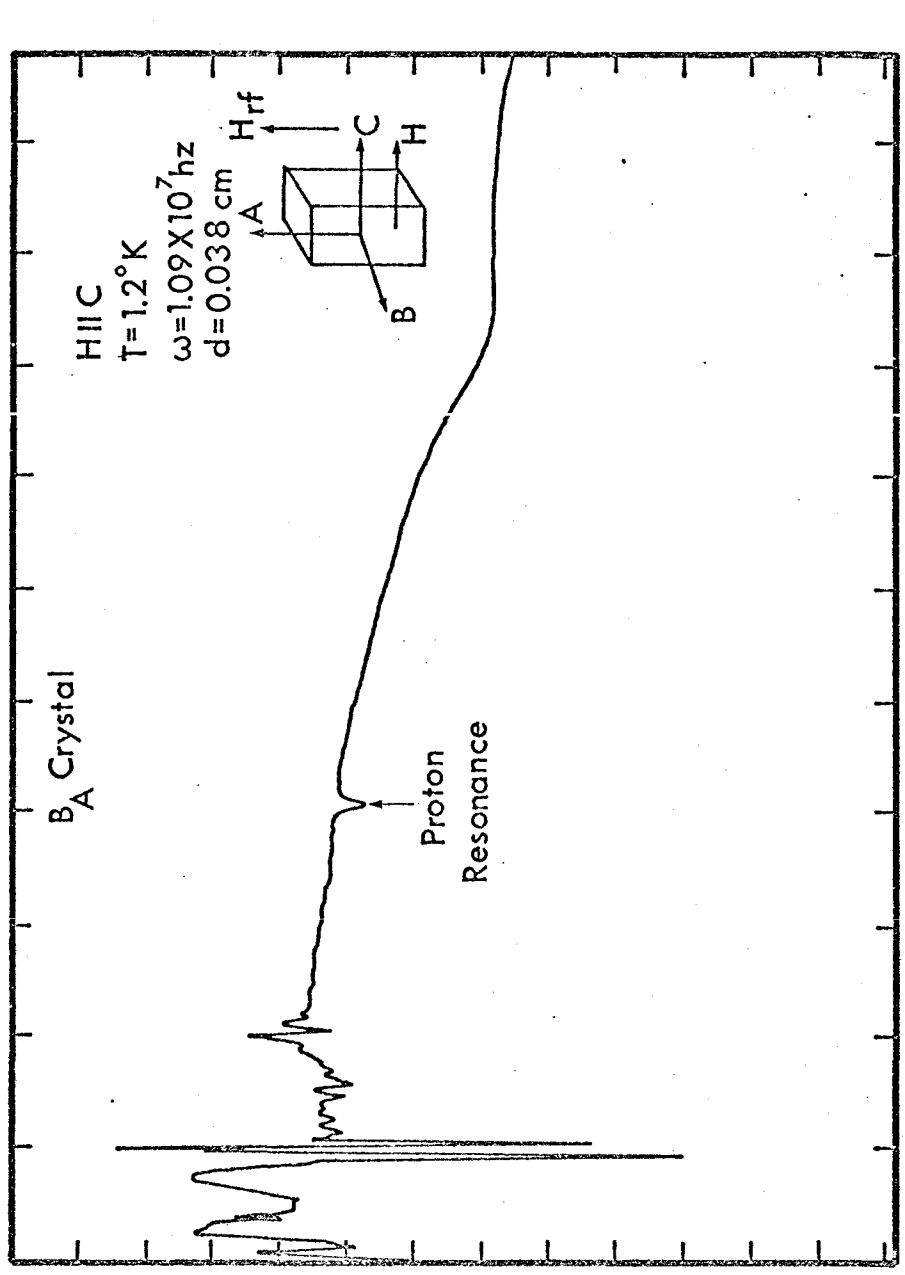
H II C
T = 1.2°K
ω = 1.09 X 10^7 hz
d = 0.038 cm
H_rf
A
B
C
H
B_A Crystal
Proton
Resonance
Change in
Transmission
Ratio
X 10^7 gauss/gauss
0.4
0
0.4
0
100
200
300
400
500
600
700
800
900
1000
1080
Magnetic Field (gauss)

Fig 6-63

Fig 6-64

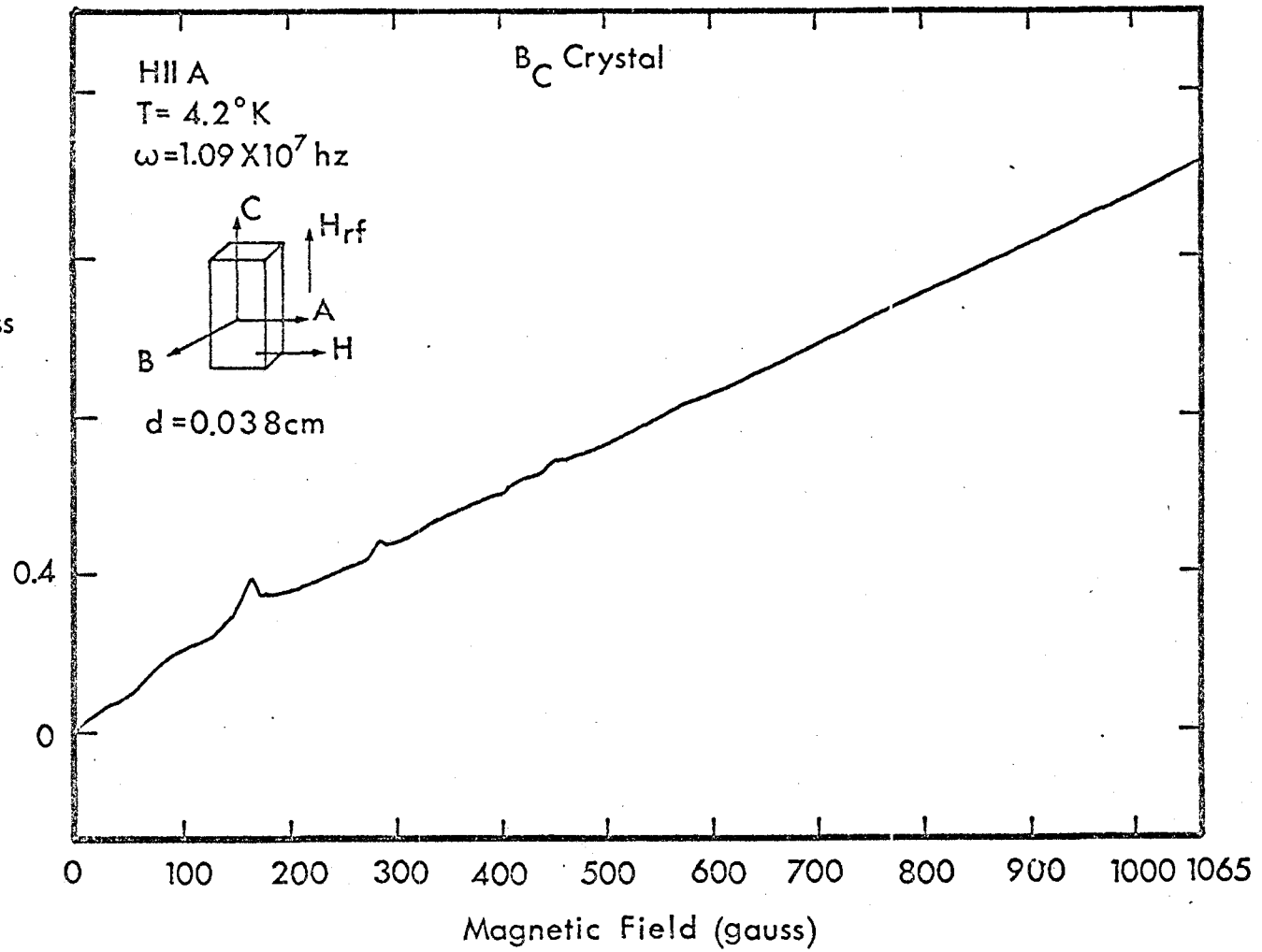
Change in Transmission Ratio X10^6 gauss/gauss
H II A
T= 4.2°K
ω=1.09 X10^7 hz
B_C Crystal
C
H_rf
A
B
H
d =0.038cm
0.4
0
0
100
200
300
400
500
600
700
800
900
1000
1065
Magnetic Field (gauss)

Fig 6-65

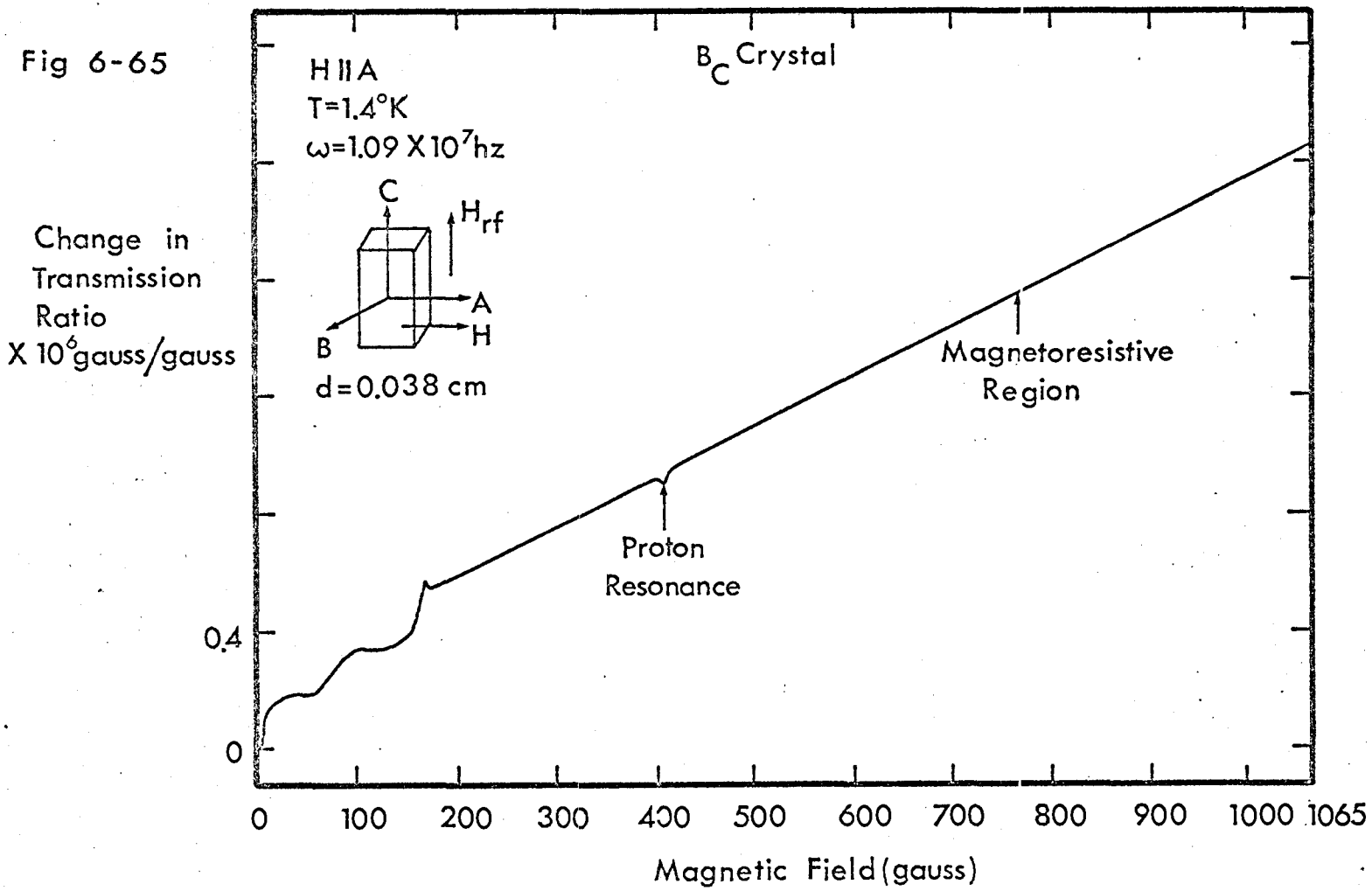
H ∥ A
T=1.4°K
ω=1.09 X 10⁷hz
B_C Crystal
C
H_rf
A
H
B
d=0.038 cm
Change in Transmission Ratio X 10⁶gauss/gauss
Magnetoresistive Region
Proton Resonance
0.4
0
0
100
200
300
400
500
600
700
800
900
1000
1065
Magnetic Field (gauss)

Fig 6-66

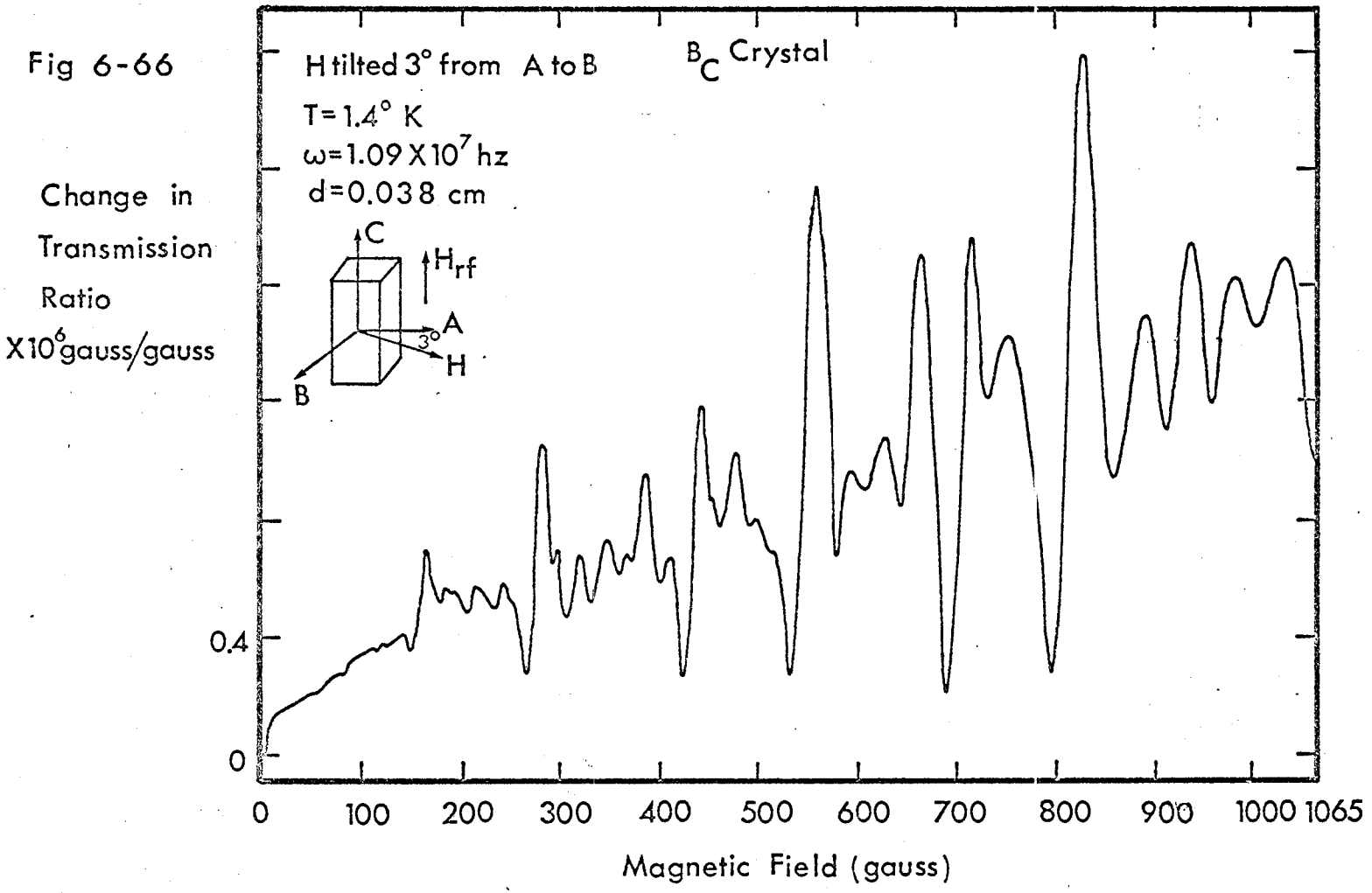
H tilted 3° from A to B
B_C Crystal
T = 1.4° K
ω = 1.09 X 10^7 hz
d = 0.038 cm
C
H_{rf}
A
3°
H
B
Change in Transmission Ratio X10^6 gauss/gauss
0.4
0
0
100
200
300
400
500
600
700
800
900
1000
1065
Magnetic Field (gauss)

Fig 6-67

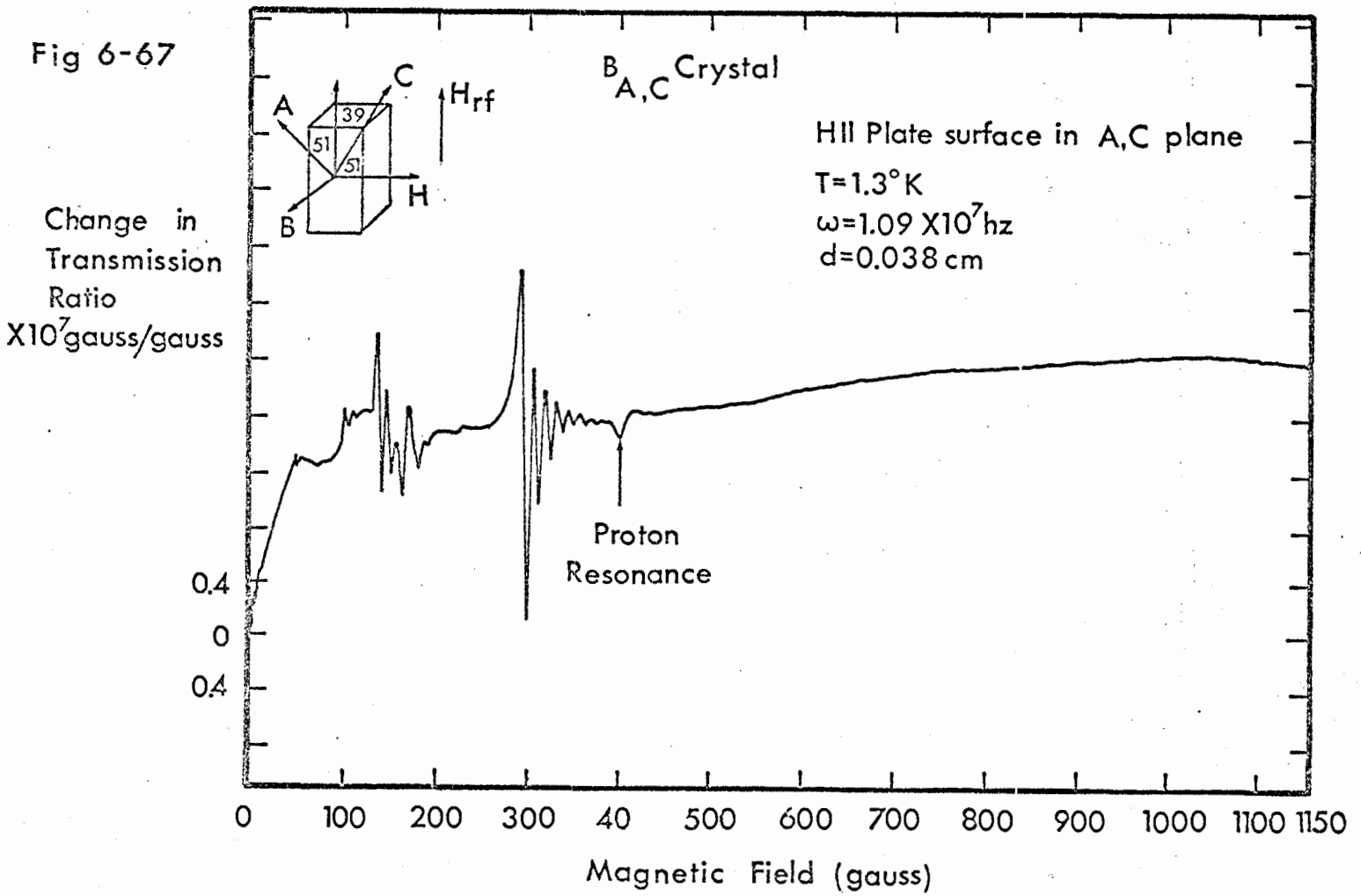
$B_{A,C}$ Crystal
H⊥ Plate surface in A,C plane
T=1.3°K
ω=1.09 X10⁷hz
d=0.038 cm
A
B
C
H
H_{rf}
39
51
51
Change in Transmission Ratio X10⁷gauss/gauss
0.4
0
0.4
Proton Resonance
0
100
200
300
40
500
600
700
800
900
1000
1100
1150
Magnetic Field (gauss)

Fig 6-68

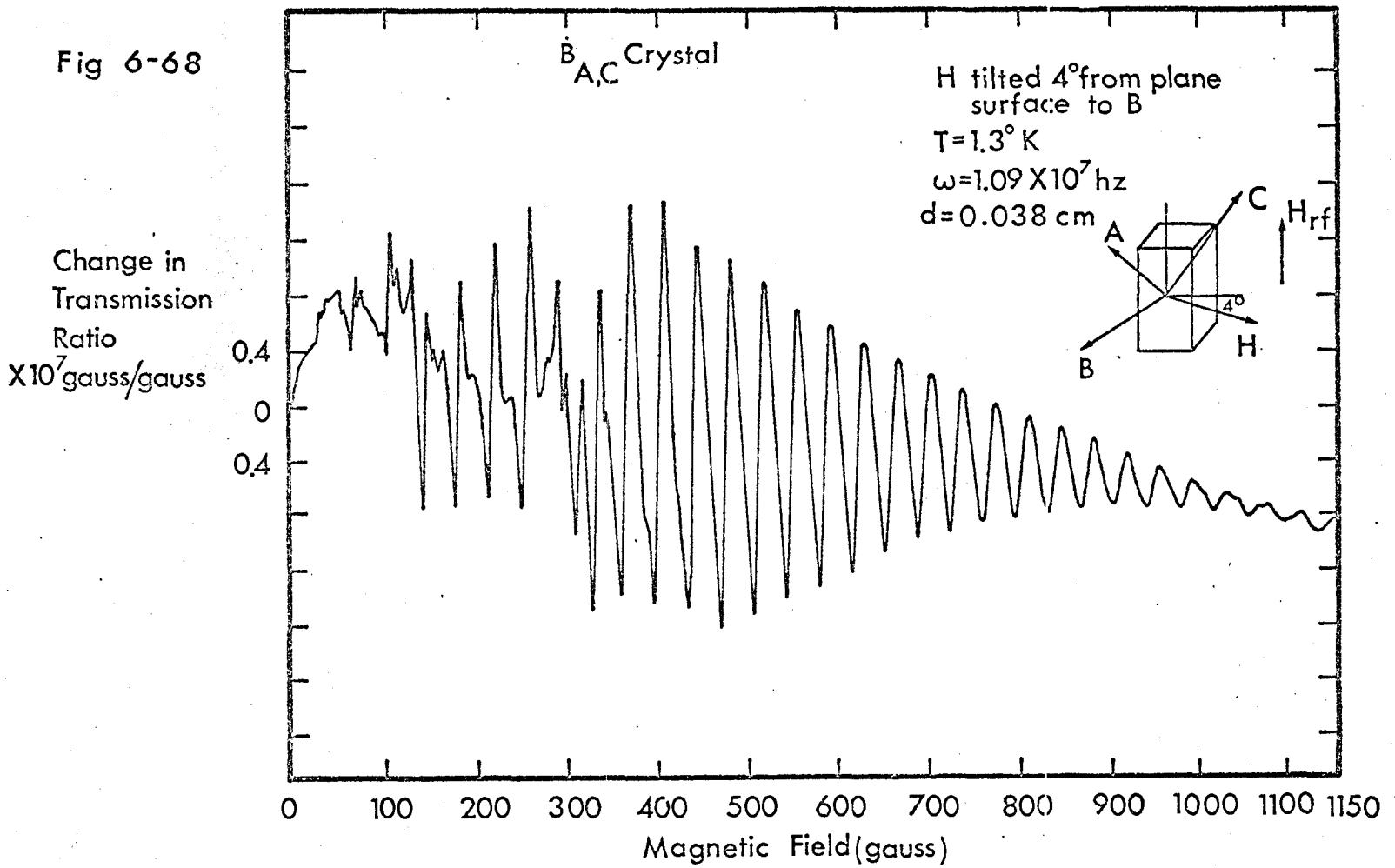
$\dot{B}_{A,C}$ Crystal
H tilted 4° from plane surface to B
T=1.3° K
ω=1.09 X10⁷ hz
d=0.038 cm
A
B
C
H
4°
H_{rf}
Change in Transmission Ratio X10⁷ gauss/gauss
0.4
0
0.4
0
100
200
300
400
500
600
700
800
900
1000
1100
1150
Magnetic Field (gauss)

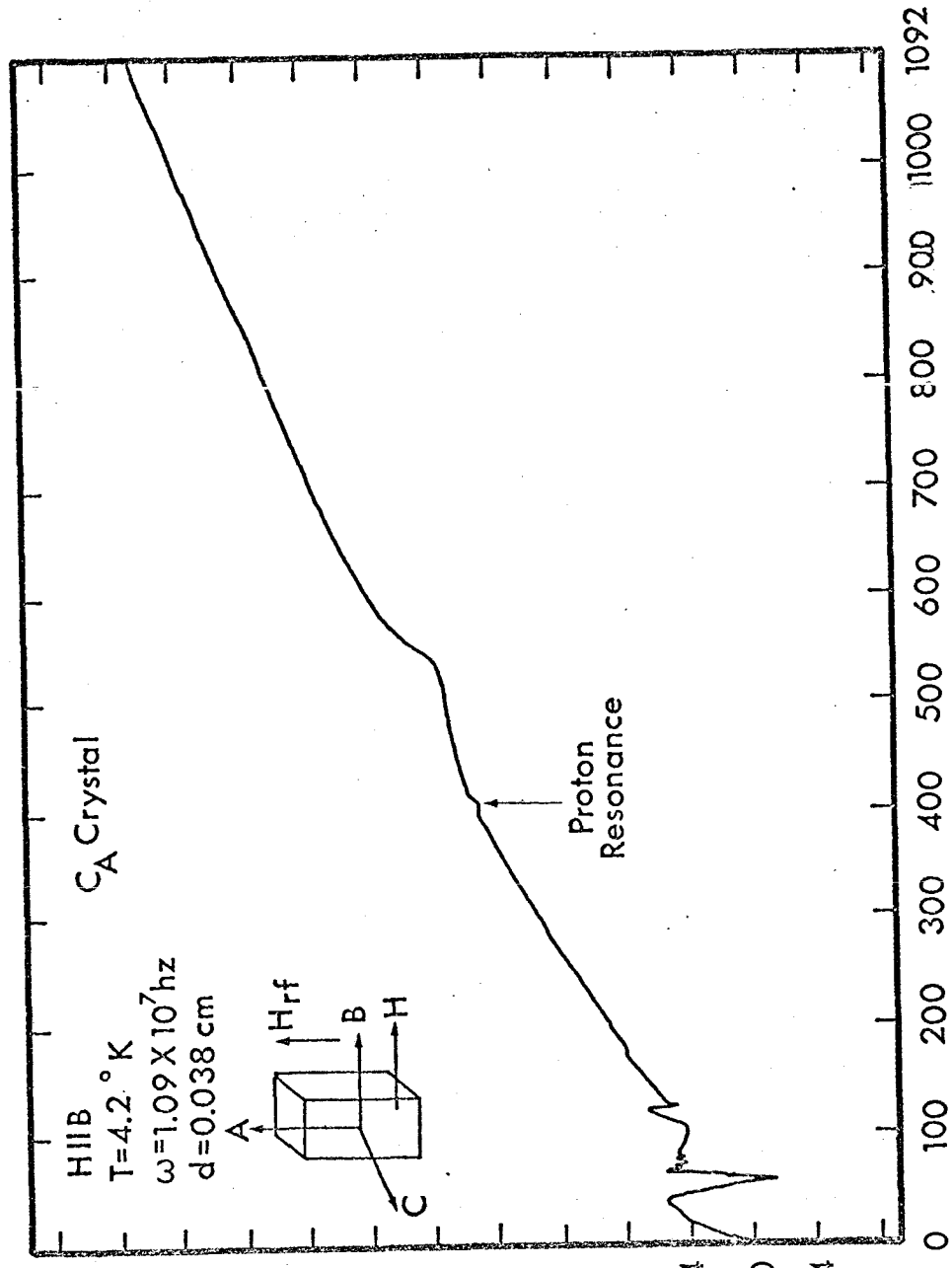
H||B
T=4.2 ° K
ω=1.09 X 10^7 hz
d=0.038 cm
C_A Crystal
A
H_rf
B
H
C
Proton Resonance
Change in Transmission Ratio X10^7 gauss/gauss
0.4
0
0.4
0
100
200
300
400
500
600
700
800
900
1000
1092
Magnetic Field (gauss)

Fig 6-69

Fig 6-70

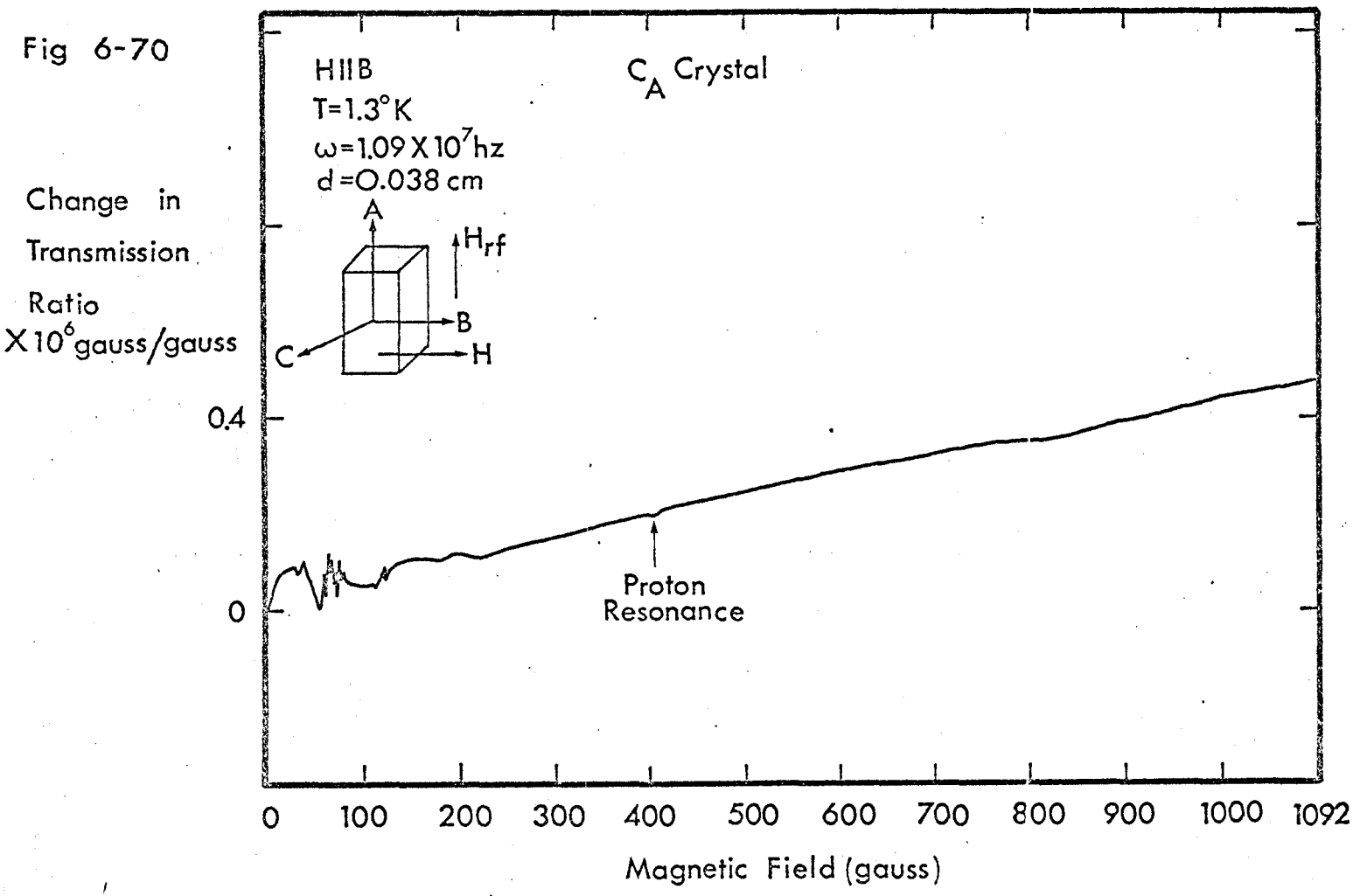
H||B
T=1.3°K
ω=1.09 X 10^7 hz
d=0.038 cm
C_A Crystal
A
H_rf
B
C
H
Change in Transmission Ratio X10^6 gauss/gauss
0.4
0
Proton Resonance
0
100
200
300
400
500
600
700
800
900
1000
1092
Magnetic Field (gauss)

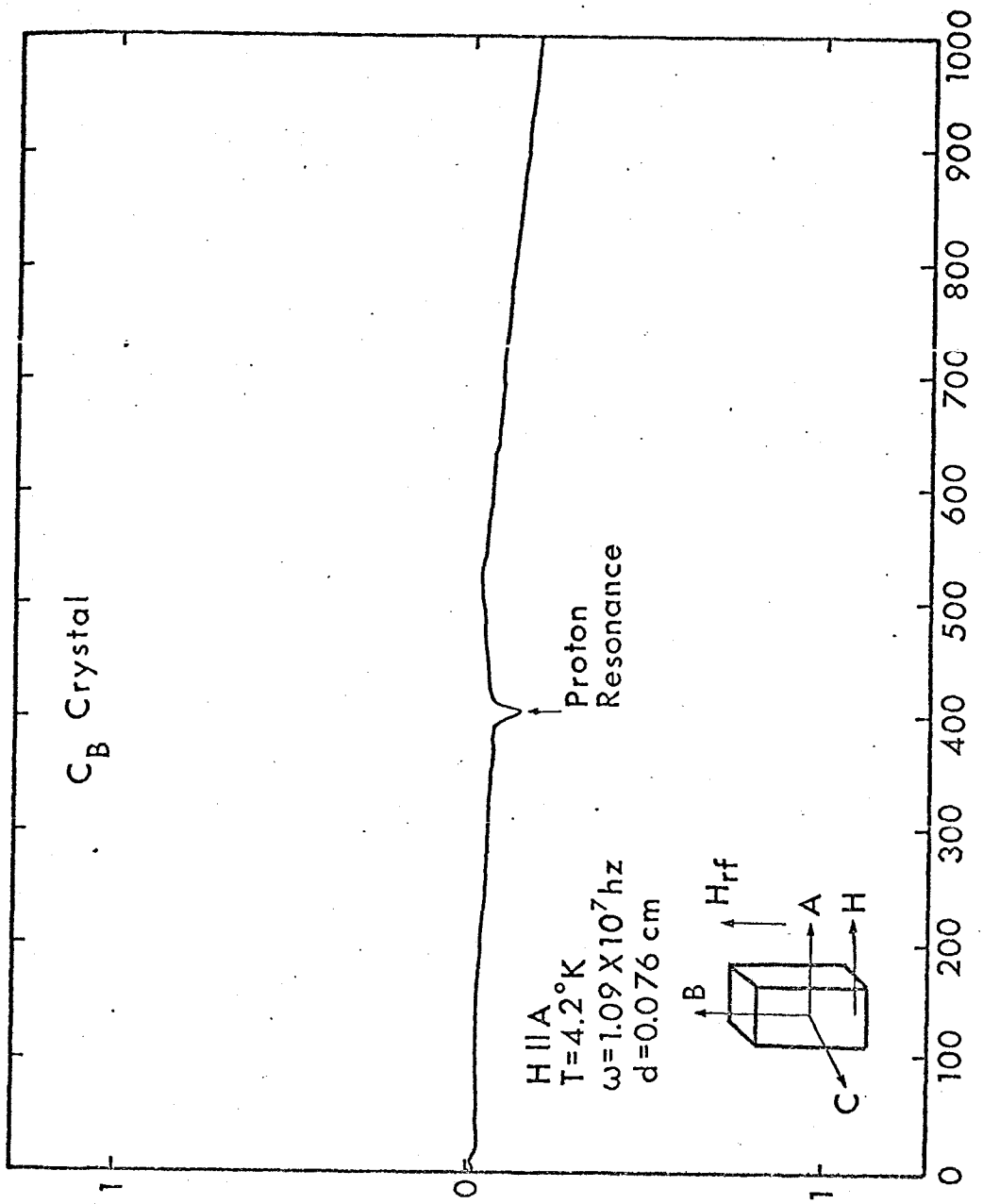
C_B Crystal
Proton Resonance
H ⊥ A
T=4.2°K
ω=1.09 X 10⁷ hz
d=0.076 cm
H_{rf}
B
A
H
C
1
0
1
0 100 200 300 400 500 600 700 800 900 1000
Magnetic Field (gauss)
Change in Transmission Ratio
X 10⁶ gauss/gauss

Fig 6-71

Fig 6-72

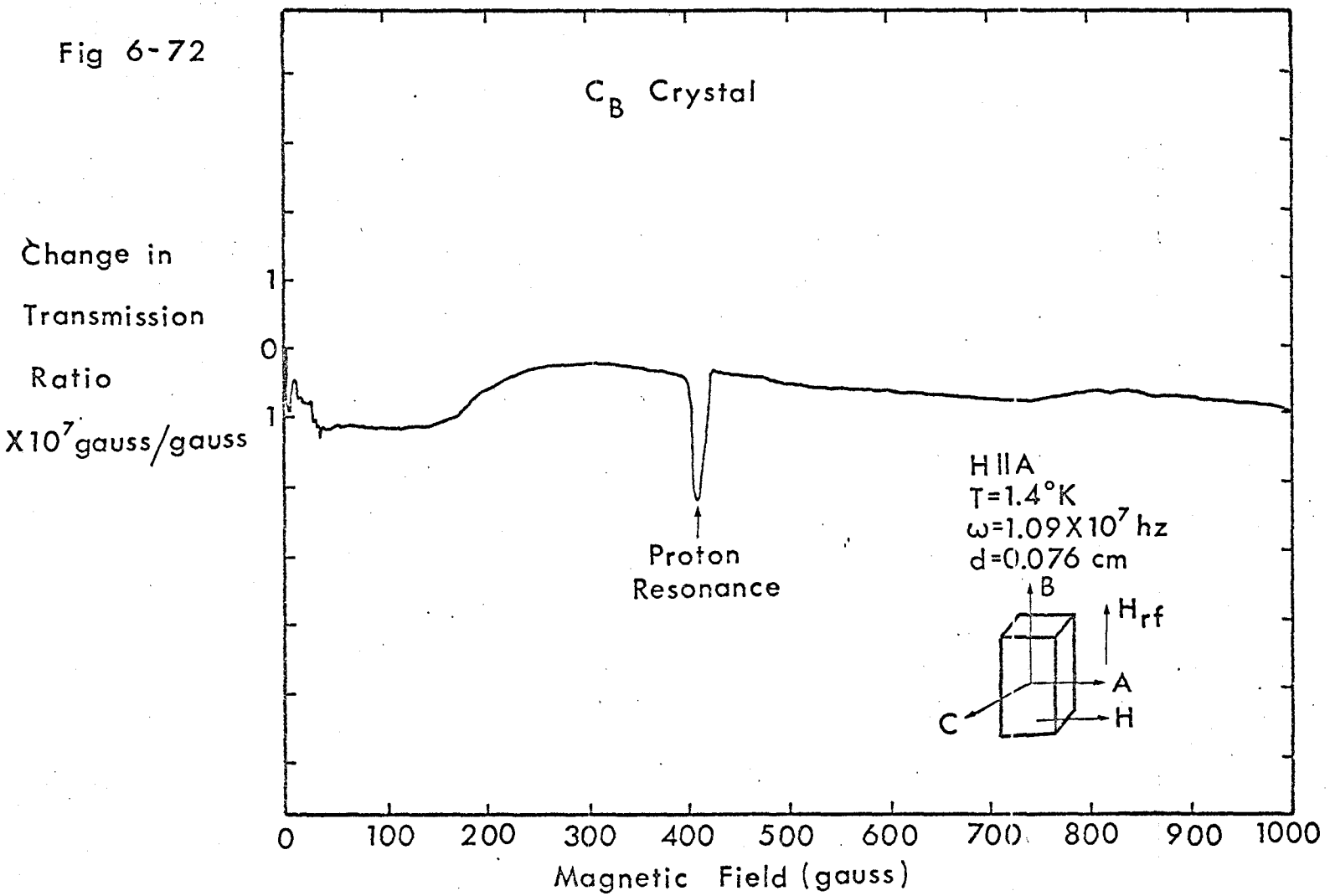
C_B Crystal
Change in
Transmission
Ratio
X10⁷gauss/gauss
1
0
1
Proton
Resonance
H ∥ A
T=1.4°K
ω=1.09X10⁷ hz
d=0.076 cm
B
H_{rf}
A
C
H
0
100
200
300
400
500
600
700
800
900
1000
Magnetic Field (gauss)

Fig 6-73

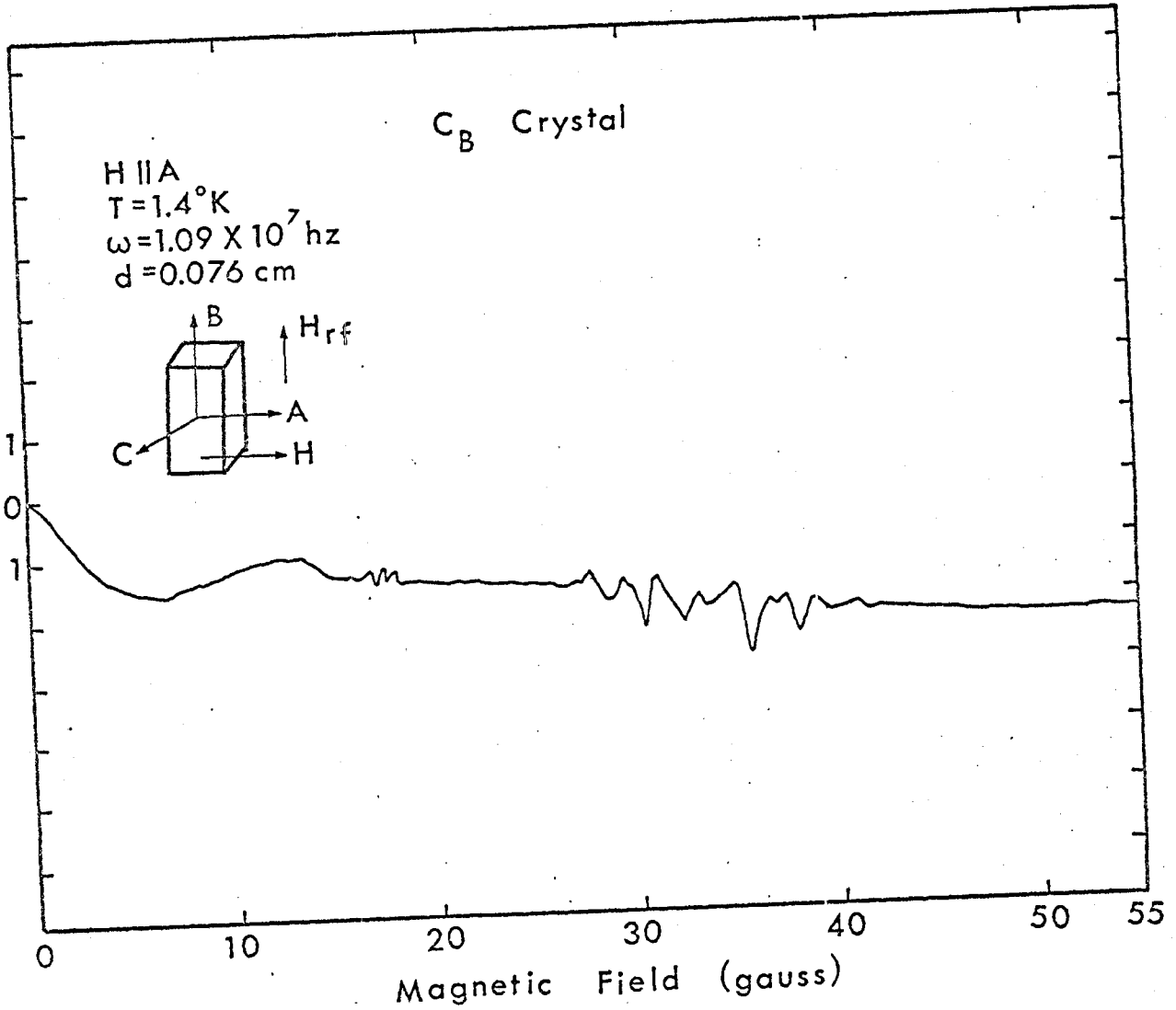
C_B Crystal
H ∥ A
T = 1.4°K
ω = 1.09 X 10^7 hz
d = 0.076 cm
B
H_{rf}
A
C
H
Change in Transmission Ratio X10^7 gauss/gauss
1
0
1
0
10
20
30
40
50
55
Magnetic Field (gauss)

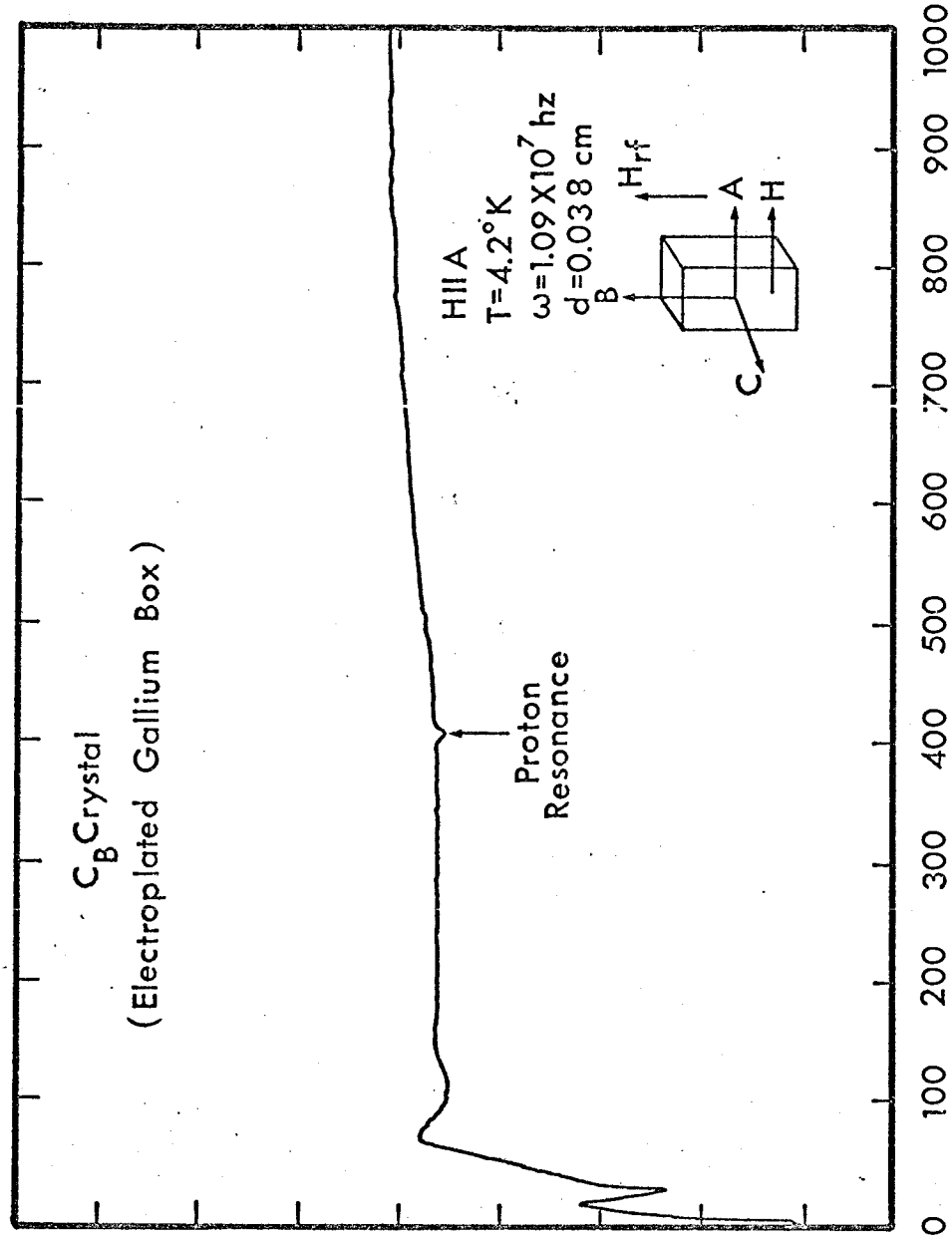
C_B Crystal
(Electroplated Gallium Box)
Proton Resonance
H⊥A
T=4.2°K
ω=1.09X10⁷ hz
d=0.038 cm
B
H_{rf}
A
H
C
Change in Transmission Ratio X10⁷gauss/gauss
1
0
0
100
200
300
400
500
600
700
800
900
1000
Magnetic Field (gauss)

Fig 6-74

Fig 6-75

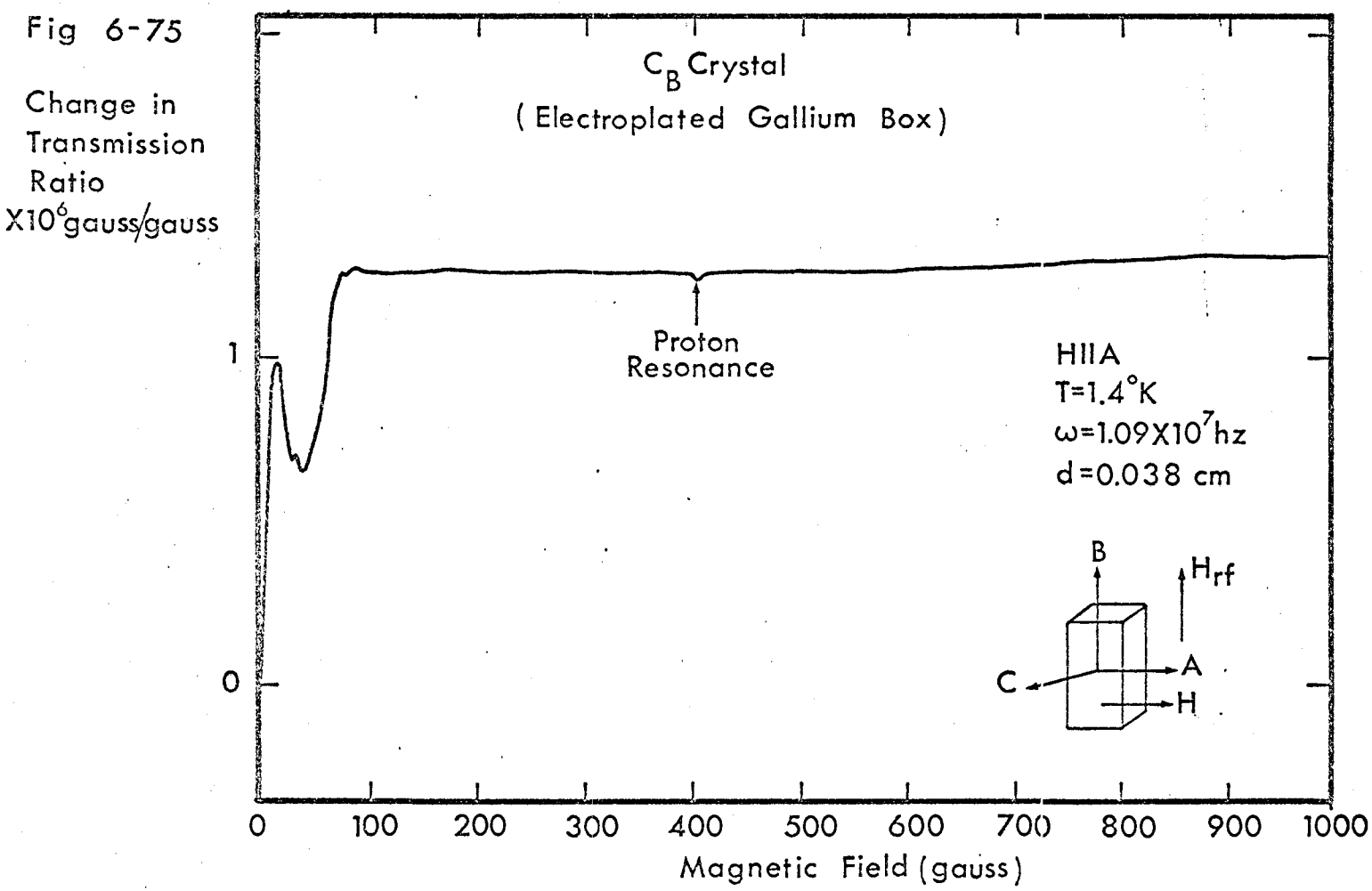
Change in Transmission Ratio X10⁶gauss/gauss
C_B Crystal
(Electroplated Gallium Box)
Proton Resonance
HIIA
T=1.4°K
ω=1.09X10⁷hz
d=0.038 cm
B
H_rf
C
A
H
1
0
0
100
200
300
400
500
600
700
800
900
1000
Magnetic Field (gauss)

Chapter 7

DISCUSSION OF THE RESULTS

7.1 Gantmakher Resonances

7.1.1 Introduction

It is clear from the results presented in Tables 6-2 and 6-3 that there is excellent agreement between Gantmakher resonance data reported in this work and that reported by other workers. The width of the low field line in the A_B crystal appears to be approximately 50% wider than that observed by Cochran and Shiffman[6]. However, the experiments on re-examined A_C crystals indicate that the line width may change with "aging". Therefore, we attach little significance to this result.

7.1.2 Fermi Surface Dimensions

Table 6-4 contains Fermi surface dimensions as deduced from the major Gantmakher resonances seen in our experiment. This data compares very favourably with that given by Cochran and Shiffman[6]. As noted by these authors the resonance line shapes varied from the simple form predicted by Fal'ko and Kaner[25] and by Juras[27] to large complexes as seen in A_C and C_A crystals. We also observe that the relative amplitude of the peaks in the A_C complex did not change with temperature, thus indicating that this may be due to a complicated piece of Fermi surface.

Data from Haberland et al.[40] and Fukumoto and Strandberg[39] have been included in Table 6-4. We have correlated all dimensions indicated by these authors with those dimensions observed in this work which compared most favourably with respect to magnitude. Table 6-4 illustrates the good agreement which was achieved by this correspondence of data. According to Haberland et al.[40] and Fukumoto and Strandberg[39] these particular Fermi surface dimensions can be correlated with bands 5, 6, 7 and 8 of the gallium Fermi surface.

It is clear from Table 6-4 that this experiment detects many Fermi surface extrema not reported by Haberland et al.[40] and Fukumoto and Strandberg[39].

7.1.3 Manifestation of the Transmission Amplitude Factor

It is appropriate at this point to comment on the interesting behaviour of the resonance labelled (11) in Fig. 6-10 in the B_A crystal. At 4.2°K a very large resonance is observed. However, at lower temperatures T = 1.3°K the resonance has decreased in amplitude by almost an order of magnitude. A similar effect has been reported by Haberland[57] and Haberland and Shiffman[31]. An examination of Fig. 3-4 suggests a possible explanation for this phenomenon. According to Fig. 3-4 the amplitude of a Gantmakher oscillation depends critically on the mean free path and on the cyclotron frequency of the electrons on the particular piece of Fermi surface under investigation (in other words, the electron effective mass). If we are dealing with a very small piece of surface, that is, $m^* << m$, then $\frac{\omega}{\omega_c} << 1$. It is clearly seen that if at 4.2°K the mean free path is such that the amplitude factor is near a maximum value for one of the curves $\frac{\omega}{\omega_c} << 1$, then upon increasing the mean free path slightly (by decreasing the temperature) a marked decrease in the amplitude factor can occur. This indeed may be the situation for this resonance.

7.1.4 Comparison of Transmission and Surface Impedance Line Shapes and Amplitudes

Juras[27] has made a theoretical calculation for the line shapes of the Gantmakher configuration radio frequency size effect. These results are for a specimen of thickness d = 0.156 cm, and the mean free path, ℓ, equal to d, which has been excited by an electromagnetic field of frequency 1 Mhz. Results are given for the surface resistance, R, the surface reactance, X, and their derivatives $\frac{\partial R}{\partial H}$ and $\frac{\partial X}{\partial H}$ as functions of the external magnetic field. Although the line shapes are for bilateral symmetric and bilateral antisymmetric excitation, the unilateral line shape can be obtained by taking the average solution. Since our experiment measures a signal proportional to the surface reactance, X, (see section 3.3), we shall restrict ourselves to the case of the unilateral line shape for the surface reactance. In Juras' paper he uses an $e^{-i\omega t}$ time dependence, as we do, but he defines $Z = R + iX$ whereas we use $Z = R - iX$. However, as indicated in section 3.3, $\Delta T \propto -X$. Therefore, the line shape applicable to the transmission experiment can be obtained by simply averaging the antisymmetric and symmetric excitation line shapes. This result is shown in Fig. 7-1. It is important to note that this line shape is for a spherical Fermi surface. An examination of our data, in particular Figs. 6-3, 6-5, and 6-10, reveals a striking resemblance to Juras' predicted line shape.

Fig 7-1 Transmission Line Shapes as Predicted by Juras[27] for Diffuse Scattering

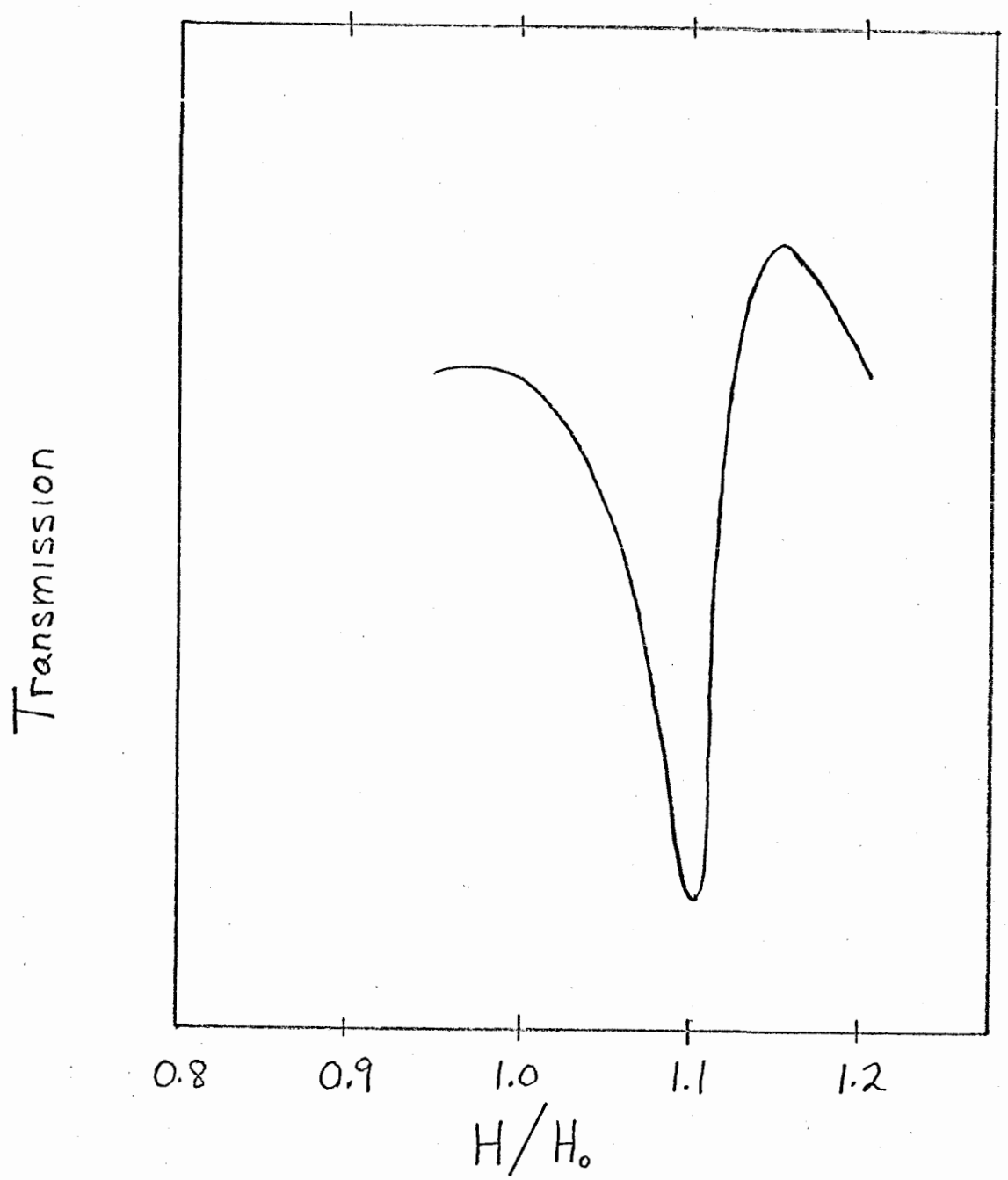

It was mentioned in section 3.3 that the change in transmission was related to the change in skin depth by the relation,

$$\Delta T = -\frac{1}{2a}\Delta\delta$$

The results obtained by Lyall[56] and Haberland et al.[40] in the investigation of the low field Gantmakher resonance in A_c crystals are shown in Fig. 6-23 (page 122). The resonance has been plotted in terms of $\frac{d\delta}{dH}$. Consequently, the amplitude is calculated in units of cm/gauss. A comparison with this data can be made if the quantity $\frac{\Delta\delta}{\Delta H}$ is determined from our experimental results. Since $\Delta\delta = 2a\ \Delta T$, then $\frac{\Delta\delta}{\Delta H} = 2a\ \frac{\Delta T}{\Delta H}$. Using the experimental values,

$a = 0.7$ cm

$\Delta T = 4.8 \times 10^{-7}$

$\Delta H = 0.15$ gauss

we calculate $\left.\frac{dT}{dH}\right|_{max} \approx 3 \times 10^{-6}$/gauss. Therefore, $\left.\frac{d\delta_x}{dH}\right|_{max} \approx 4 \times 10^{-6}$ cm/gauss. This is to be compared with Lyall's maximum $\frac{d\delta_x}{dH}$ value of 4.9×10^{-6} cm/gauss and Haberland's value of 2.2×10^{-6} cm/gauss. It is important to note that these experiments were done at different frequencies so one expects the values to be slightly different since the amplitude will depend upon frequency (reference: Gantmakher amplitude factor, section 3.2). Nevertheless, an order of

magnitude agreement is clearly obtained.

Similarly, the amplitude of the low field A_B resonance indicated in Fig. 6-3 (page 102) can be compared with that given by Cochran and Shiffman[6]. A calculation similar to that for the A_c resonance above gives $\left.\frac{d\delta_x}{dH}\right|_{max} \approx 1.5 \times 10^{-6}$ cm/gauss as opposed to the value $\left.\frac{d\delta}{dH}\right|_{max} = 3.8 \times 10^{-6}$ cm/gauss given by Cochran and Shiffman. Again, reasonable agreement is achieved.

On the basis of these calculations it can be said that Cochran's[30] hypothesized relation between surface impedance anomalies and transmission anomalies is certainly a good first approximation.

7.1.5 Aging Effect

The results on an A_c crystal, which was re-examined after being stored in a refrigerator for a period of approximately 6 months, show a marked change in transmission character. Much of the detail present in the original data is now missing (see Figs. 6-5 to 6-8). The once extremely sharp low field Gantmakher resonance now has rounded edges both at the onset and departure of the resonance. Similarly, the once sharp system of peaks in the higher field complex has all but disappeared. This phenomenon of resonances becoming indistinct is characteristic of a decrease in the electron mean free path. Similar results in the change of line shape with

mean free path have been obtained by Gantmakher and Tsoi[29] in potassium crystals. An example of a change in the mean free path is illustrated in Figs. 6-4 and 6-5. Here the mean free path has changed due to a temperature change. The low field resonances which are clearly seen at T = 1.3°K have almost disappeared at T = 4.2°K.

A possible explanation for this "aging effect" is that oxygen has diffused into the gallium over the period of refrigeration and for some reason this has reduced the mean free path. If this hypothesis is correct, all gallium specimens should be stored in a vacuum or in an inert atmosphere. It is known that the low field magnetic susceptibility of gallium for crystals grown in air is different from that of crystals grown in an atmosphere of helium gas[58].

7.2 Gantmakher-Kaner Oscillations

7.2.1 Gantmakher-Kaner Oscillations in B_A and B_C Crystals

7.2.1.1 Introduction

Investigations of B_A and B_C crystals in the normal field geometry revealed several Gantmakher-Kaner periods for each crystal. Our attention will be directed only to the most clearly defined oscillations. These were the oscillations in a B_A crystal with a period of 5.6 ± 0.02 gauss (period (1) Fig. 6-30) and those in the B_C crystal with a period of

9.5 ± 0.01 gauss (period (1) Fig. 6-35). In section 2.2 it was mentioned that for an axially symmetric piece of Fermi surface, in this case symmetric around the B-axis, one would expect the B_A and B_C crystal to give the same Gantmakher-Kaner oscillations. The period of the oscillations should be identical although the amplitude and cut-off fields may be different since the skin depth is orientation dependent.

An investigation of a $B_{A,C}$ crystal revealed oscillations characteristic of both B_A and B_C crystals appearing together. On the basis of this result it seems probable that two distinct non-symmetric pieces of Fermi surface are involved in the Gantmakher-Kaner phenomenon. It appears that the amplitude of the oscillations due to piece (1) is strong when E (the electric field) is parallel to C but diminishes rapidly with the direction of E away from C. Similarly the amplitude of the oscillations due to piece (2) is strong when E is parallel to A but diminishes rapidly as E is directed away from A.

7.2.1.2 Possible Shape of Fermi Surface Pieces

For the sake of convenience we label the oscillations seen in the B_A crystal as G-K)$_1$ and the oscillations seen in the B_C crystal as G-K)$_2$. Now one sees G-K)$_1$ oscillations in a B_A crystal but not in a B_C crystal. An explanation may be that the electric field which lies along C in the B_A crystal (and along A in the B_C crystal) does not couple to the electrons responsible for B_C oscillations. The following

model helps to illustrate this point.

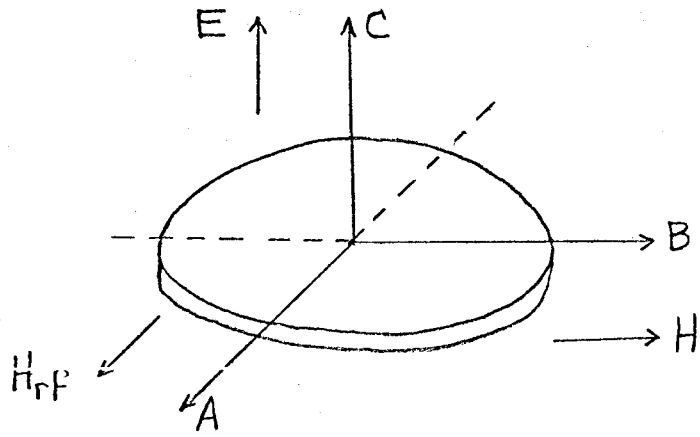

Plane of the Fermi Surface lies in the A, B plane

If one has a disc in the A, B plane then electron velocities are predominantly along C. Therefore, an electric field directed along A would not couple to this piece of surface.

Similarly, one sees G-K)$_2$ oscillations in a B_C crystal but not in a B_A crystal. The following model illustrates a shape of surface which would produce this result.

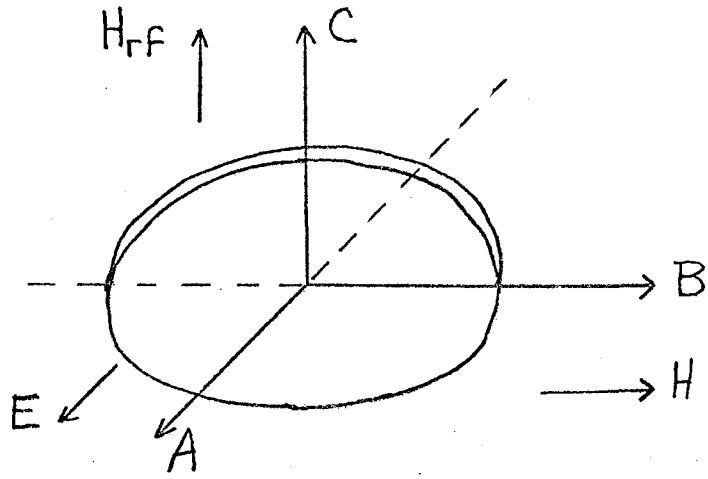

Plane of the Fermi Surface lies in the B, C plane

In this case electron velocities are predominantly along A. Therefore, an electric field along C, as in the case of a B_A crystal, would not couple to this piece of surface.

However, if the electric field was equally inclined to both A and C axes as in the case of a $B_{A,C}$ crystal, it should couple to both pieces and thus oscillations characteristic of both surfaces should arise. In fact, this is observed. Fig. 6-51 indicates that the B_A oscillations reach their maximum amplitude at a field which differs from that corresponding to the maximum amplitude position for the B_C oscillations. Therefore, oscillations characteristic of the B_A crystal predominate at low fields while those characteristic of the B_C crystal predominate at higher fields.

If the pieces of surface are thought to be approximately ellipsoidal in shape, then according to Gantmakher and Kaner[16] these oscillations are limiting point resonances. Accordingly, a value for the Gaussian curvature can be determined for these pieces of surface. Using the relation given in section 2.2,

$$d = \frac{2\pi c\hbar}{e\,\Delta H\sqrt{K}}$$

we obtain $K \approx 3.1 \times 10^{-12}$ cm^2 for the B_A crystal, and $K \approx 1.1 \times 10^{-12}$ cm^2 for the B_C crystal. Here, $K = \frac{1}{R_1 R_2}$ where R_1 and R_2 are the principle radii of curvature in k-space.

So far we have indicated the Fermi surface pieces to be disjoint discs. However, flattened ellipsoids or flatten cylinders as shown in Fig. 7-2 would produce the same effect. We have indicated the surfaces to be disjoint since a combination of the pieces, such that a "butterfly" shaped piece is formed, no longer gives rise to the limiting point resonances on the central belly. This "butterfly" shaped surface could, however, give rise to extremal helical trajectories, that is, a maximum in $\frac{\partial A}{\partial k_H}$. However, the velocities of the electrons from that belt of surface having an extremal $\frac{\partial A}{\partial k_H}$, would be in a direction that would not account for the oscillations seen by us. Therefore, we believe the pieces of surface to be disjoint.

7.2.1.3 Electron Effective Mass and Size of Fermi Surface Pieces

The oscillations which we observe are due to a group of electrons whose displacement in the field direction becomes maximal during one cyclotron period. This phenomen can be understood qualitatively from the following diagram.

Fig 7-2. Shapes Which Would Produce the Oscillations Observed in B_A and B_C Crystals

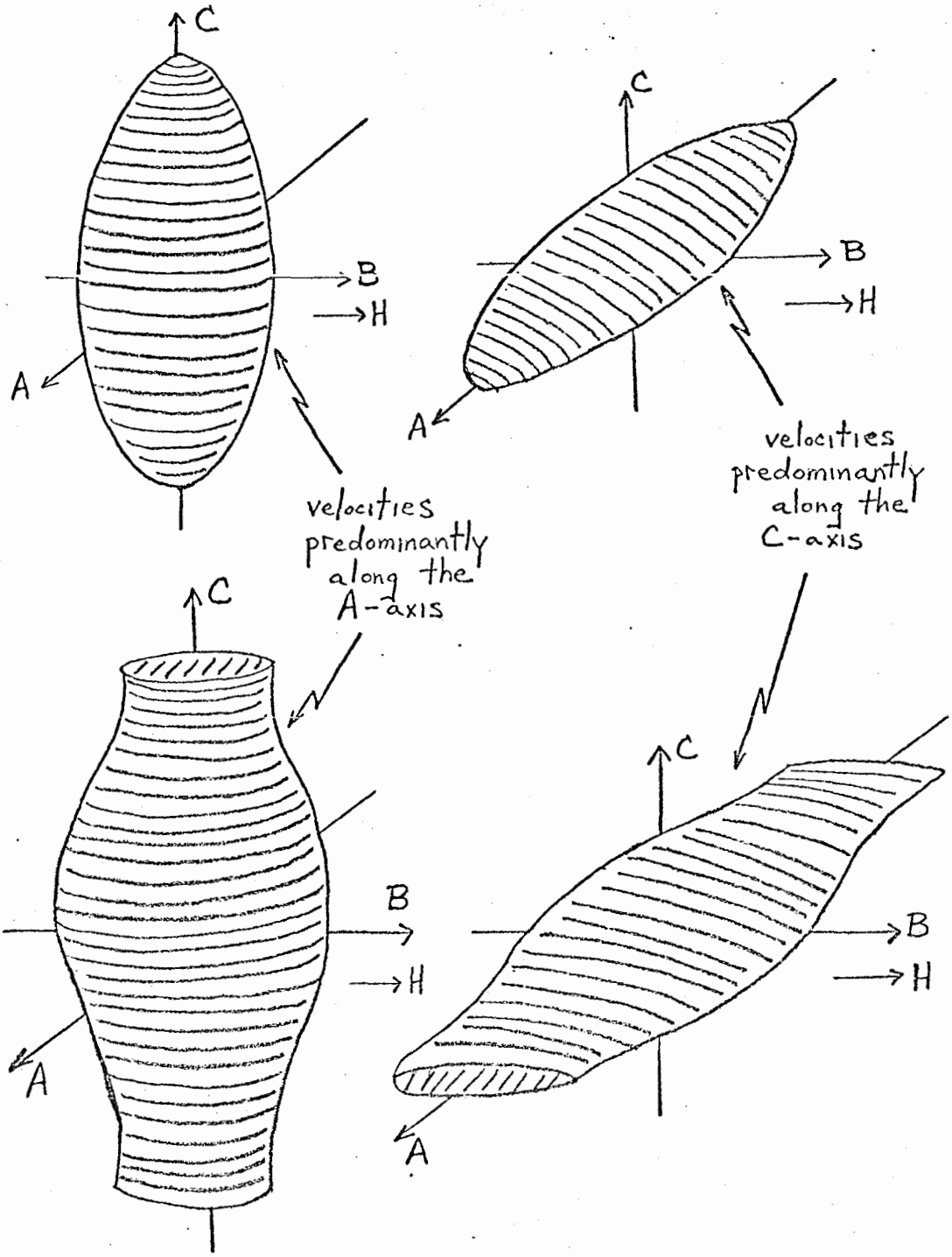

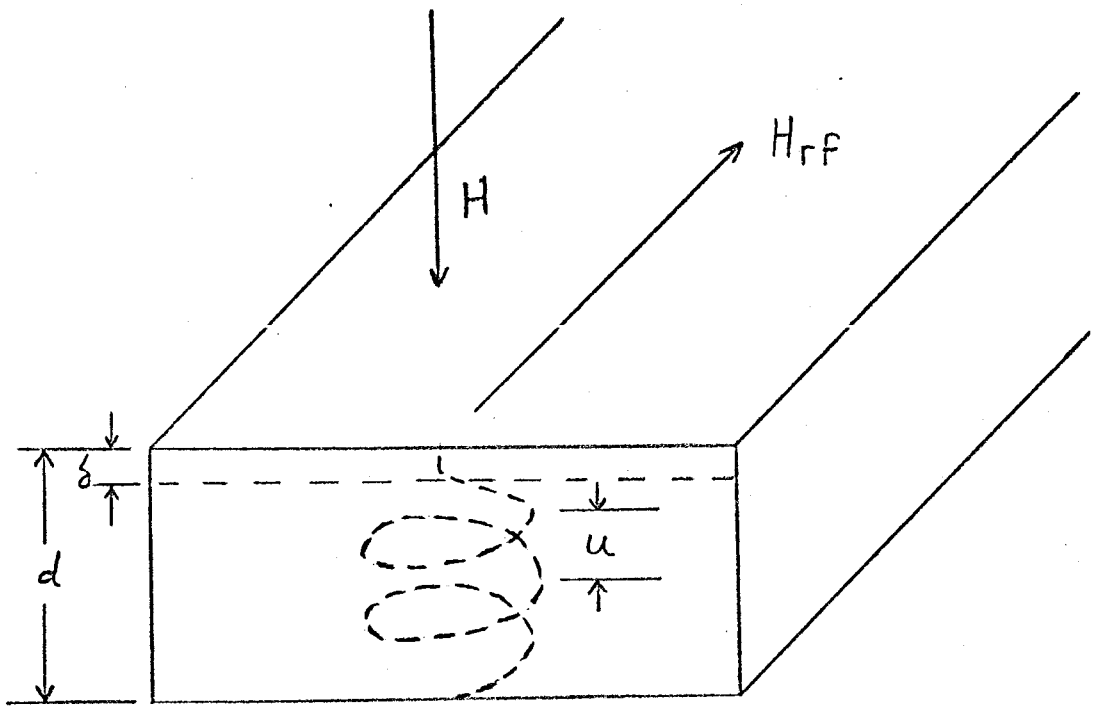

The displacement of the electrons during one cyclotron period is indicated as "u". Clearly $u = \frac{d}{n}$ where n = integer. For a limiting point resonance,

$$u = \frac{d}{n} = v_F \frac{2\pi}{\omega_c}$$

where v_F is the Fermi velocity of the electrons at the limiting point along the magnetic field direction. We can therefore write

$$\frac{e H_o}{m^* c} = 2\pi v_F \frac{n}{d}$$

or $$\frac{m^*}{m} = \frac{ed\,\Delta H}{2\pi mcv_F}$$

We take $v_F = 10^8$ cm/sec and obtain

$$\left.\frac{m^*}{m}\right|_{B_A} = 0.006$$

for the electrons involved in the B_A oscillations, and

$$\left.\frac{m^*}{m}\right|_{B_C} = 0.01$$

for the electrons involved in the B_C oscillations.

We expect in general, that the ratio $\frac{m^*}{m}$ is related to the dimensions of the Fermi surface. Roughly speaking the dimension should be given by

$$\Delta k = v_F \frac{m^*}{\hbar} = \frac{m v_F}{\hbar}\,\frac{m^*}{m}$$

But $\frac{mv_F}{\hbar} \approx 10^8$ cm^{-1}, i.e. the Brillouin zone dimension. Therefore $\Delta k \approx \frac{m^*}{m} \approx 10^{-2}$ of the Brillouin zone dimension. This result also follows from $K = \frac{1}{R_1 R_2}$.

7.2.1.4 Number of Oscillations and Significance of Oscillation Shape

The displacement of the electrons in one cyclotron period has been written,

$$u = \frac{d}{n} = v_F \frac{2\pi}{\omega_c}$$

As the magnetic field is increased more and more orbits are fitted into the slab thickness. Now this system of peaks of alternating fields and currents will be spread over a finite distance of the order of the skin depth. Clearly then only a certain number of orbits will fit within the slab before they begin to interfere with each other. The following calculation illustrates this viewpoint.

For a B_A crystal the skin depth at 1 mhz is approximately 5.7×10^{-4} cm for current flow along the C-axis according to Cochran and Shiffman[6]. They have assumed diffuse scattering and taken,

$$\delta^3 = \frac{c^2}{8\pi\omega\left(2.8\frac{\sigma}{\ell}\right)}$$

If one assumes that each field and current splash is separated by a distance of the order of δ, then the number of fringes observed should be of the order $\frac{d}{\delta}$, where d is the thickness of the slab. For a thickness, d = 0.038 cm, one should observe,

$$n = \frac{d}{\delta} \approx 66 \text{ Fringes}$$

Experimentally, at a frequency of 0.918 Mhz, approximately 32 fringes are seen.

This explanation is more clearly illustrated by the following sketch.

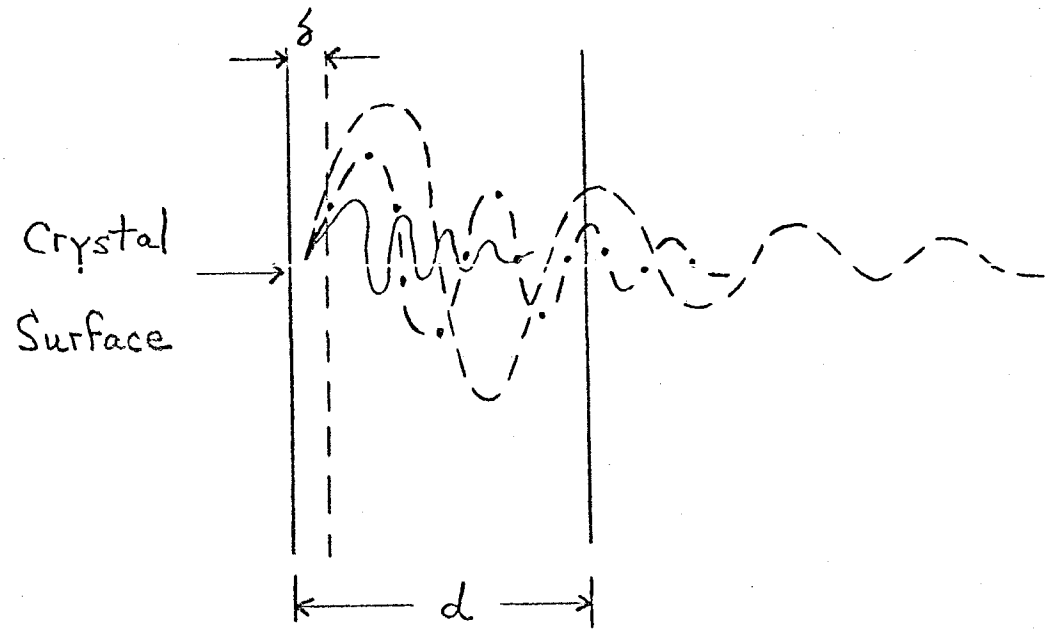

where _ _ _ _ represents effect in a weak magnetic field

_ • _ • _ represents effect in a medium magnetic field

_____ represents effect in a strong magnetic field

At sufficiently high magnetic fields, oscillations will no longer be observed. Using the above argument one would expect to see more oscillations in a thicker cyrstal and the number of oscillations should scale directly with the thickness. This in fact was observed in B_A crystals. The number of oscillations scaled almost exactly with the thickness (see section 6.3).

So far we have indicated that the number of oscillations should be of the order,

$$n = \frac{d}{\delta}$$

Now, if the shape of the particular piece of Fermi surface is rather simple, i.e. one which has cylindrical symmetry, and if the interaction of the electrons with the electric field is ineffective (as we have assumed for the B_A and B_C crystals), then one expects to observe oscillations in electric field which have a sinusoidal line shape. However, for an odd shaped piece of surface, such as a "butterfly" etc., there may be several limiting points or several points of extremal $\frac{\partial A}{\partial k_H}$. In this case there may be a set of oscillations characteristic of this one piece of surface. For example, in Fig. 6-30 we have labelled several periods in the B_A crystal as period (1), period (2), and period (3). In fact this set of periods may be due to a single odd shaped piece of surface. This type of behavior has been noted and analysed by Naberezhnykn et al.[59] in cadmium. Consequently, the line shape of an oscillation, such as the B_A and B_C oscillations, may indicate the shape of the electron trajectory around that particular piece of surface. One expects the first few oscillations to reflect the form of the trajectory most accurately.

7.2.1.5 Frequency and Field Dependence of the Oscillation Envelope

The position in magnetic field at which the Gantmakher-Kaner oscillations have a maximum amplitude is difficult to obtain analytically, according to Falk et al.[24]. However, its frequency dependence can be obtained, although the results are model dpendent. For amodel which has cylindrical symmetry about the direction of the magnetic field and has a square root singularity in the conductivity, a frequency dependence for the maximum amplitude position of $\omega^{2/5}$ was predicted. Experimentally, Weisbuch and Libchaber[60] found for the [111] direction in copper, that the field at maximum amplitude varied as $\omega^{1/3}$.

Results from measurements made on B_A crystals indicate primarily a $\omega^{1/3}$ dependence although a $\omega^{2/5}$ dependence is possible. These results are illustrated in Fig. 6-53. A frequency study of the cross-over position, H_x, in a $B_{A,C}$ crystal revealed a similar $\omega^{1/3}$ or $\omega^{2/5}$ dependence.

According to Falk et al.[24] the amplitude of the Gantmakher-Kaner oscillations should fall off as H^2 as $H \to 0$. An examination of the results for B_A and B_C crystals reveals that the amplitude decreases almost linearly with H at low fields. Consequently, we may conclude that the surfaces we are investigating, do not have a simple cylindrical symmetry about the direction of the magnetic field, in agreement with the

conclusions of section 7.2.1.3.

7.2.1.6 Dependence of Oscillation Amplitude on Specimen Thickness

The amplitude of the Gantmakher-Kaner oscillations for the case of a limiting point, according to Gantmakher and Kaner[16], should vary as,

$$A \propto \frac{\exp[-d/\ell]}{d^2}$$

where ℓ is the mean free path and d is the specimen thickness. In our experiments very pure gallium crystals were used. As a result, $\ell >> d$, and $\exp[-d/\ell] \approx 1$. Consequently, an examination of the oscillation amplitude in crystals of varying thicknesses will reveal the thickness dependence.

Experiments were done on B_A crystals with thicknesses of 0.038 cm (15 mils.) and 0.114 cm (45 mils.). The transmission signal versus field plots are shown in Figs. 6-30 and 6-33. The ratio of the amplitude of the oscillations at the maximum amplitude position was found to be approximately 5:1. At other field values this ratio was considerably less. According to the Gantmakher-Kaner theory for limiting parts which gives d^2 dependence this ratio should have been 9:1. A linear dependence on thickness would give a ratio of 3:1 while a $d^{3/2}$ dependence would give a ratio 5.2:1. It appears that our results are more consistent with a $d^{3/2}$ dependence which

according to Gantmakehr and Kaner is characteristic of extremal helical trajectories.

7.2.1.7 Temperature Dependence of the Electron Mean Free Path

Measurements of the amplitudes of the Gantmakher-Kaner oscillations as a function of temperature were made in order to determine the temperature dependent part of the electron mean free path. The results of the measurements made on a $B_{A,C}$ crystal are indicated in Fig. 6-56. The amplitude measurement was made at the position of maximum amplitude of the oscillation characteristic of a B_A crystal. This position was found to be independent of temperature.

The amplitude of the oscillations should vary as,

$$A \propto C(d) \exp\left\{-\frac{d}{\ell}\right\}$$

where d is the specimen thickness, C(d) is a constant and

$$\ell = \langle v_H \rangle \tau = \left\{\frac{1}{\ell_0} + \frac{1}{\ell(T)}\right\}^{-1} = \left\{\frac{1}{\ell_0} + \beta^{-1} T^{-\gamma}\right\}^{-1}$$

where ℓ_0 is the mean free path due to impurity scattering, and $\ell(T)$ is the temperature dependent part of the mean free path, ℓ. Therefore,

$$\ln A(T) = \ln C(d) - \frac{d}{\ell_0} - \frac{d}{\beta} T^{\gamma}$$

$$= \ln A_0 - d\beta^{-1} T^{\gamma}$$

$$\text{and } \ln \left\{ \frac{A(T)}{A(4.2^\circ K)} \right\} = \ln A(T) - \ln A(4.2^\circ K)$$

$$= d\beta^{-1} \left[(4.2)^{\gamma} - T^{\gamma} \right]$$

A plot of the logarithm of the relative amplitude $\frac{A(T)}{A(4.2^\circ K)}$ as a funciton of temperature led to a value $\gamma = 2$ (as shown in Fig. 6-56). The curve was fitted by the relation $\frac{A(T)}{A(4.2^\circ K)} = 45\ e^{-0.216T^2}$. From this plot a value of $\frac{d}{\beta} = 0.216^\circ K^2$ was determined and hence $\beta = 0.176^\circ K^2$ cm. Therefore, the electrons which are responsible for the B_A oscillations have a temperature dependent mean free path for this particular piece of Fermi surface given by

$$\frac{1}{\ell} = \frac{1}{\ell_0} + 5.7\, T^2$$

At 4.2°K and for $\ell_0 = 1$ cm, $\ell \approx 10^{-2}$ cm.

The T^2 dependence is characteristic of electron-electron scattering processes. Gantmakher and Leonov[61] mention that

a T^2 dependence is also possible for electron-phonon interactions (instead of the normal T^3 dependence) if there is large angle scattering.

7.2.1.8 Comparison of our Results with Theoretical Models and Other Experimental Data

In previous sections it was concluded that oscillations in B_A and B_C crystals resulted from two disjoint pieces of Fermi surface. These pieces were both indicated to be small with respect to the Brillouin zone dimensions. Theoretical calculations have been made recently by Reed[52] and a model of his calculation constructed (see Figs. 4-2 to 4-5). Besides this theoretical calculation recent de Haas van Alphen measurements by Condon* are of particular interest. These results are reproduced in Fig. 7-3 (page 213).

Directing our attention to Condon's data, we note that he observes several flat disc shaped sections labelled β, γ, and δ periods. De Haas van Alphen data gives information about extremal areas normal to the applied magnetic field. This area can be written,

$$A_k = \frac{2\pi e f}{\hbar c} = 9.55 \times 10^7 f \ \text{cm}^{-2}$$

---

* Condon's results are included in Reed's paper[52].

where f is the frequency of oscillation.

We wish to determine whether a correspondence can be made between our data and Condon's. We therefore require two pieces, one of which has a maximum frequency in the C direction and minimum frequencies in the A and B directions to correspond to our B_A oscillations. The other piece should have a maximum frequency in the A direction and minimum frequencies in the B and C directions to correspond to the surface causing B_C oscillations. The requirement for the B_A oscillations is satisfied by the piece in Fig. 7-3 labelled as γ period. However, a correspondence with the B_C oscillations can not be constructed from this data.

An estimation of the size of the piece of Fermi surface corresponding to the γ period can now be made.

For H parallel to the a-axis: area $\approx 4.8 \times 10^{13} = \pi$ bc

For H parallel to the b-axis: area $\approx 3.2 \times 10^{13} = \pi$ ac

For H parallel to the c-axis: area $\approx 13 \times 10^{13} = \pi$ ab

Therefore, assuming an ellipsoidal piece,

$a = 5.25 \times 10^{6}$ cm^{-1}

$b = 7.9 \times 10^{6}$ cm^{-1}

$c = 1.8 \times 10^{6}$ cm^{-1}

These values indicate that the length of the piece of surface, Δk, is approximately 1/20 of the Brillouin zone dimension. This dimension corresponds roughly with our estimated value of 1/100 of the zone dimension.

Fig 7-3

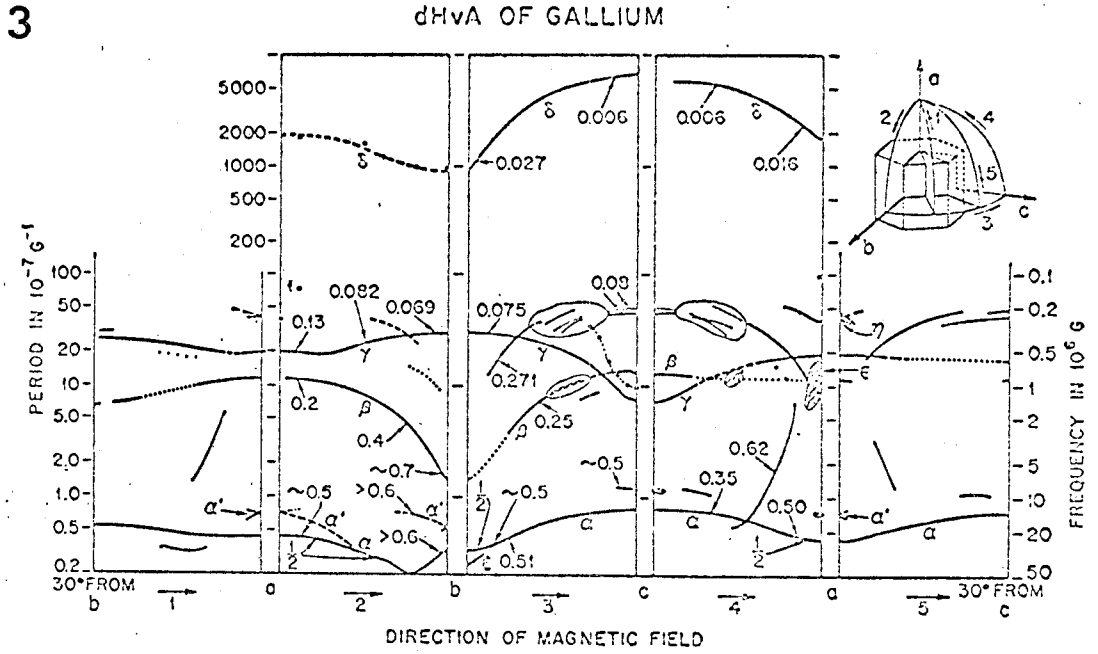

FIG. 8. de Haas-van Alphen data for gallium taken by Condon.

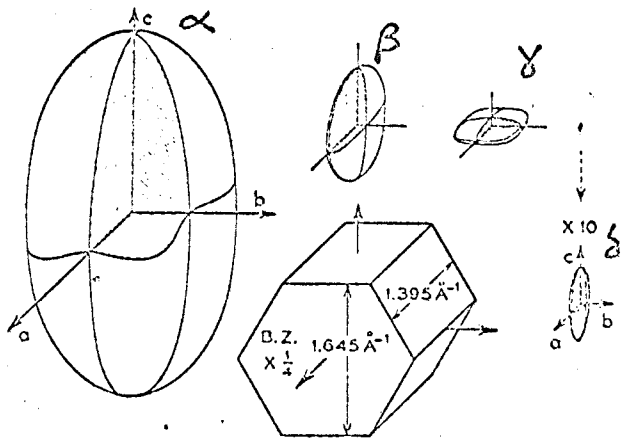

FIG. 9. Fermi-surface pieces as constructed by Condon from data in Fig. 8. In descending size, pieces represent branches α, β, γ, and δ, respectively.

It is also possible to correlate these dimensions with the results of Haberland et al.[40]. The A_2 contour indicated by these authors give the following dimensions for this piece of surface.

$$b \approx 7 \times 10^6 \text{ cm}^{-1}$$
$$c \approx 2.2 \times 10^6 \text{ cm}^{-1}$$

Resonable agreement with Condon's γ period surface and hence with our surface corresponding to B_A oscillations is achieved.

A further correspondence between these surfaces and our postulated surface can be made by calculating the Gaussian curvature of the limiting point from Condon's data and comparing it with our experimentally determined value. The Gaussian curvature for an elliptic limiting point can be calculated either using the mathematical relation,

$$K = \frac{y''}{\{1 + (y')^2\}^{3/2}}$$

where y' and y" represent the first and second derivatives of the curve at the limiting point, or by using the following geometrical argument,

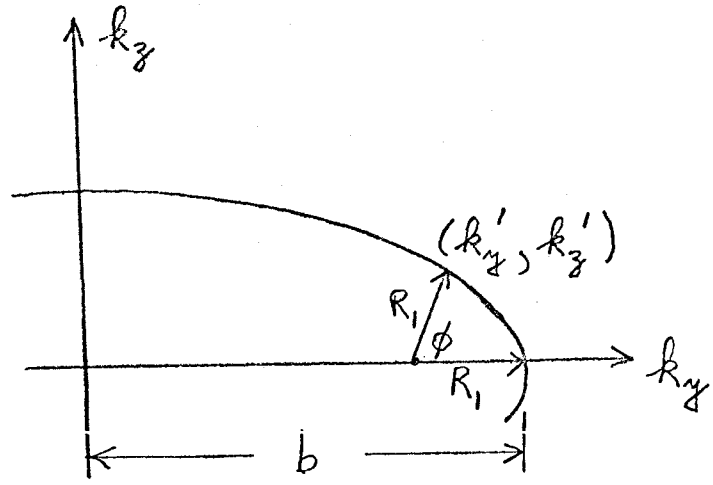

For small ϕ, the radius of curvature in the B, C plane

$$k_z' = R_1 \sin\phi \approx R_1\phi$$

$$k_y' = b + R_1\cos\phi - R_1 = b - R_1(1-\cos\phi)$$

$$\approx b - R_1\phi^2/2$$

$$\therefore (k_y')^2 \approx b^2 - R_1 b\phi^2$$

and $(k_z')^2 \approx R_1^2\phi^2$

$$\therefore \frac{(k_y')^2}{b^2} + \frac{(k_z')^2}{c^2} = 1 = 1 - \frac{R_1\phi^2}{b} + \frac{R_1^2\phi^2}{c^2}$$

and $R_1 = \frac{c^2}{b} \approx 4.1 \times 10^5\ cm^{-1}$

Similarly, for the radius of curvature in the A, B plane

$$R_2 = \frac{a^2}{b} \approx 3.3 \times 10^6\ cm^{-1}$$

$$\therefore K = \frac{1}{R_1 R_2} = 0.75 \times 10^{-12} \text{ cm}^2$$

Experimentally, we observed $K = 3.1 \times 10^{-12}$ cm^2. From this calculation we conclude that the surface may be distorted slightly from elliptical in shape.

This piece of surface characteristic of B_A oscillations is indicated by an arrow in Fig. 4-2. This small ellipsoidal shaped section has been labelled by Reed as a 6h zone on T.

Similarly in Fig. 4-3 there is another flattened cylinder shaped section indicated by an arrow which may correspond to our surface characteristic of B_C oscillations. This piece has been labelled as a 7e saucer along U by Reed. From Reed's table of experimental and theoretical data we can again calculate the Gaussian curvature.

For H parallel to the a-axis: area $\approx 48 \times 10^{13} = \pi bc$

For H parallel to the b-axis: area $\approx 6.8 \times 10^{13} = \pi ac$

For H parallel to the c-axis: area $\approx 4.1 \times 10^{13} = \pi ab$

Therefore, again assuming an ellipsoidal piece of surface,

$a = 1.36 \times 10^6$ cm^{-1}

$b = 9.6 \times 10^6$ cm^{-1}

$c = 5.04 \times 10^6$ cm^{-1}

Using a geometrical argument to calculate the radii of curvature in the B, C plane and in the A, C plane gives the

results

$$R_1 = \frac{c^2}{b} = 2.64 \times 10^6 \text{ cm}^{-1}$$

$$R_2 = \frac{a^2}{c} = 0.37 \times 10^6 \text{ cm}^{-1}$$

Therefore, the Gaussian curvature,

$$K = \frac{1}{R_1 R_2} = 1.02 \times 10^{-12} \text{ cm}^2.$$

Experimentally, a value, $K = 1.1 \times 10^{-12}$ cm^2 is determined. Clearly, remarkable agreement exists. We therefore attribute the surface characteristic of B_C oscillations to the 7e saucer along U designated by Reed.

7.2.2 Comments

7.2.2.1 Gantmakher-Kaner Periods

Table 6-5 presented a list of Gantmakher-Kaner periods which were selected "visually" in a trial and error fashion from a usually complicated transmission versus magnetic field plot. This selection of Gantmakher-Kaner periods would, in future, be best accomplished by first digitalizing the data and then performing a Fourier transform on it. This procedure would pick out individual peirods in a clear and unambiguous fashion.

It should be noted at this point that the correlation of Gantmakher-Kaner periods to properties of the Fermi surface may be complicated by the existence of harmonics that have

been excited by the fundamental Gantmakher-Kaner excitation. This phenomenon has recently been reported by Perrin et al.[62] to have been observed in single crystal copper plates. In essence, the fundamental excitation is capable of exciting harmonics which have periods that are entire fractions of the fundamental period. Consequently, periods that are representative of harmonics do not indicate sections of Fermi surface different from that described by the fundamental period*.

7.2.2.2 Shape and Position of Envelope

In the course of experiments on B_A and B_C crystals it was found that neither the shape nor the position of the oscillation envelope was temperature dependent. There was however a slight dependence of the envelope shape on specimen thickness. This dependence is seen in Fig. 6-52. Although the position of maximum amplitude has not noticeably changed, the amplitude of the tail section of the envelope is seen to decrease more slowly than for the case of the thinner crystal.

7.2.2.3 Variation of Oscillation Period with Angle of Magnetic Field

The variation of the oscillation period in a B_A crystal

---

* The fundamental period will result from relatively large pieces of Fermi surface.

with rotation of magnetic field in the B,C plane is indicated in Fig. 6-54. The vation of period with angle has been best fitted with a $\sin^2\theta$ dependence, where θ is measured from the normal position. The significance of this dependence is not known.

7.2.2.4 Complementary Oscillations

So far we have directed our attention solely to Gantmakher-Kaner oscillations in B_A and B_C crystals. An examination of the shape of the postulated piece of surface characteristic of B_A oscillations reveals that in general this piece of surface will be stongly coupled to the electric field whenever the electric field is parallel to the C-axis. The model surface is illustrated again in the following diagram.

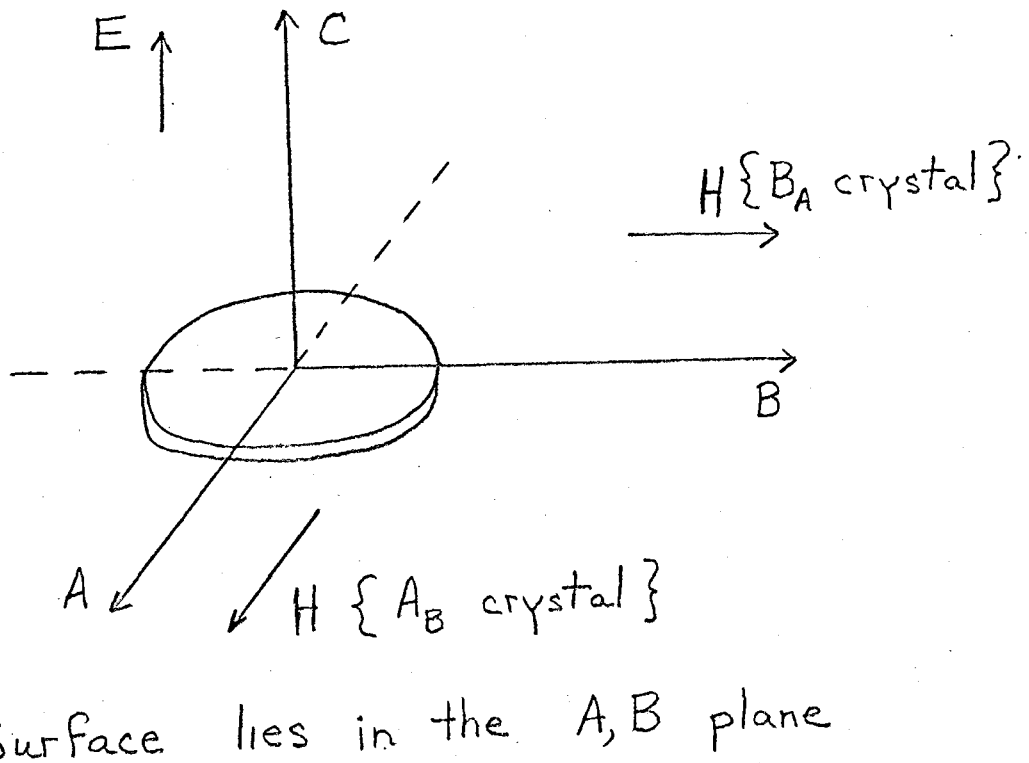

This condition is satisfied for both a B_A crystal and a A_B crystal. Therefore, the piece of surface should be coupled to the electric field for both crystals and oscillations characteristic of this piece should appear in both crystals. The periods of oscillation should have the same order of magnitude. Reference to Table 6-5 reveals that an oscillation with a period of 7.35 gauss appears in an A_B crystal. This is to be compared with the period 5.2 gauss seen in the B_A crystal.

Similarly B_C and C_B crystals should be complementary. Reference to Table 6-5 reveals that an oscillation with a period of 4.0 gauss appears in a B_C crystal. This is to be compared with the period 9.5 gauss seen in the B_C crystal.

7.2.2.5 Reference to the Results of Munarin et al.

As indicated in Table 6-5 the periods observed by Munarin et al.[36] are clearly larger than those observed by us. Evidently they are observing oscillations characteristic of larger pieces of surface. It is also interesting to note that we see many more Gantmakher-Kaner periods than do these authors.

Chapter 8

COMMENTS AND CONCLUSIONS

A comparison of the results obtained using a gallium box whose thick sides have been electroplated with copper with those obtained using a rectangular box constructed by soldering a crystal onto a rectangular trough, clearly reveals that the electroplated gallium box technique is not reliable.

In certain crystal orientations a noticeable linear variation of the transmission with magnetic field occurred at sufficiently high magnetic field strengths (see Fig. 6-65). In this case the applied magnetic field was parallel to the current direction but perpendicular to the radio frequency magnetic field. We have attributed this phenomenon to a magnetoresistive effect in the crystal. The following argument supports this conclusion.

In the low field limit it is known[63] that the resistance generally increases by an additive term proportional to H^2.

$$\frac{\Delta\rho}{\rho} \propto H^2$$

and $$\rho - \rho_0 = \alpha \rho_0 H^2$$

$$\therefore \rho = \rho_0 (1 + \alpha H^2)$$

But the skin depth varies with resistivity. For a local conductivity this relation is,

$$\delta^2 \propto \rho$$

$$\therefore \quad \delta \text{ varies as } H$$

Consequently, it is possible to experience a linear increase in transmission with magnetic field if $\frac{\rho(H)}{\rho_0} >> 1$ and if $\rho(H) \propto H^2$, and if one assumes that the field is sufficiently large that the skin effect can be described using a local conductivity.

In fact measurements made by Yaqub and Cochran[49] on the longitudinal magnetoresistance in gallium tend to support this conclusion.

In conclusion the use of a hollow box as a sample instead of a simple slab in the bilateral excitation geometry provides a very simple and convenient means for making quantitative observations on the anomalous penetration of electromagnetic radiation through metallic crystals.

Chapter 9

LIST OF REFERENCES

1. G. E. H. Reuter, E. H. Sondheimer, Proc. Roy. Soc. (London) A 195, 336 (1948).
2. E. A. Kaner, V. L. Fal'ko, JETP 22, 1294 (1966).
3. W. M. Walsh, Jr., Electrons in Metals, J. F. Cochran and R. R. Haering, Editors (Gordon and Breach, New York, 1968).
4. V. F. Gantmakher, Progress in Low Temperature Physics, Vol 5., C. J. Gorter, Editor (North Holland, Amsterdam, 1967).
5. E. A. Kaner, JETP 17, 700 (1963).
6. J. F. Cochran, C. A. Shiffman, Phys.Rev. 140, A1678 (1965).
7. see for example, C. Kittel, Introduction to Solid State Physics, 3rd edition (Wiley, New York, 1966).
8. V. F. Gantmakher, JETP 15, 982 (1962).
9. E. A. Kaner, V. G. Skobov, Advan. Phys. 17, 605 (1968).
10. C. C. Grimes, W. H. Walsh, Jr., Phys. Rev. Lett. 13, 523 (1964).
11. W. F. Druyvesteyn, A. J. Smets, Phys. Lett. 30A, 415 (1969).
12. V. F. Gantmakher, JETP 16, 247 (1962).
13. V. F. Gantmakher, JETP 17, 549 (1963).
14. A. B. Pippard, Dynamics of Conduction Electrons (Gordon and Breach, New York, 1965).

15. V. F. Gantmakher, E. A. Kaner, JETP 18, 968 (1964).

16. V. F. Gantmakher, E. A. Kaner, JETP 21, 1053 (1965).

17. M. Ya Azbel, JETP 12, 283 (1961).

18. V. P. Naberezhnykh, A. A. Maryakhin, Phys. Stat. Sol. 20, 737 (1967).

19. A. A. Maryakhin, V. P. Naberezhnykh, JETP Lett. 3, 135 (1966).

20. P. Aigrain, Proceedings of the International Conference on Semiconductor Physics, Prague 1960 (Publishing House of the Czechoslovak Academy of Sciences, Prague, 1961) p. 224.

21. J. C. McGroddy, J. L. Stanford, E. A. Stern, Phys. Rev. 141, 437 (1966).

22. P. B. Miller, R. R. Haering, Phys. Rev. 128, 126 (1962).

23. E. A. Kaner, V. F. Gantmakher, Uspekhi 11, 81 (1968).

24. D. S. Falk, B. Gerson, J. F. Carolan, Phys. Rev. 1, B406 (1970).

25. E. A. Kaner, V. L. Fal'ko, JETP 24, 392 (1967).

26. T. K. Wagner, J. F. Koch, Phys. Rev. 165, 885 (1968).

27. G. E. Juras, Phys. Rev. 187, 784 (1969).

28. J. F. Koch, T. K. Wagner, Phys. Rev. 151, 467 (1966).

29. V. F. Gantmakher, V. S. Tsoi, JETP 29, 663 (1969).

30. J. F. Cochran, CJP 48, 370 (1970).

31. P. H. Haberland, C. A. Shiffman, Phys. Rev. Lett. 19, 1337 (1967).

32. W. A. Reed, J. A. Marcus, Phys. Rev. 126, 1298 (1962).

33. American Institute of Physics Handbook (McGraw-Hill, New York, 1963).

34. A. J. Bradley, Z. Krist 91, 302 (1935).

35. C. S. Barrett, Advances in X-Ray Analysis (Plenum Press, New York, 1962) Vol. 5.

36. J. A. Munarin, J. A. Marcus, P. E. Bloomfield, Phys. Rev. 172, 718 (1968).

37. A. Goldstein, S. Foner, Phys. Rev. 146, 442 (1966).

38. J. M. Condon, Bull. Amer. Phys. Soc. 9, 239 (1964).

39. A. Fukumoto, M. W. P. Strandberg, Phys. Rev. 155, 685 (1967).

40. P. H. Haberland, J. F. Cochran, C. A. Shiffman, Phys. Rev. 184, 655 (1969).

41. Y. Shapiro, B. Lax, Phys. Rev. 138, 1191 (1965).

42. L. J. Neuringer, Y. Shapiro, Phys. Rev. 165, 751 (1967).

43. P. A. Bezuglyi, A. A. Galkin, S. E. Zhevago, JETP 20, 552 (1965).

44. P. A. Bezuglyi, A. A. Galkin, S. E. Zhevago, Soviet Physics-Solid State 7, 383 (1965).

45. J. Lewiner, Phys. Rev. Lett. 19, 1037 (1967).

46. T. W. Moore, Phys. Rev. Lett. 18, 310 (1967).

47. T. W. Moore, Phys. Rev. 165, 864 (1968).

48. J. A. Munarin, Phys. Rev. 172, 737 (1968).

49. M. Yaqub, J. F. Cochran, Phys. Rev. 137, A1182 (1965), and Phys. Rev. 140, A2174 (1965).

50. J. C. Slater, G. F. Koster, J. H. Wood, Phys. Rev. 126, 1307 (1962).

51. J. H. Wood, Phys. Rev. 146, 432 (1966).

52. W. A. Reed, Phys. Rev. 188, 1184 (1969).

53. J. R. Cook, W. R. Datars, Phys. Rev. B1, 1415 (1970).

54. F. G. Brickwedde, H. van Dijk, M. Durieux, J. R. Clement, and J. K. Logan. The "1958" He^4 Scale of Temperatures. N.B.S. Monograph 10, June 17, 1960.

55. G. T. Meaden, Electrical Resistance of Metals (Plenum Press, New York, 1965).

56. K. R. Lyall, Ph.D. thesis (unpublished).

57. P. H. Haberland, Ph.D. thesis (unpublished).

58. M. Hanabusa, A. H. Silver, T. Kushida, to be published.

59. V. P. Naberezhykh, N. K. Dan'shin, L. T. Tsymbal, JETP 28, 203 (1969).

60. G. Weisbuch, A. Libchaber, Phys. Rev. Lett. 19, 498 (1967).

61. V. F. Gantmakher, Yu. S. Leonov, JETP Lett. 8, 162 (1968).

62. B. Perrin, G. Weisbuch, A. Libchaber, Phys. Rev. B1, 1501 (1970).

63. See for example, C. Kittel, Quantum Theory of Solids, (Wiley, New York, 1963).

64. See for example, R. V. Churchill, Complex Variables and Applications, (McGraw-Hill, New York, 1960), p. 55.